NTNU – Trondheim
Norwegian University of
Science and Technology

Synkinematic intrusion of granitoid sheets, with implications for molybdenite deposits in the Knaben Zone

Sirdal Magmatic Belt, SW Norway

Martin Austin Stormoen

Geology
Submission date: May 2015
Supervisor: Rune Berg Larsen, IGB

Norwegian University of Science and Technology
Department of Geology and Mineral Resources Engineering

Abstract

The Knaben Zone represents a N-S-elongated zone with abundant xenolith screens and molybdenite deposits within the late Mesoproterozoic Sirdal Magmatic Belt (SMB) batholith in the Sveconorwegian orogen, in SW Norway. The SMB represents a significant component of the western vicinity of the Sveconorwegian orogen, and has recently received attention due to its lately defined sheer size and weak deformation. Through determining the significance of xenolith-rich zones the understanding of the evolution of the SMB can be greatly improved.

The main objective in this MSc thesis is to determine the lithological relationships and magmatic and tectonic processes for the Knaben Zone. An evaluation of the evolution and potential of the molybdenite deposits is also put forward, together with a regional comparison. Detailed fieldwork and microscopic analysis of the Knaben Zone provide the basis for this project, supported by whole-rock geochemistry and zircon geochronology.

Xenolith screens representing pre-Sveconorwegian bedrock (1252.8±8.7 Ma), and granitoid sheets (1043.3±5.6 Ma) related to the SMB, dominate the geometry of the Knaben Zone, with a pervasive moderate east-dipping parallelism. These are presented in a detailed geological map of the area. The SMB granitoids are generally undeformed to weakly deformed, with strain concentrated along xenolith screen contacts and local mylonite zones. Compressional top-to-the-W kinematics are consistent at all scales along the deformation zones, and melt-present deformation is widely documented. The deformation is largely expressed as ductile duplex ramps, ramping up towards the west. Whole-rock geochemistry and crosscutting field relations suggest a continuously evolving melt, from the least evolved K-feldspar porphyritic biotite granite to highly evolved molybdenite bearing grey granite and leucocratic granites. The whole-rock geochemistry displays a decoupling signature and distinct Nb, Pb, P and Ti anomalies, a typical active margin signature. Disseminated molybdenite of magmatic origin within the grey granite is the most economically viable molybdenite deposit, while smaller deposits are largely confined to thrust-related, subhorizontal pegmatites.

Results from fieldwork, microscopic, geochemical and geochronological analysis are synthesized to a synkinematic intrusion model for the granitoid sheets in the Knaben zone, relative to the E-W-compression. The xenolith screens are essential for the molybdenite deposits, geochemically by providing precipitating agents and structurally, by concentrating fertile melts within the shear zones and anisotropies. The emplacement model, deduced from key findings within the Knaben Zone, is likely to be scale-invariant, and provides a structurally and petrological consistent emplacement model for the SMB at whole. Timing and kinematics correlate with thrusting along major shear zones in the Sveconorwegian orogen. The vast melt volume, and the geochemical signature related to the SMB, is best explained by a tectonic setting in the vicinity of an active margin.

Sammendrag (Norwegian summary)

Knaben Sonen representerer en NS-gående sone med høy tetthet av xenolitter og molybdenittforekomster i det sen-Mesoproterozoiske Sirdal Magmatiske Belte (SMB) i den Sveconorvegiske orogenen, i SV Norge. For å forstå utviklingen av SMB er det nødvendig å definere betydningen av xenolitt-rike soner, slik som Knaben Sonen. SMB representerer en betydelig del av den vestlige delen av den Sveconorvegiske fjellkjeden, og har nylig fått oppmerksomhet på grunn av batolittiske mengder granittisk smelte og svak deformasjon. Å produsere et oppdatert og detaljert geologisk kart med en revidert tolkning av den geologiske utviklingen i Knaben Sonen, med tidligere arbeid fra Knaben Sonen som utgangspunkt og i sammenheng med nyere Sveconorvegisk forskning, er hensikten med denne masteroppgaven.

Detaljerte felt- og mikroskopiske undersøkelser av Knaben Sonen er grunnlaget for dette prosjektet, i tillegg til bulkkjemi-analyser og zirkon geokronologi. Hovedfokuset er på litologiske relasjoner og magmatiske- og tektoniske prosesser. En evaluering av utviklingen og potensialet til molybdenitt forekomstene er også sentralt, samt å vurdere Knaben Sonen i et regionalt perspektiv.

Tabulære xenolitter (eng.: screens), som representerer pre-Sveconorvegisk grunnfjell (1252,8 ± 8,7 Ma) og elongerte granittoid intrusjoner (eng.: sheets) (1043,3 ± 5,6 Ma) knyttet til SMB, definerer geometrien i Knaben Sonen, med en gjennomgående moderat øst-fallende parallellitet. Geologien i Knaben Sonen er presentert i et detaljert geologisk kart. SMB granittoidene er udeformerte til svakt deformerte, med formforandring konsentrert langs xenolittenes kontakter og i lokale mylonittsoner. Strukturelle observasjoner er konsistente med topp-mot-V kinematikk, i alle målestokker, og viser til Ø-V rettet kompresjon. Strukturer som tyder på at smelte var tilstede under deformasjonen er godt dokumentert. Deformasjonen uttrykker seg i stor grad som duktile duplex-ramper. Bulkkjemi og kuttende feltforhold tyder på en smelte som utvikles kontinuerlig, fra den minst utviklede alkalifeltspat porfyrittisk biotitt granitt til høyt utviklet molybdenitt førende grå granitt og leukokratiske granitter. Bulkkjemien viser en anrikning av kompatible sporelementer og markerte Nb, Pb, P og Ti anomalier, en typisk aktiv margin signatur. Dissemminert molybdenitt av magmatisk opprinnelse i grå granitt er den mest økonomiske molybdenitt malmen Mindre forekomster er i stor grad begrenset til skyveforkastningsrelaterte subhorisontale pegmatitter.

Resultater fra felt-, mikroskopiske-, geokjemiske og geokronologiske analyser er syntetisert til en synkinematisk intrusjonsmodell for de tabulære granitoidplutonene i Knaben-Sonen, relatert til EW-kompresjon. Xenolittene er avgjørende for molybdenitt forekomstene, geokjemisk, ved å fremprovosere krystallisering av molybdenitt, og strukturelt, ved å konsentrere malmdannende smelter i skjærsoner og anisotropier. Modellen for smelteemplassering, basert på funn fra Knaben Sonen, kan utvides til hele SMB. Kinematikken og alderen dokumentert i denne oppgaven korrelerer godt med skjærsoner i den Sveconorvegiske fjellkjeden. Det store smeltevolumet og den geokjemiske signaturen knyttet til SMB, er i best overenstemmelse med et konvergerende tektonisk miljø i nærheten av en aktiv margin.

Table of contents

Figure list

Definitions

The "Knaben Zone" refers to the N-S-striking belt of xenoliths and high density of molybdenite deposits passing through Knaben village in Vest Agder. The majority of the Knaben Zone is mapped in detail in this thesis.

When addressing the magmatic rocks in the Knaben Zone in general, the term "granitoid rocks" is used. Otherwise, the specific names presented for each rock in the chapter 3 is used. The rock names used by Lysberg (1976) are modified, due to different interpretations. In general, the rocks termed "Knaben Gneiss" by Lysberg (1976) refer to the *xenoliths* in this thesis, and similarly Lysberg's (1976) "Granitic gneiss" group refer to the *granitoid rocks* in this thesis. In addition, Lysberg's (1976) "augen gneiss" and "red granite" are termed *flaser gneiss* and *porphyritic granite* respectively, in this thesis.

Mineral abbreviations used in this thesis are from Whitney and Evans (2010). The abbreviations used are Actinolite (Act), Allanite (Al), Apatite (Ap), Biotite (Bt), Calcite (Cal), Chlorite (Chl), Chalcopyrite (Ccp), Clinopyroxene (Cpx), Epidote (Ep), Fluorite (Fl), Garnet (Grt), Hornblende (Hbl), K-feldspar (Kfs), Magnetite (Mag), Molybdenite (Mol), Muscovite (Ms), Olivine (Ol), Opaque minerals (Opq), Orthopyroxene (Opx), Plagioclase (Pl), Pyrite (Py), Quartz (Qz), Rutile (Rt), Sphene/Titanite (Spn), Zircon (Zrn).

When referring to solid-state-, submagmatic-, and magmatic flow, these terms refer to the definitions and indications for these three modes presented by Vernon (2004, p. 458). The prefixes pre-, syn- and post- are widely used in this thesis to refer to relative timing of magmatism and deformation.

Planar structures are measured as dip/dip-direction. Linear structures are referred to by trend/plunge. N, S, E, W and combinations are used to refer to bearings.

Other abbreviations:

-BGS – British Geological Survey
-CL – Cathode Luminescence
-DIRMIN – Direktoratet for Mineralforvaltning (Norwegian Directorate of Mining)
-HBG – hornblende biotite granite
-NGU – Norges Geologiske Undersøkelse (Norwegian Geological Survey)
-NTNU – Norges Teknisk Naturvitenskapelige Universitet (Norwegian University of Science
-ppl – plane polarized light
-RIC – Rogaland Igneous Complex
-SEM – Scanning Electron Microscope
-SGU – Sveriges Geologiske Undersökningar (Sweedish Geological Survey)
and Technology)
-SMB – Sirdal Magmatic Belt (Slagstad et al., 2013)
-TIMS – Thermal Ionization Mass Spectrometry
-xpl – crossed polarisers

Preface

I started my MSc degree in geology at NTNU in August 2013, with the specialisation "Bedrock and Resource geology", and contacted Trond Slagstad at NGU while searching for an interesting project. As I was hoping to find a project spanning structural geology, petrology, resource geology and with substantial fieldwork, the project in Knaben was very appropriate.

Several researchers from NGU were involved with the first field season (September, 2013), and all of them contributed to important discussions and observations which had a bearing for this project (Axel Müller, Torkil Røhr, Iain Henderson, Nolwenn Coint, Nick Roberts (BGS), Bjørn Eske Sørensen (NTNU), Trond Harstad (field assistant)). Charles Jordan and Andreas Sigersvold should be thanked for showing us around the Knaben mountains and mines. In addition, a joint excursion with NGU and SGU concerning the Sveconorwegian orogen was arranged the week before the field work, giving useful insight into the evolution of the orogen, and ongoing discussions.

After the first field season, it was clear that consistent structures and kinematics were of importance for the Knaben Zone, and Iain Henderson became a co-tutor for my project. As molybdenite deposits were one of the main reason for the previous and current interest in the Knaben Zone, Rune Larsen from NTNU got involved with the project. All three tutors, Trond Slagstad, Rune Larsen and Iain Henderson, have been available and helpful throughout the process, and they encouraged independent and critical, but at the same time creative and observant work.

The organisations Bergringen and Norsk Bergforening should be thanked for giving me the opportunity to attend the European Geoscience Union's General Assembly 2014, Unggeo 2014 and the Norwegian Geological Societies' Winter Conference 2015, where I presented preliminary work (Digital Appendix). The laboratory technicians who helped with the zircon geochronology at NGU and prepared thin sections at NTNU must also be thanked.

Finally, I want to thank my fiancée, Rebekka, for patience and understanding for my apathetic and busy behaviour during the small amount of time I have spent outside the office.

Martin Austin Stormoen

Trondheim, May 2015

Chapter 1 – Introduction

1.1 Background for thesis and rationale

The Knaben Zone is an accessible and largely well exposed area, showing the more heterogeneous parts of the rather homogeneous granitoid-dominated region. In addition, the presence of a major molybdenite deposit adds another aspect. The most recent detailed work in the Knaben Zone is done by Lysberg (1976), and shows more heterogeneity than the regional scale maps give impression of, and hence invites a different understanding.

My main supervisors, Trond Slagstad and Iain Henderson, have been working regionally in the Sveconorwegian province through several projects for NGU. Slagstad and his co-workers have identified vast amounts of undeformed to weakly deformed magmatic rocks, previously mapped as gneisses (Slagstad et al., 2013). Henderson has been involved with projects defining the structures and kinematics along major shear zones in the Sveconorwegian orogen (Henderson and Ihlen, 2004; Viola et al., 2011). This invites an approach to the Sveconorwegian orogen with stronger focus on magmatic processes than previous work, within a structural framework.

The working hypothesis, and the motivation for this thesis was to understand what the Knaben Zone represents within the magmatic complex, and the possibility that the Knaben Zone represents a boundary between individual magmatic intrusions, as speculated by Coint et al. (in press). It has also been indicated that the molybdenite deposits in the Knaben Zone could be related to shear zones (Gvein and Rui, 1980), with top-to-the-W kinematics (Jakubiak and Maund, 2012). Through detailed mapping, process oriented structural and petrological analyses, geochronological and geochemical analyses, a geological evolution of the Knaben Zone will be sought.

The existing detailed geological investigation of the northern parts of the Knaben Zone, done by Lysberg (1976), have been the basis for this project, and are re-evaluated in light of modern geological concepts, and in addition extended to cover a larger part of the Knaben Zone. Evaluating the new findings in light of the modern consensus and discussions on the regional geological setting is important.

Parallel to this project Stine Bang, from NTNU, has completed her MSc thesis on the chemistry of the different molybdenite deposits in the Knaben Zone. Hence, for more details on the deposits, see Bang (2015). The work presented in this thesis provides the geological basis for Bang (2015) and future work in the area.

1.2 Knaben – geography

Knaben is a small village at the north-eastern termination of county road 465 in Kvinesdal municipality, Vest Agder county (Fig 1). Originally, Knaben was a mining village, but is now mainly a holiday-cottage village.

Knaben lies on the south vicinity of the Hardangervidda mountain plateau, 630 m.a.s.l.. The mountainous area surrounding the village contains a gentle mountain landscape and numerous lakes. A pronounced E-W trending lineament in which Knaben village is situated, incises the area.

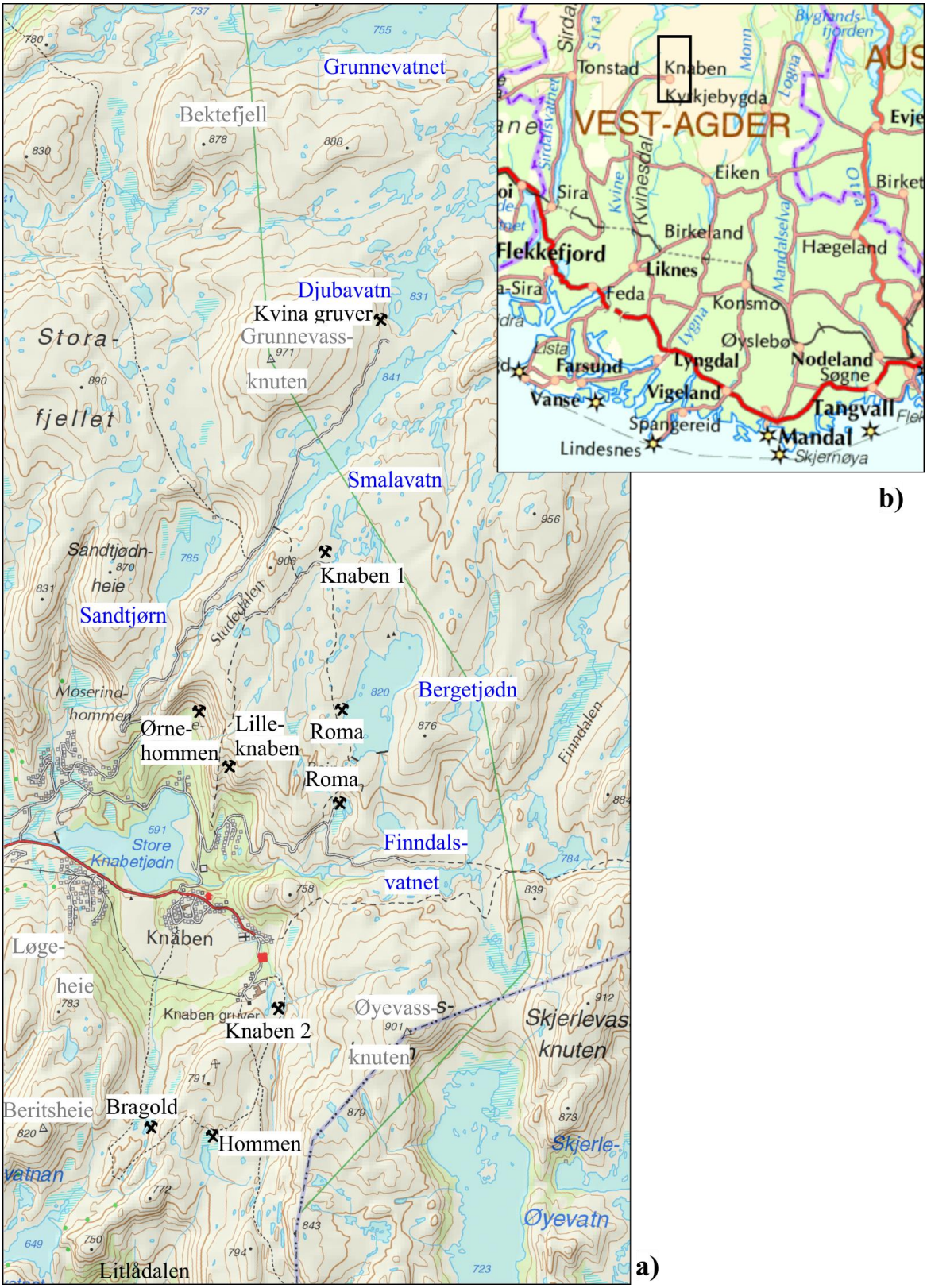

Figure 1: a) *Topographic map with the names of lakes (blue font), mountains (grey font) and mines (black font) used in this thesis. Note the pronounced lineament striking E-W through Finndalsvatnet, and the lineament following Smalavatn. Red road is Rv456.* ***b)*** *Regional map showin Vest Agder county, and the position of map a) is marked (black square).*

There are numerous molybdenite mines and claims that are mostly concentrated within a one-kilometre wide zone, that stretches approximately 5km north and south of Knaben (Fig 2a). The fieldwork for this thesis is focused on this zone, referred to as the Knaben Zone. The three largest mines in the area, from north to south, are Kvina, Knaben 1 and Knaben 2. Knaben 2 is the largest and is shown on the cover page. The Knaben village is concentrated close to the Knaben 2 mine.

Throughout this thesis, the mines, lakes and hills marked on the overview map (Fig 1) will be the reference points, besides locality numbers presented later. The topography in the Knaben Zone is defined by moderate eastward dipping structures, forming a landscape with N-S striking ridges with steeper west-facing sides, and typical rolling glacial mountains.

The history of molybdenite mining is long, and largely ceased in 1978, when the Knaben 2 mine closed. Small scale processing of remaining crushed ore in the Knaben 2 mine is still carried out by Andreas Sigersvold. Jourdan (2003) has written a comprehensive report on the mining history in the area, and details from exploration and mining are found on DIRMIN's web pages.

1.3 Geological setting

The Knaben Zone is situated in the central parts of the Sveconorwegian province within the Precambrian bedrock of SW Norway (Fig 2a). Traditionally, the Sveconorwegian orogen is interpreted as the continuation of the Grenvillian orogen, formed during the assembly of the supercontinent Rodinia during the Mesoproterozoic era (Gower et al., 1990).

Bingen et al. (2008) divide the Sveconorwegian province into four main terranes, based on crustal scale shear zones, and put forward a model for the orogeny (Fig 2a). The Telemarkia Terrane is the westernmost terrane, and includes the SMB and the Knaben Zone. Between 1050 Ma and 980 Ma, the main Sveconorwegian orogenic event, the Agder phase took place, proposed as a terminal continent-continent collision between Baltica and possibly Amazonia according to Bingen et al. (2008), resulting in crustal thickening, magmatism and metamorphism. Bingen et al. (2008) further recognise granitoid intrusions within the Telemarkia Terrane, at 1050-1030 Ma, and conclude that the tectonic setting for these intrusions is ambiguous. These granitoid rocks are termed Feda and Fennefoss augen gneiss.

As pointed out by Andersen (2005), a terrane is per definition separated from adjacent terranes by distinct lithology and geological history and Sveconorwegian terminology should comply with such definitions. Terms for crustal blocks and units employed by Bingen et al. (2008) will be used in this thesis, as they are generally accepted in recent work, and discussing other (possibly more correct) terms is outside the scope for this thesis.

Extensive mapping and geochronological studies by Slagstad et al. (2013) reveal a voluminous magmatic belt, including the Feda augen gneiss, with magmatic ages spanning 1050-1020 Ma. This magmatic belt is termed the Sirdal Magmatic Belt (SMB) and is a voluminous N-S striking elongated batholith, consisting largely of weakly deformed to undeformed K-feldspar porphyritic granite (Fig 2a). Slagstad et al. (2013) further classifies the SMB granites as calc-alkaline and magnesian, with enriched amounts of large ion lithophile elements in the primitive mantle normalized trace element diagram and a distinct negative Nb-Ta anomaly, a typical subduction signature.

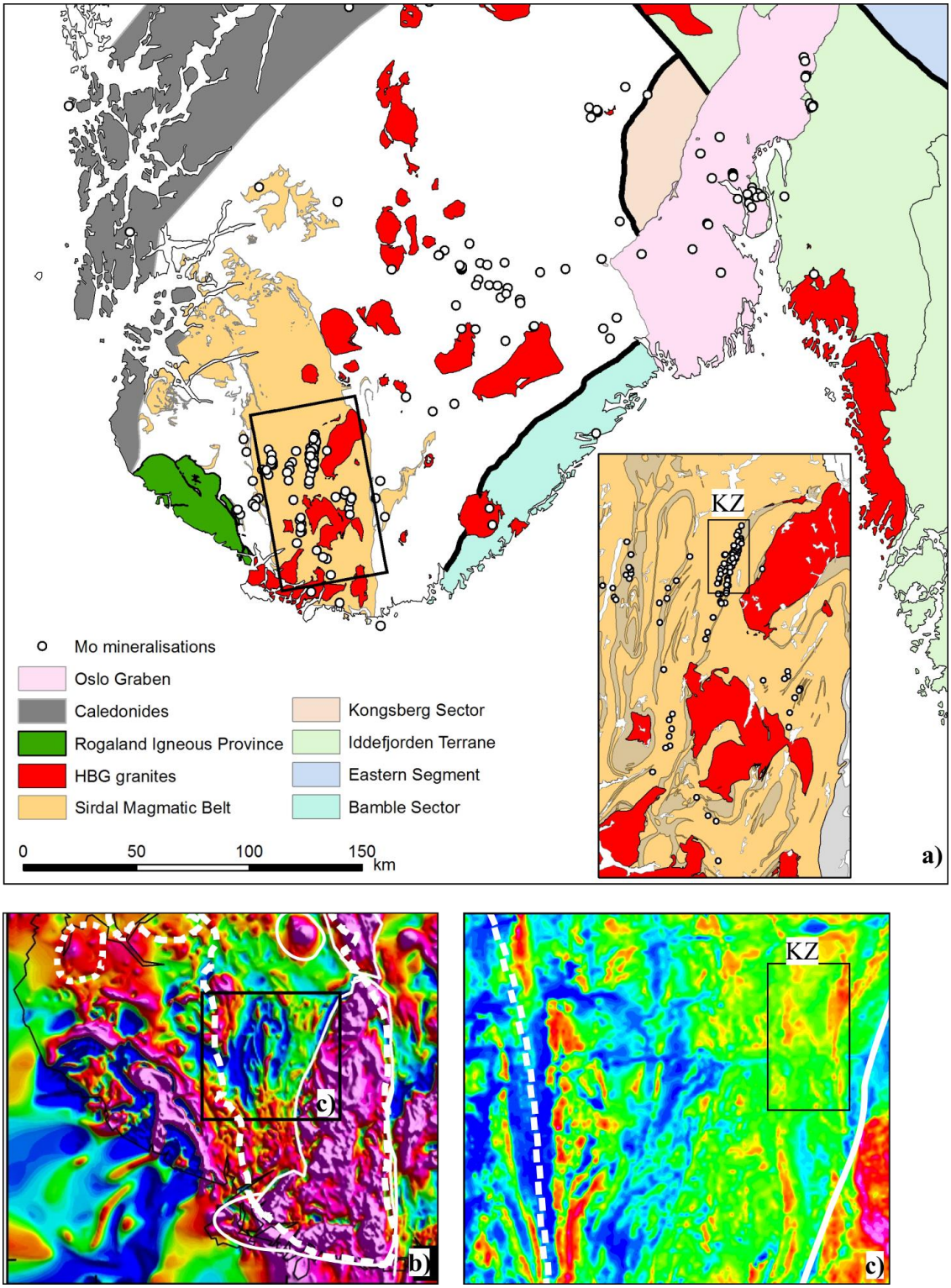

Figure 2 a) *Map showing major units in south Norway, with inset showing SMB (Slagstad et al., unpublished map). The Telemarkia terrane includes the area west of the shear zones (black lines). Westernmost equidimensional SMB pluton is the garnet granite (Coint et al., in press). Banded gneiss shown as grey bands on inset, originally from Falkum and Petersen (1980). Note that molybdenite deposits are most dense in the Knaben Zone. These banded gneiss zones consist of xenoliths representing pre-Sveconorwegian bedrock, and are speculated by Coint et al. (in press) to represent pluton contacts within the SMB.* ***b)*** *Regional areomagnetic anomaly map (Gellein, 2007). The SMB is outlined with dotted lines and the HBG is marked with full lines. Note the N-S striking anomalies within the SMB, especially the southern half.* ***c)*** *Detailed aeromagnetic anomaly map from a section (square) in map b). (Unpublished data, NGU).*

Falkum and Petersen (1980) state that the Sveconorwegian province is "*made up of a succession of synkinematic intrusions, grading into late- and post kinematic intrusions, which were emplaced into pre-existing gneisses throughout a considerable time interval*". The post kinematic intrusions are referred to as the HBG suite by Vander Auwera et al. (2003). The synkinematic intrusions have, according to Falkum and Petersen (1980), gone through "*several phases of deformation*", but the degree of deformation varies and undeformed areas with magmatic textures are common in the central parts of the magmatic region.

The synkinematic intrusions are porphyritic, and exhibit an augen-gneiss texture when deformed; hence they have been grouped as gneisses (Falkum and Petersen, 1980). These synkinematic intrusions fall within the Sirdal Magmatic Belt (Slagstad et al., 2013). Falkum and Petersen (1980) argue for a mantle derived origin rather than reworked crustal rocks, for the syn kinematic intrusions, based on low Sr content. "*Fragments of older rocks*" within the SMB, are according to Falkum and Petersen (1980), remains of older intrusions and sediments. They are grouped into units of "*banded gneisses*" and "*supracrustal rocks*". The Knaben Zone corresponds to one of these banded gneisses (Fig 2a).

An overall subduction setting for the SMB is suggested by Bingen and Van Breemen (1998) and Slagstad et al. (2013), based on the above mentioned geochemical signature. There is less agreement about how the tectonic setting evolved after the emplacement of the SMB. According to Bingen et al. (2008), the main orogenic continent-continent collision took place at 1035-980 Ma, after the commence of the SMB, resulting in crustal thickening and high grade metamorphism reaching granulite facies. Slagstad et al. (2013) argue for continuing subduction, and an Andean type orogen, without a terminal continent-continent collision.

At a later stage (990-920 Ma), the HBG ferroan intrusions perforate the SMB (Fig 2). Slagstad et al. (2013) argue for emplacement within a subduction setting, "*behind the active margin*". The well-defined Rogaland anorthosite province intrudes simultaneously in the far southwest (Fig 2). In the four-phase model for the Sveconorwegian orogeny, proposed by Bingen et al. (2008), the HBG and AMC suite falls within a period of gravitational collapse, the Dalane phase.

As a result of the Sveconorwegian orogeny, crustal thickening and voluminous magmatism is thought to cause medium pressure, ultra-high temperature (UHT) granulitic (6±1 kbar and 900±100°C) conditions (Drüppel et al., 2012). This event is often annotated M1, and was suggested to result from crustal thickening and synorogenic magmatism. Drüppel et al. (2012) and Slagstad et al. (2013) comment that a Himalaya-style collisional setting lacks the heat needed for these conditions. The later UHT metamorphism, caused by the emplacement of the Rogaland Igneous Complex (AMC and HBG) is not of importance for the Knaben Zone.

In spite of an ongoing discussion (Slagstad et al., 2013; Möller et al., 2013), the Sveconorwegian orogen differs from an Himalaya-style orogen. The need for additional heat for UHT metamorphism (Drüppel et al., 2012), large volumes of synorogenic magmatism as well as the mentioned subduction geochemical fingerprints (Slagstad et al., 2013) point towards a more complex tectonic setting than a pure continent-continent collision. Möller et al. (2013) emphasize that a subduction setting is likely to result in a terminal collision.

There are several major shear zones within the Sveconorwegian orogen, the main ones are shown in Fig 2a. Generally, the shear zones east of the Oslo graben dip towards the west,

while the shear zones defining the eastern boundary of the Telemarkia terrane dip to the east (Bingen et al., 2008). The major shear zones typically show a history of initial thrusting followed by extension, interpreted as initial orogenic collocation of the terranes and later orogenic collapse. The timing of the compressive and extensional phases is dissimilar for the different shear zones, and is the basis for the different evolutionary phases in the four-phase-model presented by Bingen et al. (2008), and the thrust phases are generally interpreted to have occurred between 1.1Ga and 970Ma.

As pointed out by Coint et al. (in press), classifications of merely undeformed granitoid rocks as gneisses, especially banded gneisses, during the last half of the 20th century, have been inherited by more recent work. This approach has underrated the importance of magmatic events during the Sveconorwegian orogeny. Similar to Coint et al.'s (in press) work, this thesis aims to explore and understand a fraction of the magmatic rocks of the SMB, in the hope that this will add to the overall consensus on the Sveconorwegian orogeny.

Molybdenite deposits are anomalously common in the Sveconorwegian region (Fig 2a), and the highest density of deposits together with the most voluminous deposits lie within the Knaben Zone. Bugge (1963) gives an overview of all molybdenite deposits in Norway, and demonstrates that the deposits in the Knaben Zone are very similar to the other deposits in the region. He also defines a 300km wide molybdenite rich belt stretching from Sokndal 300km to the NW to Drammen. The molybdenite deposits in the region now termed SMB are well documented on a local scale, and are typically related to granitic intrusions, with a simple parallel, moderately eastward dipping geometry (Bugge, 1963).

Several types of molybdenite deposits are defined by Bugge (1963). The most economic deposits occur as disseminated grains in grey-coloured granitic to gneissic rocks. Smaller deposits are often related to pegmatites and aplites or within the older gneissic rocks. All deposits were previously thought to be related to greisenisation and pnematolytic processes, indicated by the common presence of calcite or fluorite together with the molybdenite (Bugge, 1963). Modern interpretations place more confidence in magmatic processes (Bingen et al., 2015; Coint et al., in press).

The molybdenite deposits in the Sveconorwegian region lie in N-S oriented clusters following zones mapped as "banded gneiss" within the SMB, Knaben being the most prominent. The zones of banded gneiss are more heterogeneous, and are xenolith-rich zones within the dominating porphyritic granite (Coint et al., in press). The xenoliths consist of a variety of amphibolites and different gneissic rocks. A spatial relationship between the molybdenite deposits and the xenolith rich zones is certain (Fig 2a) but, as pointed out by Bugge (1963), they are not directly linked, as the largest molybdenite deposits occur as weakly deformed to undeformed granitic varieties.

1.4 Earlier work in Knaben

Summary of Lysberg's (1976) work

In this section, information that is considered significant on the Knaben Zone will be presented. This includes mining reports, consultant reports, more recent unpublished data, as well as scientific papers. The work done by Lysberg (1976) has been important for this project's fieldwork, as his mapping and interpretation was considered the most detailed and appropriate for the project. Lysberg (1976) also made use of large amounts of data from the mining industry. Drill-cores from the mining industry have been useful for estimating the geology at depth and are included in the profiles (Digital Appendix, Map 2).

Lysberg (1976) presents detailed petrographic and structural data, and a geological map of the Knaben Zone, from the Knaben 1 mine and northward. He also presents a simplified map including the southern part of the Knaben Zone, based on previous maps. Naturally, Lysberg (1976) is influenced by the geologists of his time, and presents his own work in a specific framework, especially regional work by Leake (1972).

The lithologies in the Knaben Zone are grouped by Lysberg (1976) into the "Knaben gneiss", including xenolith screens of augen gneiss, amphibolite, vein-gneiss and biotite gneiss, and "Granitic gneisses", including coarse and fine-grained varieties of a grey and red-coloured granite. In addition, Lysberg (1976) describes diabase dykes, aplites and a mafic dyke.

The geometry, rock relationships and structures in the area are used by Lysberg (1976) to put forward an evolutionary geological model of the Knaben Zone. Five deformation phases, or stages of evolution, are presented. The first phase (D1) accounts for the development of planar compositional layering (S1) in the xenoliths, a result of partial melting or metamorphic processes. This layering is folded during the next stage (D2), and as a result an axial planar cleavage (S2) is defined by mineral alignment within the Knaben gneiss. Ptygmatic and isoclinal folding of leucosomes also belong to this stage. The different units of the Knaben gneiss occur as entrained elongated xenolith screens within a red granitic gneiss, with the cleavage oriented the same direction; dipping typically 30 degrees to the east.

The red granitic gneiss is emplaced after D2, and exhibits a foliation, defined by oriented biotite, quartz and feldspar, also dipping 30 degrees to the east. According to Lysberg (1976), this foliation (S3) is not the same as the foliation within the Knaben gneiss (S2), based on deviations in outcrop scale of up to 15 degrees. The foliation within the Granitic gneisses is a result of a second fold phase during D3, where the Knaben gneiss screens themselves are folded along a N-S trending horizontal fold axis (Lysberg, 1976). S3 is not developed within the xenoliths. Quartz aggregates within the red granitic gneiss are elongated and lineated parallel to the fold axis, and the phenocrysts of microcline are locally oriented in approximately the same manner. Lysberg (1976) also states that the phenocrysts are recrystallized and broken, and rotated towards the lineation during D3.

Lysberg (1976) points out that the foliation within the Granitic gneisses (S3) and the Knaben gneisses (S2) is only sub-parallel south of the Knaben 1 mine. North of here, S2 bends towards NE, while S3 does not change, and this is thought to represent large scale folding with a fold axis plunging gently south and axial plane dipping moderately eastward, as proposed by Leake (1972).

Fine-grained granitic gneisses are reported by Lysberg (1976) to intrude the coarser granitic gneisses, but containing fragments of rotated coarse-grained granitic gneiss and still showing a foliation parallel to S3. These fine-grained varieties come in a grey and a red variety; the grey variety contains disseminated molybdenite. The fine-grained grey gneiss is mapped out by Lysberg (1976) in the Knaben 2 mine and in an area in the smaller Bektefjell claims. This is the main molybdenite ore. Molybdenite rich quartz and feldspar veins are frequent in the lithologies surrounding the fine-grained grey gneiss, and are also scattered around the Knaben Zone, being the most frequent molybdenite ore, and hence related to the intrusion of the fine-grained grey gneiss.

Lysberg (1976) mentions that the fine-grained gneissic intrusions lie parallel to S3, as do several of the molybdenite rich veins. These parallel structures are argued to have evolved during "*periods of relaxation*", when the least principle stress axis is oriented orthogonally to S3. Another population of molybdenite rich veins is similar striking, but with a shallow dip. The origin of this second vein set is unclear to Lysberg (1976).

A fourth stage of deformation (D4) is initiated by open flexural slip folds, with a fold axis plunging 25 degrees towards NE. This has resulted in slickenlines along lithological boundaries, plunging 35-65 degrees so the SE. Within the same deformation stage, Lysberg (1976) describes a couple of mafic dykes cutting the fine grained grey granite, the major one occurring as a N-S striking dyke, east of Smalavatn. These dykes belong to later mafic dykes (855±59 Ma) (Walderhaug et al., 1999). Next, in Lysberg's (1976) fourth stage of deformation, shear zones striking NE-SW to E-W cut all lithologies, and the rocks within the shear zones are altered. Finally, a conjugate set of late fractures make up Lysberg's (1976) final deformation stage (D5).

The molybdenite deposits are thoroughly described by the earlier workers (Bugge, 1963; Lysberg, 1976), and divided into several types, based on mesoscopic observations. As mentioned, the disseminated molybdenite within the grey granite is the most voluminous deposit type. Molybdenite is also disseminated, or follows the foliation in the augen gneiss variety of the Knaben gneiss. Several types of mineralisation related to quartz veins and pegmatites are described, commonly parallel to the general foliation and spatially related to the grey granite or the augen gneiss. Bugge (1963) mentions that calcite and occasional fluorite commonly occurs together with all mineralisation types. A clear spatial relationship between the augen gneiss and the molybdenite mineralisation is pointed out by Lysberg (1976).

Lysberg (1976) concludes that the molybdenite deposits are related to late granitic intrusions and associated pegmatites, possibly as a result of partial melting of the augen gneiss, explaining the spatial and concentrated relationship. During deformation of the voluminous red porphyritic granite, smaller intrusions, including the mineralized grey granite, took place, within the same stress regime, during Lysberg's (1976) D3 stage.

More recent work in the Knaben Zone

A comprehensive geochronological study of the Knaben Zone is completed by Bingen et al. (2015). They base their study on Lysberg's (1976) work, and aim to establish the time of magmatic and metasomatic events in the Knaben Zone. Due to magmatic, metamorphic and metasomatic events close in time, the geochronological data are obscured, and Bingen et al.

(2015) therefore compare results from secondary ion mass spectrometry (SIMS) and isotope dilution- thermal ionization mass spectrometry (ID-TIMS).

A sulphide bearing augen gneiss from the Knaben 1 mine gives an age of 1257±6 Ma, and is correlated with a regional pre-Sveconorwegian bimodal magmatic event (Bingen et al., 2015). The dominating poorly foliated red granitic gneiss yields a magmatic age of 1035±5 Ma, and is argued to be coeval with, and part of the same plutonic event as, the molybdenite-rich grey gneiss (1032±3 Ma). Zircon ages interpreted to represent minor magmatic events between 1065 Ma and 1000 Ma are also detected, suggesting complex relationships between veins, aplites and pegmatites, and the various granitoid sheets, correlating well with geochronology from the SMB presented by Coint et al. (in press). Hydrothermal activity, based on sparse zircon rims, is argued to endure between 1039±6 Ma and 1009±7 Ma, peaking at 1016 Ma, overlapping with monazite ages of 1013±5 Ma.

Bingen et al. (2015) proposed two models for the development of the molybdenite deposit. In one magmatogenic model, the molybdenite is transported via the molybdenite bearing grey granite and their hydrothermal fluids deposited in margins and during cooling. Several generations of magmatic and hydrothermal events close in time may cause reworking and complicating the original system. The magmatic age for the grey granite is 1032±3 Ma, according to Bingen et al. (2015). In the alternative metamorphogenic model, molybdenum is derived from the older Knaben Gneiss rocks, transported with fluids and deposited when the chemical conditions allowed it.

A different approach to the rocks in the Knaben Zone and the SMB, giving more attention to field relations and rock texture, is carried out by Coint et al. (in press). The voluminous unit, named red granitic gneiss by Lysberg (1976), is shown to be weakly deformed, with abundant magmatic textures, and is classified as a porphyritic to equigranular biotite granite, and is the dominating intrusive unit in the SMB. Coint et al. (in press) speculates that the N-S oriented xenolith rich zones represent contact zones between individual plutons making up the SMB (Fig 2a). The Knaben Zone represents one of these xenolith rich zones, and such zones could "*serve as markers for linking deformation and magmatism*". This speculation is supported by TIMS analysis from each side of the Knaben Zone, resulting in an age of 1019±2Ma on the east side and 1029±3Ma on the west side (Slagstad et al., unpublished TIMS data, 2015). Another interesting finding is the high pressure (4-5kbar) of the SMB rocks, pointing towards mid crustal depths (12-15km) (Coint et al., in press).

The possibility of a connection between the molybdenite deposits and structures in the Knaben Zone was first conjectured by Gvein and Rui (1980). They argued that molybdenite deposits occurring in thin veins are related to N-S trending, up to a metre thick shear zones, dipping parallel to the general foliation of the weakly foliated red porphyritic granite. The similar parallelism of the occasionally mineralised augen gneiss, described as "fahlbands", is also used as an argument for mineralisation within shear zones. Gvein and Rui (1980) emphasise that the amphibolite is "*twisted and torn apart in a mobile granite phase*" and is older than the augen gneiss. Three distinct N-S striking, 40-50m wide zones with molybdenite claims and mines are identified by Gvein and Rui (1980), and they speculate on whether these zones might represent larger interconnected shear zones.

Jakubiak and Maund (2012) argue that the grey gneissose molybdenite bearing granite is a separate intrusion, and that the ore deposit is not a result of alteration. They propose that these

units have intruded into weaknesses in the Knaben gneiss xenoliths, within pre-existing moderately eastward-dipping thrust ramp structures. The reason for the large size of the Knaben 2 deposit is suspected to be the intersection of deep, significant structures (Jakubiak and Maund, 2012).

Important characteristics of the magmatic system in the Knaben Zone are presented by Müller (2014). Wavy rims with oscillatory zonation is documented in quartz, visible in SEM-CL, indicating high temperatures over a long period of time (Müller et al., 2012). He estimates the closure temperature to be at 730 °C (titanium-in-quartz-geothermobarometer), and points out that this is far hotter than one would expect in more common porphyritic type molybdenite deposits. Repeating intrusive activity can explain such conditions. Müller (2014) also emphasizes that the pegmatites related to mineralisation show poorly developed grain boundaries and are clearly deformed, possibly syn-emplacement deformation, as they often lie within and parallel to the weakly deformed porphyritic granite.

1.5 Geophysical setting

On the regional aeromagnetic anomaly maps (Fig 2b, 2c), N-S trending weak magnetic anomalies define the Knaben Zone and the southern half of the SMB. The resolution of the data does not distinguish the small-scale variations within the Knaben Zone. This reflects a batholith built up by sheet-like intrusions, as indicated by Coint et al. (in press). The later E-W trending shear zones cutting the Knaben Zone are visible on the magnetic map. The later HBG pluton east of Knaben is very clear as a magnetic high, and is illustrated in Fig 2a and 2b.

Preliminary magnetic helicopter measurements were carried out in the Knaben Zone in 1971 (Gvein and Rui, 1980), and show a magnetic low area oriented N-S, including the largest mines and the major molybdenite deposits. Gvein and Rui (1980) also point to field measurements that show that the grey molybdenite-bearing granite, the main ore in the Knaben 2 mine, generally has susceptibility values two orders of magnitude less than the dominating granites and gneisses in the Knaben Zone.

1.6 Objectives and approach

The main objective in this MSc thesis is to present an updated map and a revised interpretation of the geological evolution of the Knaben Zone, using earlier work from the Knaben Zone as a starting point and in light of modern Sveconorwegian research (presented above). The project focuses on processes related to the Sveconorwegian orogeny and processes with a bearing on the molybdenite deposits. Regarding the Knaben Zone as part of the SMB and evaluating what the Knaben Zone and the SMB represents on a larger scale, is of importance.

The project's line of approach is illustrated in Fig 3. Detailed geological mapping and structural and petrological studies focused on process, combined with whole-rock geochemistry and zircon geochronology are the principle methods. Such a broad approach will result in a vast amount of data. As all findings are of potential value for future research, it is important that they are presented, even if they are of less importance for the broader picture and the following discussion in this thesis.

In the following, detailed results from fieldwork and microscopic analysis are presented for each lithology, and structural data are presented by structure type. Occurrence of molybdenite is presented continuously, and summarised in a separate section. Finally in the results-chapter, geochemical and geochronological data are presented and evaluated.

Subsequently, evaluating and systematizing the results in a synthesised model for the geological evolution of the Knaben Zone and the evolution of the molybdenite deposits, is the main outcome of the discussion. A the proposed model of the Knaben Zone is evaluated in light of the SMB at whole and put in a Sveconorwegian context.

1.7 Important concepts

As this thesis does not include a literature study, a separate theory chapter is not included, and important geological concepts are generally presented where needed. Below follows a brief review of geological concepts and restrictions of importance for the Knaben Zone.

Granitoid magmatism

This MSc thesis deals with a small heterogeneous zone within a large granitoid batholith, the Sirdal Magmatic Belt (SMB). Granitoid rocks are ambiguous at several levels. Firstly, the mineralogy is monotonous, obscuring interpretations about varying metamorphic conditions, especially in-field interpretations. Analysing quartz and feldspar microstructures can help to reveal changes in physical conditions, and well defined concepts have been important for this study (Hirth and Tullis, 1992; Parsons et al., 2005; Passchier and Trouw, 1996; Stipp et al., 2002).

Secondly, deformation is poorly recorded in granitoid rocks and, at high temperatures, it is difficult to distinguish magmatic flow and deformation in a gradually crystallizing melt, from later ductile deformation. Paterson et al. (1989) present microscopic and mesoscopic criteria for distinguishing between magmatic flow, where rotation and deformation can progress without any recrystallization, and solid-state flow, where all rotation and deformation is taken up by recrystallization. They also introduce a boundary condition at 20-40% melt, termed submagmatic flow, which results in a separate set of mesoscopic and microscopic structures. Quantifying strain in an evolving magma is difficult, as large amounts of strain can be partitioned into the melt without leaving any record, before the amount of crystallisation is significant (Paterson et al. (1998) in Vernon (2004, p. 458))

Thirdly, geochemical signatures are largely spread in felsic, highly evolved environments, so it is not always possible to distinguish different lithologies. Potential reworking of older granitoid rocks and crustal contamination further complicates petrogenetic interpretations.

In addition, the relationship between deformation and granitoid intrusions is still controversial. The general importance of tectonics and deformation for all stages of granitoid evolution is emphasized by several authors (Hutton, 1996; Vigneresse, 2004; Zellmer and Annen, 2008; Brown, 2013).

Creating space for intrusion in a compressional setting is a much discussed topic (Hutton, 1996). Ferré et al. (2012) summarise several plutons from compressive settings, and compare these with analogue models. They argue that thrusts act as convenient paths for melt migration and ascent, and that the final emplacement is spatially associated with thrusts. Dilations and flat structures can further provide space for emplacement. The depth of

intrusion is of importance for the stress regime and possible emplacement processes, largely controlled by magmatic pressure and differential stress (Brown and Solar, 1998). In a compressive setting, large amounts of strain are partitioned into a gradually crystallising melt, which can efficiently segregate more evolved melt batches (Karlstrom et al., 1993).

Large parts of the southwestern Sveconorwegian region consist of various granitoid rocks. Ambiguities, described above, regarding granitoid rocks, have resulted in research disregarding either deformation, magmatic processes or geochemistry, and has led to an ongoing debate about the evolution and regional importance of the granitoid rocks (Slagstad et al., 2013; Möller et al., 2013). In this thesis, an integrated tectonomagmatic model for the evolution of a large batholith (the Sirdal Magmatic Belt) in the Sveconorwegian orogen will be put forward.

A model for synkinematic emplacement of the SMB in a compressive tectonic setting is presented in this thesis, based on detailed mesoscopic and microscopic studies, together with geochemistry. Geochronological data are presented below, which enables the compressive setting to be delimited in time.

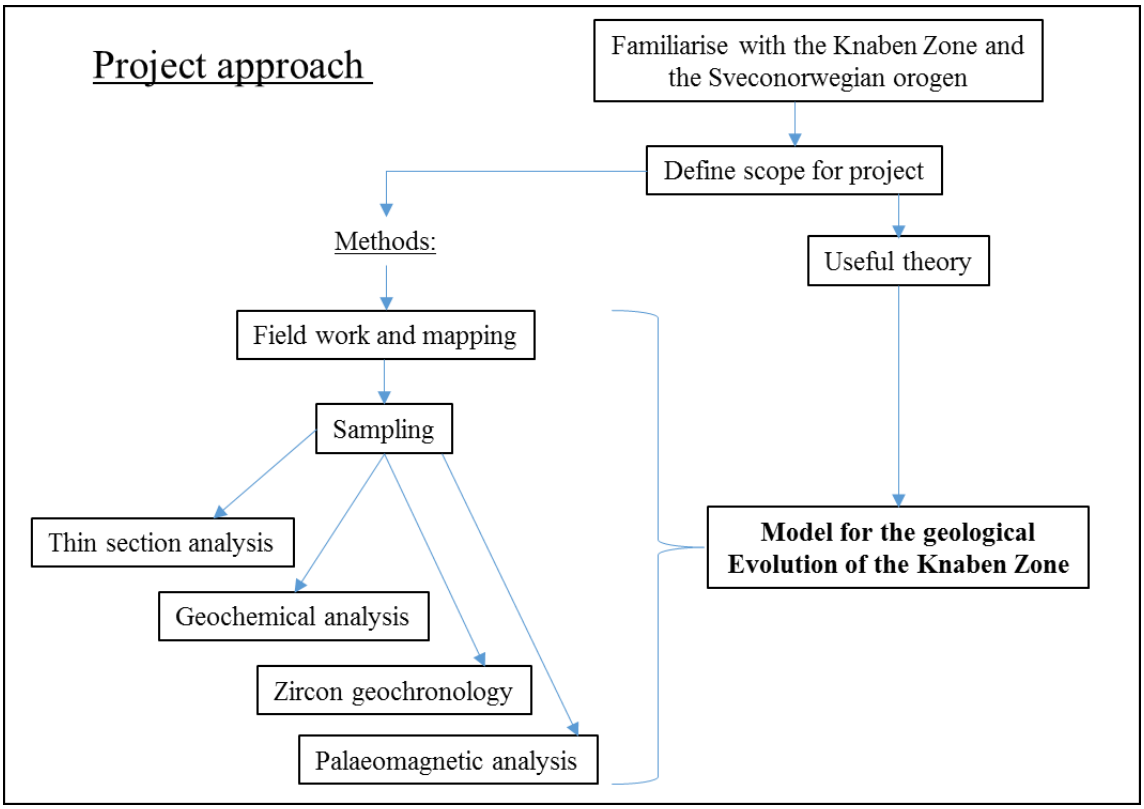

Figure 3: *Flow chart illustrating the steps of approach and methods for this project.*

Chapter 2 – Methods

2.1 Field methods

29 days have been spent in the Knaben mountains, mainly carrying out geological mapping and detailed investigations of mines, claims and outcrops of special interest. 737 outcrops have been described, and a selection of these are presented in this thesis (Fig 4). Common geological field equipment (topographic maps, notebook, hammer, 360° compass with clinometer and measuring tape), a digital camera, handheld GPS unit, and a headlamp for exploring the mines have been the main equipment. A handheld SM20 magnetic susceptibility-meter produced by "GF-instruments" (measuring SI units $x10^{-6}$) has been useful for identifying granitoid variations.

The overall aim for the fieldwork has been to produce a detailed geological map of the Knaben area, and to improve the understanding of the geological evolution. The detailed geological map produced by Lysberg (1976) has been the basis for the fieldwork. Mapping several E-W profiles through the Knaben Zone, besides following boundaries and visiting important localities, have been the main working methods, in order to identify and evaluate previous work and to extend Lysberg's (1976) detailed geological map.

Primary lithological features and relationships have been the focus for this project. Brittle structures and dykes, weathering and erosion have to some degree been neglected or given lower priority. Identifying the lithological units, magmatic and structural features and molybdenite deposits have been the main goals. Since modern research claims that magmatic processes are likely to be of importance for the evolution of the molybdenite deposits (Bingen et al., 2015; Coint et al., in press), this has been a working hypothesis.

Selected localities and samples are listed in Appendix 1 and Appendix 2 respectively, and shown in Fig 4 and the attached geological maps. Localities are referred to as L#, and samples by their sample number (K#).

2.2 Sample preparation and microscopy

Samples of all lithological units for geochemical, petrographic and structural analysis purposes were taken. Fresh samples, with minimal weathering and vegetation, were sought. Samples for geochemical purposes were taken at a distance from veins, boundaries etc, to prevent contamination. When possible, samples were oriented, especially with structural analysis in mind. Samples are listed in Appendix 2.

The laboratories at NGU and NTNU have been used for cutting, crushing and splitting samples. Slabs have been cut from each lithology, appropriate for thin section and macroscopic analysis. 30µm thin sections from all lithologies and interesting features were ordered from the laboratory at NTNU. Samples containing molybdenite or potentially interesting oxides and sulphides were produced as polished thin sections.

Thin sections have been analysed and photographed with the polarisation microscopes at NTNU's student laboratory and at NGU's laboratory. Modal amounts of minerals have been estimated visually.

2.3 Zircon geochronology

In-situ zircon geochronology is presented for two samples (K1, K36), from the fieldwork done the autumn 2013, achieved with the LA-ICP-MS (Laser ablation Inductively Coupled Mass Spectrometry) apparatus at NGU in Trondheim. Conventional methods at NGU for zircon separating, sample preparation and analysis with LA-ICP-MS were used to get a better understanding of the method and potential sources of error. The instruments and the working area were cleaned thoroughly with ethanol after each operation, to avoid contamination.

After washing and drying, the samples were crushed, using a "Fritsch Pulverisette Type 01.703" jaw crusher. A sample bag of split material was at this stage put aside for chemical analyses. The crushed sample was sieved with an "Endecott Test Sieve Shaker" for 10 minutes. Heavy minerals were separated from the <250µm fraction on the Wilfey wash table. This fraction was selected to be sure that all zircons where liberated.

After drying, magnetic minerals were separated from the concentrate by using a vertical magmatic separator ("Frantz Isodynamic Separator Model L1"). Heavy minerals, $<3{,}3 g/cm^3$, were separated with a heavy liquid (AnalaR NORMAPUR methylene iodide). Finally, the concentrate was dried and magnetic minerals were further removed by using a barrier magnetic separator ("Frantz Magnetic Barrier Laboratory Seprator Model LB-1") in 4 stages (fewer stages for small samples), 0,5A + 10° inclination, 1A + 10°, 1,5A + 10° and 1,7A + 5°.

Approximately 20 zircon grains were identified and handpicked for each sample, under a binocular microscope. Whole grains with minimal inclusions, and an uncontaminated green/brown colour were sought. The grains were mounted in epoxy and polished to approximately half thickness. Cathode luminescence images, displaying internal zonation and structures in the zircon grains, were obtained at the NGU laboratory and 10-12 grains suitable for analysis were selected. To obtain as much information as possible, both weakly luminescent and highly luminescent zircon rims and cores were sought.

The LA-ICP-MS apparatus at NGU consists of a Finnigan ELEMENT1 single collector high-resolution sector ICP–MS, coupled to a Finnigan 266 nm laser microsampler. Ablation is preformed with a 10–15 µm spot rastered over an area of ca. 60 x 38 µm, at a repetition rate of 10 Hz. Beam output energies were set to 0.1-1.0 mJ and adjusted for every sample or standard to obtain a stable ^{238}U signal around $2x10^6$ counts per second. The direction of the rastering was always towards the suction, to avoid interaction with close spot analyses.

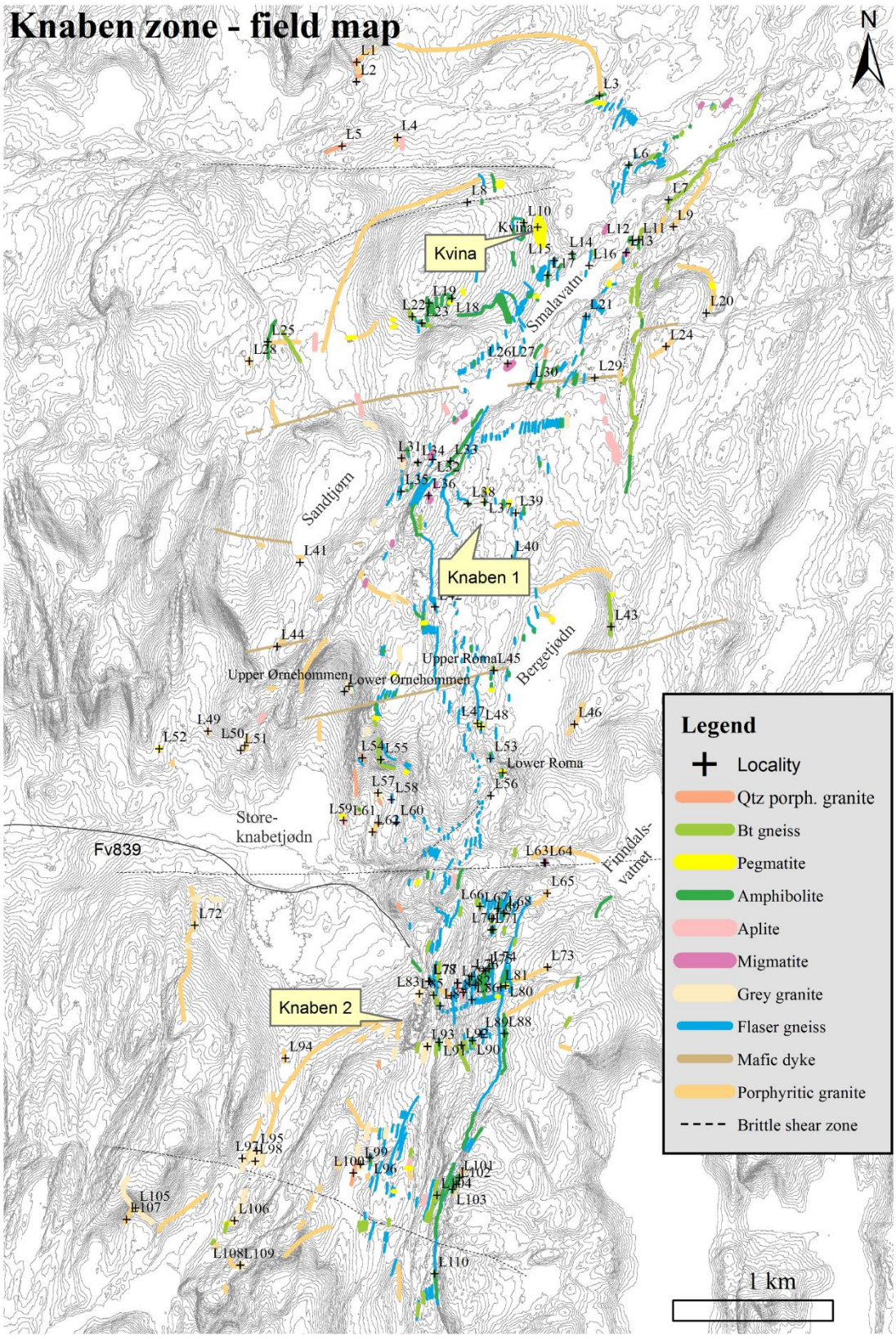

Figure 4: *Field map, indicating where fieldwork has been concentrated, and showing the localities presented in this thesis. Localities are a selection of the total 737 described localities and numbers decrease from N to S. Colours represent where the mapping is focused, and the amount of porphyritic granite is underrepresented on this map.*

The ablated mass was transported in a He carrier gas, into the plasma after mixing with Ar gas. The isotope data was acquired in a time-resolved scanning mode for 60 sec, with measurement of the masses of ^{202}Hg, ^{204}(Hg + Pb), ^{206}Pb, ^{207}Pb, ^{208}Pb, ^{232}Th and ^{238}U. The interference between ^{204}Pb and ^{204}Hg contained in the Ar gas was corrected by monitoring ^{202}Hg and assuming a ^{204}Hg/^{202}Hg ratio of 0.2293. A 60 sec gas blank analysis was performed between every second zircon analysis. Regular analysis of reference zircons was preformed to correct isotope ratios and mass-bias effects.

Results were processed and visualized with the Microsoft Excel macro program Isoplot (Ludwig, 2012). Complete results from the analysis are found in Appendix 3.

2.4 Geochemistry

Whole-rock and crushed samples were analysed at the ALS Geochemistry laboratory in Piteå, Sweden. 29 samples were analysed, mainly the Sirdal Magmatic Belt granitoid rocks, and less samples from the xenoliths. Major elements, trace elements and REE's were analysed with Lithium Borate fusion, ICP-MS (Inductively coupled plasma mass spectrometry) (analysis codes ME-MS81d and ME-4ACD81). Complete results from the analysis are found in the Digital Appendix.

The mineralogy of the granitoid rocks is relatively undiversified. Therefore, geochemical analysis often provides more information about the petrological evolution, so this was preferred to quantitative mineralogical analysis.

The IgPet® 2007 software (IgPet® RockWare website: https://www.rockware.com/product/overview.php?id=102) and Microsoft Excel has been used for analysing and visualising the geochemical data.

2.5 Mining reports

In addition to the general interactive database for scientific research, vast amounts of information about the molybdenite mining in the Knaben Zone was available from the Norwegian Directorate of Mining (DIRMIN) archives. A detailed review of all old material is beyond the scope for this thesis, and as the majority of the information is 60-40 years old, the material is outdated, regarding modern consensus. Nevertheless, geological maps, borehole data and the most recent reports have been of interest.

Chapter 3 – Results

29 days of detailed mapping, sampling and outcrop scale descriptions, have been the basis for this study, followed with thin section, geochemical and geochronological analysis on samples from the different lithologies and features of interest. In this chapter, results from fieldwork and thin section analysis will be presented for each lithology, followed by additional observations and structures. Results from geochemical and geochronological analyses are presented at the end of this section. Geochemical and geochronology data, together with coordinates and details for localities and samples are found in the appendix. The localities are placed on the field map (Fig 4) and Map 2, and samples on Map 1. A simplified map is presented in Fig 7.

A N-S-striking, 500-1000m wide, zone with abundant xenoliths and molybdenite deposits within more or less homogeneous granitoid rocks was known from previous work in the area (Lysberg, 1976), and the mapping was concentrated around this zone (Fig 2a, Fig 4). The mapping is therefore most detailed within this belt, and the surrounding areas are to a larger degree extrapolated from mapping profiles and based on ortho-photography. Areas covered during mapping are shown on the outcrop map (Fig 4). The zone rich in xenoliths will be referred to as the "Knaben Zone".

The rocks in the area have been divided into two groups, the *xenoliths,* previously termed Knaben gneiss by Lysberg (1976) and the *granitoid rocks*, previously termed Granitic gneiss by Lysberg (1976). The granitoid rocks include the main and dominating porphyritic granite, together with less voluminous varieties of granitoid rocks. The large majority of the granitoid rocks fall within the granite field in the QAP-triangle (Streckeisen, 1974). To cover all variations, the term "granitoid rocks" is preferred rather than granites (*sensu lato*). The granitoid rocks are generally undeformed to weakly deformed and lack a clear gneissic texture, apart from local deformation zones. The xenoliths are engulfed by the granitoid rocks, and exhibit deformation-related structures. Amphibolite, granitic gneisses and migmatite constitute the xenoliths.

The field area is mountainous and there is little vegetation, but the abundance of lichen obscures the outcrop. Boundaries between similar lithologies were therefore hard to define in some cases, and the variability within the granitoid rocks is therefore especially likely to be underestimated. This is to some degree compensated by detailed investigations of the granitoid rocks from accessible mines and road cuttings in the area.

Planar N-S striking structures, with a variable, moderate dip to the east, dominate the geometry of the Knaben Zone. These planes are mainly defined by foliation within the xenoliths and by primary magmatic fabric in the granitoid rocks. The dominating parallelism complicates the mesoscopic interpretations, with sparse crosscutting relations, as pointed out in previous studies. In the northern part of the mapped area, these structures bend towards a NE-SW strike (Fig 2a).

The structures in the Knaben Zone are atypical, and give the impression of a complex interplay between magmatism and syn-to-postmagmatic deformation. Primary magmatic structures and relationships are common in the granitoid rocks surrounding the xenoliths. Structures related to deformation are most common in the xenoliths, and along strained contacts between the xenoliths and granitoid rocks. The atypical structures have necessitated a creative, and to some degree unconventional, approach, bearing in mind the rheological properties of a granitoid crystal mush and the xenoliths. It has been important to determine

whether various fabric, foliation and structures originate from either magmatic or deformation processes. This is also important in view of the molybdenite deposits.

A summary of the petrography and field relationships for the different lithologies in the Knaben Zone is given in Fig 7 and Fig 6.

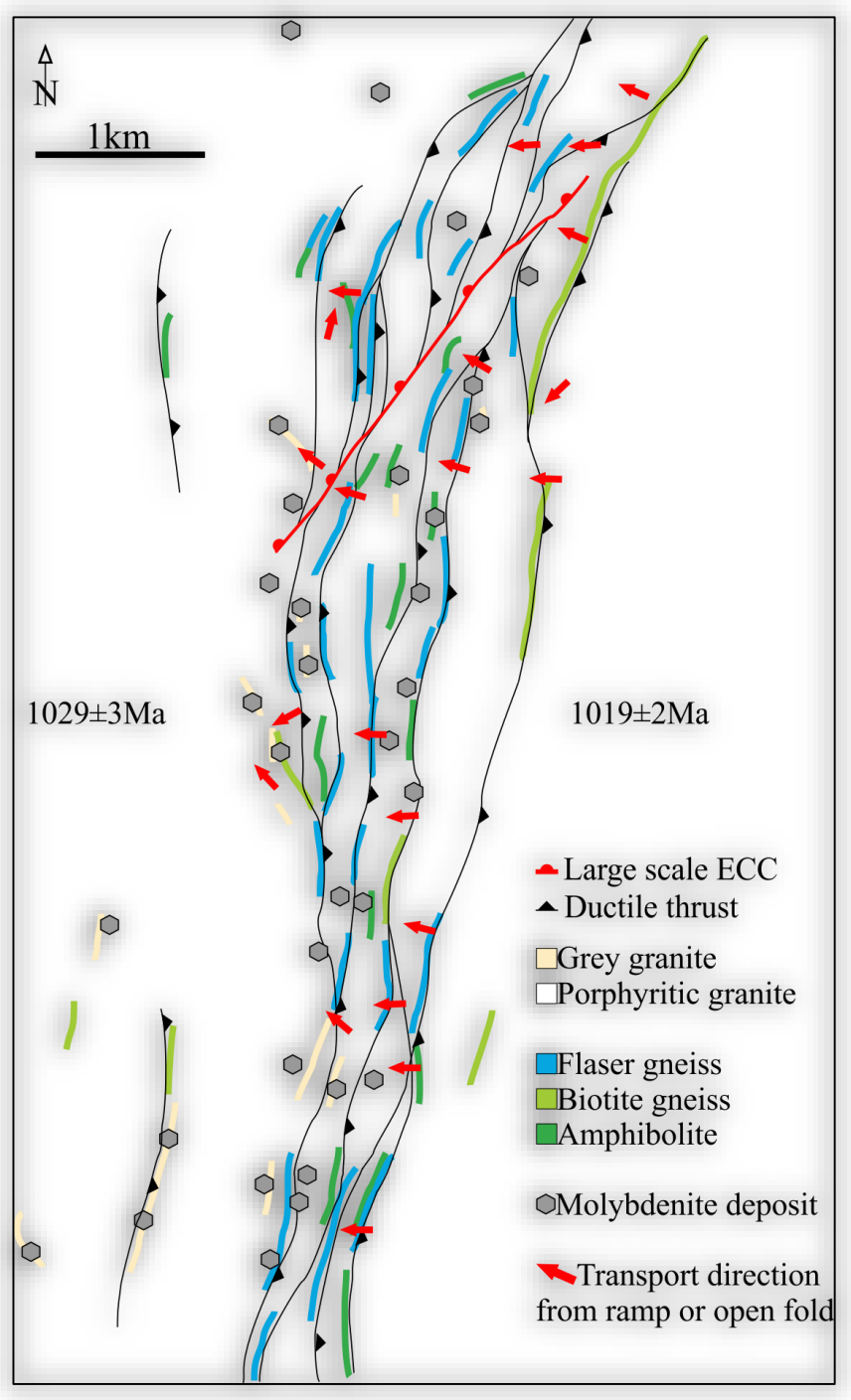

Figure 5: *Simplified geological map of the Knaben Zone, showing the most important structures, lithologies, and the anastomosing network directed by the xenolith screens. The large scale ECC-structure (explained in section 3.3.2) along the Smalavatn lineament is shown in red. Note that the xenoliths on the eastern boundary are more continuous, marking the terminal boundary towards a younger granite intrusion, unrelated to molybdenite deposits.*

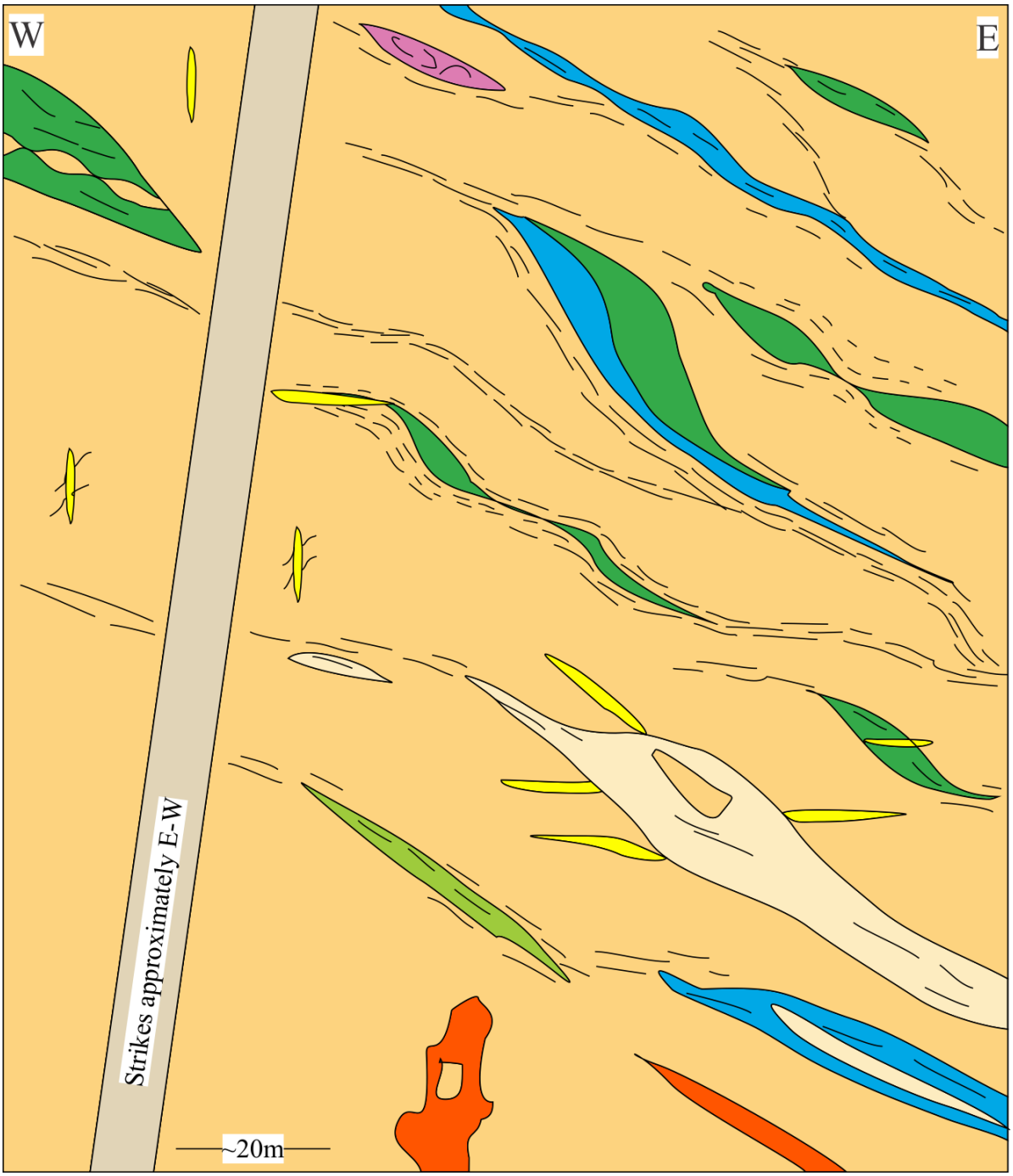

Figure 6: *Idealised summary profile showing the different lithologies and general cutting relations etc. The xenoliths are engulfed and intruded by the porphyritic granite. Deformation zones are typical along on the boundaries between the xenoliths and the porphyritic granite (indicated with dashed lines). Occasional deformation zones occur solely in the porphyritic granite. The grey granite intrudes into the porphyritic granite. Mineralised, sub-horizontal and foliation-parallel pegmatite veins (yellow) are common. The appearance of the minor granitoid variations varies, generally the melanocratic granites occur as xenolithic screens in the porphyritic granite, while the leucocratic granite cuts the porphyritic granite as irregular intrusions. The mafic dyke cuts E-W through all lithologies. Small, sub-vertical, non-mineralised pegmatites are common, and oriented E-W. Legend is shown in Fig 7.*

Lithology and map colour	Minerals (modal %)	Key textures	Occurrence and field relations
		Granitoid rocks	
Porphyritic granite (PG)	Qz (40), Kfs (40), Pl (10), Bt (10), Zrn, Ap, Chl, Rt, Mag, Al, Py	Coarse-grained, weakly foliated, pink Kfs phenocrysts, eugranitic groundmass, high-T microstructures, submagmatic flow textures with local solid-state deformation.	Dominating rock unit. Variably developed phenocrysts and foliation.
Grey granite	Qz (45), Kfs (40), Pl (10), Bt (5), Ms, Zrn, Ap, Chl, Mag, Mol, Cal, Py, Ccp, Al	Leucocratic granite with eugranitic texture. Similar microstructures as PG. Variably developed foliation. Cal only in contact with Mol.	Occurs as sheets in-, and cutting the PG. Also occurs as pods and veins in flaser gneiss.
Minor granitoid variations	Melanocratic, leucocratic, quartz porphyritic (see text)	Several local variations are observed, and are grouped into melanocratic- and leucocratic granites, in addition to a distinct quartz porphyritic granite. Generally, the melanocratic granites occur as xenoliths in the PG, while the leucocratic granite cuts the PG, as irregular intrusions. The melanocratic granite is regarded as a less foliated biotite gneiss. See text for details.	
		Xenoliths	
Amphibolite	Qz (20), Pl (35), Bt (25), Hbl (15), Opx, Cpx, Grt, Opq	Fine- to medium-grained. Lepidoblastic to grano-lepidoblastic texture, defined by Bt and Hbl laths. Porphyroblasts of garnet, with top-to-the-W kinematics. Domains with poikilitic and embayed opx and cpx. Qz shows sweeping undulating extinction.	Occurs as ductile, irregular small xenoliths, and as larger, gently folded screens with consistent FA. Generally well-developed foliation Hight-strain zones on contact to PG are common.
Flaser gneiss	Qz (40), Kfs (40), Pl (10), Bt (10), Spn, Zrn, Ap, Py, Mag, Ccp	Coarse-, to medium-grained. Flaser texture, defined by mafic foliation. Felsic domains between foliation are aggregates of felsic minerals. Otherwise, similar microstructures as PG.	Generally more enduring screens than other xenoliths, with a variable thickness. Poorly developed kinematics, mainly symmetric structures
Biotite gneiss	Qz (30), Kfs (20), Pl (20), Bt (20), Spn (5) Hbl, Zrn, Ap, Rt, Ep, Al, Fl, Opq	Medium-granied, grano-lepidoblastic, with variably developed foliation defined by mafic minerals. Similar microstructures as PG.	Similar appearance as amphibolite. Variable developed leucosomes and mafic foliation. Generally very enduring screens, up to 300-400m long.
Migmatite	Qz (40), Kfs (40), Pl (15), Bt (5), Ms, Apt, Zrn, Ep, Opq	Varying grain size, with leucosomes and melanosomes. Typically eugranitic texture.	Occurs as irregular, undefined screens. Isoclinally and ptygmatic folding is common.
Mafic dyke	Pl (50), Bt (30), Opq (20), Qtz, Act, Spn, Epi, Cal, Chl	Fine-grained, with randomly oriented, plagioclase phenocrysts, with swallowtale-, and carlsbad twinning.	Occurs as 10m thick, sub-vertical, E-W-striking dykes.

Figure 7: *Summary of the different rock units in the Knaben Zone with corresponding colours, used for maps and figures throughout this thesis. Abbreviations from Whitney and Evans (2010). Actinolite (Act), Allanite (Al), Apatite (Ap), Biotite (Bt), Calcite (Cal), Chlorite (Chl), Chalcopyrite (Ccp), Clinopyroxene (Cpx), Epidote (Ep), Fluorite (Fl), Garnet (Grt), Hornblende (Hbl), K-feldspar (Kfs), Magnetite (Mag), Molybdenite (Mol), Muscovite (Ms), Olivine (Ol), Opaque minerals (Opq), Orthopyroxene (Opx), Plagioclase (Pl), Pyrite (Py), Quartz (Qz), Rutile (Rt), Sphene/Titanite (Spn), Zircon (Zrn).*

3.1 Granitoid rocks

Within the dominating porphyritic granite, sheets and irregular bodies of various, mainly undeformed granitoid rocks occur. Variations in mineral content and grain size, together with cutting relationships, primary and secondary structures have been the main focus. As mentioned, minor variations proved hard to map due to lichen. Minor variations are typically sheets below a metre thick, hence the geological maps do not fully capture the heterogeneity. Road cuttings, mines, and other sporadic lichen free exposures have been of major importance.

In general, all the granitoid rocks have a massive appearance relative to the xenoliths. Primary magmatic structures, such as aligned minerals, weakly developed foliation and alternating colour variation banding are common. Differentiating primary magmatic structures and structures related to deformation in coarse-grained granitoid rocks is a challenge. Methods described by Paterson et al. (1989) have been of importance, and are presented below.

The field work revealed deformed xenoliths and mainly undeformed smaller granitoid variations surrounded by the voluminous porphyritic granite. Less common granitoid rocks appear as sheets aligned with the general eastward, moderate dipping geometry in the area, or as small irregular intrusions within the porphyritic granite.

3.1.1 Porphyritic granite

Field relationships and mesoscopic observations

This is the dominating lithology in the mapped area (Fig 5), and is classified as a K-feldspar porphyritic biotite granite, termed *porphyritic granite* for simplicity. The porphyritic granite surrounds the xenoliths and other granitoid rock units making up the Knaben Zone, and appears similar on either side of the Knaben Zone. Abundant 1-5cm, euhedral to subhedral phenocrysts of pink K-feldspar are distinctive, and more resistant to weathering, giving the rock a pink, knobby appearance in field, with visible perthite exsolution and Carlsbad twinning (Fig 8b). Weathering gives the rock a rusty appearance (Fig 8d)

The k-feldspar phenocrysts are locally aligned, with a shallow plunge, trending south (Fig 25a, Fig 8d and b). A poorly developed foliation defined by aligned biotite and K-feldspar is typical, with a moderate eastward dip (Fig 8a, 8b, 23a). Generally, based on the weakly developed spaced foliation together with the weakly deformed to non-deformed subhedral to euhedral phenocrysts, the texture does not classify as gneissose (Fig 8a, b, c and d) (Philpotts, 1989, p. 154; Vernon, 2004, p. 400), and is largely a product of magmatic processes.. Large fish structures, up to 1m, give an impression of deformation of a highly viscous melt, indicating top-to-the-W movement (Fig 10e).

Local gneissic to mylonitic bands occur, where the phenocrysts appear as xenoblastic aggregates, and the biotite foliation is better developed, oriented similarly to the magmatic fabric (Fig 24c, 24d). These proto-mylonite to mylonite zones display clearly recrystallized phenocrysts and an augen gneiss texture. Fig 14d shows a mylonite zone with melt present, filling deformation structures.

Within the Knaben Zone, the xenoliths appear as a few centimetre to several metre thick screens dipping moderately to the east, within the porphyritic granite (Fig 8d, e). As shown in (Fig 8d), the xenoliths thin out, becoming schlieren-horizons within the porphyritic granite, indicating a degree of assimilation. The boundaries between the xenoliths and the porphyritic granite are either sharp and undeformed (Fig 17a, 19a, 19b), or complex deformed contacts (Fig 26a, 26b). The majority of kinematic indicators and structures, generally indicating top-

to-the-W kinematics, are recorded along the deformed boundaries. Structures are presented later in a separate section.

Petrography and microscopic observations

As mentioned, the porphyritic texture is typical, with up to 1-5cm prismatic phenocrysts of K-feldspar. Elongated quartz grains, or aggregates of quartz grains up to 1 cm occur. The groundmass is eugranitic, mainly consisting of coarse-grained quartz, K-feldspar, plagioclase, biotite, and trace amounts of zircon, apatite, allanite, epidote, muscovite, and opaques.

Quartz and K-feldspar occur in similar amounts and constitute approximately 80 modal %. The quartz is anhedral, inequigranular and occurs as up to a 2mm large grains. Myrmekite intergrowths are abundant (Fig 9a, b), occasionally as "swapped rims" (Vernon, 2004, p. 251). Large quartz grains have a distinct chessboard-pattern extinction and lobate to straight grain boundaries (Fig 9d), implying high temperature deformation (Hirth and Tullis, 1992; Stipp et al., 2002). Inclusions of all present minerals occur in the quartz, and grain boundaries defined by biotite are common. Elongated quartz grains, or clusters of grains, are oriented parallel to the overall fabric in the rock. Ribbon grains of quartz, with the same orientation, occur in the samples that exhibit a clear solid-state deformation fabric (Fig 9e).

K-feldspar phenocrysts are subhedral to anhedral (Fig 9a, 9c), and show recrystallization and elongation in local solid-state deformation zones. Occasional grains show oscillatory zonation, with inclusions following the zonation pattern (Fig 9a). The phenocrysts are mainly orthoclase, with various perthite textures, mesoperthite being the most common. Tartan-twinned microcline mainly constitute the smaller grains and groundmass, and occasional phenocrysts. Asymmetric two-stage perthite exsolution, as described by Parsons et al. (2005), is abundant (Fig 9b, 10c). No consistent kinematics can be deduced from the asymmetric, two-stage perthite on a larger scale. Similar asymmetric perthite lamellae forms around quartz inclusions in the K-feldspar grains.

The biotite is typically brown, with occasional green grains, and traces of alteration to chlorite. Anomalous blue coloured chlorite alteration occurs in the highly strained sample K1004. Zircon mainly appears as inclusions in biotite. Plagioclase grains are intensely altered to sericite. Opaque minerals are mainly magnetite, with some pyrite, chalcopyrite and molybdenite when close to grey granite or pegmatite. Calcite occurs in relation to molybdenite grains.

Several microstructures point to submagmatic flow, the deformation of a 20-40% molten granitic melt, with local zones of solid state deformation (Paterson et al., 1989). The most convincing evidence on the microscopic scale is the alignment of weakly deformed to non-deformed K-feldspar phenocrysts, evidence of high temperature deformation, and late magmatic minerals filling the space between broken K-feldspar grains (Fig 9c). As pointed out by Vernon (2004, p. 459), certain microstructural criteria for submagmatic flow are sparse, and need to be supported with mesoscopic observations of melt present during deformation, and such structures are presented below (Fig 14d, Fig 26, Fig 30d).

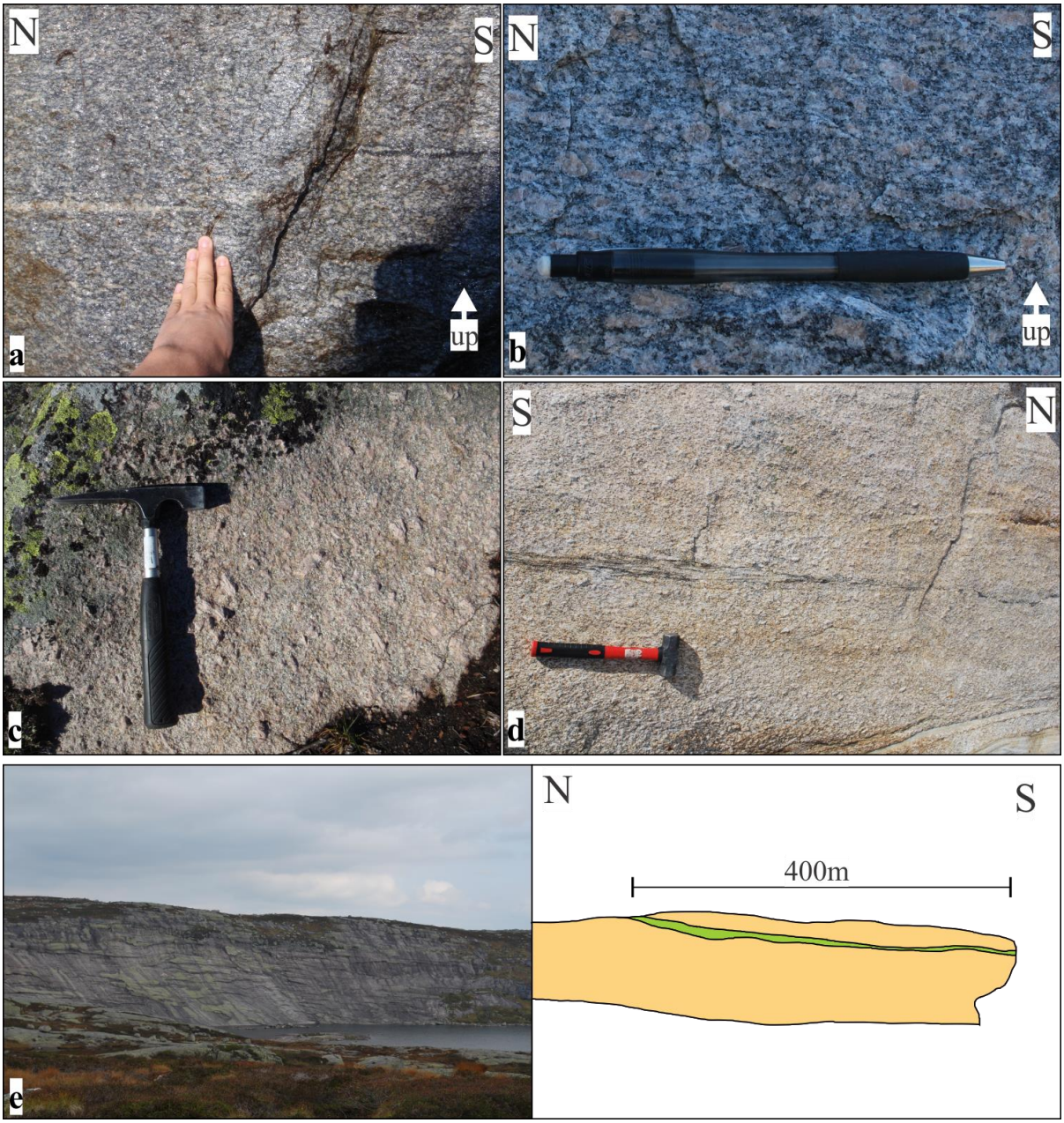

***Figure 8**: **a)**. Porphyritic granite, with a schlieren (right) and a leucocratic vein (left) oriented with the general magmatic fabric. (L52). **b)** Typical fresh porphyritic granite, with subhedral to anhedral oriented pink K-feldspar with visible Carlsbad twinning. Schlieren parallel to the foliation of the rock below the pen. (L52). **c)** Subhedral, pink, moderately aligned, up to 5cm large K-feldspar phenocrysts in porphyritic granite. (L20). **d)** A thin xenolith of flaser gneiss within porphyritic granite thins out towards the N, becoming a schlieren band before disappearing. The flaser gneiss screen lies parallel to the magmatic fabric of the porphyritic granite, defined by euhedral to subhedral K-feldspar grains and a spaced weakly defined biotite-folia-plane. (L15). **e)** Looking eastwards across Begetjødn towards L43. The slabby cliff consists mainly of porphyritic granite, with a 2-5m thick biotite gneiss screen within it, as illustrated to the right. The screen lies parallel to the general eastward foliation. Duplex structures and kinematic indicators on the boundary between the biotite-gneiss screen and the porphyritic granite show top-to-the-W kinematics.*

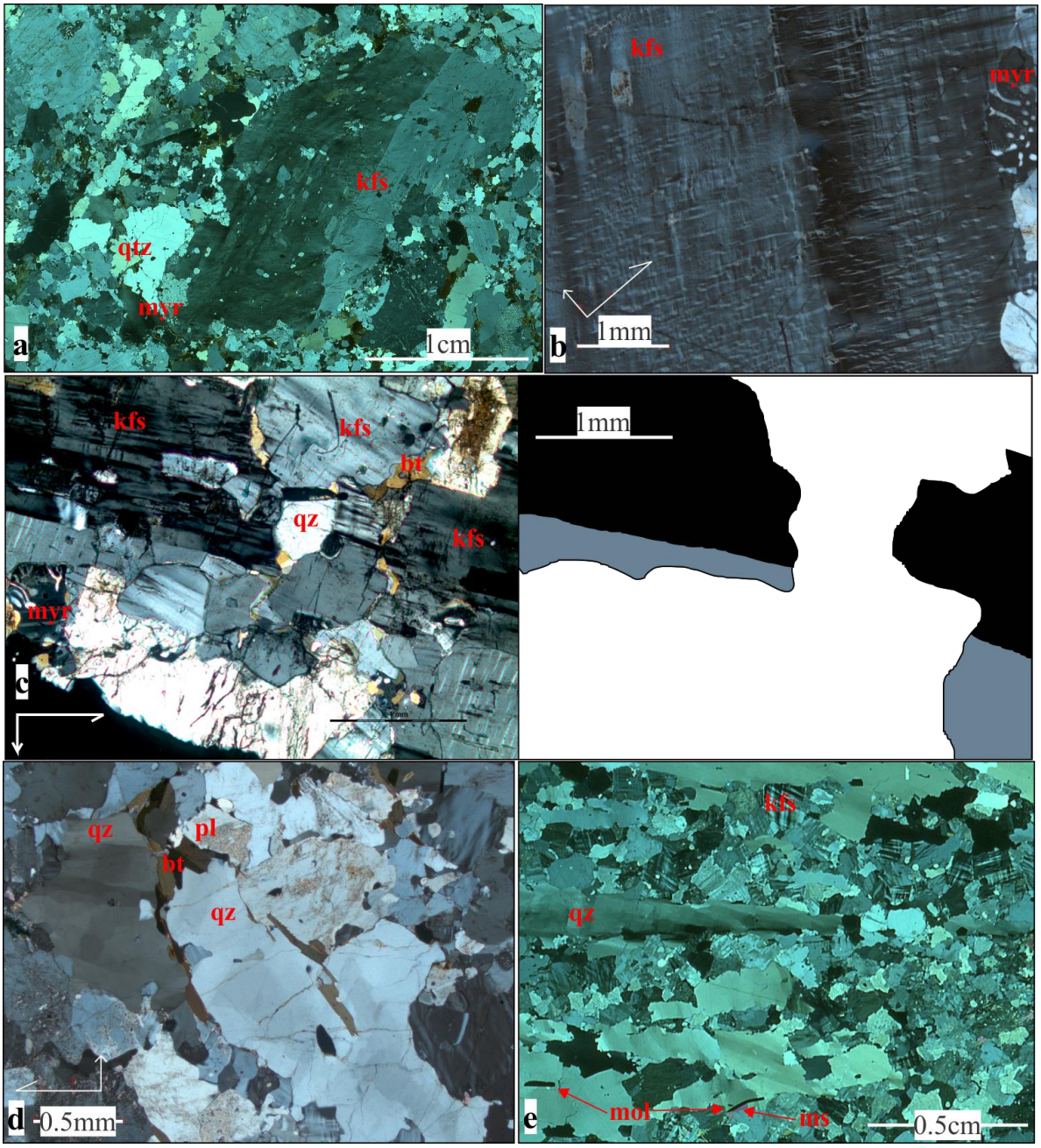

Figure 9: a) *Porphyritic granite showing a 2,5 cm subhedral Kfs phenocryst with oscillatory zoning and Carlsbad twinning. Inclusions of all main minerals occur in the phenocryst, and are aligned with the zonation planes. Myrmekite lobes occur along the phenocryst margin. Elongated quartz grains are aligned with the phenocryst. Xpl, (K15).* ***b)*** *Asymmetric two-stage perthite, as described by Parsons et al. (2005). The asymmetric shape indicates sinistral kinematics, orthogonally to the elongation of the Kfs phenocryst. Myrmekite lobe in top right. Xpl, (K122).* ***c)*** *A K-feldspar phenocryst is broken and the space between the fragments is occupied by quartz, microcline and biotite, indicating sub-magmatic fracturing of the Kfs phenocryst (Vernon, 2004, p. 460). Xpl, (K30).* ***d)*** *Quartz grains with chessboard extinction. Quartz grain boundaries are lobate to slightly angular and defined by aligned biotite grains. Plagioclase grains are sericitized. Xpl, (K128).* ***e)*** *Deformed porphyritic granite showing solid-state deformation and severely elongated grains are seen in hand specimen. The thin section photo shows well developed ribbon grains of quartz, and no K-feldspar phenocrysts. Molybdenite grains occur parallel to the quartz ribbon grains, in association with muscovite and minor calcite. Xpl, (K1004). Exact lineation is not known.*

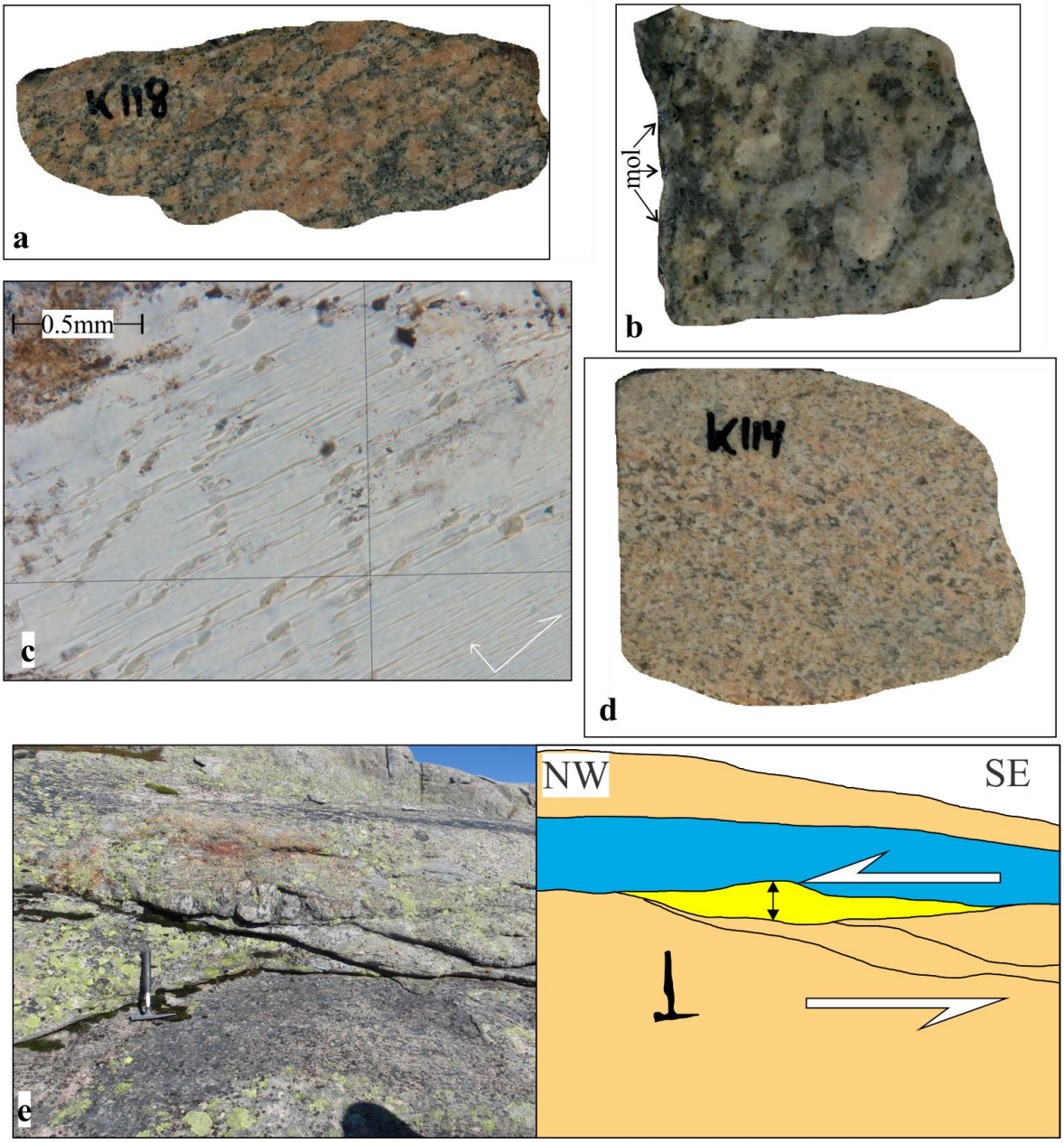

Figure 10: a) *Cut and scanned weakly deformed porphyritic granite, with oriented phenocrysts of K-feldspar. (K118)* ***b)*** *Cut and scanned porphyritic granite. Randomly oriented, subhedral K-feldspar phenocrysts. This sample is from the contact towards grey granite. A biotite layer defines the contact and molybdenite grains are visible within.(K110)* ***c)*** *Micro-photo of asymmetric two-stage perthite in porphyritic granite sample K122, as described by Parsons et al. (2005). (ppl).* ***d)*** *A medium-grained, eugranitic variety of the porphyritic granite, existing as a 20cm thick layer in the porphyritic granite. (K114).* ***e)*** *A vertical section showing porphyritic granite, flaser gneiss and a subhorizontal molybdenite bearing quartz rich pegmatite. The porphyritic granite is increasingly strained towards the boundary. Note the fish-structures apparent in the porphyritic granite, indicating ductile, submagmatic top-to-the-W kinematics (L22).*

3.1.2 Grey granite

Field relationships and mesoscopic observations

The molybdenite-bearing grey-coloured granite, referred to as *grey granite*, is the most common granitoid variety occurring within the porphyritic granite (Fig 11a). This is the main molybdenite ore lithology, and has been mined at the large Knaben 2 mine, and at several smaller mines (Gvein and Rui, 1980). It generally lacks obvious phenocrysts, appears more massive in field, and has a paler colour than the porphyritic granite (Fig 11b). The rock is mainly coarse-grained, equigranular, with visible quartz, white feldspar and biotite. Finer grained and porphyritic varieties occur. Specks of disseminated molybdenite grains up to 0,5cm and pyrite grains are common (Fig 11).

This rock unit appears as up to 10m thick sheets or thin veins, oriented with the general moderate eastward dip (Fig 12c, 12b). Notably, the grey granite only occurs on the west side, or up to 300m to the west of, the Knaben Zone and is absent to the east of the Knaben Zone (Fig 5). The largest sheets of grey granite occur in relation to the Knaben 2 and Bragold mines and north of Sandtjørn (Fig 1a, 7), and are situated within the porphyritic granite. Smaller sheets and veins of grey granite occur in the same area, and are less common in the northern part of the Knaben Zone. Grey granite veins and pods also occur within the gneissic xenoliths (Fig 12b).

The boundary towards the porphyritic granite is usually sharp and defined by a biotite rich foliation (Fig 25b, c), but can be irregular and diffuse (Fig 14b). When the boundary is sharp, a stretching lineation along the biotite film is occasionally visible (Fig 25). No clear cross-cutting relationships are seen, apart from in the Knaben 2 mine where the grey granite appears to engulf angular chunks of porphyritic granite, but this could be a result of the section through an irregular intrusive contact in the mine tunnel (Fig 12a). The angularity of the porphyritic granite within the grey granite, and the fact that the grey granite cuts the fabric in the porphyritic granite, strongly indicates that the grey granite is younger.

A variably developed foliation defined by biotite is common. Large molybdenite specks are concentrated along these planes (Fig 11a). This foliation is similar to the foliation observed in the porphyritic granite. Rusty stains are common along the foliation.

Petrography and microscopic observations

The rock is medium-grained to coarse-grained, eugranitic, with quartz and K-feldspar up to 0.6mm, and in similar modal amounts of 30-40 %. Elongate domains up to 3cm wide and 10cm long with coarse-grained quartz are common. Biotite is the main mafic mineral, typically in modal amounts of below 5%. Muscovite is more common than in the porphyritic granite, but occupies below 5 % (modal).

Molybdenite laths and flakes, up to a 5mm large, occur in all the grey granite samples and, when elongated, they are oriented with the general fabric (Fig 11a). Pyrite and magnetite are the main additional opaque minerals. Clusters of opaque minerals are not uncommon. Calcite occurs in relationship with molybdenite in most of the samples (Fig 11c, d, e and f), and is not found without being directly in contact, or very close to molybdenite.

Biotite grains are more chloritified than in the porphyritic granite. The trace minerals and microstructures are generally the same as described for the porphyritic granite.

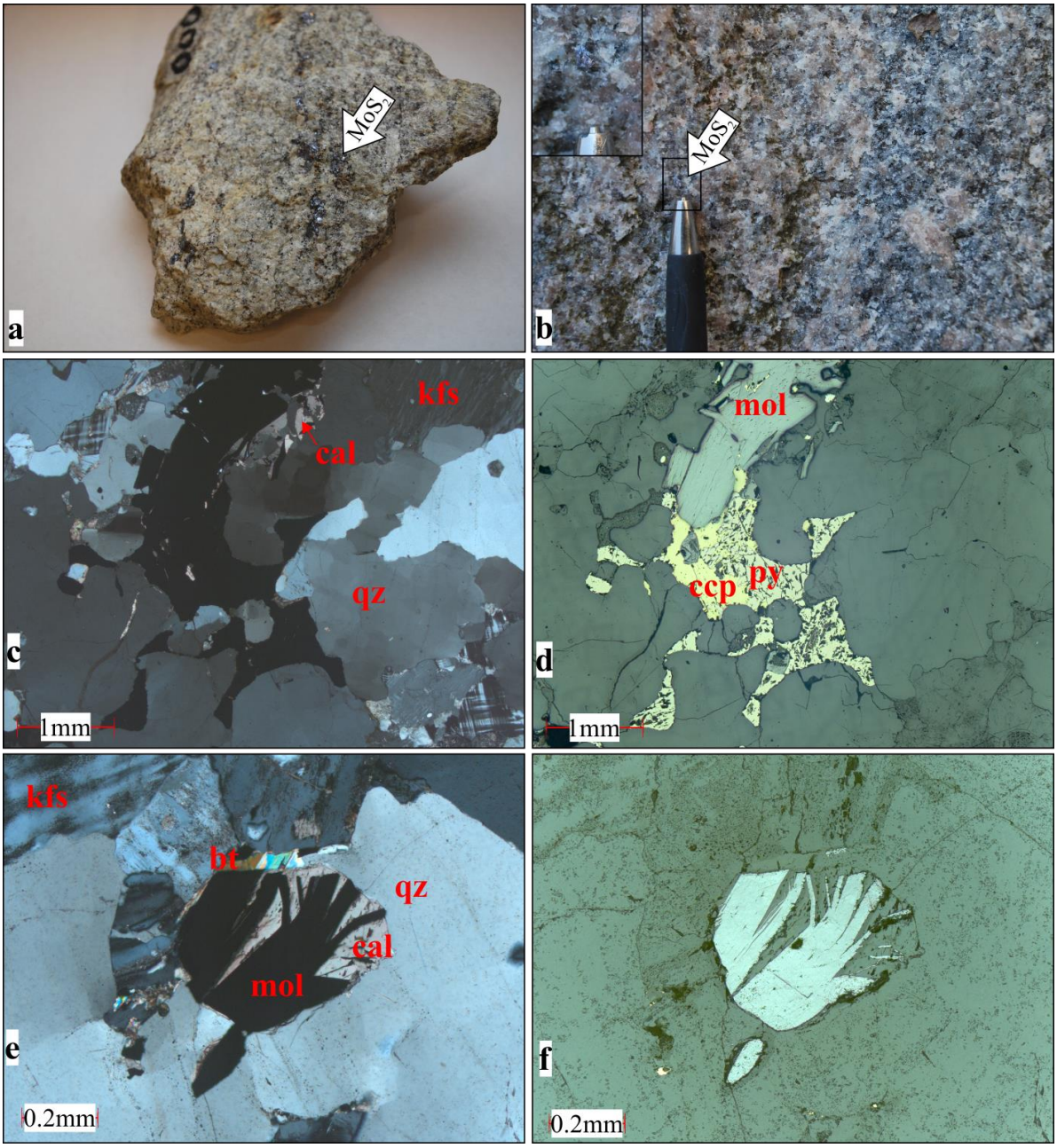

Figure 11: a) *Grey granite from the open pit at the Knaben 2 mine. A tectonic foliation has developed in the grey granite, defined by the alignment of mafic minerals. Molybdenite clots are concentrated along these foliation planes. Base of photo is 20cm. (K1000)* ***b)*** *Photo of the boundary between porphyritic granite (right) and grey granite (left). The grey granite is paler and has a eugranitic texture. A disseminated molybdenite grain is indicated by the pen (inset photo). (L57)* ***c)*** *Micrograph of grey granite sample K126 (2.5X), xpl. Photo* ***d)*** *is the same taken with reflected light. A large molybdenite grain is in contact with pyrite and chalcopyrite. Small amounts of calcite occur adjacent to the molybdenite. The quartz shows chessboard extinction and straightened grain boundaries. Small feldspar grains are microcline and the larger grain in top right is orthoclase with meso-perthite. Py and ccp appear as triangular interstitial grains.* ***e)*** *Micrigraph of grey granite sample K17 (10X) with xpl and in reflected light in* ***f)****. Lath shaped molybdenite is surrounded by calcite. Fluid inclusion trails are visible in the quartz.*

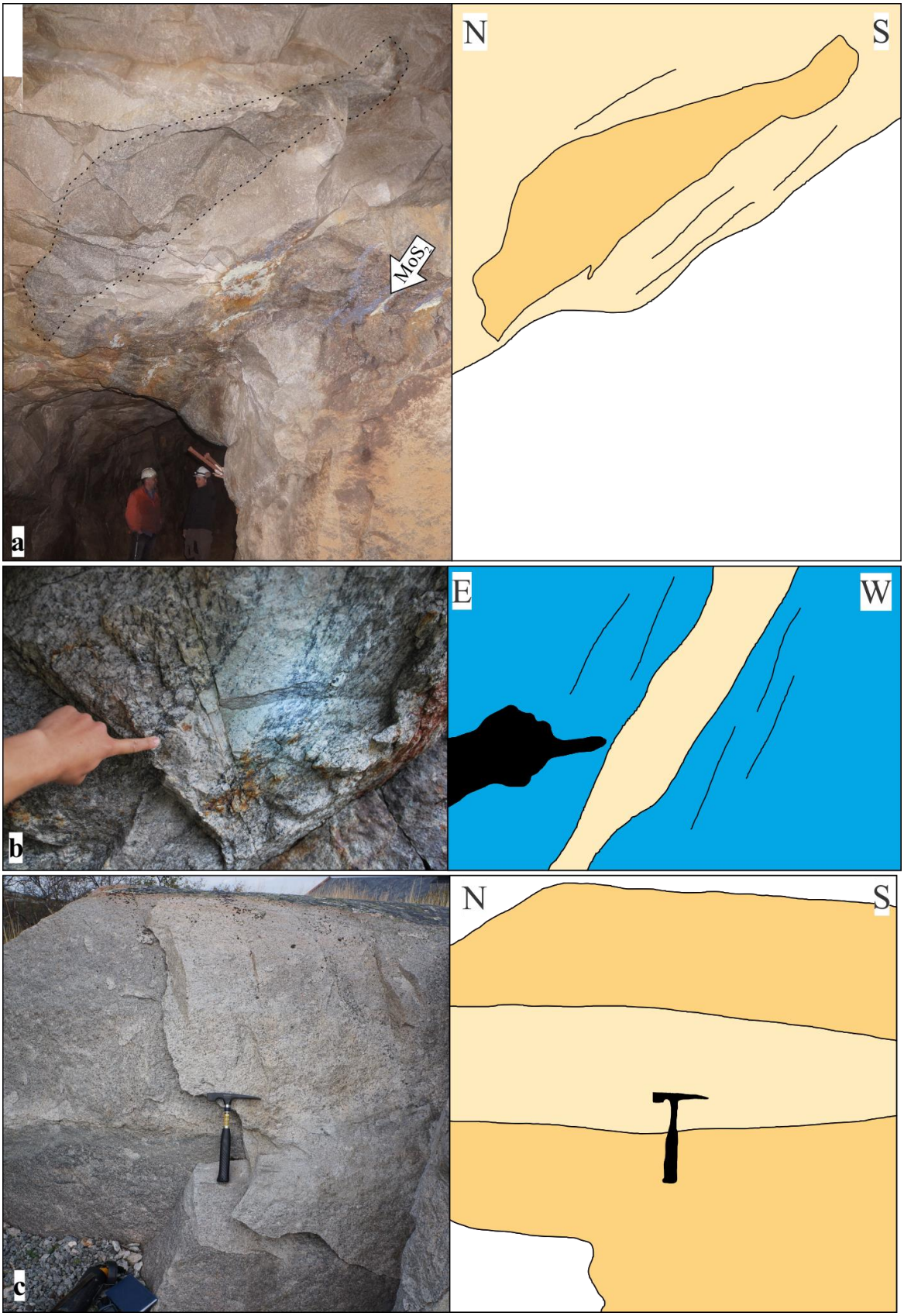

Figure 12: a) *Porphyritic granite engulfed in the grey granite. Foliation planes with molybdenite below. (Knaben 2).* ***b)*** *Thin grey granite vein within flaser gneiss. (L47).* ***c)*** *Typical grey granite screen, within porphyritic granite. The screen is parallel to the foliation in the porphyritic granite. (L72).*

3.1.3 Minor granitoid varieties

Several variations of weakly deformed to undeformed granitoid sheets and small irregular intrusions have been observed, analysed and mapped where possible. Such units are best exposed in mines and road cuttings, and are likely to be underestimated on the geological map. These rocks have a limited number of observations, and their texture and appearance is highly variable. In the section below, these observations are referred to as melanocratic and leucocratic granites, based on their colour relative to the porphyritic granite in field. An exception is a quartz-porphyritic granite, which is very distinct in the field and appears as relatively voluminous sheets, but has only been observed at a few localities.

Melanocratic granites

Small bodies of melanocratic granitoid rocks show only weak deformation, distinguishing them from the more deformed xenoliths presented later. These lithologies typically contain visible amphibole and biotite, and are typically cut by, or occur as irregularly elongated enclaves within, the porphyritic granite. It is possible that the melanocratic granites represent the precursors of the SMB magmatism. As these units display a very similar geochemistry and mineralogy to the biotite gneiss xenolith, they possibly represent less deformed domains of these xenoliths. Two examples of melanocratic granite are presented below, but they will further be regarded together with the biotite gneiss, as the few observations do not allow further differentiation.

L45, sample K101

At the Upper Roma mine (L45) an irregular, coarse-grained, dark hornblende granite (K101) is exposed at the entrance of the shaft, extending a few metres into the mine itself. It is weakly foliated, defined by the mafic minerals. Occasional K-feldspar phenocrysts and elongated domains with felsic minerals occur between the mafic foliation. 20-50 cm thick veins of porphyritic granite clearly crosscut the dark hornblende granite (Fig 13a). Smaller chunks of the dark hornblende granite appear within the porphyritic granite in the vicinity. The intruding porphyritic granite has a weakly irregular boundary, but clearly dips moderately eastwards.

Hornblende and biotite constitute approximately 20 modal % each. The mafic minerals are oriented, and occur in elongated clusters, defining a fabric in the rock. Quartz, altered plagioclase and some K-feldspar dominate the rock. Chessboard extinction and other similar microstructures as in the porphyritic granite occur in the quartz. Titanite is the main trace mineral, occurring together with the biotite and hornblende. Calcite, apatite and opaque minerals are additional trace minerals.

Knaben 1, sample K9

At the end of the left adit in the northern part of the Knaben 1 mine, a 50cm wide mafic, subvertical, NW-SE-striking dyke-like melanocratic granite (sample K9) cuts through the flaser gneiss (Fig 13b). It is fine-to-medium-grained, with visible biotite, quartz and feldspar. The rock is weakly foliated parallel to the dyke, with a foliation defined by mafic minerals. The dyke is zoned, with a 20-30cm more felsic core. The rim towards the porphyritic granite has a pale and altered appearance.

In thin section, sample K9 displays well developed shear bands, defined by fine-grained biotite, epidote and calcite grains. They create an anastomosing pattern, wrapping around coarse-grained, recrystallized felsic domains and phenocrysts. Recrystallization tails around plagioclase and quartz domains form sigma-clasts. The plagioclase is intensely sericitized.

The amount of biotite is below 20%. The quartz mainly shows a sweeping undulating extinction, and lacks the chessboard extinction typical for the granitoid rocks previously described.

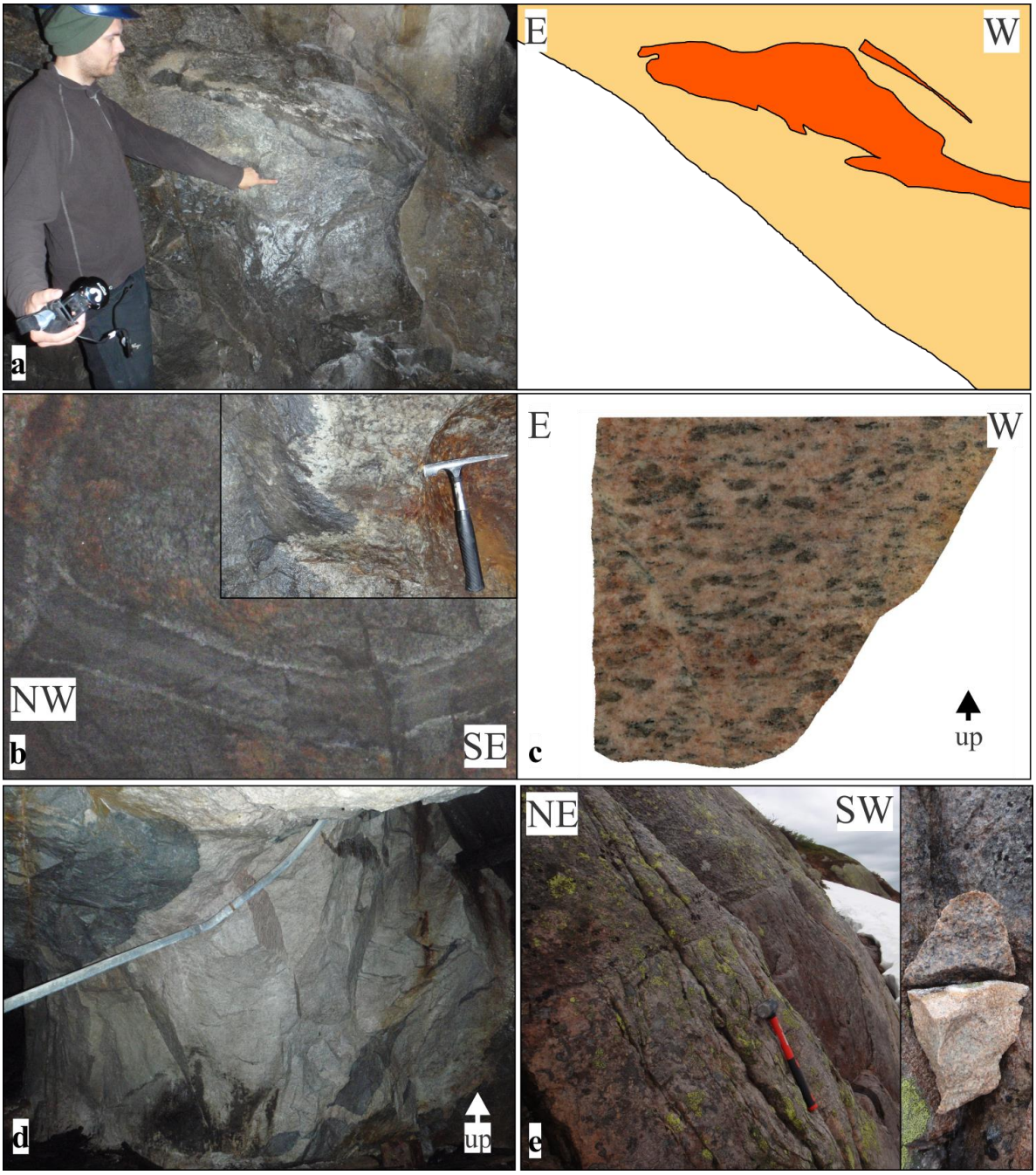

Figure 13: a) *A weakly deformed, melanocratic hornblende granite (K101) is engulfed by porphyritic granite. (L45).* ***b)*** *From the left adit in the northern part of Knaben 1 mine, with NW-SE striking dyke-like melanocratic granite. The large photo shows the roof of the mine. The sub-vertical, melanocratic, granitic dyke (K9) cuts through the flaser gneiss. The dyke is zoned, with a more felsic core, and displays a distinct pale reaction rim (inset photo). Photo is 5m across.* ***c)*** *Quartz phenocrystic granite with aligned qz grains and clusters of qz grains (K28). (L100).* ***d)*** *Porphyritic granite (dark) is engulfed by a leucocratic granite (K11). Note the angular fragments of porphyritic granite in the lower right. (lower Ørnehommen mine).* ***e)*** *A 3m wide sheet of a medium-grained leucocratic granite (K114) is situated within the porphyritic granite, and parallel to its foliation. Inset photo shows fresh samples. The leucocratic sheet dips 32° towards 102°. (L5).*

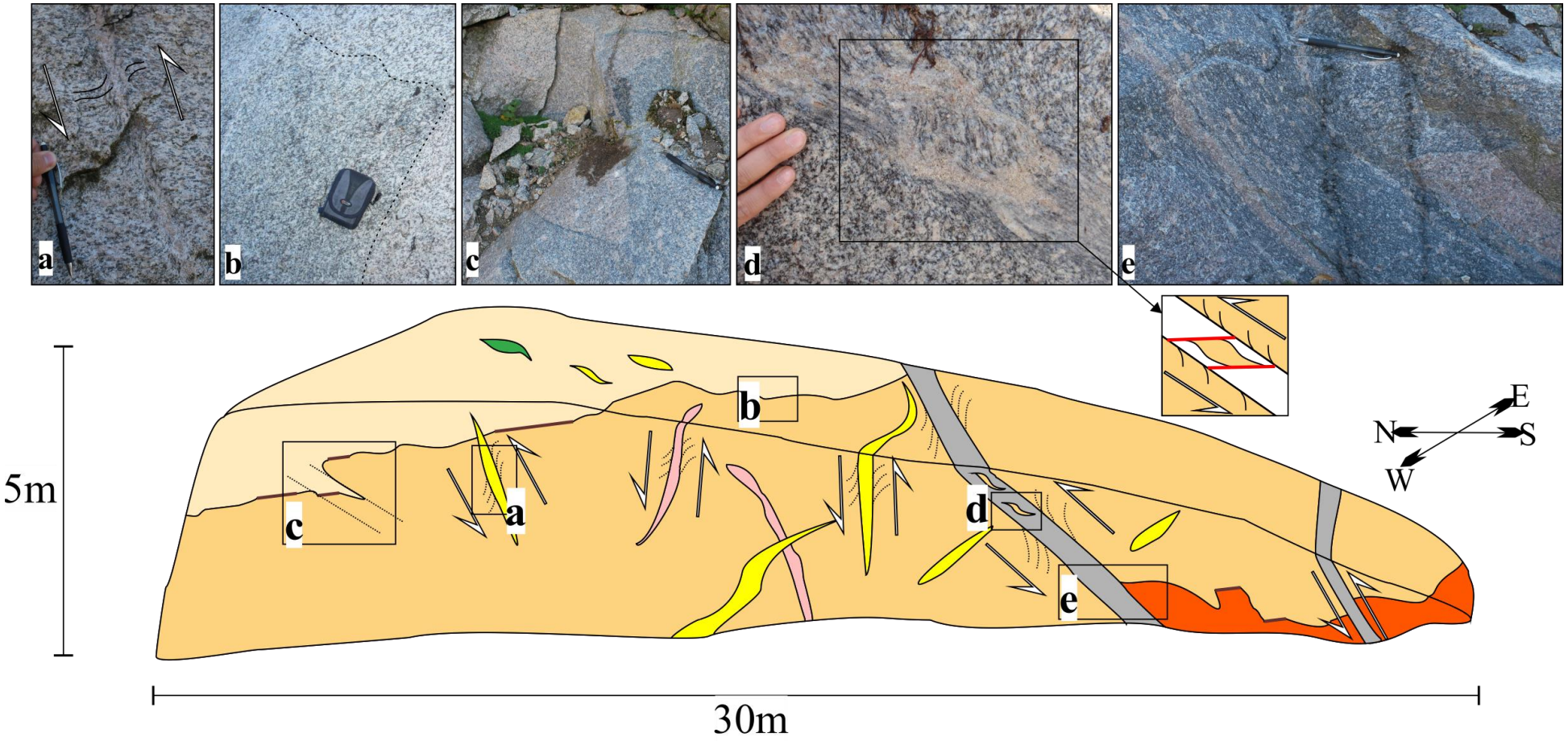

Figure 14: *Sketch of L57, with photos from key features. The outcrop shows the porphyritic granite in contact with two different granitoid variations. At the upper part, the porphyritic granite is in contact with a coarse-grained mineralised grey granite* ***(b)****, and at the bottom in contact with a quartz phenocrystic pink granite* ***(e)****. The contact is partly irregular and partly planar and defined by a dark biotite-rich schlieren horizon* ***(c)****. The planar parts of the contact have a moderate dip towards the east. A primary magmatic fabric within the granitoid varieties is parallel to the planar contacts. Numerous pegmatite and aplite veins* ***(a)*** *and two semi-parallel mylonitic shear zones (dipping 40° towards 140°)* ***(d, e)*** *are visible. Sinistral kinematics along the mylonitic zones are deduced from drag folds, fish structures and ECC fabric. Photo* ***(d)*** *with illustration shows melt filling ECC structures in mylonitic porphyritic granite, indicating that melt was present during deformation.*

Leucocratic granites

Pale-coloured, non-mineralized and massive granites, generally with a non-deformed appearance, occur as irregular bodies, sheet-like intrusions or most commonly as foliation-parallel or irregular veins. The appearance together with the evolved, felsic composition strongly suggests that these rocks represent the final stages of the SMB magmatism. Three exposures of leucocratic granites from the more voluminous occurrences are presented below. K11 is the only sample analysed in thin section.

Lower Ørnehommen, sample K11

At the lower adit of the Ørnehommen mine, an irregular pale intrusive unit (K11) clearly crosscuts the porphyritic granite (Fig 13d). The contact towards the porphyritic granite is sharp and slightly angular, with chunks of the porphyritic granite situated within the pale granite. The pale unit is medium-to-coarse-grained, highly leucocratic with a pink tint and massive with no alignment of minerals. Randomly oriented K-feldspar grains up to 5 cm dominate the rock.

The modal amount of k-feldspar is 70%, with equal amounts of quartz and plagioclase constituting the majority of the remaining 30%. Minor and trace minerals are green biotite, locally altered to chlorite, zircon and apatite. Microstructures are similar to the porphyritic granite.

L5, Sample K114

A 3m thick sheet of massive leucogranite (K114) is exposed in the NW part of the mapped area at L5 and L1. This unit is mapped as fine-grained grey granite by Lysberg (1976). No molybdenite is documented within the leucogranite, and the rock is less deformed and finer-grained with a stronger red colour than typical grey granite. The rock is equigranular, medium-grained, with visible quartz, plagioclase and pink K-feldspar. Minor biotite grains are scattered randomly, and no fabric or foliation is apparent (Fig 13e). This is in strong contrast to the bordering porphyritic granite, with a clear magmatic fabric parallel to the border. Both the lower and upper boundaries are sharp and planar, dipping moderately to the east.

L108, sample K27

On the ridge 400m east of Øyevatnet, in the SW-corner of the mapped area, a pale granite is exposed as an irregularly shaped body (K27), and distinctive in the surrounding porphyritic granite. The elongated unit is 10 m wide in the E-W direction and 50m in the N-S direction. It is a coarse-grained, equigranular granite, lacking foliation. Biotite and pyrite are the visible mafic minerals.

Quartz-porphyritic granite (QPG)

At L100, 70m west of the tailings at the Bragold mine, a N-S-striking quartz-phenocrystic pink coloured granite sheet continues southward for 200m. It crops out as a 10m wide sheet, dipping moderately to the east. The pink colour and smoky quartz phenocrysts give the rock a distinct appearance (Fig 13c). The porphyritic granite, grey granite and quartz porphyritic granite all appear within 10 metres at this locality, as parallel sheets. Thin sheets of this lithology are exposed in the Ørnehommen mine, at L93 and L57 (Fig 14).

Elongated quartz crystals, or aggregates of quartz crystals, are up to 20mm long and 4mm wide (Fig 13c). The phenocrysts are aligned with a S-SW-trending, weakly plunging lineation, creating a distinct fabric. This lineation coincides with sparse lineation measurements in the porphyritic granite (Fig 25a). Occasional K-feldspar phenocrysts are

oriented similarly to the quartz. The petrography is otherwise similar to the porphyritic granite.

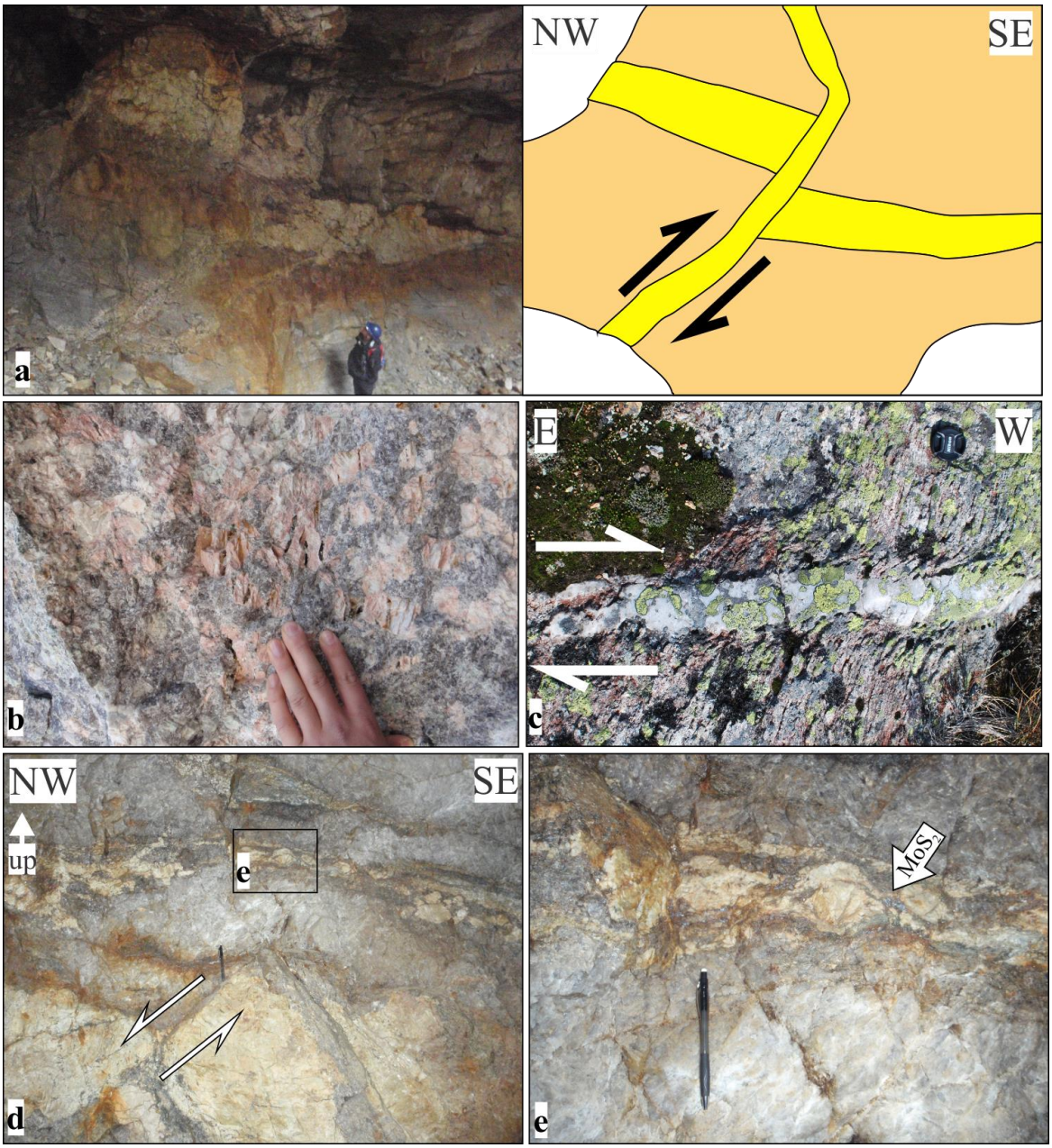

Figure 15: a) *An irregular, mineralized, sub-horizontal pegmatite is cut by a sub-vertical, non-mineralised E-W-striking pegmatite. The sub-horizontal pegmatite is dextrally displaced along the sub-vertical pegmatite. (Kvina)* ***b)*** *A section through a sub-vertical pegmatite. The identified minerals are smoky quartz, Kfs, amazonite and white, green and brown mica. Crystal faces are well-preserved, indicating little deformation. (L57).* ***c)*** *Drag-folds along a sub-vertical pegmatite, indicating dextral displacement. (L48).* ***d)*** *Within the dominating sub-horizontal pegmatite of the Kvina mine. The pegmatite is quartz rich, with large, irregular feldspar domains. Deformation structures are abundant. Note shear-band cutting the large feldspar domain below pen.* ***e)*** *Close up of d), showing boudinaged, ductile Kfs, with quartz and molybdenite accumulated in thin bands and in the neck-structures.*

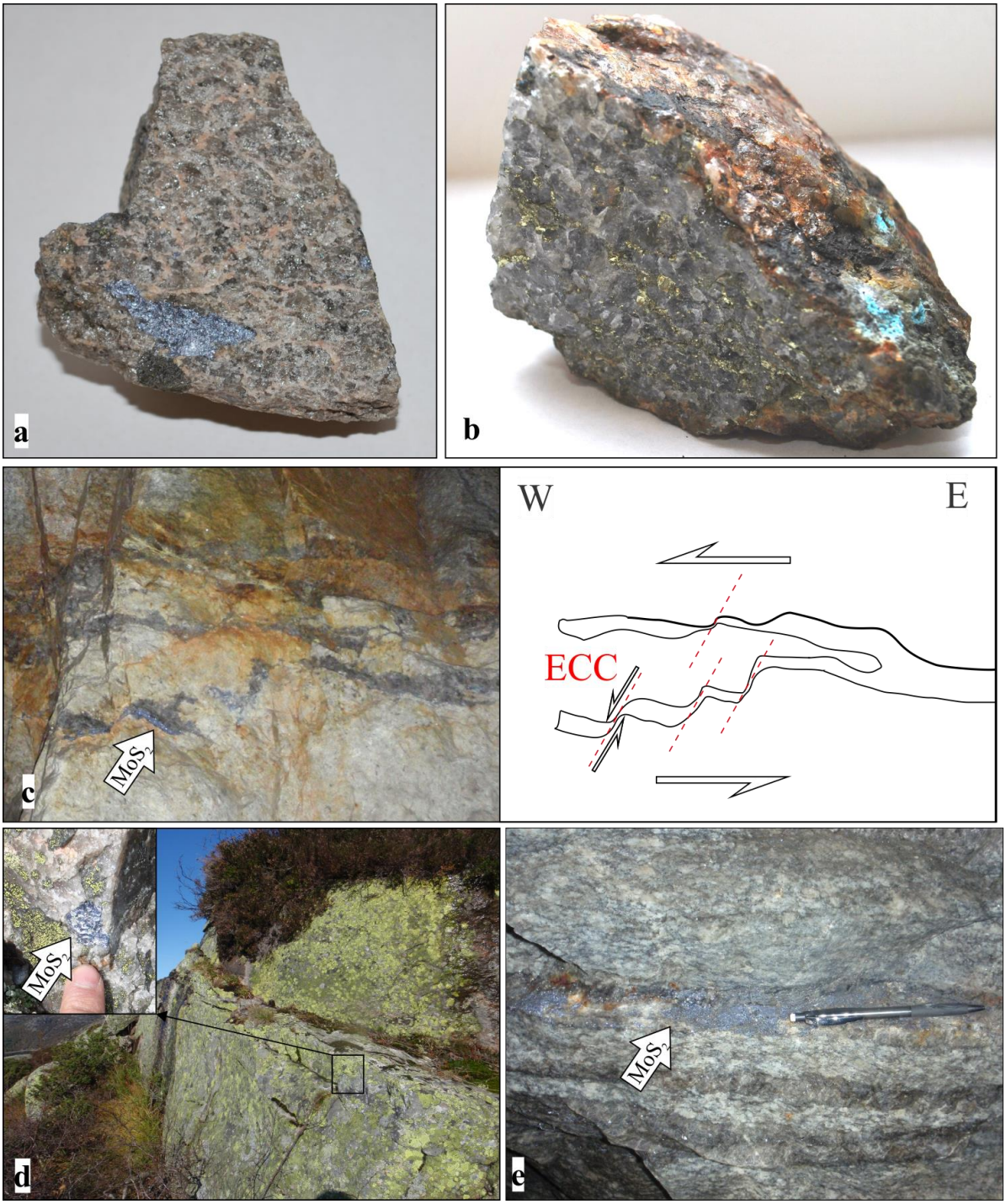

Figure 16: a) *Large molybdenite speck in deformed, sub-horizontal, quartz rich pegmatite. The molybdenite speck is 4cm across. (K1003) (L96).* ***b)*** *From minor Cu-claim, on a mineralized irregular pegmatite. Visible chalcopyrite and pyrite together with smoky quartz and minor feldspar. Note malachite on weathered surface. (K1001) (L21).* ***c)*** *From the Kvina mine, within the main pegmatite. Molybdenite mineralized quartz rich bands, are displaced by ECC-fabric, indicating top-to-the-W kinematics.* ***d)*** *Horizontal, 30cm thick pegmatite within porphyritic granite, cutting the general foliation. Inset photo is a close-up showing a molybdenite speck, and K-feldspar in the quartz rich pegmatite. (L92).* ***e)*** *Typical molybdenite bearing, sub-horizontal, foliation-parallel, quartz rich pegmatite within porphyritic granite. Bottom levels of the Kvina mine.*

3.1.4 Pegmatites, aplites and veins

Subvertical E-W-striking pegmatites

Subvertical, E-W-striking, lensoid shaped, granitic pegmatites, from 1-10m, have been documented at 30 localities, crosscutting the xenoliths and the granitoid rocks (FIG 34a). These pegmatites are not mineralized with molybdenite. Well-developed crystal faces (Fig 15b) indicate that these pegmatites are less deformed than the subhorizontal pegmatites described below. They also cut the latter, as seen in the Kvina mine (Fig 15a). Drag folds (Fig 15c, Fig 14a) indicate movement along the pegmatite vein, but without systematic kinematics. Granitic aplite veins and lenses with less systematic orientations are common, and show a mutual crosscutting relationship with the E-W-striking pegmatites. Both the E-W-striking pegmatites and the aplites are cut by shear bands, indicating top-to-the-W kinematics (Fig 31a).

The main minerals identified in the subvertical pegmatites are, K-feldspar and smoky quartz, and minor amounts of amazonite, plagioclase, biotite, muscovite and green mica (Fig 15b).

Subhorizontal pegmatites and aplites

Subhorizontal pegmatites, and less abundant aplites, cut the eastward dipping foliation in the xenoliths, granitoid rocks and the strained boundaries between xenoliths and granitoid rocks (Fig 10e, Fig 16d, Fig 32a, Fig 36f). They also occur as gently-to-moderately eastward dipping pegmatites, parallel to the general foliation (Fig 36b, Fig 16e). They are cut by the subvertical pegmatites (Fig 15a).

The pegmatites that display an angular relationship with the east-dipping foliation show a consistent clockwise relationship to the foliation, suggesting a shear component with a subhorizontal compressive stress regime. The importance of the pegmatite orientation and kinematics within the context of the tectonic development will be discussed later.

The pegmatites are typically quartz rich with minor feldspar, and are 5-10cm thick (Fig 16d, 16e). Deformation structures and poorly developed crystal faces indicate that these pegmatites are deformed (Fig 15d,e, Fig 16c). These pegmatites are mineralised, and the molybdenite mineralisation occurs within the pegmatites and on their contacts (Fig 16a, b, c and e, Fig 36c).

The majority of the smaller claims in the Knaben Zone have exploited subhorizontal pegmatites, and the larger Kvina mine has exploited a large subhorizontal pegmatite, 240m long in the N-S direction, 80 metres long in the E-W direction and 16 metres wide (Gvein and Rui, 1980).

On the east side of Smalavatn, two pegmatite sheets are related to massive chalcopyrite mineralisation (Fig 16b), and malachite is visible on rusty surfaces. Otherwise, smoky quartz and minor K-feldspar are documented.

3.1.5 Magnetite rich layers

Layers, or pods within the porphyritic granite, following the magmatic fabric, with extreme susceptibility values, occur at L51 and L90 (Fig 22f). These layers are only 10cm thick, and consist of 20-30 modal % of magnetite, 40-50% plagioclase, 30% quartz and minor biotite, zircon, titanite and apatite. The magnetite appears as an interstitial mineral occurring in triangular pits. Susceptibility values range from 100^{-3} to 300^{-3} SI units. The large variation in susceptibility and the variation of oxides and sulphides within the granitoid rocks, indicate large variations in oxygen fugacity and other chemical thresholds. Such factors are likely to be crucial for the molybdenite mineralisation, and the variations are possibly very large over short distances as inferred from the magnetite layers.

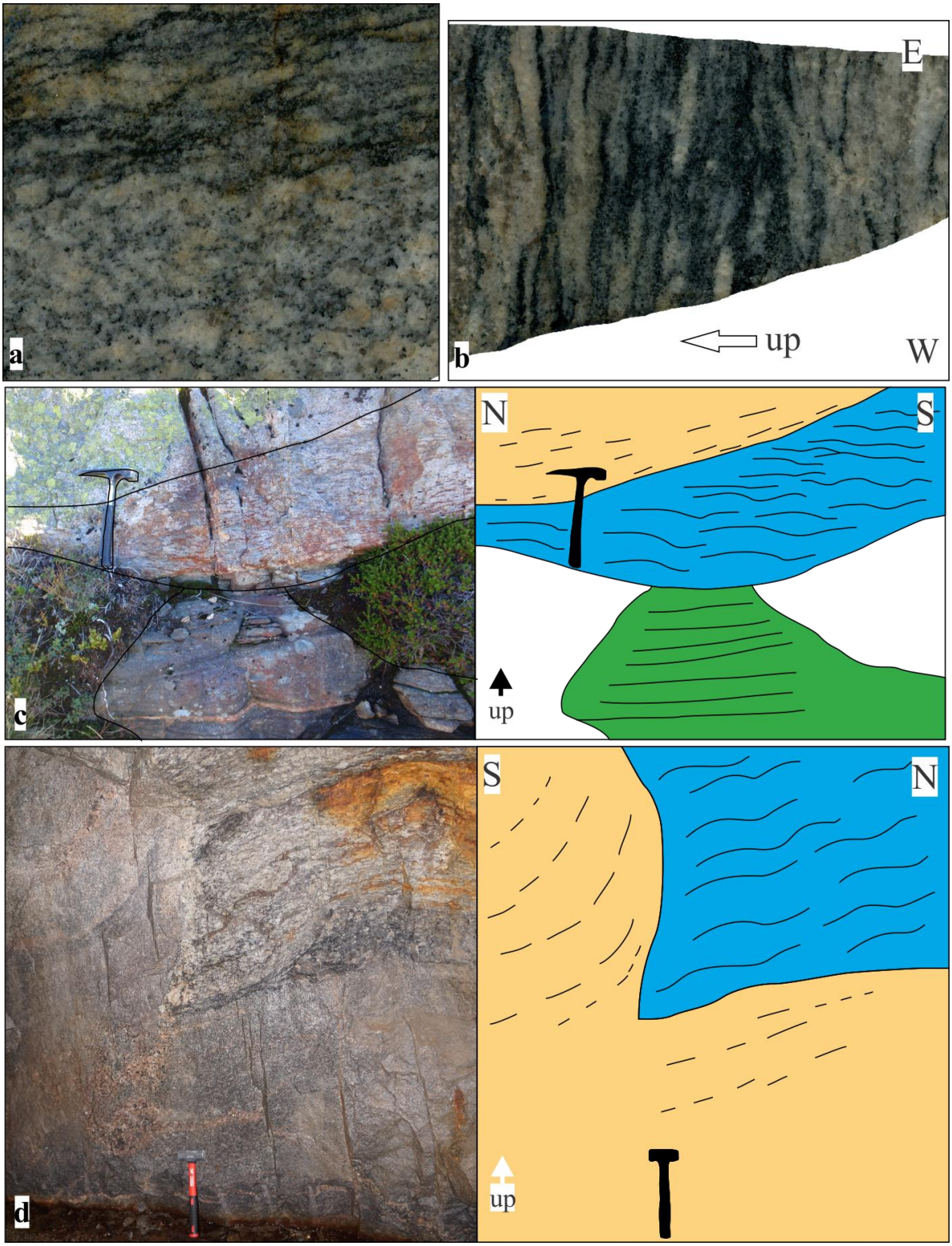

Figure 17: a) *Sharp contact between the flaser gneiss (top) and porphyritic granite. Note the anastomosing, flaser texture. Base of photo is 10cm and is N-S oriented. (K102)* ***b)*** *Flaser gneiss with well-developed, symmetrical flaser texture. (K127).* ***c)*** *A composite screen, with amphibolite at the bottom, and flaser gneiss above. The porphyritic granite cuts the foliation in the flaser gneiss. (L14).* ***d)*** *A xenolith of flaser gneiss is cut by porphyritic granite. The fabric in the porphyritic granite bends around the flaser gneiss. Note an irregular coarse-grained, pegmatitic pod above the hammer, extending to the cutting boundary between the flaser gneiss and porphyritic granite. (Knaben 2).*

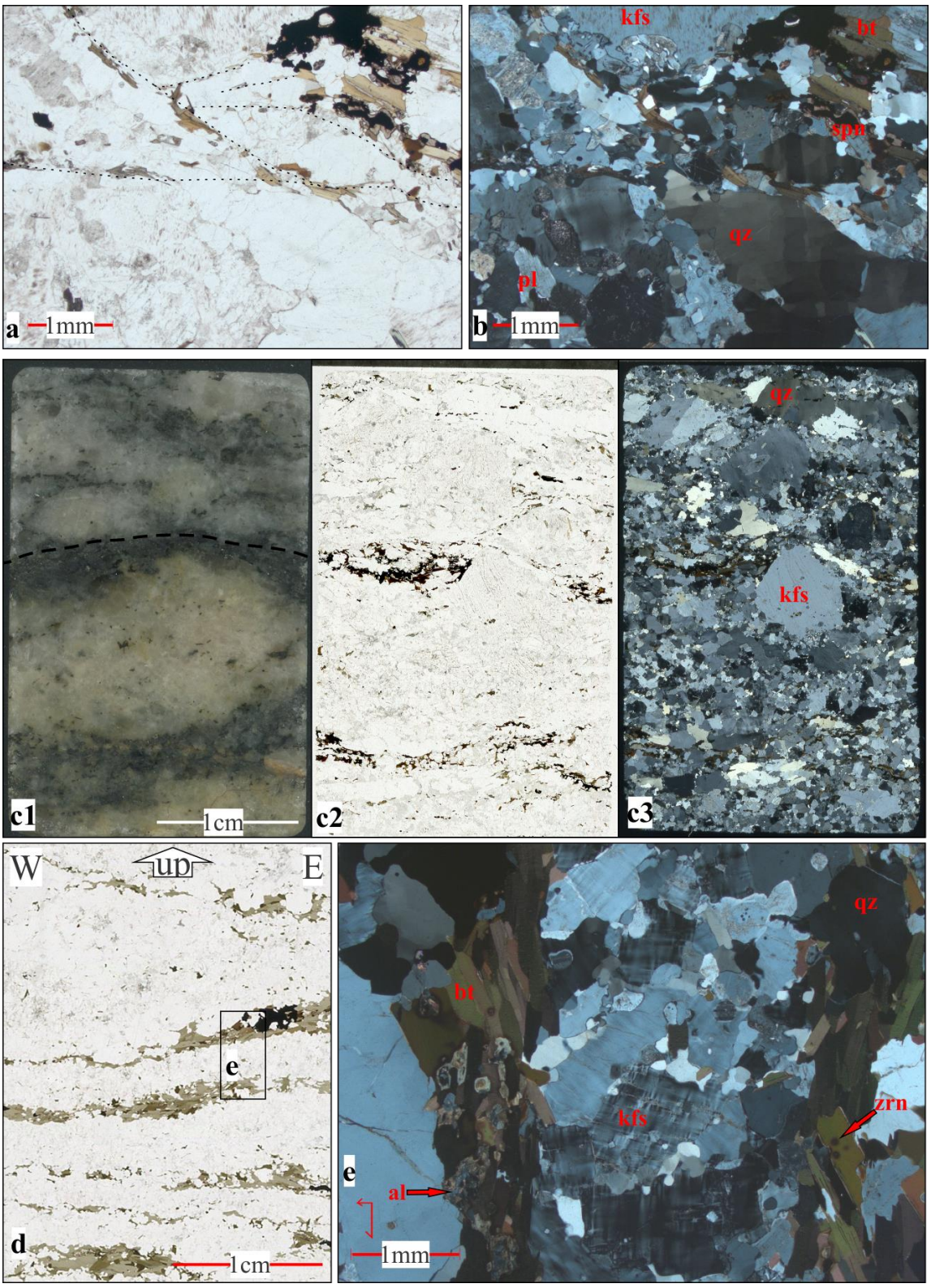

Figure 18: a) *Flaser gneiss sample K100, x2.5, ppl. Anastomosing foliation defined by biotite. (ppl).* ***b)*** *Same as a), with xpl, displaying chessboard extinction in quartz, and myrmekite intergrowth.* ***c1)*** *Sample K100, displaying the boundary (dashed line) between flaser gneiss (below) and porphyritic granite (above). The flaser gneiss has a rusty tint, and distinct mafic bands.* ***c2)*** *K100, ppl. Note the augen texture on the boundary, defined by aligned biotite.* ***c3)*** *K100, xpl. Gneissic texture and recrystallization is more pronounced in the flaser gneiss.* ***d)*** *Flaser gneiss sample K127, displaying well-defined mafic foliation. (ppl).* ***e)*** *Close up of d), showing the mineralogy of the mafic foliation. (xpl).*

3.2 Xenoliths

N-S trending, generally foliation-parallel Xenoliths are abundant in the Knaben area, and are particularly associated with the N-S zone of numerous molybdenite deposits (Fig 5). These xenoliths consist of amphibolite, flaser gneiss, biotite gneiss, and migmatite. The flaser gneiss and amphibolite are the most common xenoliths.

The xenoliths form screens from a few centimetres (Fig 8d) to several metres thick (Fig 8e), and vary in length from below a metre to a couple of kilometres, and thin out to schlieren horizons within the granitoid rocks (Fig 8d). Along the strike, away from a screen, another screen regularly appears, or the screen merges with an adjacent screen, forming a complex anastomosing network (Fig 27c, 27d). The network is interrupted by later E-W-striking shear zones.

The distribution of xenoliths is shown on the geological map (Map 1, Fig 5). Because of a varied mountainous topography, the parallel geometry of the moderate eastward dipping screens appears more complex on the geological map (Map 1). Where the topography is flat or planar, the parallelism is kept, and the Knaben Zone appears narrower, as is the case for most of the area south of the Knaben 2 mine and between Smalavatn and Bergetjødn. In areas with significant topography, the screens seem to bend or broaden, or even form ring-patterns on the map, as seen north of Smalavatn.

Granitoid rocks typically form veins and layers within the xenoliths (Fig 26), with sharp, primary contacts or as complex and deformed relationships. Hence, the structures within the xenoliths seem to be of importance for the granitoid emplacement and evolution. However, features within the xenoliths are also likely to be pre-existing and unrelated to the evolution of the granitoid rocks. Therefore, it is has been necessary to describe and compare all structures within the xenoliths and structures related to strained contacts between xenoliths and granitoid rocks.

3.2.1 Flaser gneiss

Field relationships and mesoscopic observations

The flaser gneiss is the most abundant xenolith, and it appears as screens from a few cm to 10m thick, with a very consistent moderate eastward dip (Fig 8d, Fig 17a, b and c). The boundary to the surrounding lithologies is generally sharp, and the width of the screens vary with the strike, creating a wavy and boudinaged pattern, thinning out to schlieren horizons (Fig 8d). The screens can be followed for up to several hundred metres, and are generally more continuous than the other xenolith screens, apart from a few anomalous amphibolite screens on the western side of the Knaben Zone. Composite screens, with both amphibolite and flaser gneiss are common (Fig 17c). Smaller amphibolite xenoliths within the flaser gneiss also occur, indicating that the amphibolite is older (Fig 20e). A handful of localities show that the porphyritic granite clearly cuts the flaser gneiss (Fig 17c, d). This relationship is supported by geochronological U-Pb analyses on zircon, presented below (Fig 45).

The rock is medium-grained, with oblate lenses of felsic minerals defined by an anastomosing foliation of mafic minerals, giving it a distinct appearance (Fig 17a, b). The felsic lenses are commonly one cm wide and 3-5cm long. Based on the texture, the rock is generally well described as a flaser gneiss, with local augen gneiss when the lenses are less elongated (Philpotts, 1989, p. 153). K-feldspar, plagioclase, quartz and scattered fine-grained biotite constitute the lenses, while biotite and minor mafic minerals (Fig 18d, 18e) mainly define the foliation.

Structures indicating simple-shear kinematics are rare; occasional shear bands within the flaser gneiss, defined by the foliation, occur, indicating top-to-the-W kinematics, as described below (Fig 31b). More commonly, the biotite layers in the flaser gneiss suggests a predominant component of pure-shear, as symmetric lenses and flaser texture. The significance of this observation, in relation to the interpreted early appearance of the flaser gneiss in the tectonic evolution will be discussed later. Subhorizontal, mineralised pegmatites and pods of grey granite occur within the flaser gneiss (Fig 12b). Molybdenite mineralisation along the biotite foliation is common (Fig 36a). Weathered flaser gneiss has a more rusty appearance than the porphyritic granite (Fig 17c, Fig 18c1).

Petrography and microscopic observations

The flaser foliation occurs at all scales, and consists mainly of strongly aligned biotite, and traces of pyrite, chalcopyrite, magnetite, molybdenite, apatite and zircon (Fig 18). The interstitial felsic lenses are mainly aggregates of medium-grained quartz and feldspar, or consist of one 1-2 cm sized equidimensional K-feldspar grains mantled by finer-grained feldspar and quartz (Fig 18c). Sparse biotite occurs within the lenses.

Microstructures in quartz and K-feldspar are similar to the porphyritic granite. Occasional brittle deformation, imbricate-structures, and tapering deformation twins occur in the plagioclase. The biotite is mainly brown-coloured and partly altered to chlorite. Clusters of zircon grains along the mafic foliation planes occur, in addition to the more common zircon inclusions in biotite. Trace amounts of metamict allanite are also concentrated in the mafic foliation (Fig 18e).

3.2.2 Amphibolite

Field relationships and mesoscopic observations

A garnet-bearing biotite amphibolite schist is one of the main types of xenoliths (Fig 19e). Garnet is sporadically present. Due to its dark colour, distinct lichen growth and crumbly weathering, this rock unit is easily recognisable in the field (Fig 19a). Its schistocity is generally well-developed and defined by hornblende, biotite, or both.

Contacts between the amphibolite and granitoid rocks or the other xenoliths are mainly sharp (Fig 17c, Fig 19a, c). In relation to the porphyritic granite, contacts can also be deformed (Fig 26a, b). Fig 19b shows a coarse-grained reaction-rim developed on the contact towards the porphyritic granite engulfing an amphibolite xenolith. The amphibolite is typically weakly folded. Folds in large xenoliths generally have a consistent fold-axis (Fig 28c). Smaller amphibolite xenoliths appear twisted and folded, and have a large variation in fold axis resembling folding caused by magmatic flow (Fig 28). Xenoliths smaller than 2 m display more irregular relationships, with felsic melt pods, relationships resembling assimilation and are occasionally oriented with the magmatic lineation (Fig 19d, Fig 20a). Boudinaged amphibolite xenoliths occur (Fig 30). Detailed descriptions of structures are presented below.

The schistocity in the amphibolite is occasionally weakly developed, as seen in FIG 19b and Fig 30a. Here, the relationship to the granitoid rocks is less deformed, displaying a primary magmatic relationship.

Petrography and microscopic observations

The amphibolite is fine-grained with varying amounts of hornblende and biotite, and occasional pyroxene and porphyroblasts of garnet (Fig 20b, c, d and e). Two amphibolite samples have been analysed in thin section. The amphibolite has a strong lepidoblastic to grano-lepidoblastic texture (Bard, 1986), defined by hornblende and biotite laths (Fig 20b, c). Typically, it contains 10-20 modal % hornblende, and up 30-40% biotite, with polygonal to

heterogranular quartz (10%-20%) and plagioclase (30-40%). Occasional garnet porphyroblasts, up to 1cm, with asymmetric biotite and hornblende wrapping indicates top-to-the-W kinematics (Fig 20b, c).

In sample K19 a 3cm sized grano-porphyroblastic domain is apparent, with 2cm elongated, strongly poikilitic clino-and orthopyroxene, together with fine-grained isogranular pyroxene, hornblende, quartz and plagioclase (Fig 20d, e).

The quartz is generally fine-grained, moderately polygonal, with sweeping undulating extinction. Plagioclase grains are weakly sericitized, with tapering deformation twins. Biotite grains are brown, and often bent. Hornblende has a distinct blue-green pleochroism.

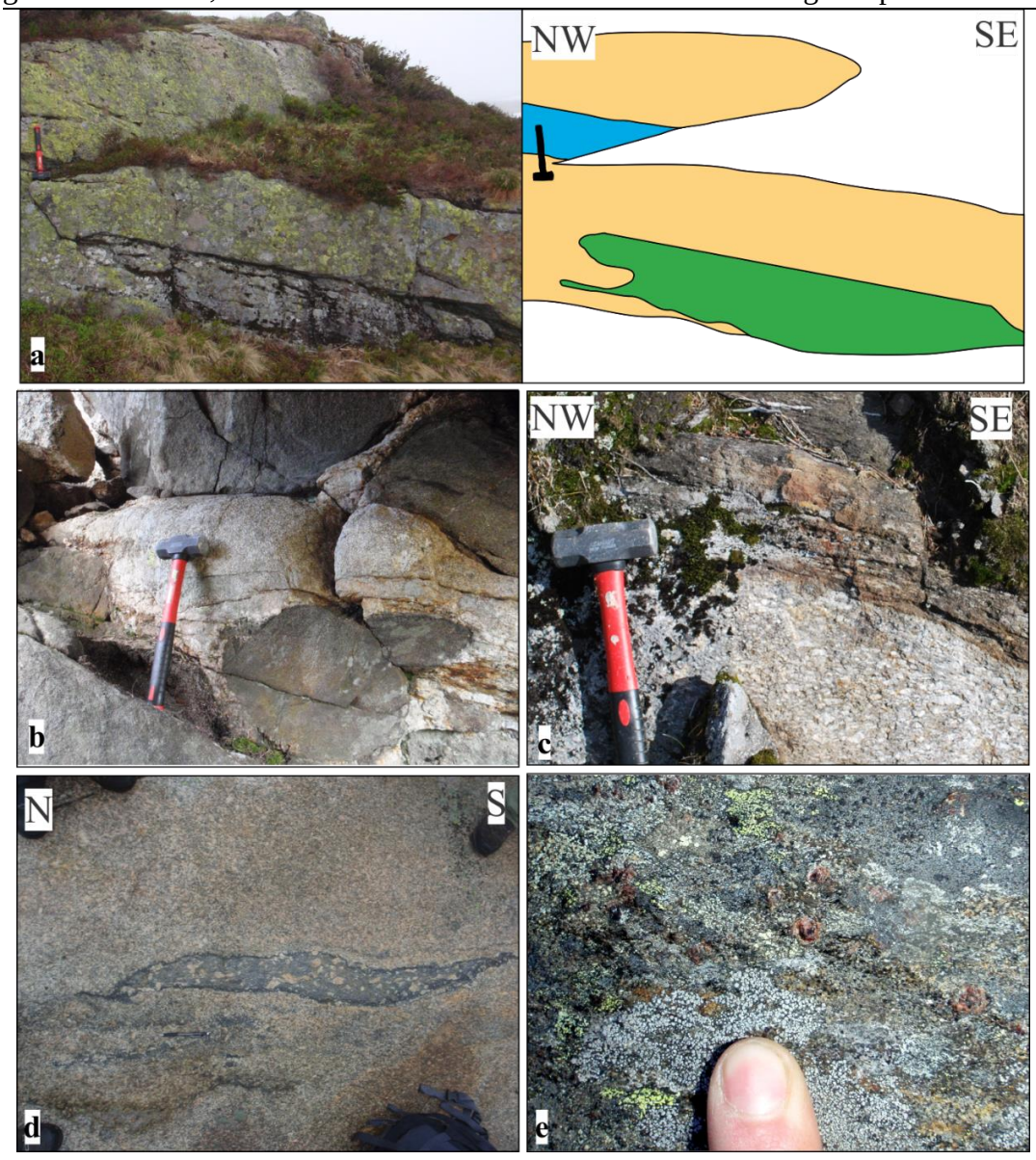

Figure 19: a) *Typical amphibolite xenolith (darker, grey lichen) in porphyritic granite (more massive with bright green lichen). (L38).**b)** Amphibolite xenoliths engulfed by a pale granite. Coarse-grained rims around the amphibolite. (L110).* ***c)*** *Sharp contact between amphibolite (brown) and porphyritic granite. Note the alignment of euhedral to subhedral Kfs grains parallel to the contact and the foliation in the amphibolite. (L67).* ***d)*** *Small mafic xenolith in porphyritic granite, aligned with the phenocrysts. Note the dark reaction rim and thinning out to schlieren horizons at the ends. Ductile clasts of K-feldspar and granite within the xenolith. (L35).* ***e)*** *Garnet rich domain in the amphibolite. (L91).*

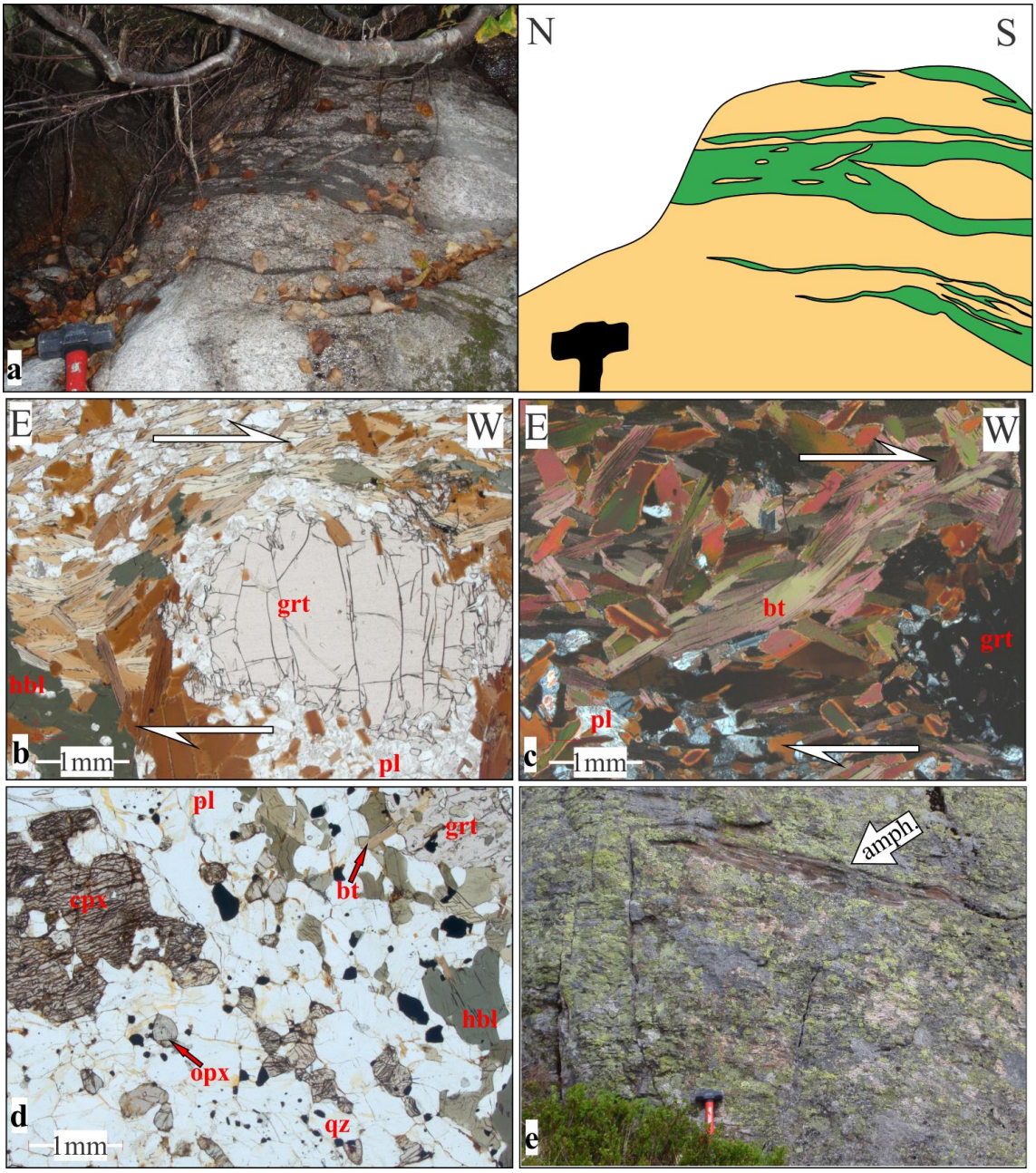

Figure 20: a) *Ductile, assimilating relationship between amphibolite and porphyritic granite. Magmatic flow and mingling relationship, including felsic melt pods within the xenolith. The xenolith thins into schlieren horizons. (L77).* ***b)*** *Amphibolite sample K33, x2.5. Biotite (brown) and hornblende (green) laths, wrap around a garnet porphyroblast (pink tint). The steep, ramping fabric on the upper left side, and the lack of wrapping on the right side indicates dextral, top-to-the-W kinematics. (ppl).* ***c)*** *Displaying a different garnet (black) in the same sample as photo b), with identical wrapping of biotite and hornblende around the garnet. (xpl).* ***d)*** *Amphibolite sample K19. (ppl).* ***e)*** *Amphibolite enclave in flaser gneiss (L104).*

3.2.3 Biotite gneiss

Field relationships and mesoscopic observations

Generally, the geometry of biotite gneiss screens and field relations are similar to the amphibolite (Fig 21b). The biotite gneiss has a distinct planar spaced foliation, defined by biotite, occasionally hornblende and other mafic minerals (Fig 21a). Occasional hornblende grains of up to 2cm occur (Fig 21c). The spacing between the mafic planes vary, when at the densest, its appearance is similar to the amphibolite. The rock has a very weathered and crumbly altered appearance (Fig 21a, b).

At L7 (sample K23) a sheet of dark grey, medium-grained biotite granite stands out from the surrounding porphyritic granite. The sheet is 1-2m thick, dipping moderately to the east. It has a massive appearance, with no clear fabric. Biotite, quartz and plagioclase are the main minerals, and the rock lacks pink k-feldspar phenocrysts. As shown in a later section, the geochemistry is very similar to the biotite gneiss (Fig 40, 41). Hence, K23 is likely to represent a variety of the biotite gneiss with less deformation. This is similar to the melanocratic granite presented above.

Development of leucosomes occur at a few localities (Fig 22e), and the leucosomes are occasionally folded, making the rock similar to the migmatite.

Petrography and microscopic observations

The texture is grano-lepidoblastic (Bard, 1986), with fine-grained to medium-grained felsic minerals and minor aligned biotite between the mafic foliation planes. Clusters of zircon, titanite, opaque minerals and traces of rutile, allanite and fluorite occur along the foliation planes (Fig 21e, f).

The quartz generally has the same appearance and microstructures as in the porphyritic granite, and typically occurs in amounts of 40 modal %, but the amount varies with the density of mafic foliation. Elongated clusters of quartz are common. Rusty stains in the quartz are typical. K-feldspar generally constitutes below 10%, as microcline with tartan twinning, and occasional two-stage perthite. Heavily sericitized plagioclase occurs in modal amounts of 10-20 %

3.2.4 Migmatite

Field relationships and mesoscopic observations

Undefined lenses of granitic migmatite with clearly defined leucosomes and melanosomes, with local augen-texture are exposed at a few localities along the Smalavatn lineament (Fig 1a, Map 1). In addition, a 2x4m migmatite xenolith crops out within the lineament east of Store Knabetjødn (L64, sample K123). The rock is fine-to-medium-grained, with pink leucosomes and dark-grey melanosomes.

The leucosomes appear as veins up to 5cm thick and are folded. The folds are tight to isoclinal, and when vergence is apparent, they generally indicate top-to-the-W kinematics (Fig 28e, Fig 22c). More randomly oriented ptygmatic folding also occur (Fig 22a, Fig 28d). Alteration gives the migmatite a rusty colour.

Along the southwestern side of Smalavatn the leucosomes create a fabric, with a steep dip to the west (Fig 23a, 23b). They are isoclinally folded, indicating top-to-the-W movement (Fig 28e). This observation is interpreted as a large scale ECC-structure (Fig 5), and is explained below in the structures-section.

Petrography and microscopic observations

The grain size and texture is highly variable, with fine-grained eugranitic domains and coarser grained and clearly strained domains. Biotite is the main mafic mineral, constituting 5-20 modal %. Medium-grained epidote occurs in trace amounts in sample K35. Zircon, titanite, apatite and rutile occur in trace amounts in all samples.

The quartz occurs in modal amounts of up to 40%, as polygonal, annealed grains and as elongated grains, with similar microstructures as in the porphyritic granite, parallel to the foliation. Brittle imbrication-structures occur in the plagioclase, which constitute 5-20%, and is sericitized.

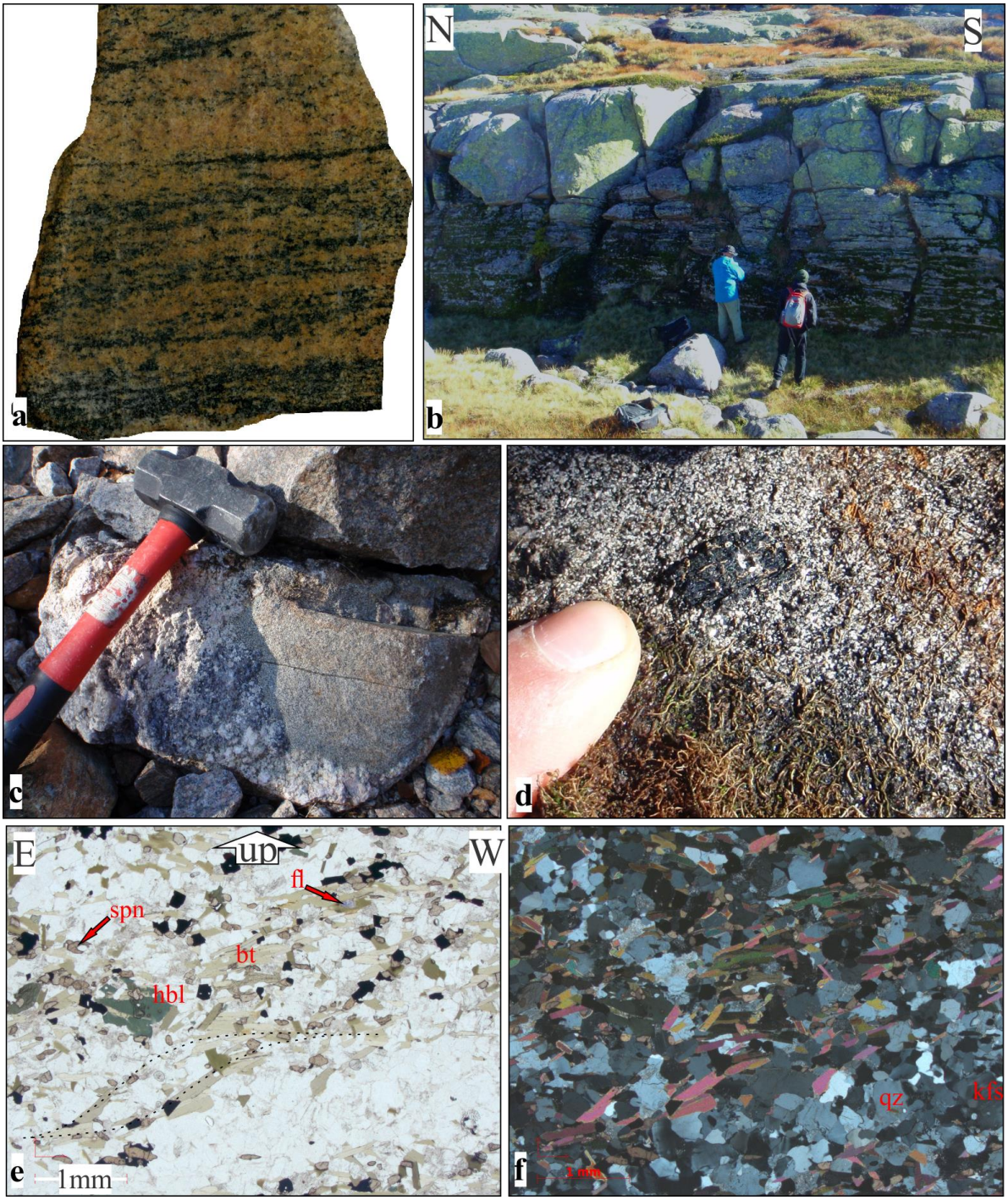

Figure 21: a) *Biotite gneiss sample K16, with typical rusty alteration and variable density of mafic foliation.* ***b)*** *A screen of biotite gneiss, with distinct foliation and weathering, below massive porphyritic granite. (L25).* ***c)*** *Poorly foliated granitic gneiss, engulfed in coarse-grained leucocratic granite. (L78).* ***d)*** *Poorly foliated biotite gneiss with a large hornblende grain. (L87)* ***e)*** *Biotite gneiss sample K116, ppl, x2.5. Biotite, hornblende and titanite are the major mafic minerals. Traces of fluorite occur. Biotite laths are oriented in S-C relationship (dashed line), indicating top-to-the-W kinematics.(ppl).* ***f)*** *Same as e), in xpl.*

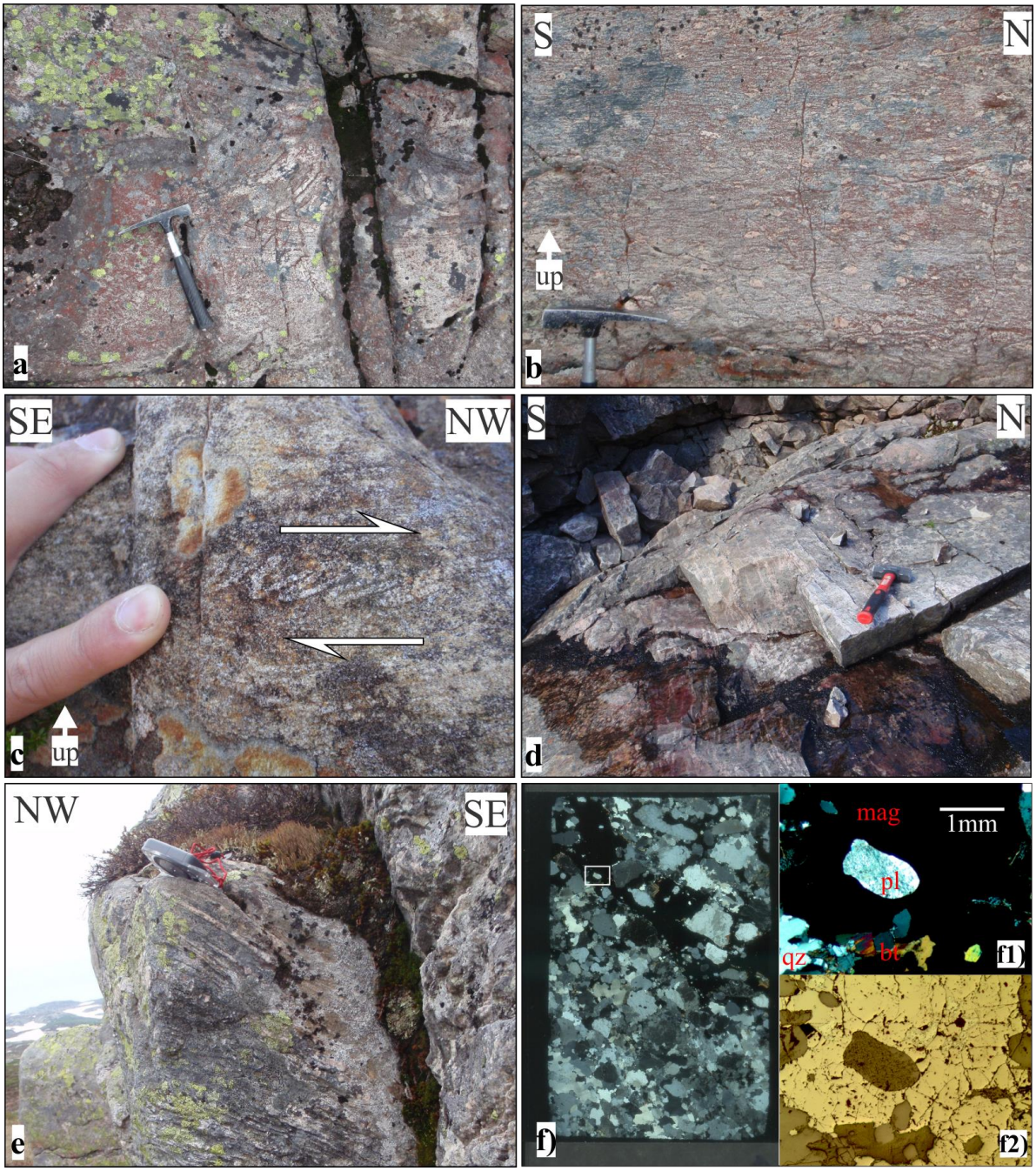

Figure 22: a) *Fine grained, irregularly folded migmatite, with well-developed leucosomes. (L26).* ***b)*** *Strained migmatite, with augen texture and leucosomes. (L33).* ***c)*** *Small leucosome in migmatite with isoclinal, NW-vergent folds. (L13).* ***d)*** *Migmatite with planar leucosomes and sigmaclast development and steep foliation. (L64).* ***e)*** *Leucosome development in the biotite gneiss. The leucosomes are folded and show augen texture, but are generally parallel to the foliation in the biotite gneiss. (L3).* ***f)*** *Magnetite rich band in porphyritic granite. (K104, xpl). White square is shown in f1) (xpl) and f2) (reflective light).*

3.3 Structural geology and tectonics

In this section, observations of the different types of structures occurring in the Knaben Zone are presented. Whereas most of the Sirdal Magmatic Belt is not significantly deformed, in localised zones, complex deformation relationships occur (pers. comm., Henderson & Slagstad). The Knaben Zone is an example of such a deformation zone. An interpretation of the structures with profiles is presented in Map 2, and key localities in Map 3 (Digital Appendix)

Both ductile and brittle structures are observed but, as the following section and the discussion will demonstrate, the ductile structures are more predominant and appear to have some bearing on the emplacement of the granites, their subsequent deformation and the molybdenite mineralisation. Many different structural types are observed and these are documented separately below. The structures involve several lithologies and, moreover, tend to occur at lithological contrasts, and are therefore presented separately in this section.

At the outset the appearance of the ductile structures in the Knaben Zone are atypical and ambiguous, when compared with tectonic structures, particularly in other parts of the Sveconorwegian Orogen (Henderson & Ihlen, 2004; Viola & Henderson, 2008). In addition, the pervasive parallelism of the different lithologies, primary and secondary structures complicates an interpretation of the geological evolution, as pointed out by Lysberg (1976). The reasons for this will become apparent when the observations are incorporated below in a tectonic model for the area. However, the consistency of the structural geometries and styles, and their spatial relationship to the different lithological units throughout the Knaben Zone, indicates that they are important features in the tectonic evolution.

3.3.1 Foliation, magmatic fabric and lineations

Within the xenoliths, foliation is well developed, clearly as a secondary, tectonic foliation as described for each lithology above. This tectonic foliation is exploited by the sheeted granitoid intrusions (Fig 23c). Both primary magmatic, to submagmatic, foliation and locally a more developed tectonic foliation are evident in the granitoid sheets.

Distinguishing between magmatic fabric and foliation in the weakly deformed granitoid rocks is, at times, problematic and ambiguous. However, during several long field seasons with many observations recorded, a pattern of recognition was developed. Criteria presented by Paterson et al. (1989) have been particularly useful. Examples of primary magmatic fabric and secondary tectonic foliation are shown in (Fig 24). Stereonet data for both magmatic and tectonic foliation for the whole of the Knaben area is presented in Fig 23. A moderate eastward-dipping foliation with coinciding magmatic fabric and tectonic foliation dominates the Knaben Zone, similar to the findings of Lysberg (1976).

Where there is only an alignment of subhedral to anhedral phenocrysts, a weakly developed and homogeneous alignment of mafic minerals or alternating colour variations within the weakly deformed to undeformed granitoid sheets, this has been interpreted to represent a primary magmatic fabric, possibly intensified locally post-magmatic (Fig 24). Where a heterogeneous fabric is present, with a recrystallized and gneissose appearance within the granitoid rocks, particularly with the key observation of kinematic indicators on several scales, this is interpreted as tectonic foliation (Fig 24c, d). However, small amounts of recrystallization and development of a distinct foliation can be formed during submagmatic flow, and continuing post magmatic deformation (Paterson et al., 1989). Convincing foliation caused by solid-state deformation within the granitoid rocks is only observed in local, narrow bands (Fig 24c, 24d).

Such high strain, mylonite zones occur at a few localities, and are approximately 5 to 20cm thick. At L60, the porphyritic granite is clearly mylonitic, with sigma clast development indicating top-to-the-W kinematics, and a heterogeneous fabric (Fig 24c, d). The mylonitic foliation at L60 is parallel to the magmatic fabric in the porphyritic granite. Similarly, in the porphyritic granite sample K1004 at L106, the deformation is clearly solid state, with sigma clasts and ribbon grains (Fig 9e), with a tectonic foliation parallel to the magmatic fabric.

A 20-30cm wide mylonite band at L57 is shown in (Fig 14). The band falls 40° towards 140°, cutting through the magmatic fabric in the granitoid rocks (oriented 20-30° towards 80°) with a distinct angular discontinuity at this locality. Kinematics derived from internal structures and external drag folds support an interpretation with top-to-the-W kinematics, possibly with an oblique northward component. Structures filled with undeformed granitic veins indicate that melt was present during deformation (Fig 14d).

As pointed out by Paterson et al. (1989), "*distinguishing foliations formed by magmatic flow in granitoids from those formed by tectonic processes is critical for understanding the timing and means of emplacement of plutons, which in turn influence interpretations of the age and significance of structures and metamorphism in the surrounding country rock*". Because the molybdenite is thought to be closely related to magmatic activity (Gvein and Rui, 1980; Bingen et al., 2015) , such an approach is in addition important for evaluating the molybdenite deposits.

The amount of strain typically decreases with distance from the deformed boundaries between the xenoliths and the granitoids (Fig 23c, Fig 26a). In the same manner, the thickness of porphyritic granite sheets within the xenoliths also increases. This heterogeneous strain distribution, with strain concentrated along lithological contrasts, is distinct.

In addition to the foliation, several types of lineation occur in the Knaben Zone, originating from different processes. A shallow plunging S to SE-trending, local K-feldspar phenocryst lineation and lineation of quartz aggregates, occurs in the porphyritic granite and the quartz porphyritic granite (Fig 25a). These new data are very similar to the data presented by Lysberg (1976). What this lineation represents is not clear, but the phenocrysts appear to be aligned to this position without significant recrystallization, and with occasional parallel small xenoliths displaying a magmatic relationship (Fig 19d). Hence, the mineral lineation is likely to be caused by magmatic to submagmatic flow.

Stretching lineations occur on biotite rich lithological boundaries (Fig 25), and are most likely to have formed post magmatic, or at least in domains with significant crystallisation. They display a moderate plunge towards the southeast, again coinciding with older data (Lysberg, 1976), and partly overlapping with the more widely spread phenocryst lineations. These stretching lineations are more confined than the magmatic to submagmatic mineral lineations. The tectonic significance of the concurrence of the interpreted lineation structures created during the magmatic phase of the tectonic evolution and those interpreted to have been formed post-magmatic will be discussed later.

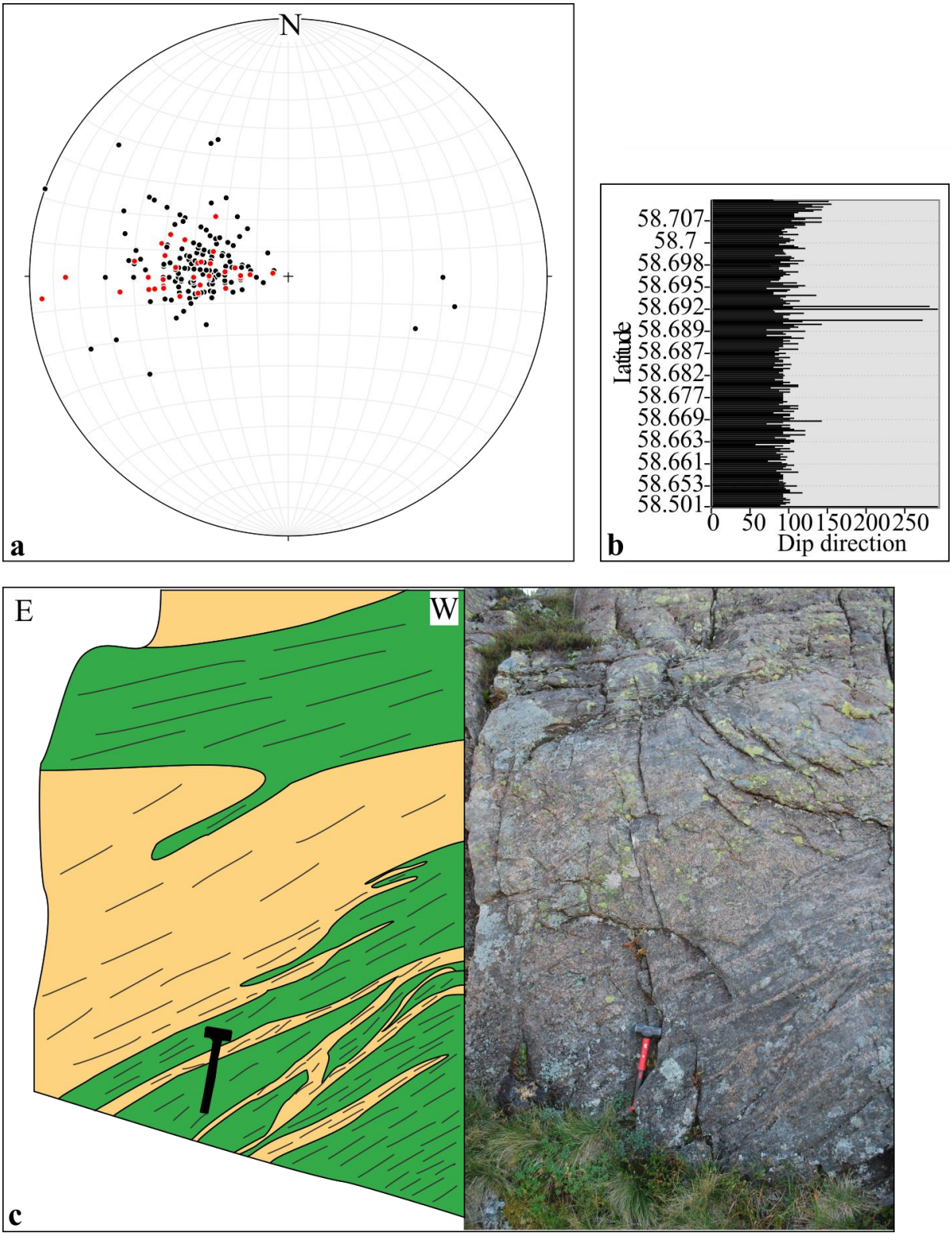

Figure 23: a) *Stereonet with poles to tectonic foliation (black dots) and magmatic fabric (red dots).* ***b)*** *A diagram showing the variation in dip-direction in relation to latitude. Note the increase in dip-direction in the northern (upper) parts. The three anomalies around 58.692 degrees north show the westward dip in around Smalavatn.* ***c)*** *500 m east of Knaben 2 mine, on the eastern margin of the Knaben Zone (L88). Porphyritic granite, with a weakly developed foliation lies in thin sheets parallel to the tectonic foliation in the amphibolite. The foliation within the porphyritic granite increasingly better developed towards the amphibolite screen, indicating that strain has been concentrated here, and that the porphyritic granite intruded synkinematically..*

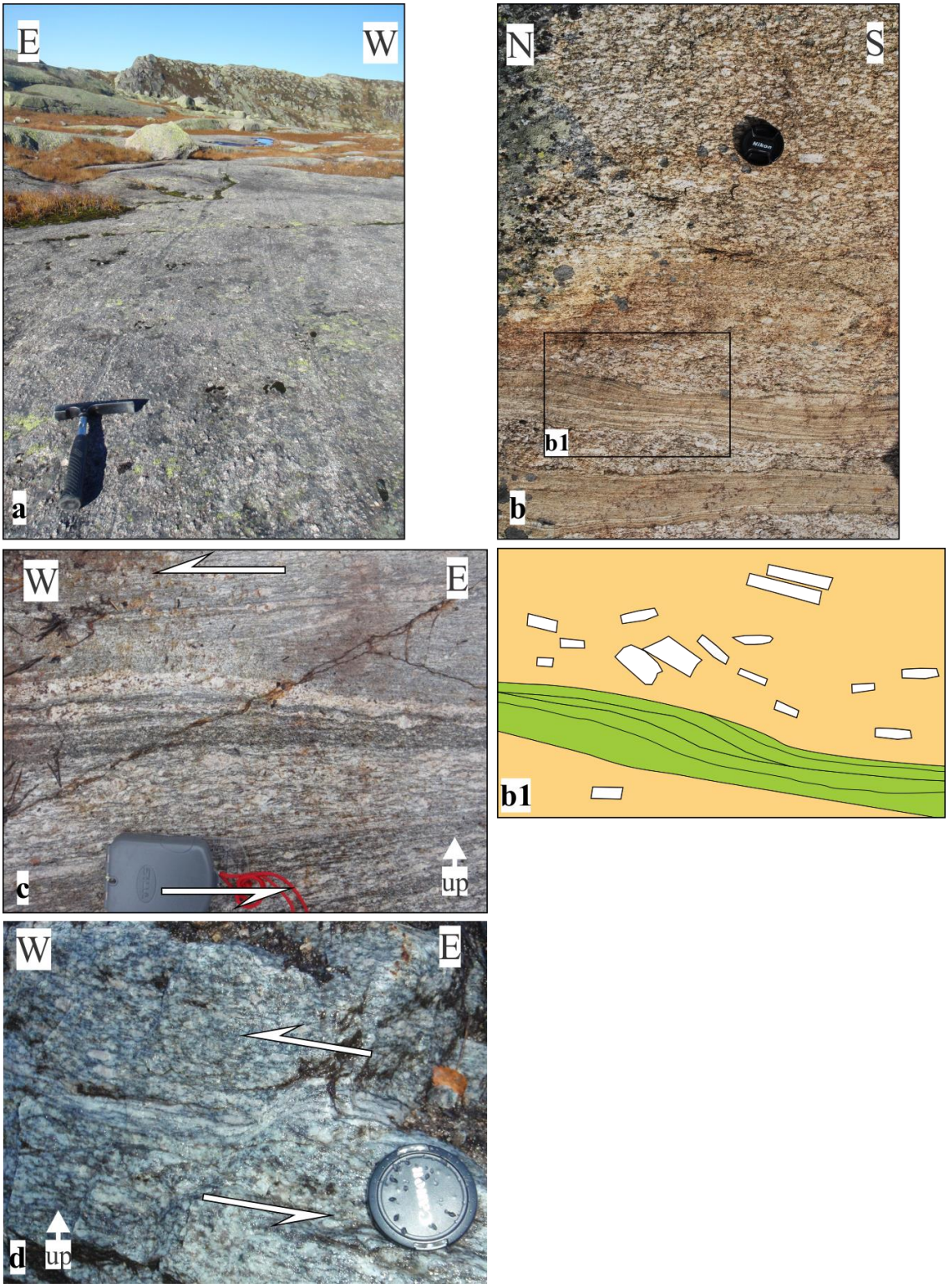

Figure 24: a) *Altered surface of porphyritic granite with magmatic fabric. Aligned subhedral phenocrysts, and banding with variable amounts of phenocrysts. (L24).* ***b)*** *Planar outcrop, magmatic fabric within the porphyritic granite, aligned euhedral to subhedral K- feldspar phenocrysts. At the bottom, two thin screens of biotite gneiss lie parallel to the magmatic fabric. (L15).* ***b1****) sketch of b), showing Imbricated phenocrysts in the porphyritic granite just above the biotite gneiss.* ***c)*** *Highly strained, mylonitic porphyritic granite, with augen-texture, sigmaclast development and heterogeneous fabric. Top-to-the-W kinematics deduced from sigmaclasts. (L60).* ***d)*** *Thin (4cm) mylonitic band within weakly deformed porphyritic granite. ECC band indicating top-to-the-W deformation. (L58).*

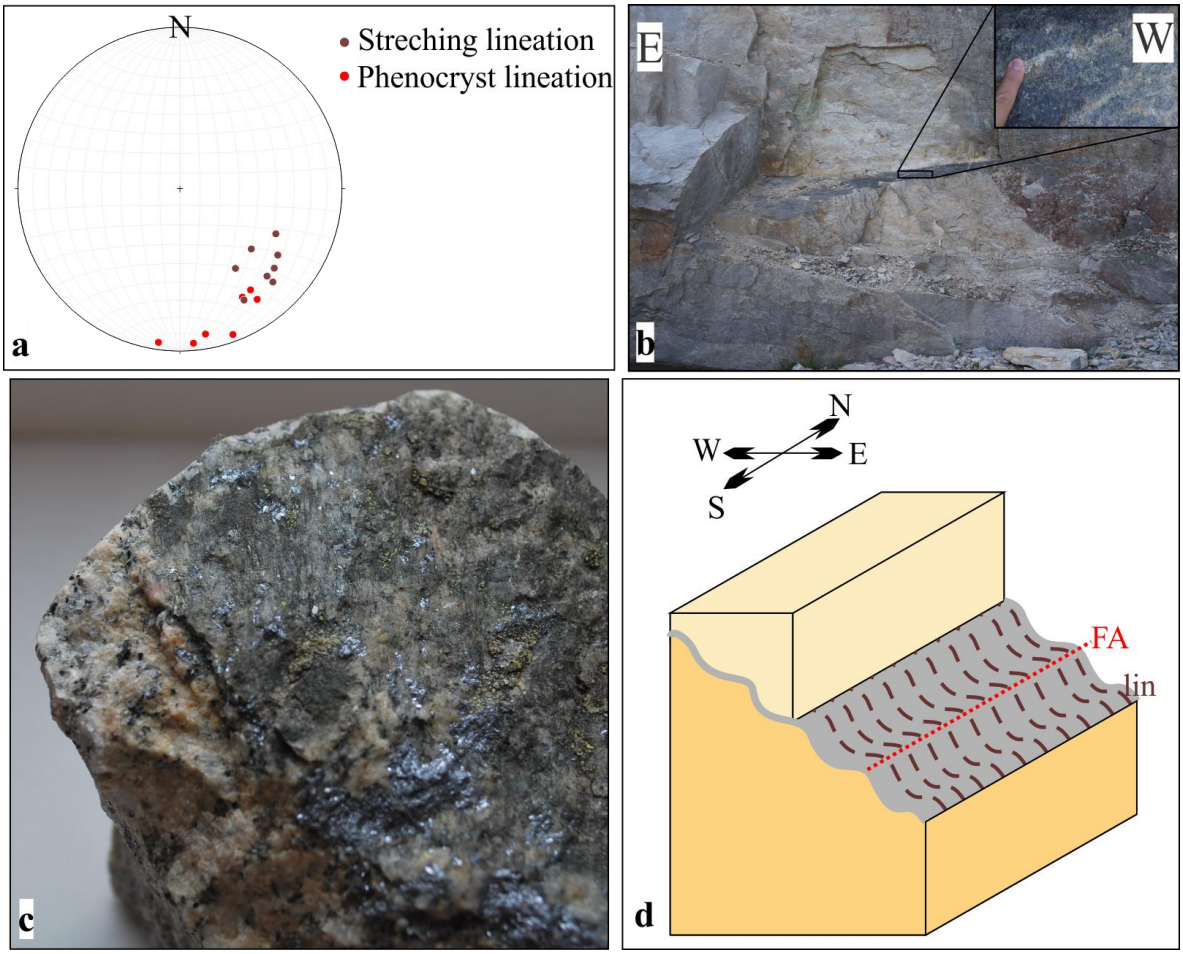

Figure 25: a) *Stereonet with lineation measurements from the Knaben Zone. Phenocryst lineation and lineation of quartz aggregates in the granitoid rocks (red dots) fit with Lysberg's (1976) data, but are more spread. The stretching lineations (brown dots) are typically defined by biotite grains, and occur on well-defined contacts between the different rock units.* ***b)*** *In the open pit at the Knaben 2 mine the contact between grey granite (above) and porphyritic granite (below) is well defined by a biotite film with stretching lineation. The interface is also weakly folded.* ***c)*** *Sample K110. A sample of a contact similar to b). Molybdenite is concentrated on the interface. (L95)* ***d)*** *Sketch of photo b), showing the contact between grey granite (paler) and porphyritic granite, with stretching lineations and orthogonal small folds.*

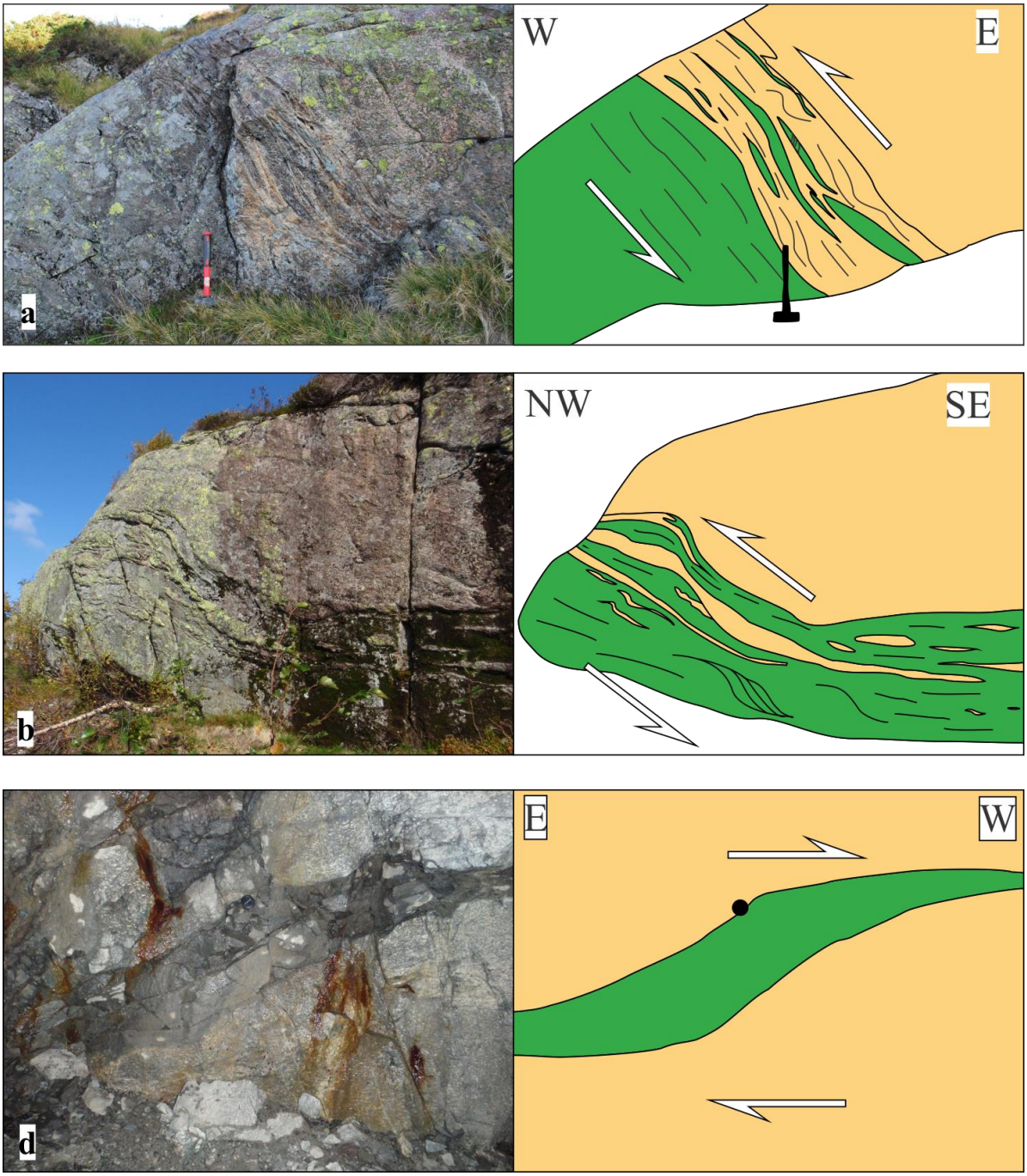

Figure 26: a) *The boundary between porphyritic granite and amphibolite forms a complex duplex structure, with smaller imbricates within, indicating top to the west kinematics, supported by small folds, and SC-structures. The porphyritic granite within the shear zone is more strained than above. (L89).* ***b)*** *Base of photo 5m. Layers of porphyritic granite lie within the foliated amphibolite, and form a ramping duplex structure, ramping similarly to a). Smaller ramps and imbricates within the amphibolite, and ramping porphyritic granite layers indicate top-to-the-W kinematics. The porphyritic granite is only weakly deformed. (L86).* ***c)*** *Within the Lower Roma mine, lens cap for scale. A sigmoidal amphibolite screen within weakly deformed porphyritic granite, ramping up to the W.*

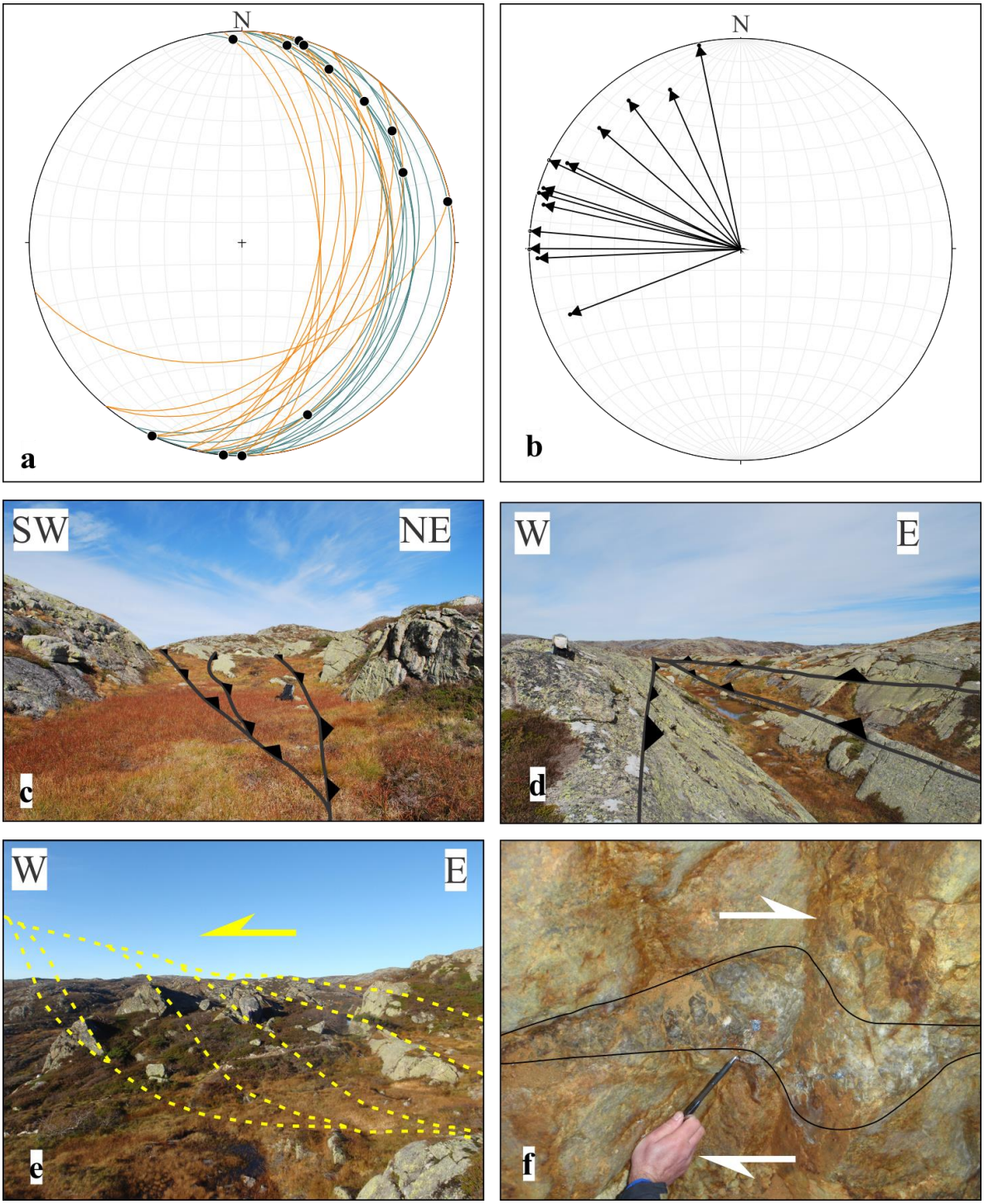

Figure 27: a) *Measurements from 13 duplex structures in the Knaben Zone. Gentle dipping parts of duplex structures are shown in orange and steep parts in green. The ramp intersection point for each duplex is marked black.* ***b)*** *All ramp intersection points are rotated 90° either clockwise or anti-clockwise, giving cluster of points in the W-NW. Arrows indicate inferred kinematics from the duplex structures, respectively top-to-W-NW* ***c), d)*** *Deformation zones in field are seen to merge together, resulting in an anastomosing network, and a stepped terrain. Photo c) is from L42, rucksack for scale. Photo d) is from L81, rucksack for scale.* ***e)*** *An idealized sketch of how the strain zones in the stepped terrain are connected based on small variations in dip, and duplex structures on smaller scales. Photo e) is from L68, man for scale in middle of photo.* ***f)*** *Molybdenite mineralisation related to a folded pegmatite. The fold has dextral kinematics. (Kvina mine).*

3.3.2 Compressional ductile structures

Ductile structures are common both within the xenoliths, on the deformed boundaries between the xenoliths and granitoid rocks, and related to structures cutting the granitoid rocks. Folds, duplex structures, boudinage and deformation bands are the main observed structures, and will be described separately below. Predominantly, the discrete structures are formed parallel to the otherwise weak SE-dipping foliation. However, some critical ductile structures for the interpretation of the tectonic evolution have distinct angular relationships to this regional foliation. The kinematics inferred from these structures, largely indicate consistent, top-to-the-W kinematics, related to the dominating moderate eastward dipping geometry.

Duplex structures

Structures ramping upwards towards the west are the most common and consistent structural features in the Knaben Zone. These structures have a distinct sigmoidal shape, which is why they are termed duplex structures, though they are not clearly restricted by floor and roof thrusts (Boyer and Elliott, 1982). The structures are similar to duplex structures presented by Casini et al. (2007).

Duplex structures form at all scales, either along deformed boundaries between granitoid rocks and the xenoliths (Fig 26a, b), or within the xenoliths themselves (Fig 26c). Within larger duplex structures, smaller duplex structures occur as imbricates (Fig 26b, Fig 32c). Duplex structures are also apparent at the microscopic scale (Fig 21e). The scale invariance and frequency of these structures imply that the geometry of the Knaben Zone as a whole reflects a network of duplex structures, as evident from the structural pattern on the geological map and profiles (Fig 21e, Map 2). As a result of the duplex network, the deformation zones appear as weakly weaving, anastomosing N-S striking structures on the map.

Fig 27a shows the data collected from duplex structures across the Knaben Zone. The intersection between the shallow and steep plane of a duplex structure gives a point, referred to as the ramp intersection. Measurements, covering the whole Knaben Zone, show that the majority of ramp intersections cluster in the northern and southern hemisphere of the stereonet. On this basis, the inflection axis of the duplexes is generally N-S striking.

Together with kinematic indicators, such as sigma clasts, asymmetric or vergent small-folds, imbricate structures and shear bands, the duplex structures are interpreted to indicate top-to-W kinematics (Fig 27b).

The duplex structures appear as ductile, melt-involving structures. As mentioned above, the granitoid rocks follow the foliation within the xenoliths, and ramping duplex structures involve the granitoid rocks and xenoliths. Top-to-the-W(-NW) structures associated with duplex structures are found within the xenoliths (Fig 26b), along the deformed contacts between granitoid rocks and the xenoliths (Fig 26a) and within structures cutting the granitoid rocks (Fig 14d). This suggests that the duplex structures and corresponding top-to-the-W kinematics have been important for the geological evolution, at least syn-emplacement and post-emplacement.

Folds

Folding in the Knaben Zone is not easily systematized. Magmatic processes interacting with, and post-dated by, tectonic processes are likely to cause a chaotic pattern and, in addition, there are pre-existing structures in the xenoliths.

In this study, the number of observed folds in the Knaben Zone are limited, leading to a rather small dataset (Fig 28a). Open folds along boundaries (Fig 28c) between xenoliths and granitoid rocks are common. These folds show a relatively consistent fold axis, trending

approximately N-S with a shallow plunge, with a few observations overlapping with Lysberg's (1976) observations.

Folds within the xenoliths are typically isoclinal, or occasionally ptygmatic within the migmatite xenoliths (Fig 28d).The kinematics deduced from the isoclinal folds, and tight vergent folds, do to some degree correspond to top-to-the-W kinematics (Fig 28d, e), but there is some variation, indicating that some structures were pre-existing.

Small xenoliths, mainly amphibolite, engulfed within the porphyritic granite are complexly folded and twisted, probably as a result of magmatic flow (Fig 28b). Fold axis measurements for these outcrops are scattered, but include a small cluster of shallow-plunging E-SE trending fold axis.

Boudinage

Boudinage structures occur at exposures with alternating thin xenolith screens and granitoid sheets, were there may be an enhanced competency contrast during deformation. Both boudinaged granitoid sheets (Fig 29) and boudinaged xenolith screens (Fig 30) occur. The former are mainly symmetrically boudinaged, while the latter can be both asymmetric (Fig 30d) or symmetric (Fig 30c). No systematic asymmetry has been deduced from the asymmetric boudinage.

The boudinage is generally lens-shaped, apart from the amphibolite boudinage in Fig 30b, which is has a ductile rectangular appearance. Neck-folds are visible in the surrounding flaser gneiss and amphibolite (Fig 29b, c, Fig 30b).

The granitoid rocks appear as boudins within the xenoliths, both in high-strain zones, with well-developed foliation in the xenoliths (Fig 29), and in zones with less strain (Fig 30a). In the high strain zones, the granitoid sheets were probably passively boudinaged, while magmatic pressure emplacing the granitoid melt into the xenoliths could be an important mechanism in the zones with less strain. This could explain the irregular and bulgy appearance of the porphyritic boudins within the amphibolite in (Fig 30a).

As shown, boudinaged granitoid rocks occur, indicating that these are less competent than the xenoliths, and vice versa. This could indicate that the structures formed before the granitoid rocks were fully crystallized and at a stage when the xenoliths were less competent. An increasingly cooling magmatic system, with continuous deformation could explain this, and is also inferred from the evolution of the foliation and lineation in the magmatic rocks presented above.

Accumulation of felsic melt in boudin-neck structures occur around occasional boudinaged xenoliths (Fig 30d). This indicates that melt was present during the deformation event that formed the boudinage structures.

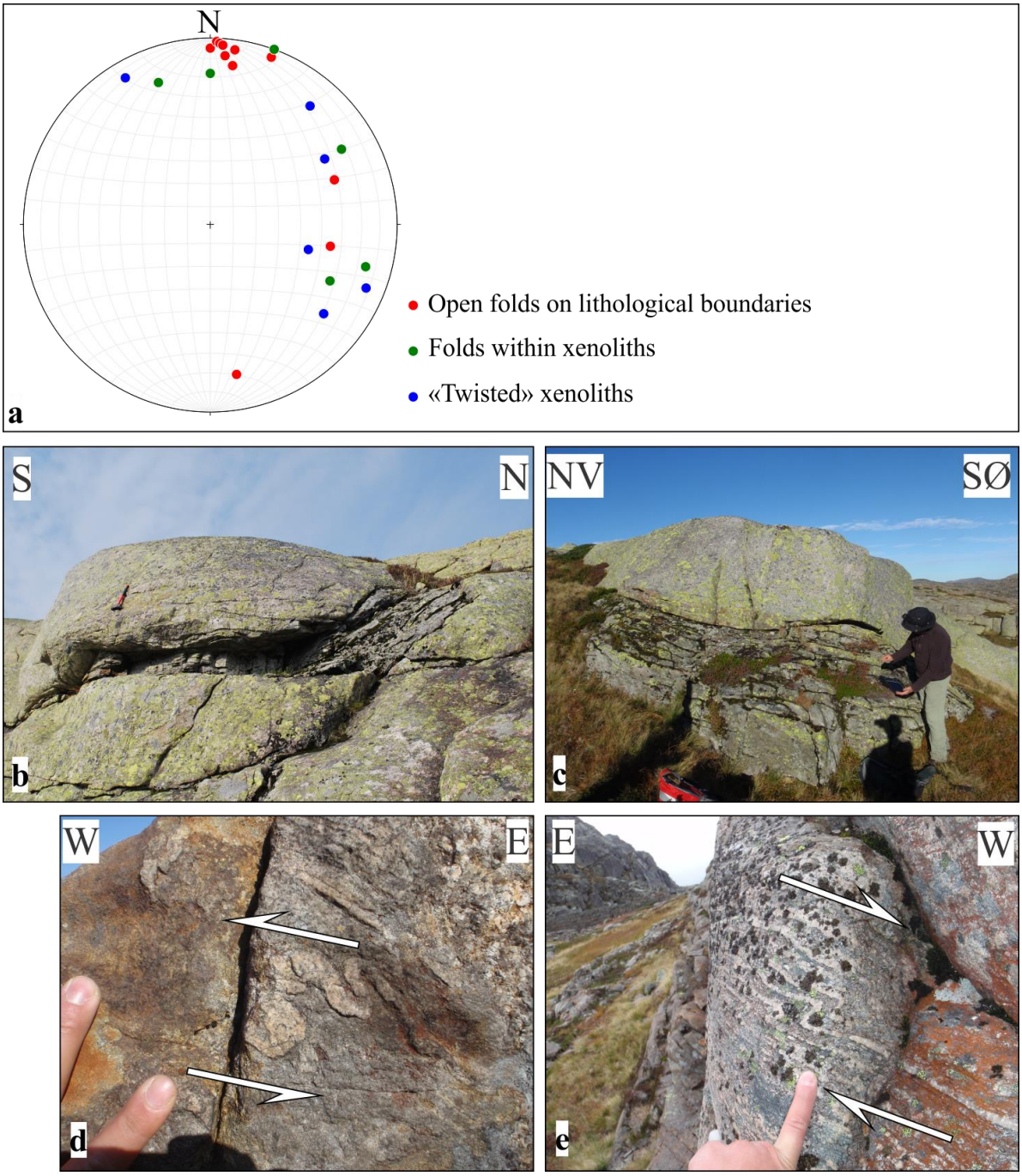

Figure 28: a) *Stereonet showing all measured fold axis in the Knaben Zone.* ***b)*** *Hammer for scale. An amphibolite xenolith (eroded, fractured rock with grey lichen) surrounded by porphyritic granite (massive rock, with more green lichen). The xenolith is complexly folded and twisted, resulting in non-consistent fold axis. (L34).* ***c)*** *Open folds on the boundary between biotite gneiss and porphyritic granite. (L19).* ***d)*** *Ptygmatic to isoclinal folding within a migmatite xenolith screen, with top-to-the-W vergens. (L13)* ***e)*** *Folded leucosome bands indicating top-to-the-W movement in a migmatite xenolith. The westward dipping foliation, together with the kinematics have been interpreted as a large scale ECC structure along the Smalavatn lineament. (L32).*

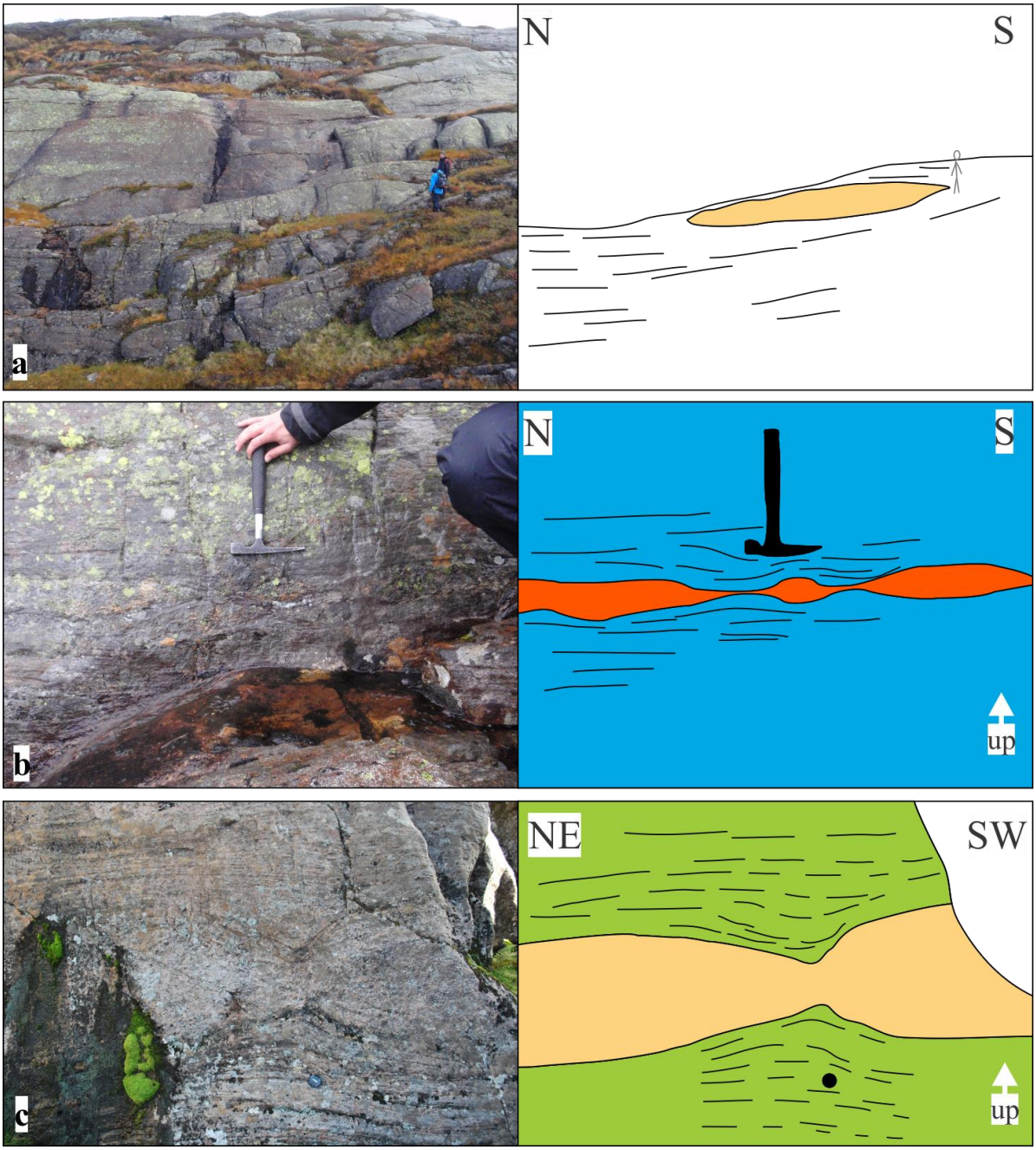

Figure 29: a) *Lensoid body of weakly deformed porphyritic granite, interpreted to be a boudin, within a thick screen of flaser gneiss and amphibolite. (L70), man for scale.* ***b)*** *Thin boudinaged vein of equigranular, weakly deformed granite, within flaser gneiss. The foliation is passively folded around the boudin neck. (L70).* ***c)*** *Weakly deformed porphyritic granite within biotite gneiss, foliation in the biotite gneiss is passively folded around the boudin neck. (L102), lens cap for scale.*

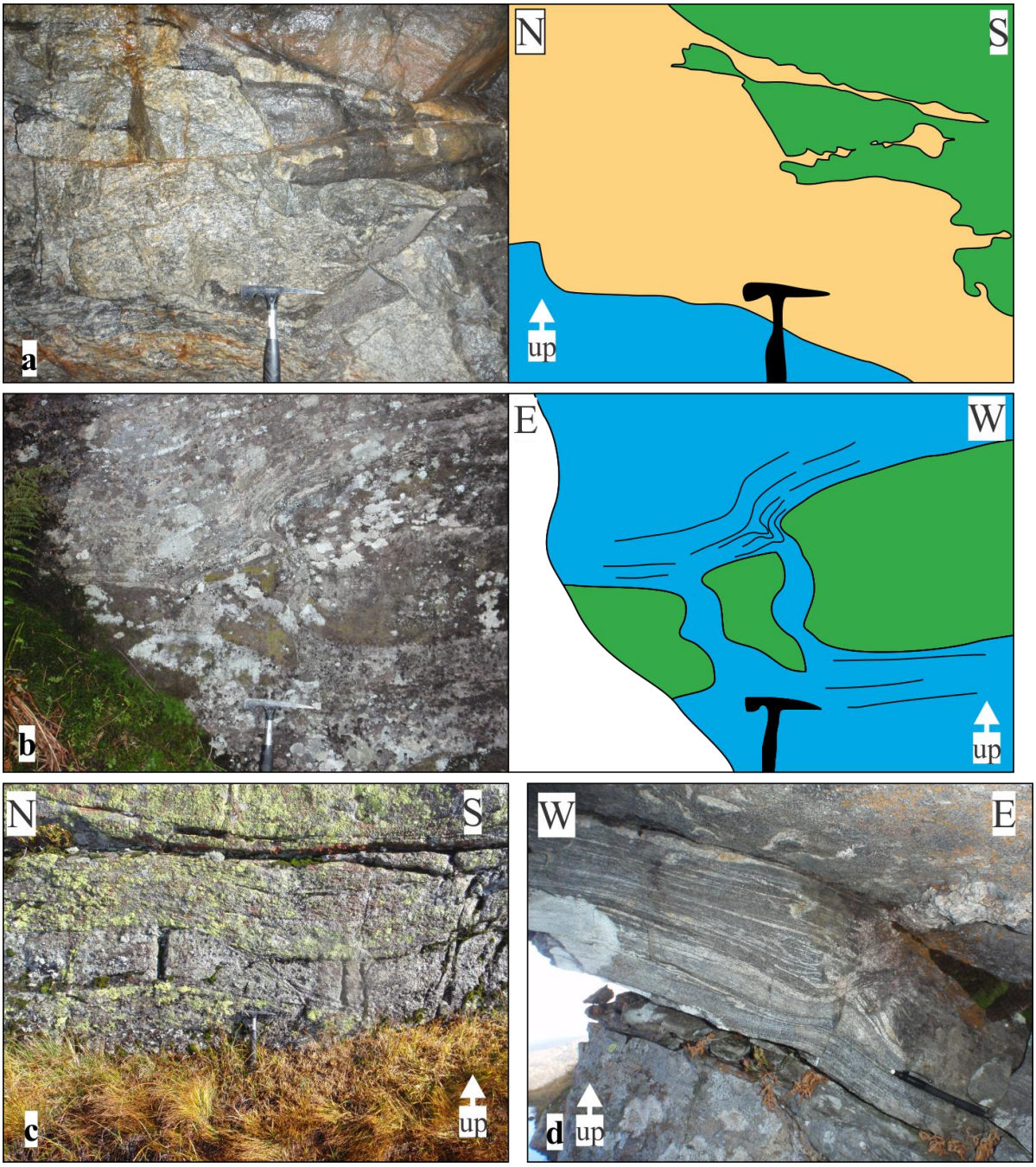

Figure 30: a) *Boudinaged veins from the porphyritic granite into amphibolite. The highly bulbous boudins are interpreted to result from forceful melt intrusion, rather than passive boudinage. (L40).* ***b)*** *Ductile, rectangular boudinaged fragments of amphibolite within flaser gneiss. The foliation is bent into the boudin neck. (L104).* ***c)*** *Asymmetric boudinaged amphibolite, indicating N-S extension. (L70).* ***d)*** *Boudinage structure in amphibolite, with accumulation of felsic melt in the boudin neck. Small-scale folds show opposing sense of shear, dominantly top to-the-W kinematics. (L75).*

SC-structures and extensional crenulation cleavage (shear bands)

Shear bands are important strain and kinematic indicators in deformation zones, and this also applies to the high-strain zones in the Knaben Zone. Their presence is related to zones of enhanced strain, along boundaries between xenoliths and granitoid rocks. These bands are observed in several varieties, cutting foliation and late veins, and influencing the granitoid melt migration and the molybdenite deposits.

Extensional crenulation cleavage (ECC), as described by Platt and Vissers (1980), is the most commonly observed shear band in the Knaben Zone. ECC-fabric defined by the distinct foliation in the flaser gneiss is shown in (Fig 31b). Shear bands are not well developed within the coarse-grained granitoid rocks, and they become more apparent when the foliation is well developed, or when cutting marker veins. Fig 31c shows ECC fabric cutting a pegmatite vein parallel to the foliation in the porphyritic granite, with 20cm apparent displacement along a poorly developed biotite surface, while the porphyritic granite itself is only weakly deformed, indicating deformation in a porphyritic granite that is not fully crystallized.

A thin mylonitic zone within the porphyritic granite shows similar ECC-fabric (Fig 24d), indicating top-to-the-W kinematics. A more flat-lying shear band within the porphyritic granite, cutting an aplite and a pegmatite vein, is shown in (Fig 31a). SC-fabric (Berthé et al., 1979) is less commonly documented than ECC-fabric, which is expected, as ECC fabric overprints SC-structures associated with the initial deformation (Fig 32).

As previously discussed, most of the foliation (both magmatic and tectonic) observed within the Knaben Zone is moderately eastward-dipping. However, a few observations of westward dipping foliation are restricted to several exposures along the Smalavatn lineament (Fig 23a, Fig 28e). This is a NE-SW oriented lineament following Smalavatn and extending a few kilometres from both ends of the lake (Fig 5). Other than alongside the lake, the lineament is filled with boulders and vegetation, obscuring the outcrop. Limited, but consistent, top-to-the-W kinematic indicators, give an apparent extensional kinematic in this structure. This is interpreted to represent a large scale ECC-structure, that cuts and displaces the east-dipping foliation along the Smalavatn lineament. The lineament is likely to be reactivated at a later stage, resulting in the brittle structures occurring in the prolongation of the lineament (Fig 34).

As described above, the granitoid rocks follow the foliation in the xenoliths and exploit structures related to top-to-W deformation (Fig 31d, Fig 14d). In addition, the granitoids are deformed in a top-to-W manner (Fig 32e, f). This indicates synkinematic intrusion of the granitoid melt.

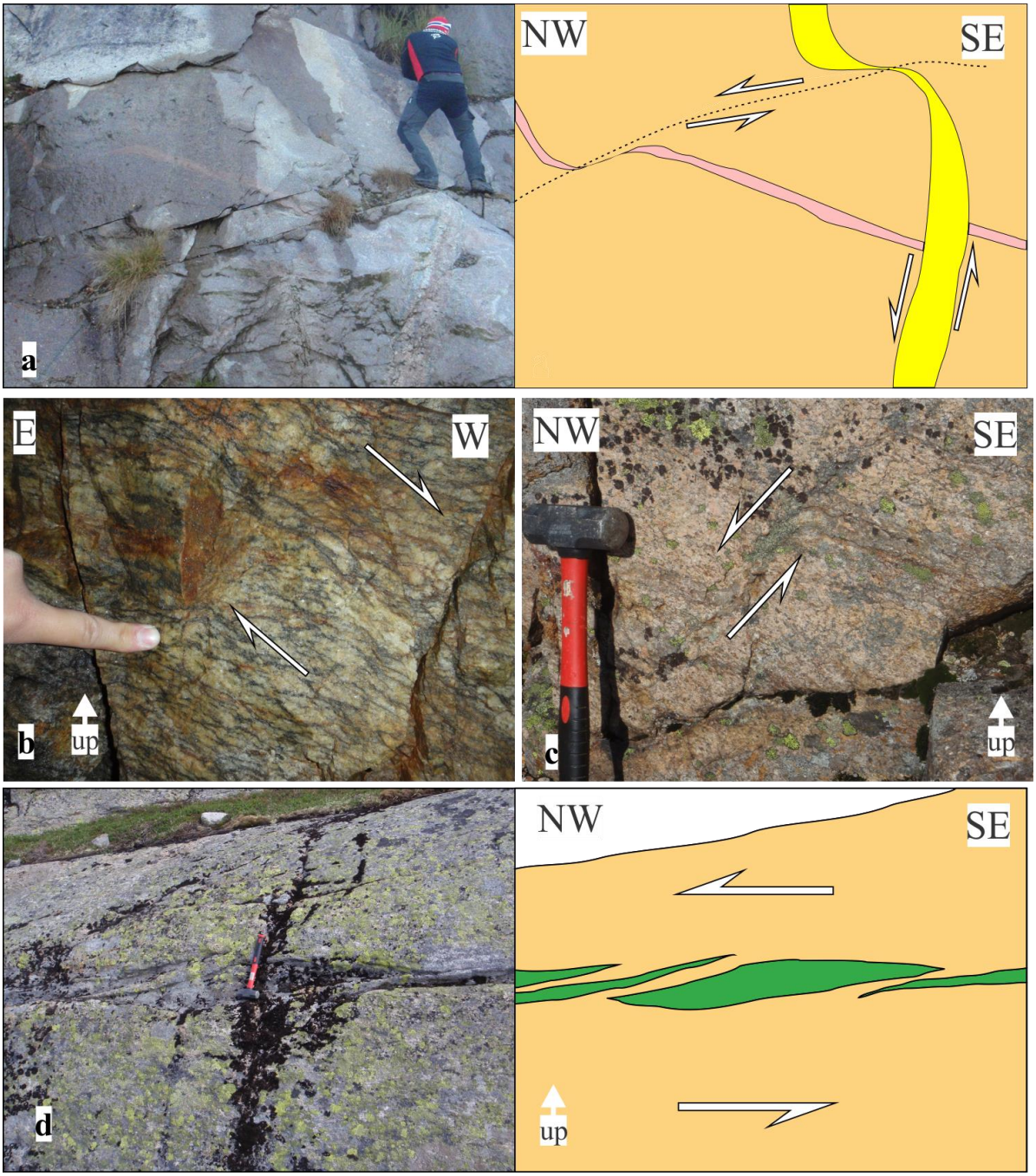

Figure 31: a) *A subvertical pegmatite displaces an aplite vein in a sinistral fashion. Both the pegmatite and the aplite are cut by a later ductile shear band, with top-to-the NW kinematics. The shear zones dip shallowly to the east, but are optically obscured due to the geometry of the outcrop. (L59)* ***b)*** *Weakly developed ECC-fabric, cutting the foliation in flaser gneiss. Knaben 1 mine, NE adit.* ***c)*** *ECC cutting a sub-horizontal pegmatite within porphyritic granite, in a top-to-the-W manner. (L16).* ***d)*** *Veins from the porphyritic granite cut an amphibolite xenolith. The orientation of the porphyritic granite veins is similar to the orientation of ECC-fabric. (L74).*

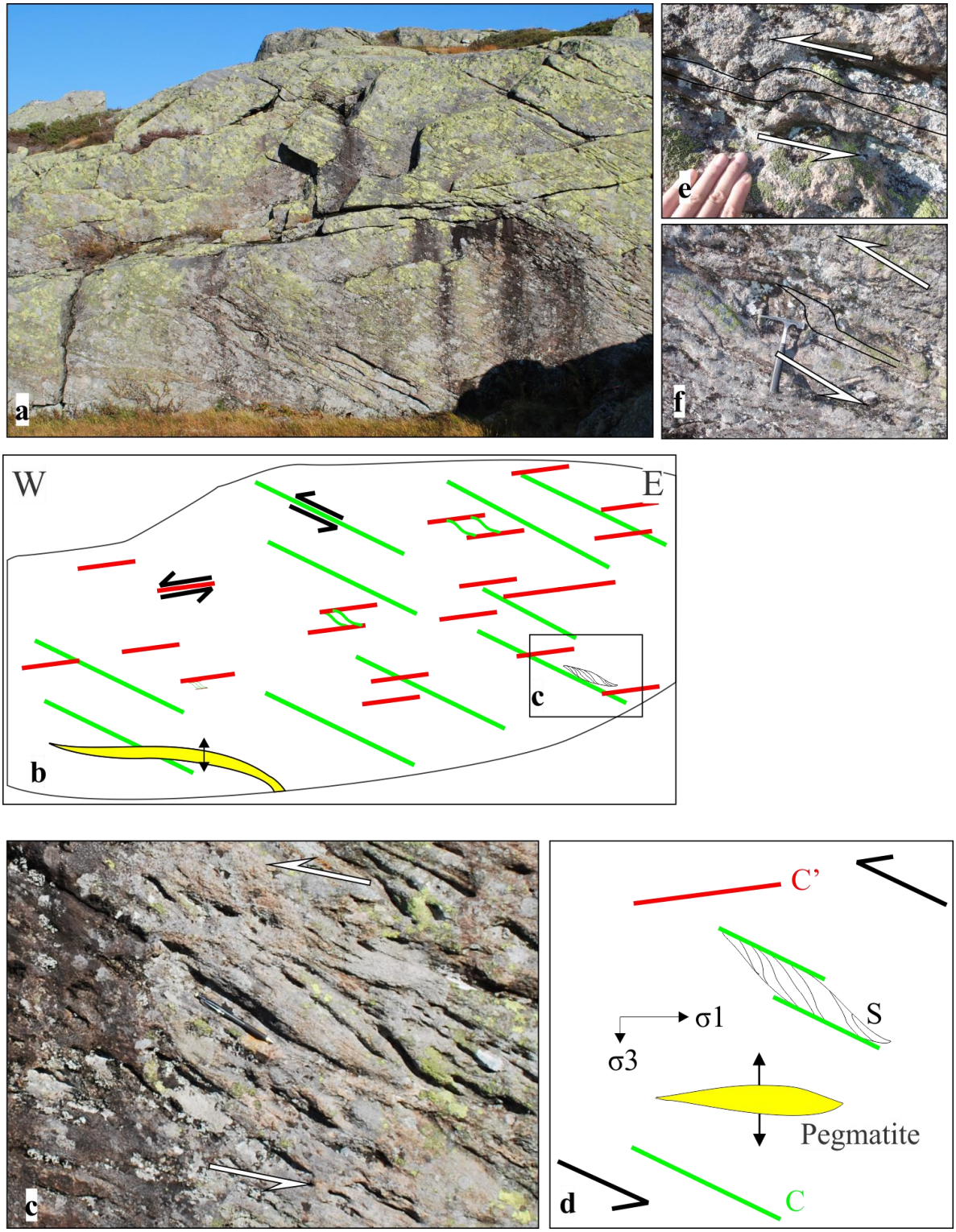

Figure 32: *The whole outcrop (L88) is shown in* ***(a)****, and the important structures are sketched in* ***(b)****. Close up photos of structures are shown in* ***(c), (e), (f)****. Kinematics, structures and principle stress axis are shown in* ***(d)****. This outcrop is a well-exposed high strain zone, consisting mainly of a variety of biotite gneiss and thin sheets of porphyritic granite. SC and ECC-fabrics are weathered, and easily recognised, indicating top-to-the-W movement. Weakly deformed thin sheets of porphyritic granite intrude along the C-fabrics, and are folded, indicating top-to-W kinematics (e and f). As indicated in (b) a pegmatitic vein intrudes sub horizontally suggesting a sub-vertical least principle stress axis.*

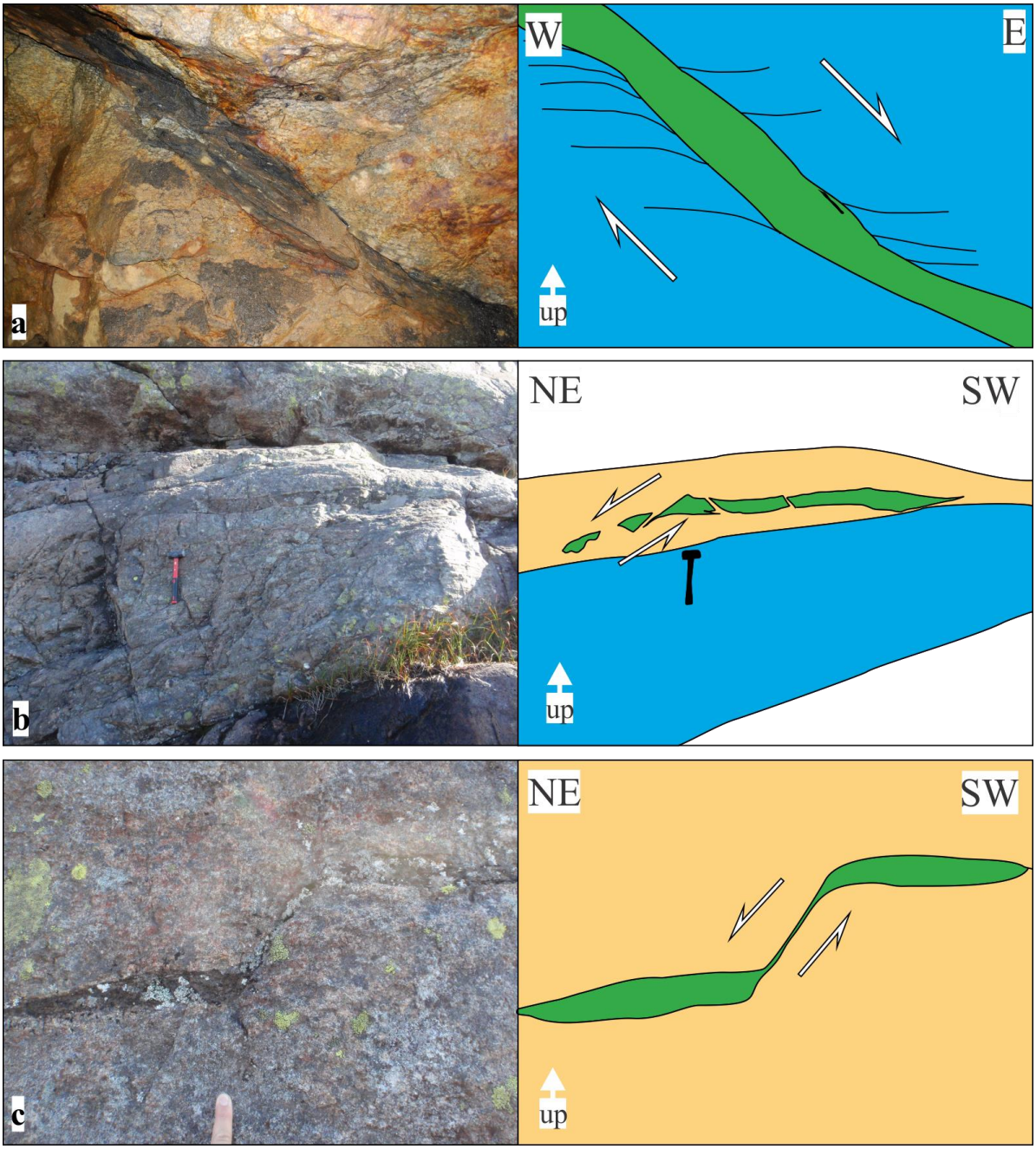

Figure 33: a) *A biotitized amphibolite screen in the roof of the north adit of the Knaben 1 mine. The foliation of the surrounding flaser gneiss is folded, indicating down towards E extension. Pen for scale.* ***b)*** *An amphibolite xenolith within porphyritic granite, close to a larger flaser gneiss screen, at L6. The amphibolite screen is boudinaged into angular pieces. The left part of the xenolith is dragged, indicating down towards NE extension.* ***c)*** *A small amphibolite xenolith within porphyritic granite at L30. The xenolith is cut by a shear band indicating down towards NE extension. The surrounding porphyritic granite is only weakly deformed, indicating syn-magmatic, ductile deformation.*

3.3.3 Extensional ductile structures

Limited evidence for a relatively late ductile extension, coaxial to the approximate E-W-compression, but with an extension down towards the SE, is observed at a small number of localities. The disposition of these structures suggests an extensional phase postdating the top-to-the-W kinematics.

Well exposed in the roof of the north end of the Knaben 1 mine is a 20-30cm thick biotitized amphibolite screen. The amphibolite screen, dipping 40-50° eastwards, apparently cuts through the surrounding flaser gneiss with an eastward foliation dipping roughly 20°. The flaser gneiss foliation is dragged along the amphibolite screen, in a dextral, normal fault manner, indicating top-to-the-E kinematics (Fig 33a).

Two localities (L30 and L6) show thin amphibolite screens, within weakly deformed porphyritic granite, cut by shear bands, with drag folds indicating ductile down towards NE extension (Fig 33b, c). These observations do not fit the general kinematics, but show the ductile behaviour of the thin amphibolite xenoliths in the granitoid melt.

3.3.4 Field relations and map scale structures

The topography in the Knaben Zone is influenced by the heterogeneity, with weaker anisotropic xenoliths and more resistant massive granitoid rocks. Two different types of terrain forms are therefore present in the Knaben area. Firstly, where there is little or no deformation, or the presence of xenoliths, the granite is homogeneous and the topography is rounded. However, where there are xenoliths and the development of strain zones, the terrain has a distinct stepped appearance (Fig 27c, d, e).

Hence, ridges in the terrain, defined by the xenolith screens and deformation zones, can be followed along the strike, and at several localities, the screens are seen to merge together (Fig 27c, d). This forms a network of xenolith screens and granitoid sheets. The duplex geometry of the screens appears to lead to the geometry, and to the anastomosing network of shear zones seen on the geological map (Map 2, Fig 5). Such nuances in the variation of topographical form allow a more detailed mapping of the anastomosing duplex structures.

3.3.5 Brittle structures

Steeply dipping brittle structures and mafic dykes cut through the granitoid rocks, xenoliths and all of the ductile structures discussed above, and are clearly younger and not related to the evolution of the granitoid rocks or the molybdenite deposits (Fig 34). This conclusion is also drawn by previous authors (Lysberg, 1976; Gvein and Rui, 1980). These structures have been given limited attention in this project, but will be presented shortly here.

Approximately ENE-WSW striking, 70-80° dipping mafic dykes were known from previous maps (Lysberg, 1976). Their orientation is similar to the regionally related Hunnedalen dykes which have been dated to approximately 850Ma (Mauer and Verschure, 1998; Walderhaug et al., 1999). Five dykes, or fragments of dykes, have been mapped in the field (Map 1, Fig 34b). The dykes are seen as pronounced, approximately 10m wide and weathered steps in the terrain cutting through all other lithologies, with remains of the actual dyke on the walls, and rock scree within the step (Fig 35f). The two northernmost dykes both stop abruptly towards either side of a pronounced N-S striking lineament, parallel to a screen of deformed biotite gneiss. The orientation of the western part of the dyke cutting the south end of Sandtjørn is anomalously ESE-WNW oriented, but this is consistent with variations in the dyke orientations presented by Mauer and Verschure (1998).

The dyke appears as a dark grey, massive fine-grained rock, with some visible biotite and feldspar, and it breaks into sharp pieces in hand specimen. In thin section, phenocrysts of subhedral to euhedral randomly oriented plagioclase are estimated to a modal amount of 50%. The plagioclase is approximately 0.5mm in grain size, but can reach 1mm. Plagioclase zonation, Carlsbad-, and skeletal swallow-tale twinning is common, and the grains are moderately to strongly altered (Fig 35d). Brown, anhedral biotite grains are generally below 0.5mm. Fine grained biotite and epidote give the rock an altered appearance. Domains are completely occupied by epidote and biotite. Such domains could represent completely altered mafic minerals, as is pointed out for the Hunnedalen dykes by Mauer and Verschure (1998). Opaque grains constitute the majority of the remaining minerals. A distinct veinlet with amphibole, calcite, epidote and titanite grains cuts the thin section. Mauer and Verschure (1998) classify the dykes as monzonoritic, and their geochemical results are similar to results in this study (presented below). The alteration of the dykes observed in this study obscure the original mineral assembly, and they will be referred to as mafic dykes.

There are several distinct lineaments dissecting the Knaben Zone (Fig 34c, e), and are referred to as faults, shear zones or crush zones by previous authors (Leake, 1972; Lysberg, 1976). The zones are 5-20m wide depressions in the terrain, filled will rock scree and vegetation, hampering detailed geological investigations. No displacement has been determined along these zones. Rocks within these zones are typically altered, with red k-feldspar, chloritified biotite and saussuritised plagioclase (Fig 35e). E-W-trending shear zones are the most abundant, and most pronounced is the lineament following the valley with the road to Knaben village, following up the stream to Finndalsvatnet (Fig 34d, e), referred to as "Råtagangen" by Leake (1972) (Fig 34). According to Lysberg (1976), Råtagangen cuts the southernmost mafic dyke a few kilometres west of Knaben. Irregular veins with vuggy quartz occur sporadically along the lineament cutting Finndalsvatnet (Fig 35a).

A less pronounced shear zone occurs along prolongation of Smalavatn. A similarly oriented lineament occurs south of Bergetjødn (Fig 34e). These lineaments could represent reactivated large scale ECC structures, as defined for the Smalavatn lineament above. The shear zone cutting the Hommen mine in the south is oriented ESE-WNW.

Late brittle fractures, or joints, are common (Fig 34d), with no obvious displacement, and are typically oriented approximately N-S. North of the lower Roma mine, conjugate fractures striking ENE-WSW occur in a conjugate manner (Fig 35bc). These fractures are filled with milky quartz, and lie within the shear zone south of Bergetjødn.

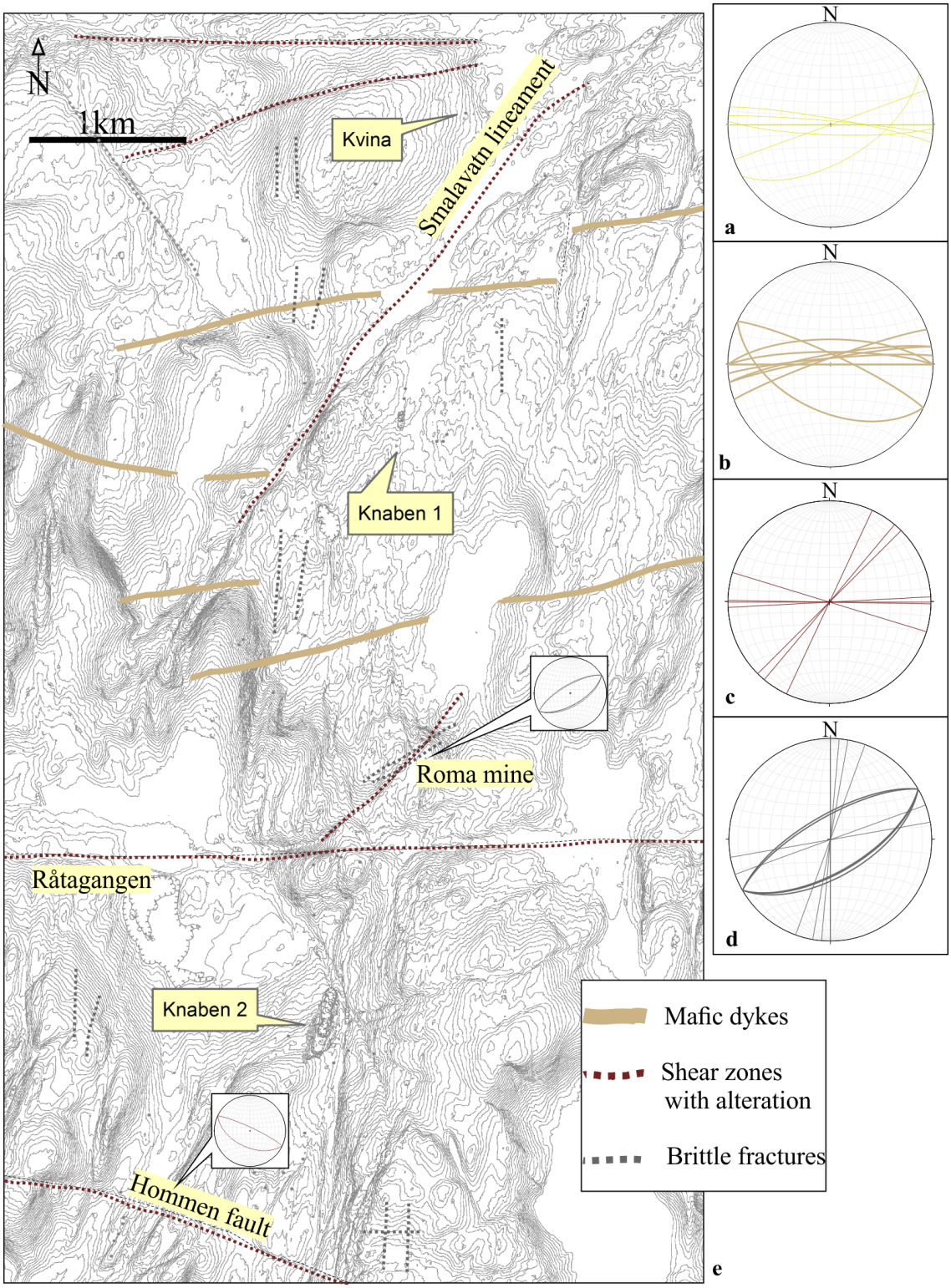

Figure 34: a) *Stereonet displaying sub-vertical, E-W striking, non-mineralised pegmatites.* ***b)*** *Stereonet displaying measurements of the mafic dykes.* ***c)*** *Stereonet displaying directions of major shear zones, mainly obtained from analysis of ortho-photography.* ***d)*** *Stereonet displaying late, brittle fractures measured in field.* ***e)*** *Map showing late to post-Sveconorwegian brittle structures. The orientation and petrology of the mafic dykes correlate well with the Hunnedalen dykes dated 850Ma (Walderhaug et al., 1999). The major shear zones that are related to alteration are marked dark brown. Brittle fractures (grey) are mainly N-S-striking, with large variation. Measurements from anomalously oriented Hommen fault and quartz filled fractures close to Roma mine are shown.*

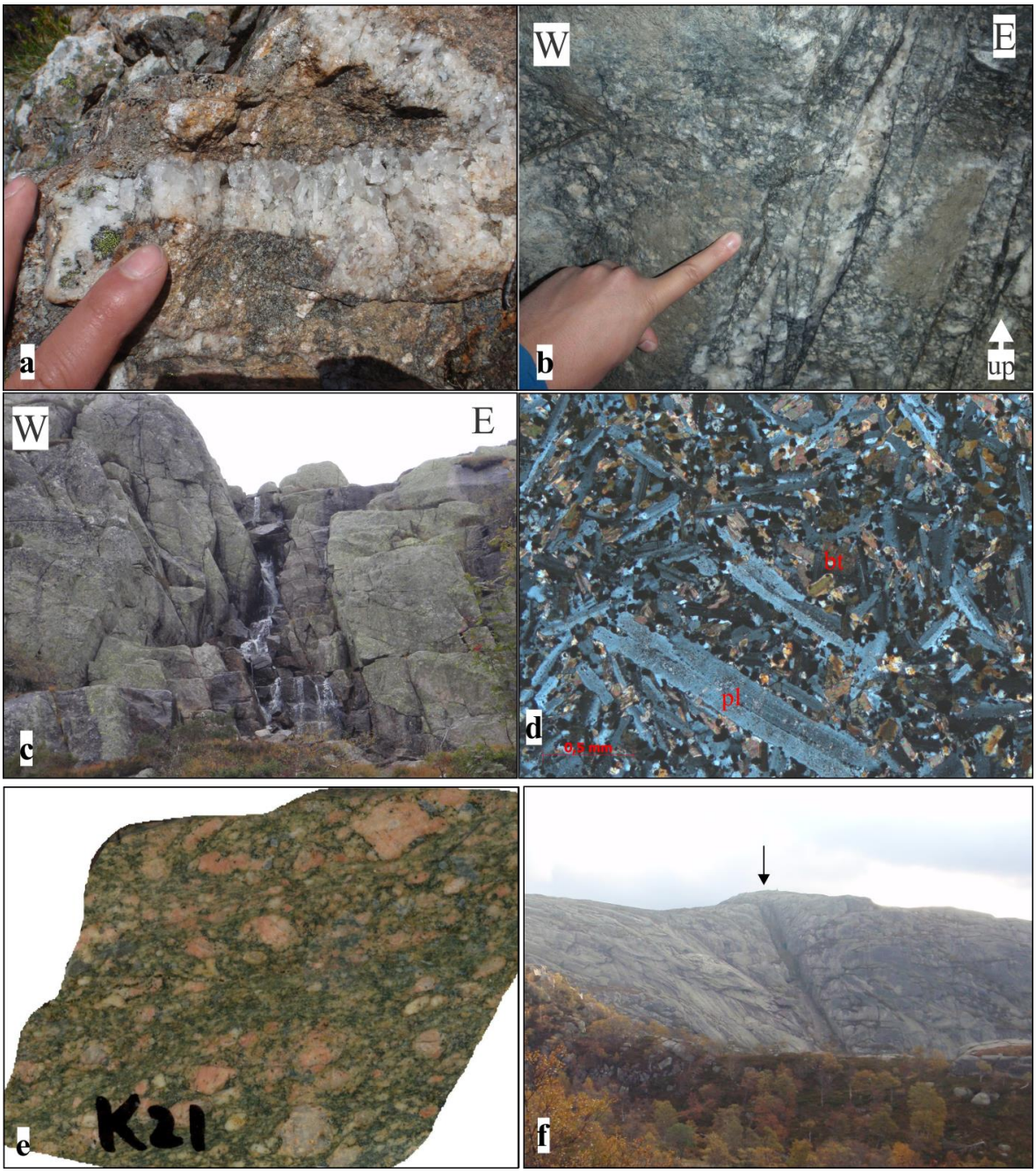

Figure 35: a) *Breccia within the Finndalsvannet lineament, with bridging quartz veins filling fractures. (L63).* ***b)*** *Brittle fractures in the lower Roma mine filled with milky quartz.* ***c)*** *Conjugate fracture pattern seen from the Lower Roma mine, corresponding to the fractures in figure b). Cliff is approximately 15m high.* ***d)*** *Microphoto (xpl) from a sample of the mafic dyke at L44, sample K117. Skeletal swallow tale twinning is evident in the plagioclase phenocrysts.* ***e)*** *Altered mylonitic porphyritic granite from L8, sample K21.* ***f)*** *View of the E-W striking mafic dyke, south of Ørnehommen mine. The dyke is 10m wide.*

3.4 Molybdenite mineralisation

As pointed out in previous studies (Lysberg, 1976; Gvein and Rui, 1980), the concentration of molybdenite along the Knaben Zone is striking. Another notable feature is the concentration of molybdenite along, or up to 1km west of, the western part of the xenolith rich zone, especially in the southern half of the mapped area (Fig 5,Map 1). The deposits west of the xenolith rich zone are still directly related to, or close to, sheets of granitoid variations or occasional xenoliths.

The molybdenite deposits generally occur in two groups: disseminated within the grey granite (Fig 11b), or within thrust-related structures.

The disseminated deposits give the most economical deposits, as exploited in the Knaben 2 mine. Specks of disseminated molybdenite are present, independent of the size of the grey granite sheets. As described above, the grey granite is variably deformed and hence the foliation is variably developed. When deformed, the molybdenite grains are generally elongated with the deformation and foliation, and concentrated along the foliation planes.

When directly related to structures, the molybdenite is more concentrated and often coarse-grained. The most common structure-related molybdenite deposits occur along the foliation planes (Fig 36a, b) or related to subhorizontal thrust-related pegmatites (Fig 36b, c and f, Fig 16e). In addition, molybdenite occurs in fold hinges (Fig 27f), boudin-structures (Fig 15e) and in pressure shadows around deformed phenocrysts (Fig 36d). The subhorizontal molybdenite bearing pegmatites are described above in a separate section, and are generally deformed (Fig 15, 16). Biotite rich foliation planes displaying stretching lineations typically contain specks of molybdenite, when within, or close to a sheet of grey granite (Fig 25a, b).

Minor molybdenite deposits occur within the porphyritic granite, but these deposits are related to biotite-rich schlieren bands parallel to the general foliation (Fig 36e), or spatially close to a sheet of grey granite or pegmatite vein. The biotite rich schlieren bands are rustier and more finely grained than the surrounding porphyritic granite, and appear similar to thin xenolith screens.

No direct relationship between the grey granite and the molybdenite bearing pegmatites has been observed. A genetic relationship between the two is the most obvious conclusion, and has been noted by previous workers (Lysberg, 1976; Gvein and Rui, 1980). The amount of grey granite is largest in the southern half of the Knaben Zone, related to the Knaben 2 mine (Map 1, Fig 5). In the northern half of the Knaben Zone, thrust related pegmatites are the most abundant molybdenite deposits, and the anomalously large Kvina mine pegmatite occurs here, together with a few other molybdenite bearing large pegmatites.

In thin section the molybdenite typically occurs as laths, elongated with the foliation when present (Fig 9e, Fig 11c, d). As previously mentioned, calcite is commonly in contact with parts of the molybdenite grain. Clusters of molybdenite and other sulphide minerals are common when the foliation is well developed.

The presence of molybdenite within the porphyritic granite in the vicinity of grey granite sheets and mineralised pegmatites points towards a component of metasomatosis. A lower susceptibility is measured in the mineralised parts of the porphyritic granite. As pointed out by Müller (2014), the large majority of the quartz is magmatic, and there is little evidence for significant hydrothermal activity. The occurrence of fluid inclusions (Fig 11e) and calcite related to the molybdenite, indicates a component of metasomatosis, but not with significant bearing on the molybdenite deposits.

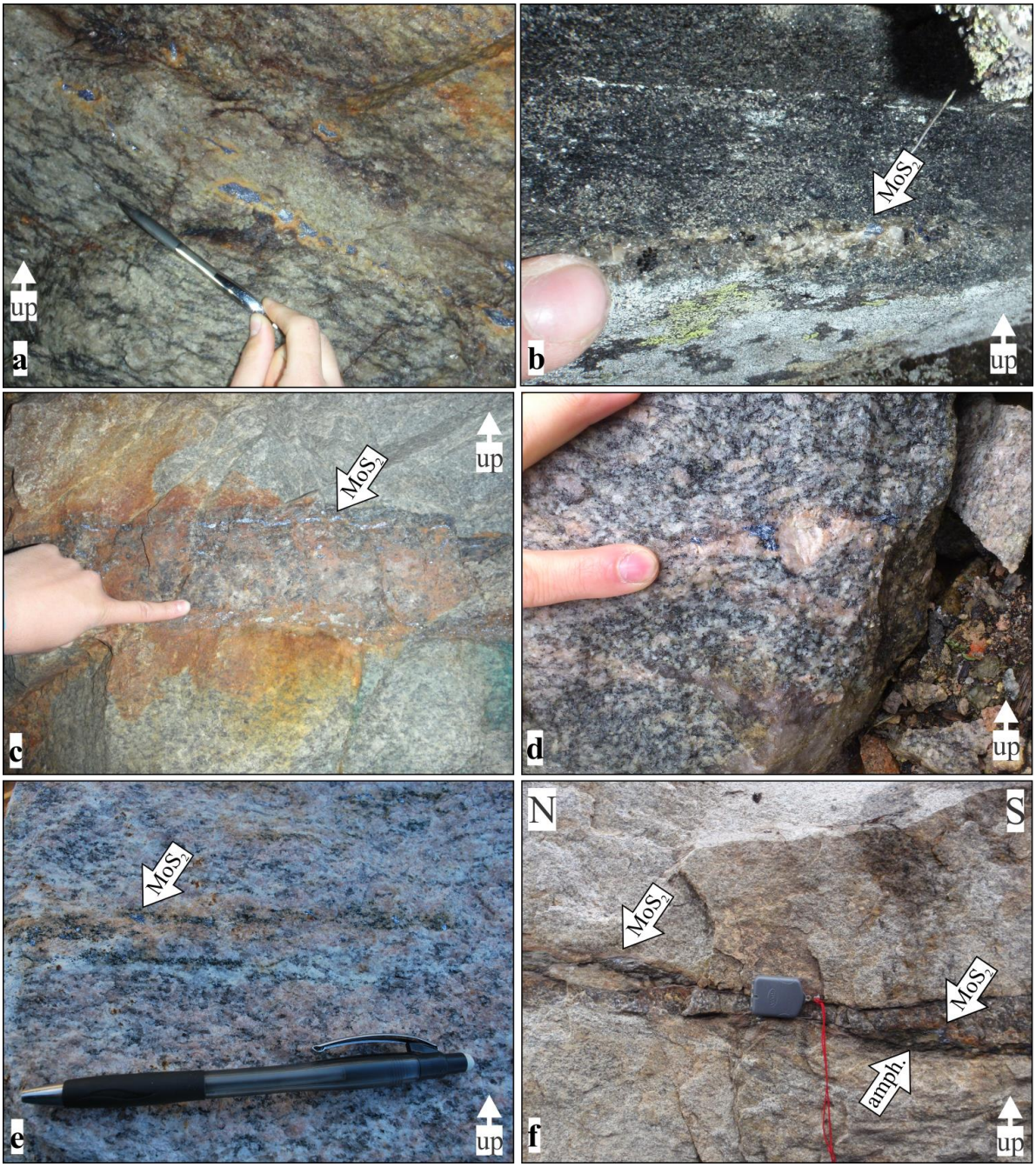

Figure 36: a) *Knaben 1 mine, NE adit. Elongated molybdenite specks within the flaser gneiss foliation. A grey granite vein without foliation lies parallel to the flaser gneiss, and close to the deposits.* ***b)*** *A mineralised, sub-horizontal pegmatite vein within the foliation in the amphibolite. (L91).* ***c)*** *Sub-horizontal, deformed quartz rich, molybdenite-bearing pegmatite vein in porphyritic granite. Note the ribbon grains of molybdenite on the rims of the pegmatite. (Knaben 2).* ***d)*** *Molybdenite is located in the pressure shadows, around a sigma clast within deformed porphyritic granite. (Open pit, Knaben 2)* ***e)*** *Molybdenite specks clearly related to a rusty, mafic schlieren band, in a leucocratic granite. (L57).* ***f)*** *A mineralised, sub-horizontal quartz rich pegmatite cuts through the porphyritic granite. The pegmatite follows a thin amphibolite xenolith. (L61).*

3.5 Magnetic measurements

The marked contrast in susceptibility between the porphyritic granite and the grey granite (Appendix 4), as previously pointed out, has been an important tool for distinguishing the two units in the field. In addition, the mineralized grey granite has a lower susceptibility than other non-mineralized granitoid varieties, and hence, very low magnetic susceptibility generally indicates occurrence of molybdenite. Susceptibility measurements for the grey granite range between $0.001*10^{-6}$ and $0.2*10^{-6}$ SI units, while the porphyritic granite and the other granitic varieties typically measure around $8*10^{-6}$. As mentioned, thin magnetite rich veins show extreme susceptibility values from $100*10^{-6}$ to $300*10^{-6}$ SI units.

Susceptibility measurements are less consistent for the xenoliths, but generally, screens directly linked to, or adjacent to molybdenite deposits show low susceptibility measurements. For field use, the susceptibility is less useful, as the xenoliths are easily recognisable in field.

A preliminary magnetic study has been carried out, as a project for a university course, at the paleomagnetic laboratory at NGU. An interesting outcome of this study was the inclination of the natural remanent magnetism (NRM) for the porphyritic granite on each side of the Knaben Zone. The NRM inclination from the east side of the Knaben Zone (sample K30) deviates with approximately 90° from the western side (sample K26) (Appendix 4, Map 3). As only two samples are analysed weight should not be attached to these results. However, it is plausible that NRM measurements could be used to distinguish separate intrusions making up the SMB.

3.6 Geochemistry

The characteristic geochemical features for the different lithologies are presented below, and the raw data is shown in the Digital Appendix. In general, the geochemical results are of little value for drawing detailed petrogenetic conclusions within the scope of this thesis, due to the highly evolved signatures for the granitoid rocks, and the large variations in the xenoliths.

3.6.1 Granitoid rocks

Major elements

High SiO_2 content, typically 70% to 77%, characterizes the granitoid rocks (Fig 38a). Most extreme is the grey granite reaching 81.9% (possibly influenced by silicification). The rocks are weakly peraluminous to metaluminous (Fig 37a). Considering the Fe-number, these rocks are generally ferroan (Fig 39a). In the MALI diagram (Fig 38a), the grey granite falls within the calc-alcalic series, while the other granitoid rocks are alkali-calcic, but this is most likely an effect of the high SiO_2 content.

The three leucogranite samples are very spread apart, and plot outside the general trend in all major element diagrams. Samples from aplitic granite sheets, deformed porphyritic granites and the quartz porphyritic granite, display similarly to the porphyritic granite. There is no obvious difference between the eastern and western porphyritic granite samples, regarding the major elements.

One sample of the mafic dyke is analysed. Its silica content is 54.1%, it is weakly peraluminous, with a high alkalinity index, ferroan and plots on the boundary line between alkali-calcic and calc-alcalic.

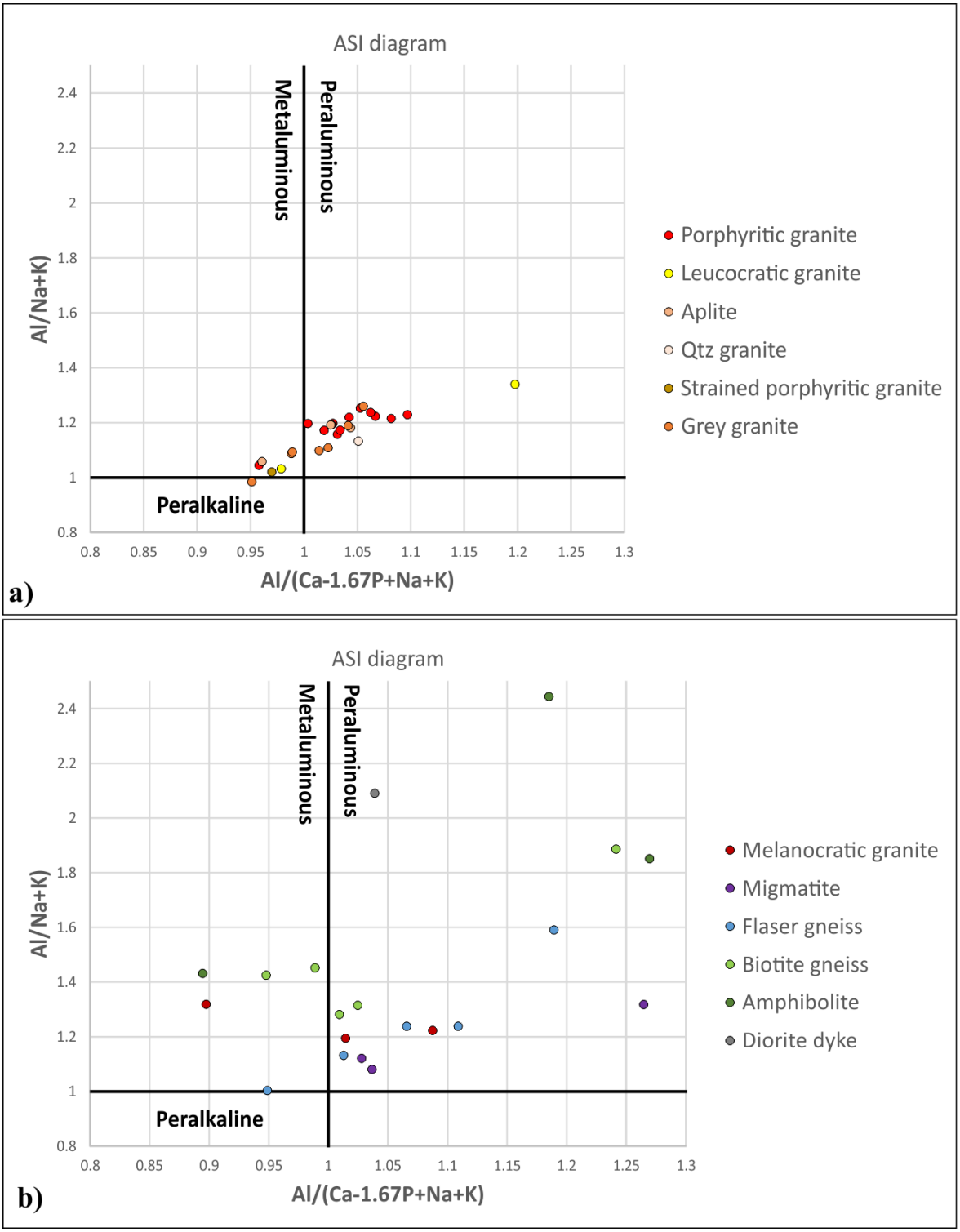

Figure 37: *Aluminium Saturation Index (ASI) diagram (Shand (1943) in Frost et al. (2001)).* ***a)*** *Granitoid rocks from the Knaben Zone, generally alkali-calcic and the most evolved calc-alkalic.* ***b)*** *Xenoliths and mafic dyke (marked "diorite dyke") from the Knaben Zone, amphibolite is more alkalic. Diagram is made using Microsoft Excel.*

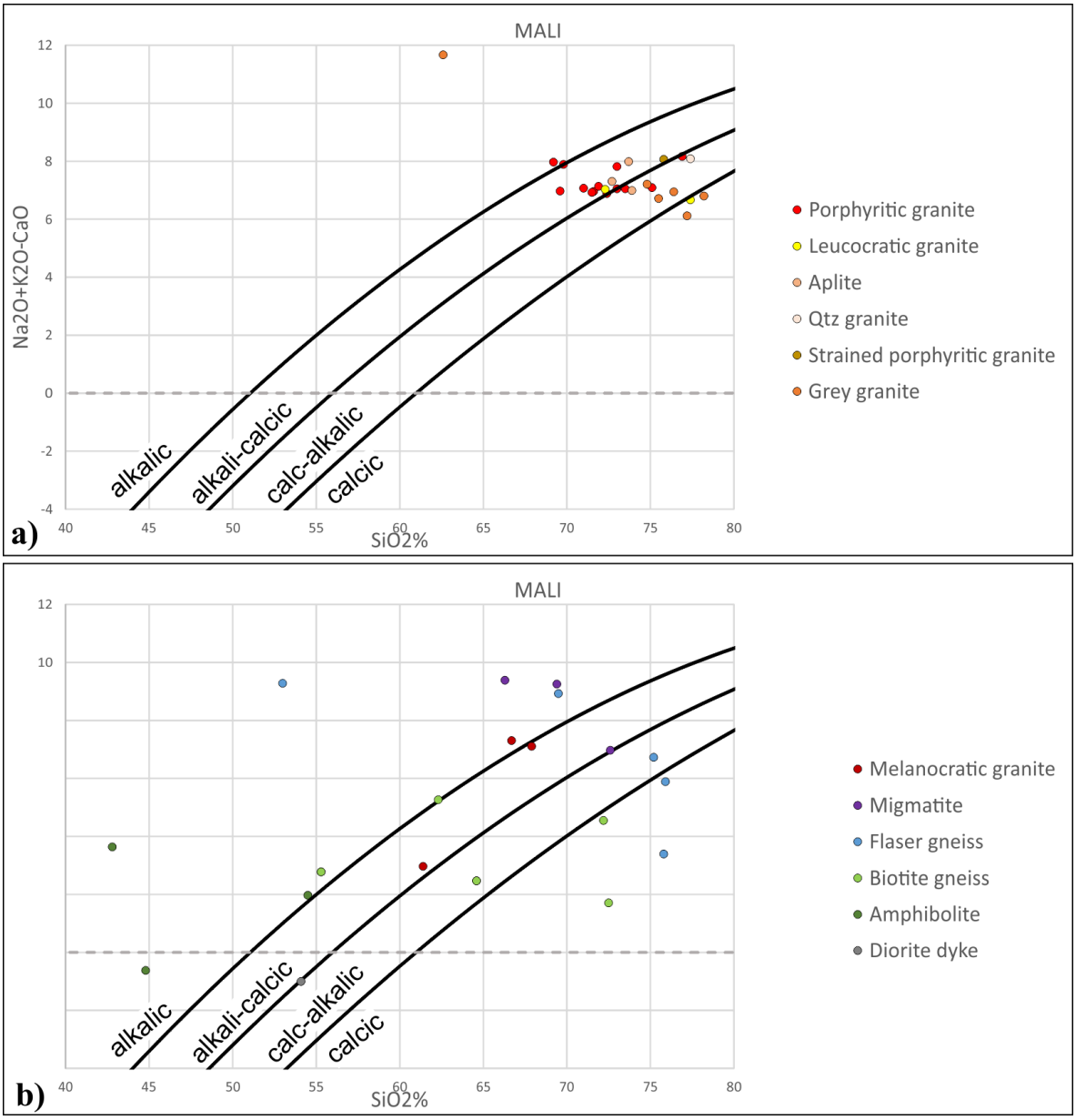

Figure 38: *Modified Alkali-Lime Index (MALI) diagram (Frost et al., 2001).* ***a)*** *Granitoid rocks from the Knaben Zone, metaluminous to weakly peraluminous.* ***b)*** *Xenoliths and mafic dyke (marked "diorite dyke") from the Knaben Zone. Diagram is made using Microsoft Excel.*

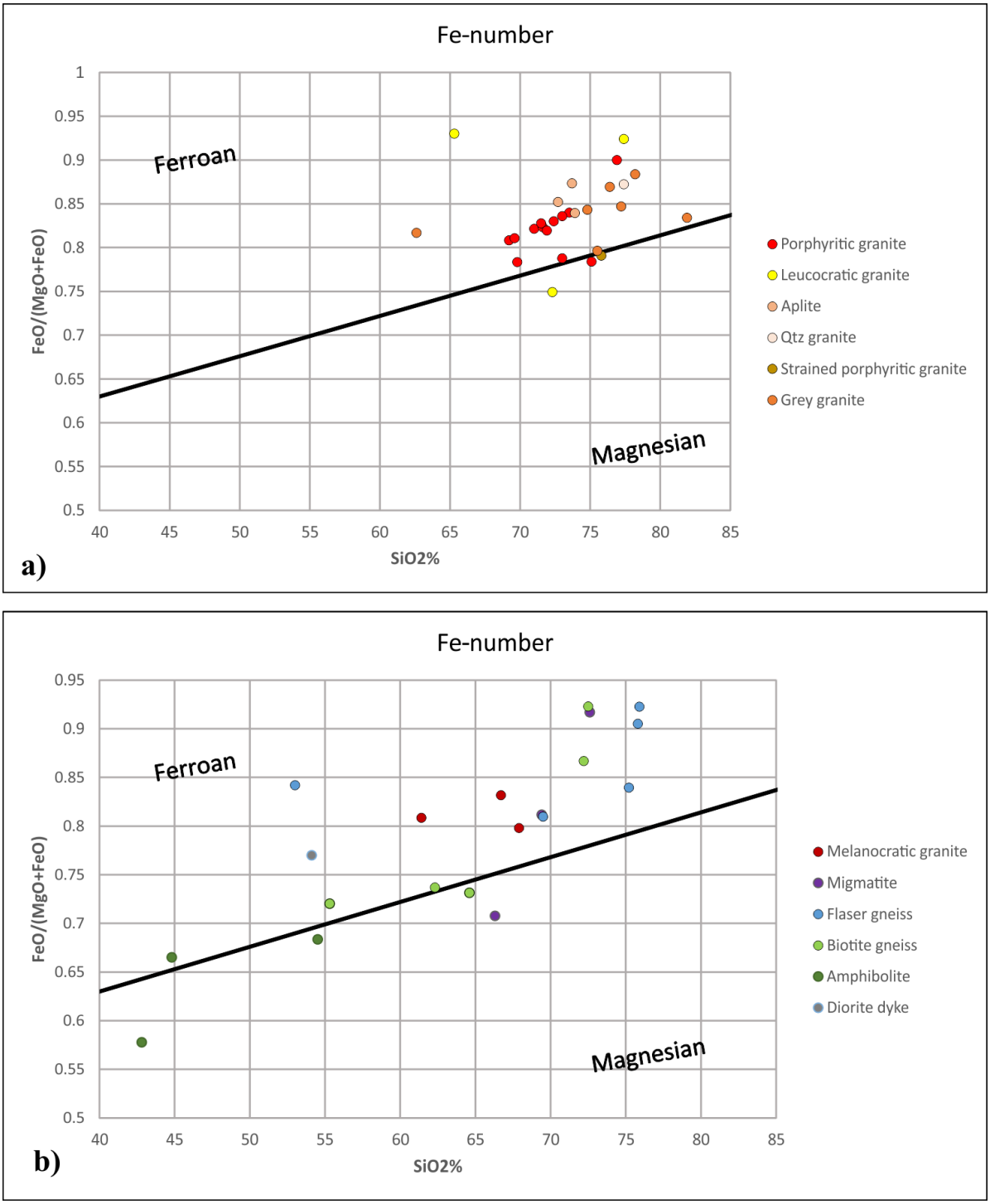

Figure 39: *Fe-number diagram (Frost et al., 2001).* ***a)*** *Granitoid rocks from the Knaben Zone, generally ferroan.* ***b)*** *Xenoliths and mafic dyke (marked "diorite dyke") from the Knaben Zone, generally ferroan. Diagram is made using Microsoft Excel.*

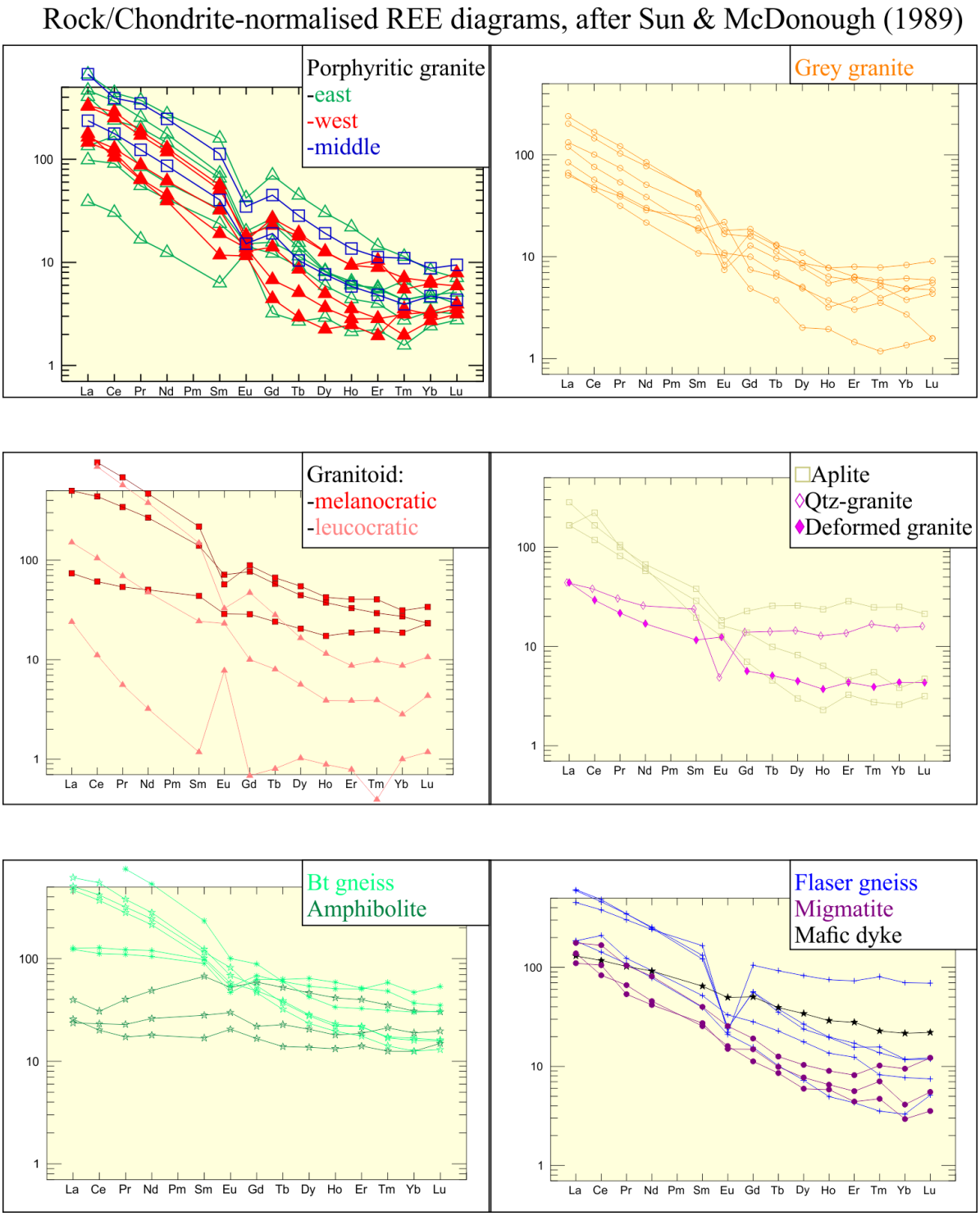

Figure 40: *Rock/chondrite normalised REE-diagrams, after Sun and McDonough (1989). Porphyritic granite is separated into samples east of the Knaben Zone, west of the Knaben Zone and within (middle) the Knaben zone. Diagrams are made using IgPet.*

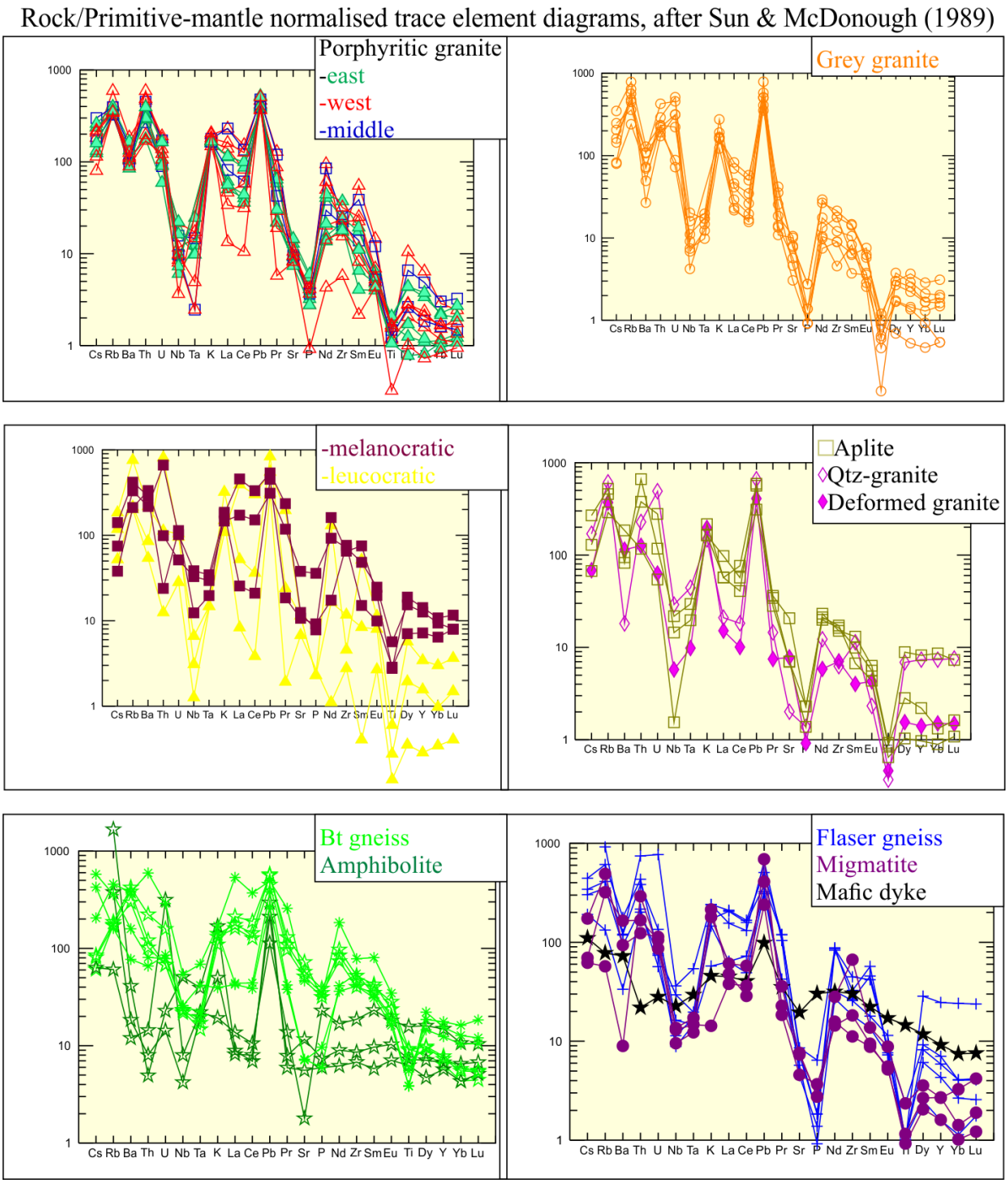

Figure 41: *Rock/primitive mantle normalised trace element diagrams, after Sun and McDonough (1989). Porphyritic granite is separated into samples east of-, , west of and within (middle) the Knaben zone. Diagrams are made using IgPet.*

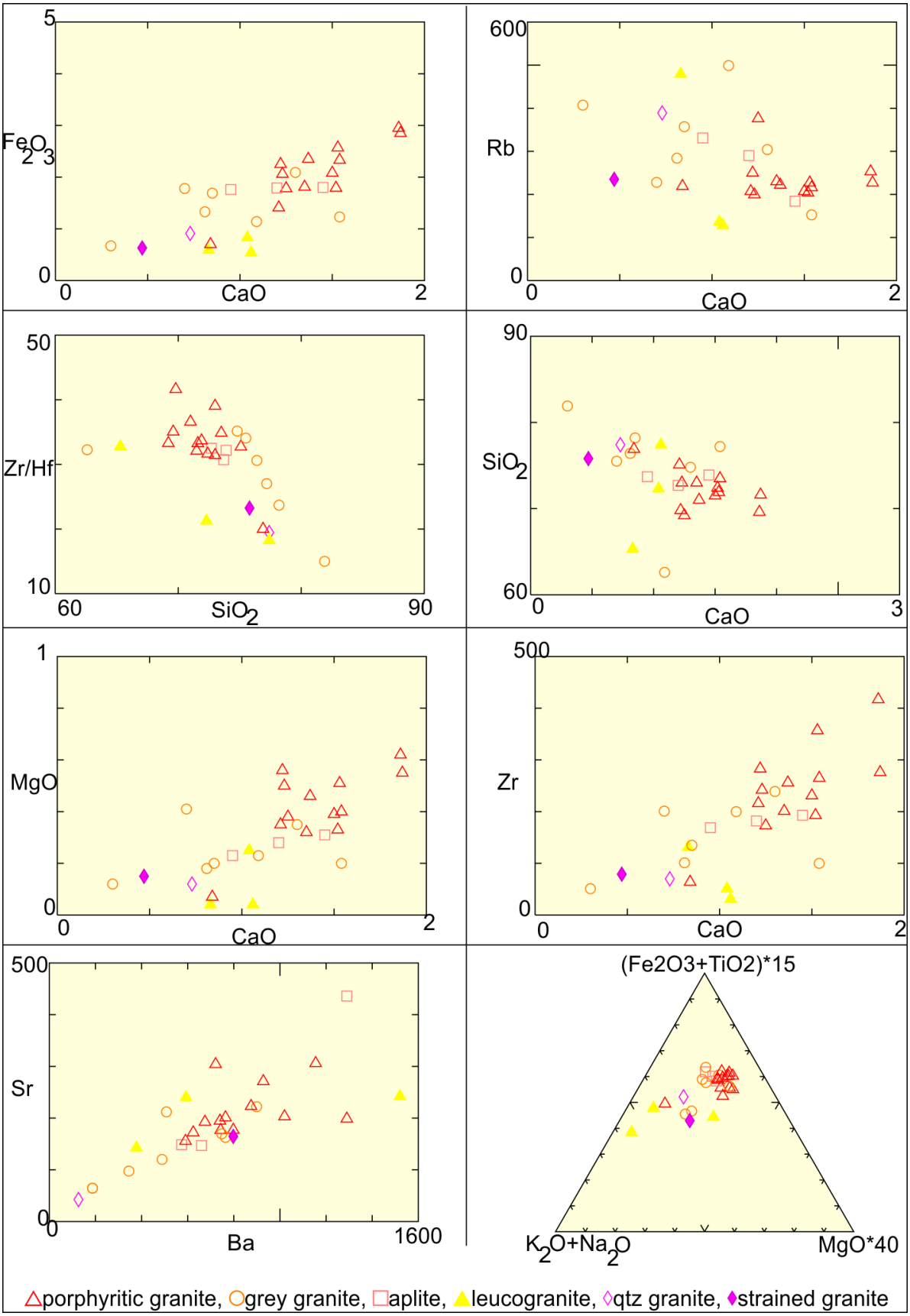

Figure 42: *Various diagrams indicating an evolutionary trend. The porphyritic granite is the least evolved, and it is proposed that it evolves into the more felsic granitoids by fractionation and strain-aided segregation. Diagrams are made using IgPet.*

Trace elements and REE

Chondrite-normalised REE-diagrams (Fig 40) display enrichment in the light rare earth elements (LREE's) (La-Sm) compared to the heavy REE's (Gd-Lu). The slope is similar for all the granitoid rocks, except the quartz phenocrystic granite, with a flatter trend.

A large vertical spread is evident for the porphyritic granite and grey granite, but the slope and anomalies are quite consistent. Both positive and negative Eu-anomalies occur, with the latter occurring in the most elevated samples and the opposite, resulting in a wasp-waisted pattern. Both the lateral variation and the Eu-anomalies can be explained by varying plagioclase fractionation. Variations in the heaviest HREE's are visible, especially for Tm, but these variations are likely to be of analytical origin, due to the low values.

The aplite samples show similar trends to the porphyritic granite, except sample K120, displaying an anomalous increase in HREE's. The leucocratic granites show a large variation in total REE, and an anomalously positive Eu-anomaly in sample K114. Large variations in the most evolved granitoid rocks are expected, as these melt batches are more isolated, and trace minerals have a larger influence. The increase in HREE's for the aplite sample K120 could be explained by local assimilation of a garnet bearing rock, e.g. the amphibolite xenolith.

Primitive mantle normalized diagrams are presented in Fig 41, and show a similar pattern for all granitoid rocks, again with some scatter for the most evolved leucocratic granite. A decoupling, with increased large ion litophile elements (LILE) relative to the high field strength elements (HFSE), is clear. This decoupling, together with the negative Ta-Nb and Ti anomaly is commonly interpreted as a subduction signature (Gill, 1976; Pearce and Stern, 2006). The negative Ba anomaly is likely to reflect plagioclase fractionation. Contamination of crustal rocks is clearly present with large positive Pb anomaly, and the slightly elevated Nd (Winter, 2010, p. 357). The negative P-anomaly could indicate apatite fractionation.

The anomalies for the granitoid rocks are generally well defined, and a subduction signature with significant crustal contamination is clear. A continental arc setting is typical for such signatures (Winter, 2010, p. 357). Signatures inherited from an original subduction-related magmatism will be inherited by potential reworking of these rocks. Reworking of the subduction signature in a later collision zone would only increase the crustal contamination signature.

Fig 42 indicates a continuous evolution of the SMB granitoids, from the least evolved porphyritic granite towards the more evolved grey granite, leucocratic granite, aplite and quartz porphyritic granite. With evolution, the amount of SiO_2 and Rb increases, while MgO, Fe_2O_3, Zr, Sr, Ba and CaO decreases. Fractionation of plagioclase, zircon and other mafic minerals would cause such trends. The leucocratic granites are more scattered, but following the argument above, together with crosscutting relations and general undeformed and irregular appearance, they could be regarded as the most evolved SMB granitoid rocks.

The mafic dyke has a weak negative REE pattern without any anomalies, and lacks the decoupling signature in the trace element diagram. A positive Pb-anomaly, and a negative Sr-anomaly are weakly developed.

3.6.2 Xenoliths

Major elements

All xenolith samples show a significantly larger spread in the major element diagrams than the granitoid rocks. The migmatite and flaser gneiss appear similar to the granitoid rocks on the major element diagrams, but with a few significant outliers.

The amphibolite and biotite gneiss samples are widely spread on all diagrams, though a few features should be mentioned. The amphibolite is clearly the least silicic, principally around 50% SiO_2. One amphibolite sample (not shown in the diagrams) has a silica content of 28.6%, most likely a result of alteration (Digital Appendix). The biotite gneiss has similar silica content as the granitoid rocks. Both the amphibolite and the biotite gneiss display a relatively high alkalinity index in the ASI diagram. In the MALI diagram, the amphibolite samples are alkalic while the biotite gneiss samples are more calcic, but the variation is very large. The alkalic properties of the amphibolite indicates that it originates from a separate magmatic system than the more calcic granitoid compositions.

Trace elements

Chondrite normalized REE diagrams are presented in (Fig 40). The biotite gneiss, flaser gneiss and migmatite show similar trends as the granitoid rocks. Two biotite gneiss samples have a distinct flatter REE pattern. Trace element diagrams for these xenoliths (Fig 41) display similar decoupling and anomalies as for the granitoid rocks, but with more variation.

The REE pattern for the amphibolites is flat, with no significant anomalies. No decoupling is evident for the amphibolites.

Xenoliths	Sample	ppm Mo	Granitoids	Sample	ppm Mo
Amphibolite	K14	3	**Porphyritic granite**	K15	1
	K33	22		K112	1
Flaser gneiss	K6	2		K8	7
	K36	3		K131	13
	K24	4	**(*)**	K1004	1040
	P	27	**Leucocratic**	K11	2
Biotite gneiss	K7	1	**Aplite**	K22	3
	K130	1	**Aplite**	K120	8
	K2	2	**Melanocratic**	K9	1
	K16	15	**Melanocratic**	K23	1
	K29A	27	**Melanocratic**	K101	9
Migmatite	K32	2	**Grey granite**	K29	4
				K12	83
				K1005	186
				K17	397
				K31	543
				K126	1240
				K13	2560

Figure 43: *Table showing the Mo content in different lithologies in the Knaben Zone.*

3.6.3 Molybdenum content

Samples containing molybdenum are listed in Fig 43. As expected, the grey granite contains the most molybdenum. The porphyritic granite and other granitoid varieties only show traces, generally below 10 ppm Mo, apart from sample K1004 with 1040 ppm Mo. Sample K1004 is a deformed porphyritic granite adjacent to a grey granite screen, which explains the high value.

Generally, the xenoliths include Mo amounts similar to the granitoid rocks around 20-30 ppm Mo, apart from occasional xenolith samples with anomalously high Mo content.

3.7 Geochronology

Zircon geochronology for one sample of porphyritic granite and one flaser gneiss sample is presented below. As crosscutting relations between the two units were sparse in field, and that thin screens of flaser gneiss resemble deformed porphyritic granite, documenting their temporal relationship with geochronology is important for understanding the evolution of the Knaben Zone. Samples analysed and presented below are shown on Map 3 (Digital Appendix).

Originally, samples of the grey granite, the biotite gneiss and the migmatite were prepared for zircon geochronology, but due to an error in the polishing process the majority of the zircon grains were lost. Data from sample K29 and K26 turned out severely discordant, and are not regarded any further.

Complete data from all analysis are found in Appendix 3.

3.7.1 Porphyritic granite (sample K1)

The porphyritic granite sample K1 is from the western side of the Knaben Zone, L28. The zircon grains obtained from this sample are prismatic with well-rounded edges, up to 200µm large (Fig 44b). Bright, distinct strongly cathode-luminescent cores and dark weakly luminescent rims of variable width are typical. Oscillatory zones showing varying degrees of luminescence are common within the core itself, and occasionally within the rim. The luminescent cores regularly have a more angular appearance than the rounded terminal rims. Grains without luminescent cores are quite common. The grains resemble igneous zircon grains, according to Corfu et al. (2003).

In thin section, the zircons appear as small (<0.25mm) rounded grains with visible zonation, often as clusters of small grains (Fig 44d, e). Grains occurring as inclusions in biotite are generally very dark, only revealed by the metamict halo.

Ten zircon grains from sample K1 have been analysed, and give a concoridia age of 1043.3±5.6 Ma (2σ) (Fig 44a). Two outliers are eliminated from this age (Fig 44c), but are relatively concordant. One of the outliers, a zircon core with strong cathode luminescence, gives a 207Pb/206Pb age of 1256±26Ma (1σ) (Appendix 3). This age is similar to the concordia age calculated for the flaser gneiss sample K36 (below), and could represent an inherited zircon grain from assimilated flaser gneiss. This process is supported by field evidence presented above (Fig 8d).

The second outlier, gives a 207Pb/206Pb age of 966±22 Ma (1σ) (Appendix 3), and is obtained from a very weakly luminescent ellipsoid zircon rim, possibly representing a metamorphic overgrowth. In that case, the age is concurrent with the post-kinematic, regional, voluminous HBG intrusions.

3.7.2 Flaser gneiss (sample K36)

12 grains are analysed from flaser gneiss sample K36, from L39. The zircon grain morphology is similar to sample K1. The number of grains with cathode luminescent cores is larger, showing more complex oscillatory zoning, domains of weaker luminescence etc. (Fig 45b). Zircon grains are more abundant than in the porphyritic granite, and concentrated in the mafic, biotite-rich foliation (Fig 45d, e and f).

By removing two outliers, the two weakest luminescent zircon grains, a Concordia age of 1252.8±8.7 Ma (2σ) is fitted for flaser gneiss sample K36 (Fig 45a, c).

In addition to a distinct weaker luminescence and the lack of visible oscillatory zoning, the two outliers stand out from the other analyses with a lower Th/U ratio (Appendix 3). For the outliers, the ratio is 0.18 and 0.17, while for the remaining analyses, the ratio above 0.26 and 0.32 on average. Low Th/U ratios could indicate that the zircons are metamorphic, as Th is less compatible in zircon than U, but this also depends on other factors, such as the presence of monazite (Hoskin and Black, 2000).

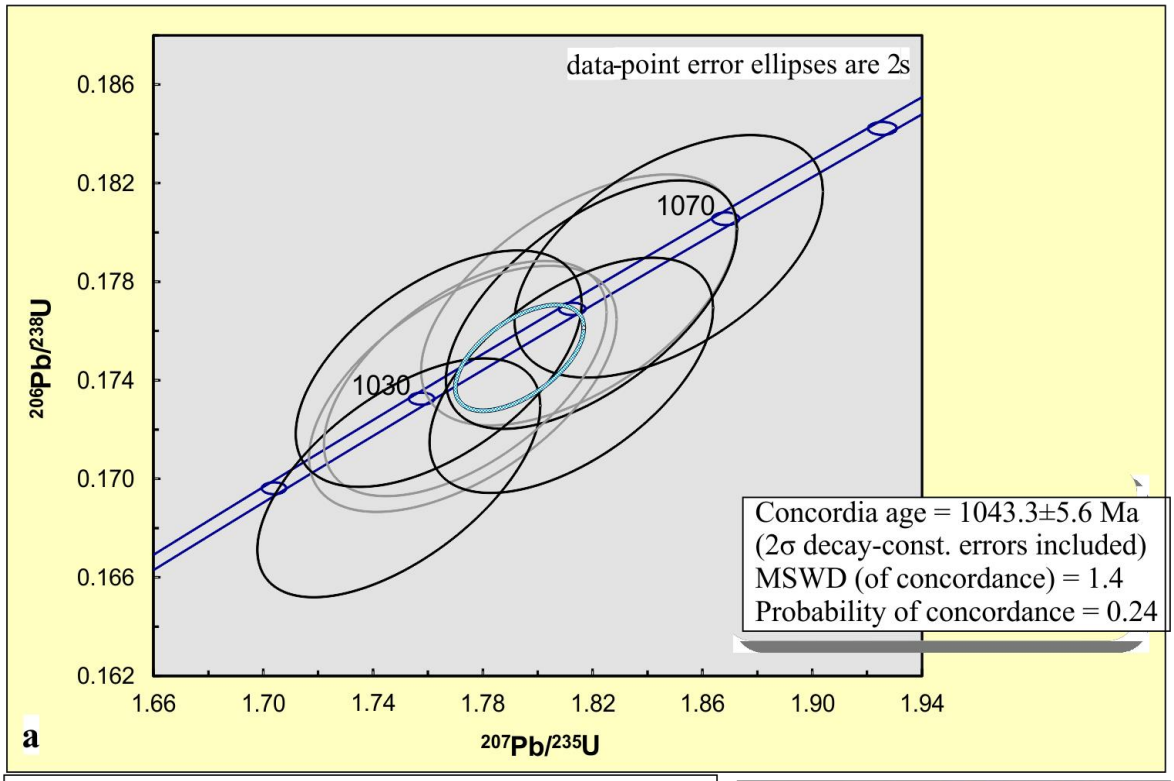

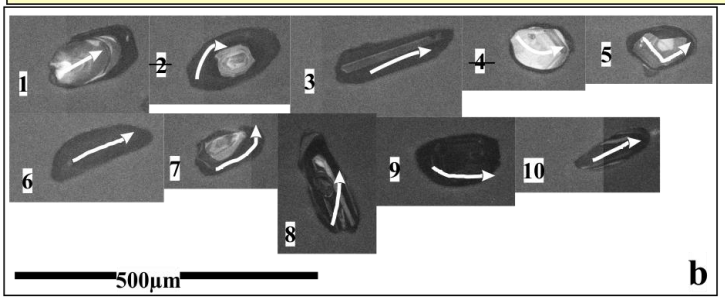

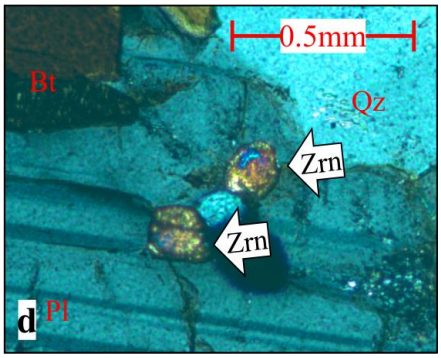

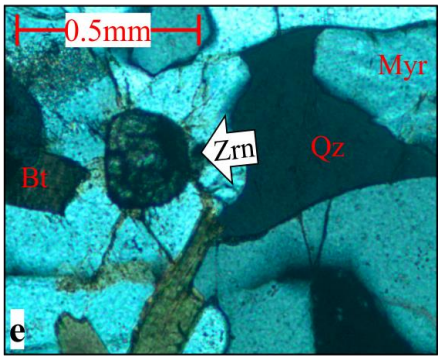

Analysis_#	Pb207 U235	1s%	Pb206 U238	1s%	roh
K-1_01	1.8149	1.29	0.17726	1.17	0.56
~~K-1_02~~	~~1.5714~~	~~1.21~~	~~0.15995~~	~~1.17~~	~~0.60~~
K-1_03	1.8196	1.19	0.17707	1.16	0.61
~~K-1_04~~	~~2.3838~~	~~1.45~~	~~0.20991~~	~~1.20~~	~~0.50~~
K-1_05	1.7727	1.29	0.17365	1.17	0.56
K-1_06	1.7494	1.20	0.17004	1.16	0.60
K-1_07	1.8477	1.24	0.17903	1.12	0.53
K-1_08	1.7736	1.19	0.17407	1.12	0.56
K-1_09	1.8123	1.16	0.1742	1.12	0.57
K-1_10	1.7639	1.21	0.17447	1.12	0.55

c

Figure 44: a) *Condordia plot displaying zircon geochronological data from porphyritic granite sample K1. Diagram is made using Isoplot.* ***b)*** *CL images for the analysed zircons. Arrows indicate ablation trace.* ***c)*** *Table displaying data for the different zircons. The two outliers are outlined.* ***d) and e)*** *Micro-photo of porphyritic granite sample K122, showing typical zircon appearance.*

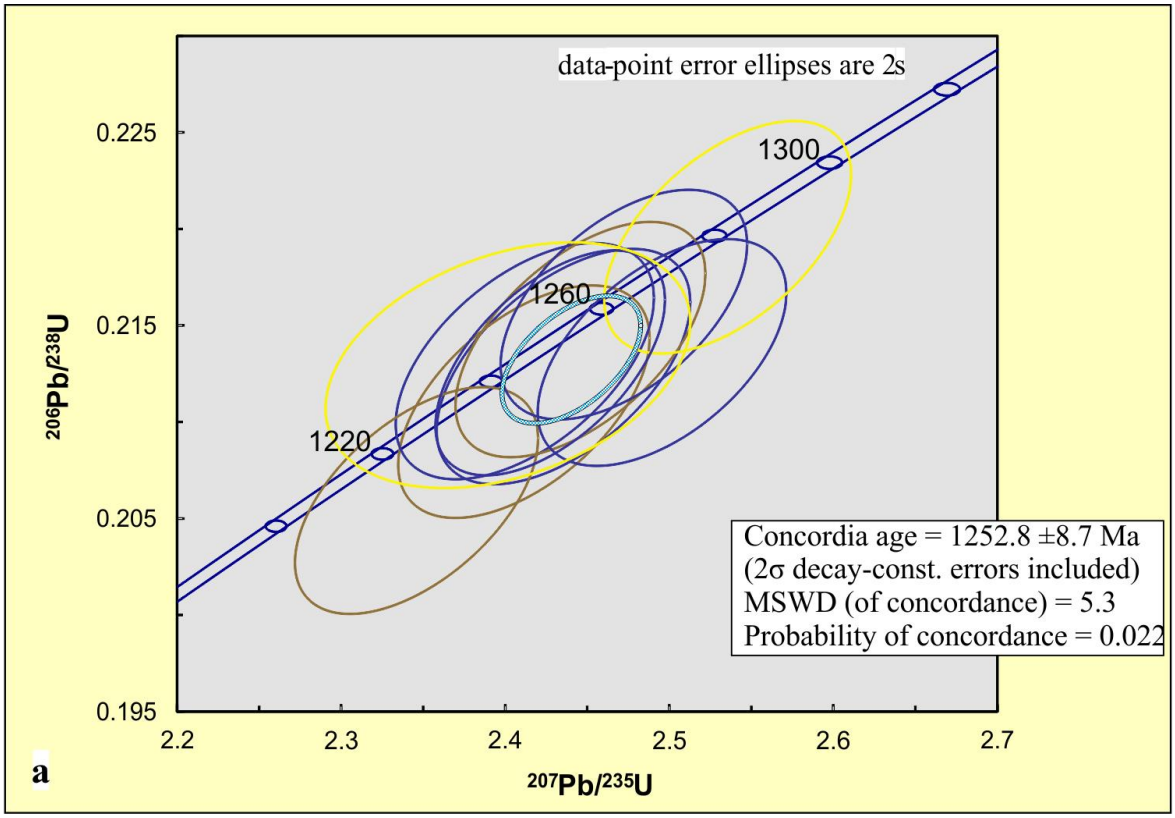

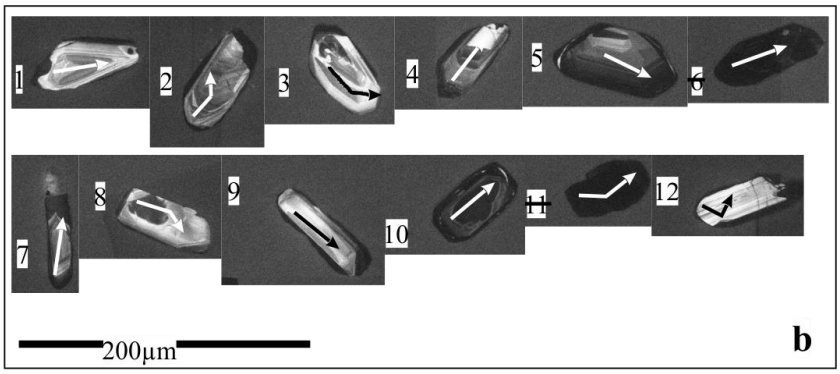

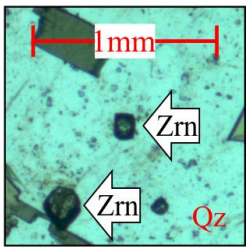

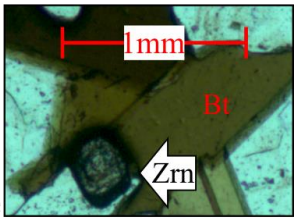

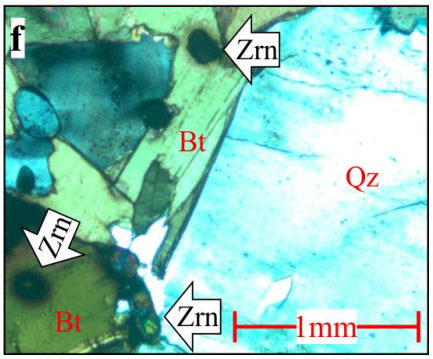

c

Analysis_#	Pb207 U235	1s%	Pb206 U238	1s%	roh
K-36_01	2.4355	1.30	0.21287	1.17	0.55
K-36_02	2.4114	1.30	0.21105	1.17	0.54
K-36_03	2.4120	1.33	0.21315	1.17	0.53
K-36_04	2.3460	1.29	0.20593	1.17	0.55
K-36_05	2.4459	1.27	0.21427	1.16	0.56
~~K-36_06~~	~~2.1541~~	~~1.23~~	~~0.19318~~	~~1.16~~	~~0.58~~
K-36_07	2.4724	1.24	0.21608	1.12	0.53
K-36_08	2.4956	1.24	0.2136	1.12	0.53
K-36_09	2.5356	1.21	0.21957	1.12	0.54
K-36_10	2.4275	1.18	0.21306	1.12	0.56
~~K-36_11~~	~~1.8835~~	~~1.17~~	~~0.18127~~	~~1.11~~	~~0.56~~
K-36_12	2.4017	1.89	0.21294	1.22	0.35

Figure 45: a) *Condordia plot displaying zircon geochronological data from flaser gneiss sample K36. Diagram is made using Isoplot.* ***b)*** *CL images for the analysed zircons. Arrows indicate ablation trace.* ***c)*** *Table displaying data for the different zircons. The two outliers are outlined.* ***d) e) and f)*** *Micro-photo of K36, showing typical zircon appearance.*

Chapter 4 – Discussion

4.1 Focus areas and main outcome

The overall aim for the discussion is to shed light on processes that are important for the magmatic and tectonic evolution in the Knaben Zone, especially focusing on the SMB during the Sveconorwegian orogeny and, in addition, to place the molybdenite deposits in a robust tectonic framework. The regional significance of the findings and proposed models for the Knaben Zone will be of importance, both on a batholith and orogen-scale.

Lithological relationships, style of deformation and mineralisation and other results from the study which help to understand the evolution of the Knaben Zone, are evaluated and systematized, with a view to developing a model for emplacement of the SMB and the molybdenite deposits. Observations of folds, duplex structures and kinematic indicators have led to the important conclusion that a (sub-) horizontal maximum principle stress axis (σ_1) has been dominant during the evolution of the Knaben Zone and has resulted in the present general geometry and lithological relationships. An examination of key processes for the geological evolution is the core of the following discussion.

4.2 Tectonomagmatic evolution of the Knaben Zone

4.2.1 Summary

In the previous chapter, evidence for synkinematic intrusion of the SMB granitoid rocks in the Knaben Zone was presented. This allows for an integrated understanding of the magmatic and structural evolution of the Knaben Zone, and considering these findings in a regional perspective.

Evidence for synkinematic intrusion is presented in the previous chapter consists of: (1) Coinciding moderate eastward-dipping foliation in the xenoliths and magmatic to submagmatic fabric (Fig 23a), parallel to the elongated SMB batholith and large scale magnetic anomalies (Fig 26c); (2) Evidence for magmatic to submagmatic flow in the SMB granites on the microscopic scale (Fig 9c, 9d), together with mesoscopic structures indicating that melt was present during deformation (Fig 4d, 10e, 24b, 30d) and only local solid-state deformation (Fig 9e, 24c, 24d), with consistent top-to-the-W kinematics in an E-W-compressive environment with consistent duplex geometries (Fig 26); (3) Structural observations, at all scales, in the xenoliths, along strained contacts to the xenoliths (Fig 26b, 32), melt filled structures and in solid state deformation zones within the granitoid rocks which are generally consistently top-to-the-W, indicating continuing kinematic conditions with cooling of the granitoid melts; (4) Geochemical indications of progressive crystallisation and melt-segregation during deformation (Fig 42).

Observations of the relationship between the country rock and the intrusion are commonly critical when studying magmatic evolution and proposing emplacement models. The Knaben Zone represents a xenolith rich zone within the SMB, and a well-defined contact to the country rock is not available in this area. The abundance and parallelism of the xenolith screens and granitoid sheets, together with common kinematic conditions imply that the Knaben Zone represents an important component in the SMB batholith, rather than randomly positioned xenoliths, and that conclusions considering the tectonomagmatic evolution in the

Knaben Zone are coupled with the SMB. Possible ways to understand which evolutionary stage the Knaben Zone represents, within the SMB at a larger scale, are discussed later.

The evolution of the Knaben Zone can be divided into three major stages, which are discussed in detail below and summarized in Fig 46. The detailed structural mapping and kinematic relationships, combined with the knowledge of the geometry and cross-cutting relationships of the various intrusive units and xenoliths, allows a model of tectonic evolution to be constructed in three dimensions, based on key outcrop descriptions previously described, and pre-existing borehole data (Gvein and Rui, 1980). Profiles through the Knaben Zone (Map 2) illustrate the widespread duplex geometry, mainly with deformation zones along xenolith boundaries. Local, well-developed, solid-state strain zones in the granitoid rocks are likely to connect to the duplex network, as well as strain being partitioned into melt rich zones. The interpreted large-scale ECC structure along the Smalavatn lineament is shown in profile A, Map 2. A close relationship between the grey granite and the flaser gneiss is illustrated in the profiles (Map 2) and discussed below.

	Pre-Sveconorwegian	Schematic Sveconorwegian evolution in the Knaben zone				Post-Sveconorwegian
	Stage 1	Stage 2a	Stage 2b	Stage 2c	Stage 2d	Stage 3
The Knaben zone	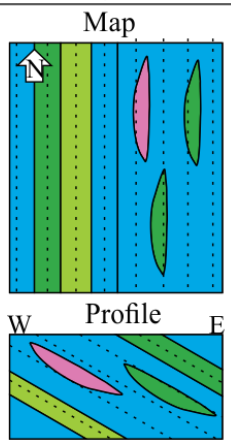	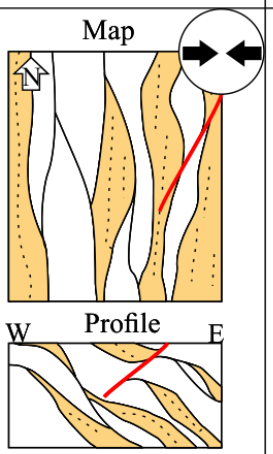	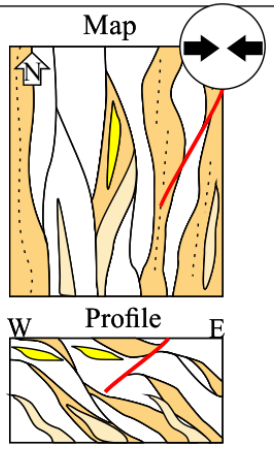	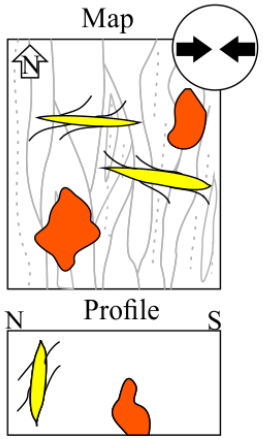	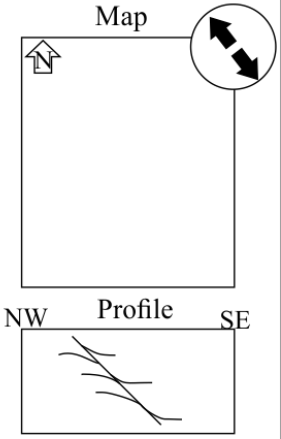	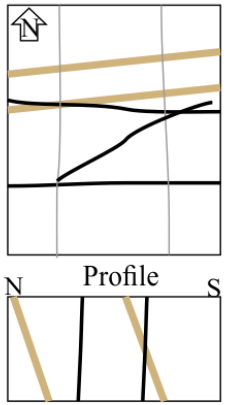
Structural expression	Developement of regional foliation	-Ductile top-to-the-W duplex-thrusting, kinematics and E-W compressive folding -N-S directed lateral extrusion and corresponding E-W-oriented pure shear component		-More heterogenous and s.-s. strain + open folds -E-W pegmatites along duplex transfer zones	-Sparse observations of down-to-SE extension, cutting general foliation, reactivating weaknesses	1) 850Ma dykes 2) Calledonian shear zones 3) Late brittle joints
Magmatic events	Flaser gneiss -1260Ma	-Porphyritic granite 1040-1020Ma -Synkinematic emplacement	-Grey granite (1030Ma) and Mo-pegmatites -Strain-assisted melt-fractionation	-Irregular leucogranitic intrusions -Subvertical E-W pegmatites	(possibly close in time and related to Stage 2c)	Hunnedalen dykes -850Ma -Approximately E-W striking
Regional correlation	Lithological and geochronological regional correlation	-SMB - correlation -Similar kinematics as PKFZ and KTBZ			Extensional reaktivation along all major shear zones in the orogen, related to gravitational collapse	

Figure 46: *A schematic summary table for the geological evolution of the Knaben Zone. Legend for the lithologies are shown in Fig 7. The abbreviations used are PKFZ (Porsgrunn Kristiansand Fault Zone) (Henderson and Ihlen, 2004), KTBZ (Kongsberg Telemark boundary zone) (Scheiber et al., 2015). Stage 1 includes the colocation of the pre-Sveconorwegian bedrock, and formation of east-dipping geometry. The emplacement of the SMB initiated at 1060Ma (Coint et al., in press). The Knaben Zone is interpreted to represent the boundary between two separate intrusions (see text for discussion). Stage 2a to 2c involves synkinematic intrusion of increasingly evolved plutons into a compressive duplex environment, with structures evolving from magmatic and submagmatic to solid-state (s.-s.). 2d represents later poorly constrained ductile extension. Stage 3 involves very late to post-Sveconorwegian events.*

4.2.2 Stage 1 – Collocation of pre-Sveconorwegian bedrock

As described in the previous chapter, fragments of amphibolite occur within the flaser gneiss (Fig 20d), hence the flaser gneiss is assumed to be younger, but this temporal relationship is obscured, as both units are deformed. No crosscutting relationships that further restrict the biotite gneiss are documented. The foliation within the flaser gneiss, amphibolite and biotite gneiss, is consistent and moderately dipping eastwards (Fig 23a). Less foliated domains of biotite gneiss and amphibolite occur. Kinematic observations within the xenoliths are largely restricted to the contacts with the later granitoid intrusions. Symmetric flaser texture, indicating pure-shear deformation, dominates the flaser gneiss (Fig 17a, b). A few observations of weakly developed ECC-fabric occur within the flaser gneiss, with top-to-the-W deformation (Fig 31 b), presumably as a result of the kinematic conditions during Stage 2.

On this basis, it is proposed that the proto-flaser gneiss intrudes into the amphibolite, and also the biotite gneiss, as the foliation and physical appearance is similar for the biotite gneiss and the amphibolite. Zircon geochronology from this study, matching with other research (Bingen et al., 2015), delimits this event to 1252.8±8.7 Ma (Fig 45a). The timing of the formation of the foliation in the xenoliths is not clear, other than that it existed before intrusion of the porphyritic granite. The foliation is likely to be intensified during Stage 2, together with the formation of the sparse top-to-the-W kinematics in the xenoliths. It is possible that most of the symmetric, pure-shear related structures in the flaser gneiss are a result of forceful intrusion of the granitoid sheet-intrusions in a compressive setting, which will be discussed below.

Bingen et al. (2015) argue that the age and lithology of the xenoliths indicate that they represent pre-Sveconorwegian basement, intruded by the SMB. This fits well with the model proposed in this thesis, and further supports the suggestion that the xenoliths represent remnants of country rock.

Geochemical signatures (Fig 40, Fig 41) for the flaser gneiss and biotite gneiss are assigned to subduction and significant crustal contamination. Geochemically, reworking and assimilation of rocks with such signatures could result in signatures similar to the SMB granitoid rocks. However, the flat REE pattern, together with the more alkalic signature, indicates a different tectonic setting and melt source for the amphibolite.

Migmatite is documented at a few localities, but its part in the evolution is not well determined. As it occurs as elongated screens, generally with foliation and kinematics correlating with the other xenoliths, it is considered to be part of the pre-Sveconorwegian bedrock. The migmatite is documented spatially close to major lineaments (Map 2, Fig 5), and a relationship between large-scale ECC structures and partial melting is possible.

4.2.3 Stage 2 – Synorogenic deformation and magmatism

As pointed out in the previous chapter, the geochemistry of the SMB granitoid rocks of the Knaben Zone show an increasingly evolved signature, from the porphyritic granite, through the grey granite and finally the leucocratic granites (Fig 42). Crosscutting field relations and a temporal relationship support this model of evolution (Fig 12a, Fig 13d, Fig 16d). As argued in the previous chapter, the structures in the Knaben Zone suggest synkinematic intrusion of the SMB granitoid rocks, relative to ductile top-to-the-W thrusting (Fig 10e, Fig 24d, Fig 14d).

Karlstrom et al. (1993) argue that continuous fractional crystallisation of a melt in a compressive environment can result in highly effective melt segregation and discrete melt batches with an increasingly evolved petrology. With this in mind, an evolutionary model for the SMB granitoid rocks in the Knaben Zone, combining petrological evolution and deformation is suggested, and summarized in Fig 46.

Based on crosscutting relationships and the nature of the deformation, Stage 2 is interpreted to progress from a magmatic-ductile environment into an environment where heterogeneous solid-state deformation accounts for the deformation. Such a change is expected as the SMB-melts cool.

Local N-S-trending magmatic to submagmatic lineations (Fig 25a) and pure-shear structures (Fig 29, Fig 30) (boudinage) indicate a small component of N-S-directed movement of granitoid melt and ductile units. Below, it is argued that lateral extrusion induced by the E-W compression can cause such structures. Finally, a small number of, but unambiguous structures imply ductile NW-SE oriented extension post-dating the compression (Fig 33a).

Stage 2a – synkinematic SMB intrusion in an E-W-compressive setting

During this stage, an E-W compressive stress regime is proposed to account for the formation of a ductile, anastomosing duplex-network of deformation zones, in which the majority of the SMB granitoid melts have intruded as multiple sheeted intrusions and migrated synkinematically, resulting in the moderate eastward-dipping network of xenolith screens and granitoid sheets. Geochemistry and mineralogy demonstrates that the porphyritic granite is the least evolved SMB granitoid, which is supported by crosscutting relations (Fig 12a, 13d). Strain is best localised along contacts between xenoliths and the granitoid rocks, and it is here the bulk of the kinematic indicators and the majority of structures are observed. The porphyritic granite intrusion was emplaced at 1043.3±5.6 Ma, according to zircon geochronology from one sample in this thesis (Fig 44, Map 3), which fits existing data well (Bingen et al., 2015; Coint et al., in press).

Although evidence for a synkinematic intrusion is convincing, and the granitoid melt was influenced by top-to-the-W kinematics, the possibility that the intrusion was prekinematic and experienced deformation and migration after intrusion is hard to disprove. The submagmatic structures are not necessarily related to the initial intrusion, but could have formed later during magma migration caused by the compressive stress. In fact, an evolution from magmatic to solid-state flow is highly likely in such a tectonic environment (Paterson et al., 1989). Existence of local solid-state deformation with top-to-the-W kinematics shows that the deformation was active at the late stages of the intrusion. Since the top-to-the-W structures are important for the final geometry of the intrusion and molybdenite deposits, understanding the tectonic processes which formed these structures are important.

The large majority of the structures presented in the previous chapter can be explained within the proposed model. Duplex structures, ramping up towards the west, occur on all scales, and are best developed along the contacts between xenoliths and granitoid rocks. The thickness of the granitoid sheets increases away from deformation zones, and similarly the development of foliation in the granitoid rock is typically seen to decrease away from the highest strain deformation zones. ECC-fabric (Fig 31, Fig 32), SC-structures (Fig 32), small duplex structures (Fig 26) and sigma-clasts (Fig 24c) occur along the deformation zones and outcrop-

scale duplex structures, indicating a top-to-the-W transport direction, with a sub-horizontal maximum principle stress axis (σ_1) and a sub-vertical minimum principle stress axis (σ_3).

As is evident from Map 2 and Fig 5, transport direction is highly variable and far from well-confined top-to-the-W. This variation is partly a result of the irregular melt-flow-resembling nature of the observed ramps, folds and other kinematic indicators. In a ductile thrusting environment with significant amounts of melt, such irregularities may be expected.

The anastomosing network of both synmagmatic deformation zones and local solid-state deformation zones with consistent top-to-the-W kinematics argue for an E-W oriented compressive stress regime. Domains of less strain separate the deformation zones, where the relationship between the xenoliths and the granitoid rocks is of a more magmatic character, with irregularly folded xenoliths (Fig 28a 28b) and irregular contacts between granitoid varieties, but still with an overall similarly orientated fabric. This suggests that strain was partitioned into melt rich zones.

Local N-S oriented lateral extrusion

Shallow-plunging, N-S-trending K-feldspar phenocrysts and quartz aggregates occur locally (Fig 13c, 24b, 25a), and are similarly oriented to occasional small xenoliths (Fig 19d). They are interpreted by Lysberg (1976) to originate from a N-S-compressive fold phase, succeeding the emplacement of the granitoid sheets. Mesoscopic and microscopic observations presented in the previous chapter argue that these lineations are of magmatic to submagmatic origin, and no N-S-oriented compression is documented kinematically. The amount of solid-state recrystallization is considered insufficient to have formed the N-S-oriented mineral lineations. These lineations could suggest a N-S-directed, prekinematic intrusion. As mentioned above, an initial, prekinematic intrusion is hard to disprove. Alternatively, local N-S oriented foliation-parallel lateral extrusion (Jones et al., 1997) could produce such lineations, which fit well with the overall compressive setting, as has been argued to be an important component of melt migration in compressive regimes (Brown and Solar, 1998) .

At the point of inflection in a duplex-structure, one would expect an increased local amount of pure-shear over simple-shear, in the E-W compressive direction, at a high angle to the foliation (Fig 47). This shortening would most efficiently be consumed by unconsolidated granitoid sheets or partly molten xenoliths, resulting in lateral melt extrusion perpendicular to the pure-shear, channelled by the E-W-compressive folds and duplex structures. The largest and least ductile xenolith screens represent anisotropies which could channel and direct the extrusion. Such a process could cause the locally documented magmatic or submagmatic, foliation-parallel N-S-lineations and weakly developed imbrication of phenocrysts (Fig 24b). This component of pure-shear also allows for the formation of boudinage structures, typically observed in the N-S sections, presented in the results chapter.

Both boudinaged granitoid sheets (Fig 29) and thin xenolith screens (Fig 30) occur, reflecting the ductile behaviour of the thin xenolith screens. In addition, this indicates that pure-shear structures formed at times when the granitoid sheets were the least competent and at times when the thin xenoliths were the least competent, indicating that the deformation outlasted the magmatism.

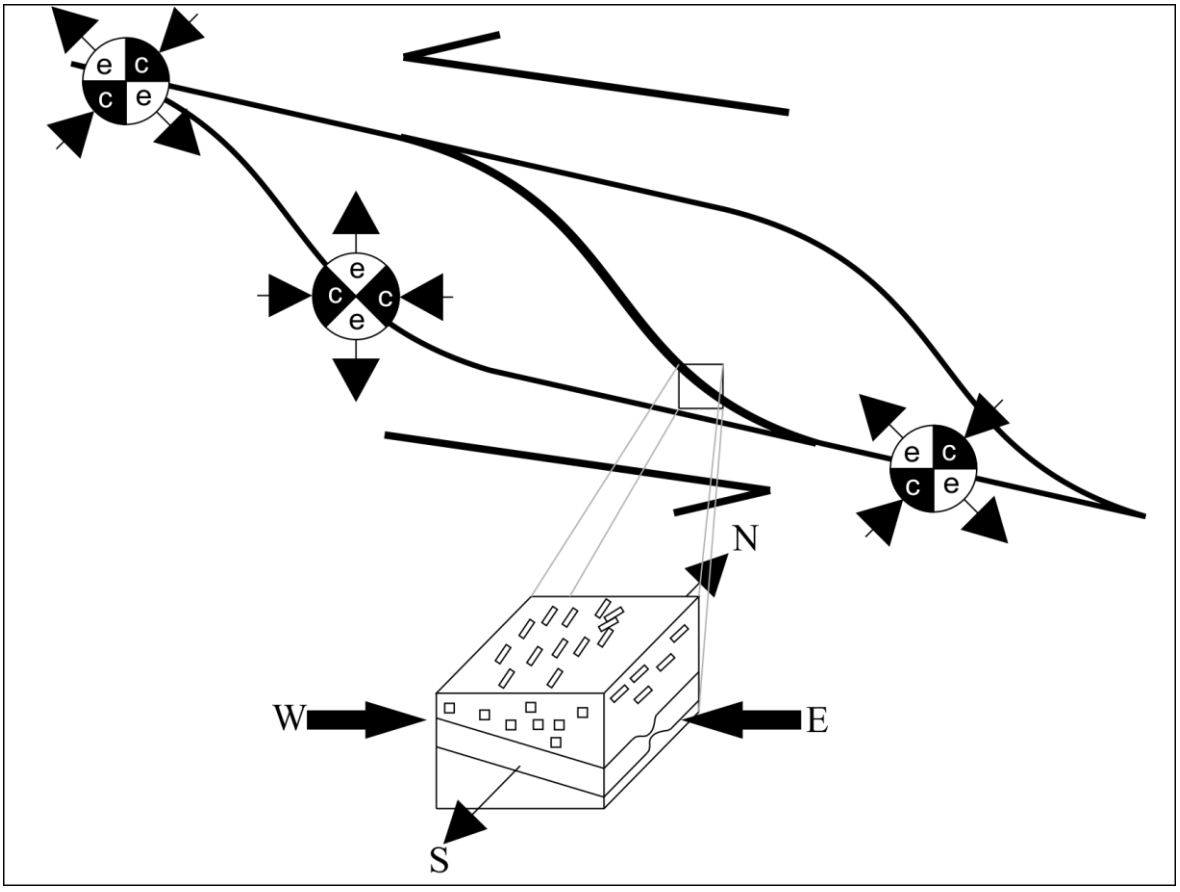

Figure 47: a) *Conceptual extrusion model of molten to partly molten granitoid melt, due to pure-shear in the inflection point in a duplex structure. This is indicated by the direction of extension (e) and compression (c) in relation to the duplex geometry in the Knaben Zone. More rigid xenolith screens would act as anisotropies relative to molten rock and cause extrusion of the molten granitoid orthogonally to the screens, creating N-S oriented magmatic to submagmatic lineations, imbricates of phenocrysts and boudinage structures. Duplexes and folds may channelize the extrusion in a N-S direction.*

Stage 2b – Strain-assisted melt segregation and migration of the grey granite

Foliation-parallel sheets of granitoid rocks are described in the previous chapter. They are more evolved than the porphyritic granite and display similar kinematics and structures, and the grey granite is the best differentiated evolved unit. The geochemistry and mineralogy strongly implies that the grey granite represents a more evolved melt, genetically related to the porphyritic granite (Fig 42). In addition, assimilation of the xenoliths and mixing with partial melts from the xenoliths is likely to affect the grey granite; this is discussed later. Zircon geochronology presented by Bingen et al. (2015) suggests that the grey granite is more or less coeval with the porphyritic granite at approximately 1030Ma. One crosscutting observation from the Knaben 2 mine (Fig 12a) indicates that the grey granite is relatively younger than the porphyritic granite.

As mentioned, strain-induced melt segregation could be an efficient process explaining the development of more evolved intrusive sheets. While the porphyritic granite continuously crystallises, remaining melt could be segregated efficiently in the compressive environment, forming a more evolved melt. Likewise, partial melt from the xenoliths will be effectively squeezed out, and possibly mix with the existing melts. The large spread of ages documented

for the SMB (Slagstad et al., 2013; Bingen et al., 2015; Coint et al., in press) suggests a long-lived magmatic event and multiple sheeted intrusions. Hence, a closed-system with continuous fractionation is not likely to occur on a batholith-scale, and the granitoid variations, such as the grey granite, may be locally dependent on assimilation of xenoliths etc..

Subhorizontal, foliation-parallel and subvertical pegmatites are well documented (Fig 15, Fig 16). The former two are related to molybdenite deposits and display a deformed appearance. A low angle compressive stress component is required, to allow subhorizontal dilation and corresponding pegmatites, fitting well with the proposed tectonic model (Fig 49). If the anisotropies in the rock are large enough, they could possibly override the theoretical σ_1-paralell dilation, and influence the foliation-parallel pegmatites. As argued by Brown and Solar (1998), high differential stress or high melt-pressure can result in an equal likelihood of intrusion parallel to the anisotropies and intrusion parallel to σ_1. Alternatively, continuous deformation could rotate originally horizontal pegmatites to a foliation-parallel position, as described in the Bamble terrane (Henderson and Ihlen, 2004). Previous authors argue for a genetic relationship between the grey granite and the mineralised pegmatites (Lysberg, 1976).

Stage 2c – late to postkinematic leucocratic intrusions and pegmatites

Stretching lineations along foliation planes and lithological boundaries are clustered in the SE quadrant of the stereonet (Fig 25a). Folds along lineated surfaces indicate that the lineations are related to the thrusting, rather than the later extension, while the system was still hot and ductile. Despite the small data-set, these mineral lineations indicate that the late-stage thrusting was top-to-the-NW oriented and with a more confined thrust direction than interpreted from synmagmatic duplexes. When evolving from a magmatic system to a solid-state system, more consistent structures are expected (Buettner, 1999). Weak folds with a N-S-trending fold axis are in accordance with this stage (Fig 28a).

Solid-state mylonitic shear zones, with top-to-the-W kinematics, cut the subvertical pegmatites (Fig 31a), indicating that the E-W oriented subvertical pegmatites should be regarded within Stage 2 of the tectonic model. On the other hand, the subvertical pegmatites are undeformed, and cut the general foliation (Fig 15c) and the subhorizontal pegmatites (15a), indicating that they at least occurred late in Stage 2. Ductile drag-folds typically occur along the contacts to the pegmatites, but with no systematic kinematics. Transfer structures between duplexes could result in such structures, fitting well with the structural evolution. Alternatively, later N-S extension could generate E-W-oriented tensile fractures, possibly related to the mafic dykes, but this model fails to explain the ductile drag folds, and necessitates a complex history with a rapidly changing stress regime.

Irregular, leucocratic granitoids occur sporadically in the Knaben Zone (Fig 13d). Clear crosscutting relations and a highly evolved geochemistry indicates that these intrusions occurred at a late stage of the SMB. The typical lack of pervasive deformation indicates that the tectonomagmatic system is at a late, brittle-ductile stage, with more confined heterogeneous, solid-state strain zones (Paterson et al., 1989). The irregular appearance of the leucogranite, together with the subvertical pegmatites (if regarded as extension-related tensile fractures) could imply the initiation of an approximately NW-SE directed extensional stage. Alternatively, as will be discussed below, increased melt-pressure and differential stress within a compressive environment can lead to irregular intrusions (Brown and Solar, 1998).

The lack of molybdenite in the later subvertical pegmatites and leucocratic granites contradicts the possibility of continuous evolution from porphyritic granite to grey granite to leucocratic granite. This further suggests that the grey granite melt is influenced by the xenoliths or other components from depth, and is discussed below. Conditions strongly favouring molybdenite mineralisation could alternatively remove all molybdenum at stage 2b, hence the remaining evolved melts at stage 2c are barren.

Stage 2d – NW-SE-directed ductile extension

The structure in the Knaben 1 mine (Fig 33a) strongly indicates a ductile NW-SE extensional stage, post-dating the compression. Otherwise, the documentation of this stage is poor.

4.2.4 Stage 3 – Late to post-Sveconorwegian influence

As noted in the previous chapter, one metamorphic zircon rim correlates with the timing of the emplacement of Rogaland Igneous Complex (RIC) (950-920Ma) (Fig 44c, Appendix 3), indicating a metamorphic event at this stage. The RIC is associated with massive and hot magmatism (Drüppel et al., 2012), possibly perforating the SMB (pers. com. Slagstad), and a metamorphic influence is expected.

The SSE-NNW-oriented mafic dykes (Fig 35f) are dated to 850Ma (Walderhaug et al., 1999) and are argued to relate to extensional tectonics during the opening of the Iapetus Ocean (Sundvoll (1990) in Mauer and Verschure (1998)). Greenschist metamorphism of the dykes and veinlets with greenschist minerals are argued to be of Caledonian origin (Mauer and Verschure, 1998), based on mineralogical similarities. The greenschist metamorphism along the major lineaments (Fig 35e), or shear zones in the Knaben Zone, is also suggested to occur during this event.

Joints and fractures with less pronounced alteration (Fig 34b, 34c) and deformation are the latest structures and are likely to relate to exhumation and isostatic processes, as recent as Holocene postglacial isostasy.

4.2.5 Evolution of molybdenite deposits

The molybdenite is interpreted to initially occur with the grey granite, during Stage 2b, based on the disseminated magmatic appearance of the molybdenite grains (Fig 11b). This is supported by the lack of hydrothermal quartz (Müller, 2014). Subhorizontal molybdenite-bearing pegmatites are likely to be genetically connected to the grey granite, as argued by earlier workers (Lysberg, 1976; Gvein and Rui, 1980). No direct relationship is observed, other than a spatial concentration of both units within the Knaben Zone. That the grey granite is the primary molybdenite-bearing unit, and that the molybdenite related to pegmatites and other structures is secondary, but still within the magmatic system, is supported in this thesis.

Hydrothermal quartz occurs in minor quartz rich molybdenite deposits where chalcopyrite and pyrite replace molybdenite (Fig 16b), indicating that these deposits result from later hydrothermal circulation (Müller, 2014). Such deposits are only documented on the eastern vicinity of the Smalavatn lineament, also associated with later alteration, and will not be discussed further.

The fact that molybdenite is concentrated within a xenolith rich zone, strongly suggests a genetic connection. Three concepts for the origin of the grey granite are presented: (1) The connection is purely structural, meaning that the presence of xenoliths facilitates the top-to-the-W kinematics acting as a pathway for grey granite from depth, not genetically related to

the xenolith; (2) A genetic link exists between the country rock, represented by the xenoliths, and the grey granite; (3) Both structural control of the magmatic system and a chemical influence from the xenoliths have been important for concentrating the molybdenite deposits in the Knaben Zone.

Distinguishing between these concepts is difficult, based on studies of the Knaben Zone alone. As pointed out in the introduction, N-S striking zones with molybdenite deposits are related to xenolith-rich zones in the SMB, but are restricted to the southern parts of the batholith (Fig 2). The general structure and lithology of the xenolith rich zones in the southern parts of the SMB are very similar (pers. comm. Slagstad), while the non-molybdenite-bearing northern parts of the SMB possesses more flat-lying structures and with metavolcanic (and other dissimilar), xenoliths (Roberts et al., 2011; Roberts et al., 2013). This strongly implies a connection between the gneissic and amphibolitic xenolith lithologies and the molybdenite deposits. The reason for the anomalous abundance of molybdenite in the Knaben Zone relative to the similar N-S-striking xenolith rich zones is less clear.

The style of mineralisation is similar for all the molybdenite deposits in the SMB (Bugge, 1963; Olerud, 1980; Vel, 1981), related either to grey granite screens or pegmatites. A relationship between the grey granite and gneissic rocks, similar to the flaser gneiss, is indicated by Vel (1981), but is argued to be unlikely due to the lack of evidence for anatexis. The grey granite that is documented in other areas is less voluminous than in the Knaben Zone, and only occurs as thin veins and lenses (Bugge, 1963; Leake, 1972; Olerud, 1980; Vel, 1981). Hence, an increased amount of grey granite is distinct for the Knaben Zone.

A structural control of the molybdenite deposits is argued by Leake (1972), pointing out that the deposits disappear when the foliation deviates from the general moderately east-dipping geometry, as is the case in the northern end of the Knaben Zone. Gvein and Rui (1980) question whether the molybdenite rich zones are remnants from country rock or related to shear zones. Jakubiak and Maund (2012) interpret the Knaben Zone as a thrust ramp, in which the grey granite is emplaced, and that dilation, possibly due to intersection of deep thrusts, results in the large volume of grey granite.

Thin pods and sheets of grey granite occur within the flaser gneiss xenolith in the Knaben Zone. This relationship is ambiguous, but is also documented by previous workers (Lysberg, 1976; Jakubiak and Maund, 2012), and implies a genetic relationship between the two lithologies. Partial melting of the flaser gneiss, driven by heat from the porphyritic granite, possibly mixing with late fractions of the SMB melt, could result in a melt similar to the grey granite. Strain related to the compressional setting would aid the segregation of small percentages of melt, and possibly leave few traces of partial melting processes. Geochemical data presented in this thesis indicates that the xenoliths do contain molybdenum, but this could be a result of metasomatosis, smilar to the elevated molybdenum content within the porphyritic granite that is in contact with the grey granite.

Smaller molybdenite deposits, in thrust-related pegmatites (Fig 36b, c, f) along foliation planes (Fig 12a, Fig 36a) and within other structures (Fig 15e, Fig 27f, Fig 36d), have a clear link to the compressive deformation during Stages 2b-2c. These deposits are minor and regarded to be related to the grey granite directly, as evolved pegmatite melts segregated from the grey granite. Understanding the evolution of the voluminous grey granite sheets is of most interest with further prospecting in mind. A direct structural control of the grey granite is not

observed, but, as discussed below, the sheet-intrusion geometry in a compressional setting is largely dependent on anisotropies and shear zones for it to be mechanically possible. It is proposed that grey granite sheets are guided along foliation planes and within actively deforming shear zone driven by high melt-pressure and strain-aided segregation.

Evolved granitoid melts acting as the main mineralizing fluids are structurally controlled, similar to common granitoid melts, hence creating space for voluminous emplacement which is important to create a large deposit. Emplacement in a compressional setting is discussed below, and sheeted intrusions guided by anisotropies are considered important for the Knaben Zone. An example of a structure controlled mineralized granitoid is given by Küster (2009), and suggests that large scale shear zones are important to localize mineralising fluids. Duuring et al. (2001) and Ferré et al. (2012) shows how ramp-flat geometries can cause dilation and be of importance for a granitoid related deposit (Fig 48c).

Molybdenum partitions into melt relative to solid phases, and into aqueous fluids relative to the melt (Candela and Holland, 1984). As calculated by Coint et al. (in press), the magmatic system is at 4-5kb pressure, meaning that the melt can contain significant amounts of water before reaching saturation (Burnham, 1979). Hence, molybdenum will concentrate in the latest melts and fluids in the SMB. No estimate of the amount of aqueous fluids is calculated in this study, but it is assumed to be low (Müller, 2014). Hence, an evolved felsic melt is the main ore-forming agent.

Strain-induced segregation of evolved melt in the cooling porphyritic granite, and/or from partially melted flaser gneiss could result in molybdenum rich melt batches. These melts are likely to be directed along strain zones, similar to the Knaben Zone. Alternatively, the molybdenum-rich melts could be derived from depth, similarly to the process described by Muñoz et al. (2012), where crustal thickening initiates dehydration melting of the sub-continental lithospheric mantle, and fertile melt rises and is channelled by crustal scale shear zones. A genetic link between the flaser gneiss and the grey granite is preferred in this study, based on the mentioned spatial relationship between the two. See (Bang, 2015) for a detailed chemical approach to the molybdenite deposits in Knaben, also favouring a coupling between the flaser gneiss and the grey granite.

No molybdenite deposits are documented east of the xenolith screens, while the grey granite and other minor deposits do occur slightly west of this zone (Fig 5, Map 2). In addition, the porphyritic granite on the east side is proved to be 10My younger than the porphyritic granite on the west side (Slagstad et al., unpublished TIMS data, 2015). The grey granite is coeval, in terms of the resolution of the data, with the western intrusion (Bingen et al., 2015). Hence, it is proposed that the western porphyritic granite and the grey granite intruded before the eastern porphyritic granite, and the xenolith screens in the Knaben Zone represent the pre-existing country rock, also explaining the lack of grey granite east of the xenoliths. This also delimits the Knaben molybdenite deposit in time.

Melts and fluids from the xenoliths in the deformation zones are most likely to have a different chemistry than the porphyritic granite, and these conditions could hypothetically be favourable for molybdenite precipitation. Sulphur enrichment or a low oxygen fugacity would provoke molybdenite crystallisation (Zhang et al., 2012). Graphite from the xenoliths could generate a reducing environment, and occurs in amphibolite close to a molybdenite deposit west of the Knaben Zone (Vel, 1981). The gneissic xenoliths are rich in sulphide minerals,

and are likely to be a source of sulphide. The contrast in magnetic susceptibility (Appendix 4) and occurrence of extremely magnetic and magnetite-rich veins (Fig 22f) points towards large contrasts in the oxygen fugacity.

The occurrence of calcite closely related to the molybdenite in the grey granite, and the lack of calcite elsewhere, as described in the previous chapter (Fig 11), could indicate CO_2 rich fluids (Fein and Walther, 1987). Increased CO_2 would also create a more reduced environment (Simakin et al., 2012), promoting molybdenite precipitation. CO_2 rich fluids could originate from the xenoliths or from greater depths, and be channelled into the deformation zones.

In summary, a model considering tectonics and magmatism responsible for the formation of the molybdenite deposits is proposed (Fig 48a). Molybdenum is concentrated in evolved melt fractions, and perhaps volatile-rich fluids, and channelled into an active, ductile, compressive shear zone, such as the Knaben Zone. Addition of sulphur and/or reducing agents, from the xenoliths or from a deeper source, promotes molybdenite precipitation with the evolved grey granite melts along the deformation zones that act as geochemical traps. With further cooling and continuing deformation, the last fractions of melt and volatiles from the grey granite are emplaced as subhorizontal, mineralised pegmatites. The deformation locally concentrates molybdenite in foliation planes and other structures related to top-to-the-W thrusting (Fig 48b). The majority of the molybdenum is likely to originate from the xenoliths, particularly the flaser gneiss, or possibly from dehydration melting of the mantle, but evolved melts from the porphyritic granite will also concentrate any available molybdenum.

Voluminous grey granite intrusions are the most interesting economical deposits. In that sense, a structural investigation of the other N-S striking molybdenite zones in the SMB could indicate why the grey granite in the Knaben Zone is anomalously voluminous. The width of a sheet-intrusion is controlled by melt viscosity, amount of available melt, melt-pressure and the local stress regime (Brown and Solar, 1998). Local dilation, for example in a thrust flat, or intersection of large-scale structures could be important for creating space for larger volumes of grey granite (Fig 48c). No such relationship is observed in the Knaben Zone, but it is likely that this is evident on a larger scale, resulting in the large volumes documented in the Knaben Zone.

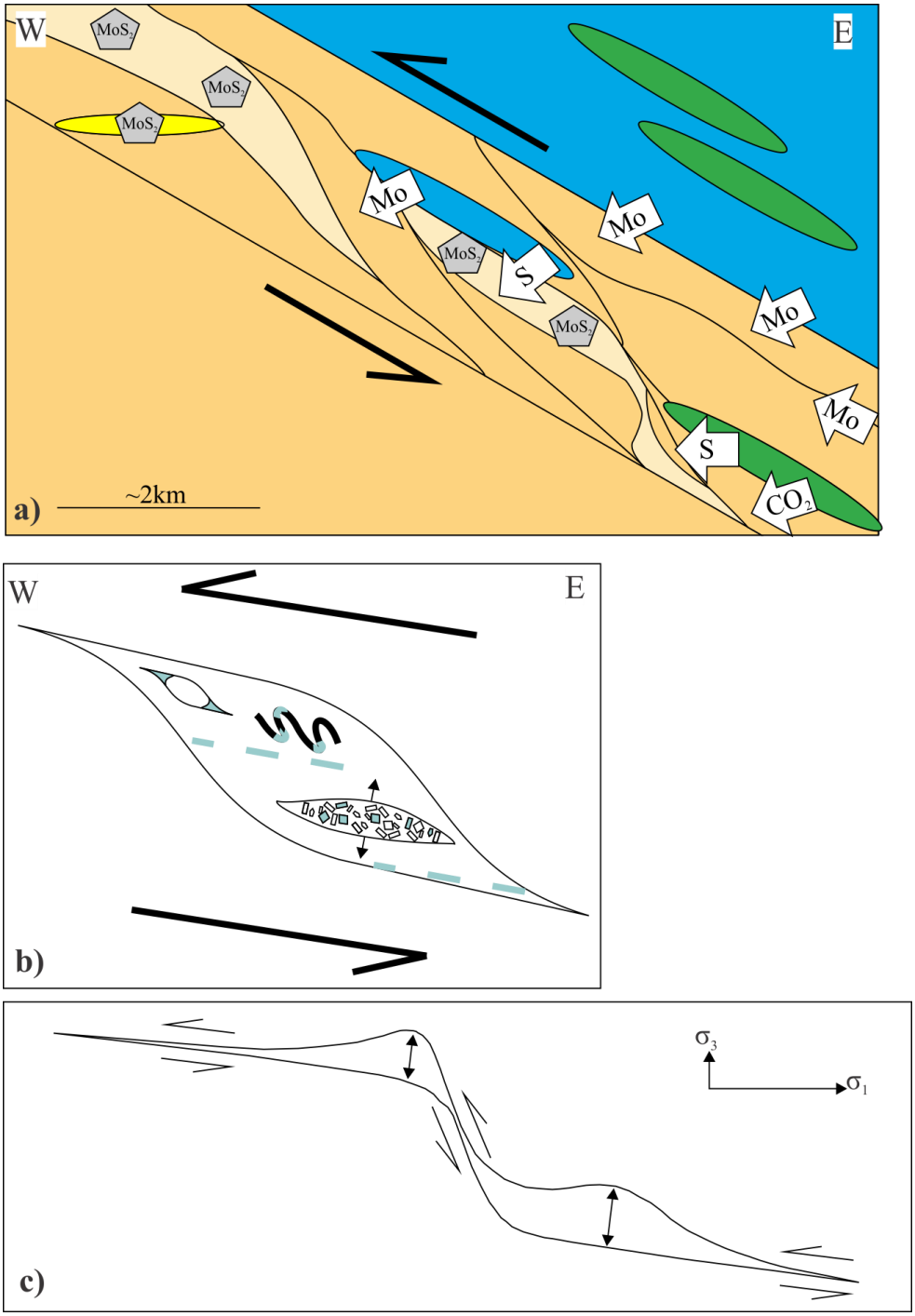

Figure 48: a) *A schematic model of the ore forming processes forming the molybdenite deposits. Mo is concentrated in late magmatic fluids from the porphyritic granite, extracted from the flaser gneiss or possibly comes from depth (see text for discussion). Molybdenite rich magmatic fluids are concentrated in the shear zone (similar to the Knaben Zone). Sulphur and possibly reducing agents from the xenoliths generate a chemical trap where molybdenite is precipitated in the evolved grey granite and related pegmatites. On a local scale, continuing deformation concentrates molybdenite in structures related to top-to-the-W thrusting, and volatiles enrich lithologies adjacent to the grey granite and pegmatites with molybdenite.* ***b)*** *An illustration showing that molybdenite is locally concentrated within top-to-the-W related structures, in the duplex setting. Molybdenite occurs in pressure shadows, in fold hinges, along foliation planes and most importantly within subhorizontal pegmtites.* ***c)*** *A schematic figure, modified after Ferré et al. (2012), indiacting where dilation is expected within a thrust ramp, and crates space for potential voluminous melt emplacement.*

4.2.6 Comparison with previous work from the Knaben Zone

The model for the geological evolution presented in this thesis (Fig 46) is contrasted to the work done by Lysberg (1976), which has until now served as the geological basis for modern research in the Knaben Zone. In addition, the model presented here is applicable when evaluating the SMB in light of a modern Sveconorwegian framework.

The relative temporal relationship between lithological units presented by Lysberg (1976) is similar to that presented here, but the processes controlling this evolution are fundamentally different. As presented in the introduction, Lysberg (1976) argues that the foliation in the xenoliths pre-date the occurrence of porphyritic granite, and that the grey granite and pegmatite occur later, due to partial melting. The model in this thesis places emphasis on the magmatic and tectonic processes in a compressional setting, while Lysberg (1976) explains the geometry with a number of fold phases and does not evaluate the emplacement mechanism for the granitoid rocks or recognize any kinematics. This difference is underpinned by the importance of distinguishing between magmatic, submagmatic and solid-state deformation. Similarly to the model for molybdenite deposits presented here, Lysberg (1976) recognises the relationship between the molybdenite deposits related to grey granite and the flaser gneiss.

Lysberg (1976) describes foliation parallel sheet-like granitoid intrusions and pegmatites, in addition to subhorizontal pegmatites cutting the foliation, but couples these features with periods of relaxation (σ_3 orthogonally to the sheets). As explained above, in this thesis such structures have been critical for evaluating the system as an ongoing compressive setting.

Lysberg (1976) delineates four folding phases, where the first two (F1 and F2) were interpreted as pre-existing structures in the xenoliths. The third phase (F3) is argued to be an incremental fold phase, occurring simultaneously with the granitoid intrusions, creating NS-striking fold axis, and associated with the pervasive parallelism in the area and related to N-S trending shallow mineral lineations in the granitoid rocks. Finally, Lysberg (1976) documents open folds (F4), with a moderate plunging NE-trending fold axis interpreted as a later event, associated with the SE-trending moderately plunging stretching lineations. In this study, the N-S trending mineral lineations are interpreted to be of magmatic to submagmatic origin, related to N-S lateral extrusion, or possibly an early extensional phase allowing N-S directed magmatic intrusion. The four distinct fold phases delineated by Lysberg (1976) are not recognised in this thesis. In combination with kinematic indicators, the small cluster of shallow N-trending fold axis (Fig 28a) is connected to the compressional phase, while the large spread of more irregular folds are considered a product of magmatic processes and possibly pre-existing structures (Fig 28a). The N-S-striking mafic dyke, emphasised by Lysberg (1976) is in this thesis regarded as a regular biotite gneiss screen.

Similarly to the work done by Bingen et al. (2015), the results from this thesis do not show any clear origin for the molybdenum. Late fractions of SMB melt, small amounts of melt or fluids from the pre-Sveconorwegian flaser gneiss or a deeper source are all plausible. The metamorphogenic model presented by Bingen et al. (2015) emphasizes the relationship between the flaser gneiss and the grey granite, a view supported in this thesis, but the importance of aqueous fluids is more contentious. Magmatic processes are crucial in the

model argued in this thesis. The concentration of late melts and fluids in compressive structures is an important finding presented in this thesis.

A connection between the structures and the molybdenite deposits is proposed by Gvein and Rui (1980). They argue that the minor deposits are clearly structure-controlled and speculate on whether they are linked together in a larger network, but they do not document any kinematics or stress regimes. Jakubiak and Maund (2012) recognize the top-to-the-W thrust ramps in which the grey granite has intruded, but do not point out the temporal relations between the structures and the granite emplacement which has been the main focus in this study. In addition, they propose that a dilatational jog, due to intersection of deep-going structures, cause the anomalous large volume of grey granite in the Knaben Zone. This proposal is hard to confirm by studying only the Knaben Zone, as the structures are largely parallel. Future studies should compare structures and geometries of other molybdenite deposits in the SMB, in order to understand regional-scale structural features responsible for large volumes of grey granite.

4.3 The Knaben Zone in the Sveconorwegian orogeny

4.3.1 Emplacement in a convergent setting

The interplay between deformation, metamorphism and intrusion in convergent settings is complex, and the mechanics are examined by among others Hutton (1992) and Brown and Solar (1998). Sheet-like flow through anisotropies or crustal-scale shear zone systems is commonly proposed as a possible melt ascent and migration mechanism in convergent settings.

Falkum and Petersen (1980) argue that large parts of the area, now referred to as the SMB, are formed by repeated synkinematic granitoid intrusions forming N-S-striking sheets and domes, with successive stages of deformation and emplacement throughout the Sveconorwegian orogeny. These conclusions are seldom referred to in more recent Sveconorwegian work. In the Bamble terrane, synkinematic intrusion of pegmatites relative to a top-to-the-W thrusting setting is documented by Henderson and Ihlen (2004). The pegmatites are progressively deformed, and evolve from intruding as sub-horizontal pegmatites cutting the regional foliation, to deformed foliation-parallel pegmatites, similar to the pegmatites in Stage 2c in the Knaben Zone. On a larger scale, the emplacement of a batholith, such as the SMB, in a convergent setting is a mechanical challenge, and is addressed below. Coint et al. (in press) recognise that deformation accompanied the SMB emplacement, and that the emplacement was apparently continuous between 1070Ma until 1020Ma, as sheet-like intrusions. They do not conclude whether the sheet-like geometry is purely a result of pre-existing structures, or else governed by the regional stress-field.

Buoyancy of the melt, melt-pressure and extrusion pressure are important for melt migration to overcome the compressional stresses, together with local stresses related to the sheet-intrusion and viscous flow of the melt (Brown and Solar, 1998). Multiple pulses of granitoid sheets are necessary to maintain a high melt-pressure, consistent with the common sheeted structure of batholiths in compressive settings, including the SMB. Positive volume change due to metamorphic and melt-producing reactions, together with confining pressure of the melt source, can maintain a high melt-pressure (Hutton, 1996). The melt-pressure reduces the effective normal stress and causes melt fracturing, in accordance with hydraulic fracturing (Brown and Solar, 1998).

According to Brown and Solar (1998), anatexis synchronous with the deformation is effective for weakening the crust and causing faster strain rates. Further, tectonic forces are important for extracting melt from the partially melted crust, and the melt flow is strongly controlled by anisotropies in the crust. Due to the viscous properties of granitoid melt, a critical width of the sheets is required to prevent the melt from stalling. Extrusion can help melt migration and extract melt from partially molten rock, but the efficiency depends on the orientation of anisotropies relative to the maximum principle stress axis.

Volumes of intruding melt batches are argued to increase with the number of sheets, because internal intrusion, similar to sheeted dykes, is more efficient (Brown and Solar, 1998). In addition, increased amounts of partial melting will reduce the melt-pressure, as the connection between individual melt batches is larger and may produce instabilities where melt can accumulate. As the melt intrudes the country rock, strain is consequently applied to the country rock (Hutton, 1992). This could explain the typical symmetric deformation documented in the flaser gneiss in the Knaben Zone.

The orientation of anisotropies and shear zones is important for the possibility to act as pathways for melt and to a large degree control the sheet-orientation (Hutton, 1996). Theoretically, tensile fractures will occur at high angles to the minimum principle stress axis. As shown by Brown and Solar (1998) for a compressive setting with vertical anisotropies, the melt-pressure (P_m) must exceed σ_1 (σ_h) to allow a granitoid sheet to intrude along the anisotropies, and for horizontal anisotropies P_m (Fig 49c) must exceed the vertical load (σ_v). High differential stresses can lead to fracturing across the foliation, and is expected at shallower levels. Similarly, high melt-pressure can cause fractures at an angle to the anisotropies. Horizontal and more equidimensional plutons can form at such conditions.

Fowler (1994) argues that intrusion styles in a compressive setting, with subvertical anisotropies, evolve from early foliation-parallel sheets to more irregular plutons and finally discordant angular dykes, depending on the emplacement depth. This evolution is caused by increasing melt viscosity and melt-batch volume. Increased pressure destabilizes the regular sheet geometry, as explained above, resulting in more equidimensional plutons, aided by the continuous heating of the country rock due to repeated intrusions.

Xenolith-rich zones representing country rock separating individual plutons are well documented in the Sierra Nevada batholith (Mahan et al., 2003). The Sierra Nevada batholith consists of both sheeted tabular plutons related to compressive tectonics, and equidimensional plutons which are commonly argued to relate to extension. Magmatism lasted for 140My, and the equidimensional plutons are overrepresented in the final 20My. Mahan et al. (2003) argue that this reflects temporal, and spatially restricted changes in the tectonic setting, which evolve with the active margin.

The McDoogle pluton represents one of the tabular plutons within the Sierra Nevada batholith, and it contains remnants of a synmagmatic compressive shear zone within it and on the margins, and fabrics and kinematics in the xenolith screens reflect the fabrics in the pluton, ranging from magmatic to solid state (Mahan et al., 2003), similarly to the SMB. The kinematics are consistent along either side of the tabular pluton, indicating that the shear zone localized the intrusion and not the opposite. Mahan et al. (2003) argue that buoyancy together with differential stress resulted in magma ascent and migration along an active shear zone in the country-rock. The number of xenolith-screen zones is smaller than the number of tabular

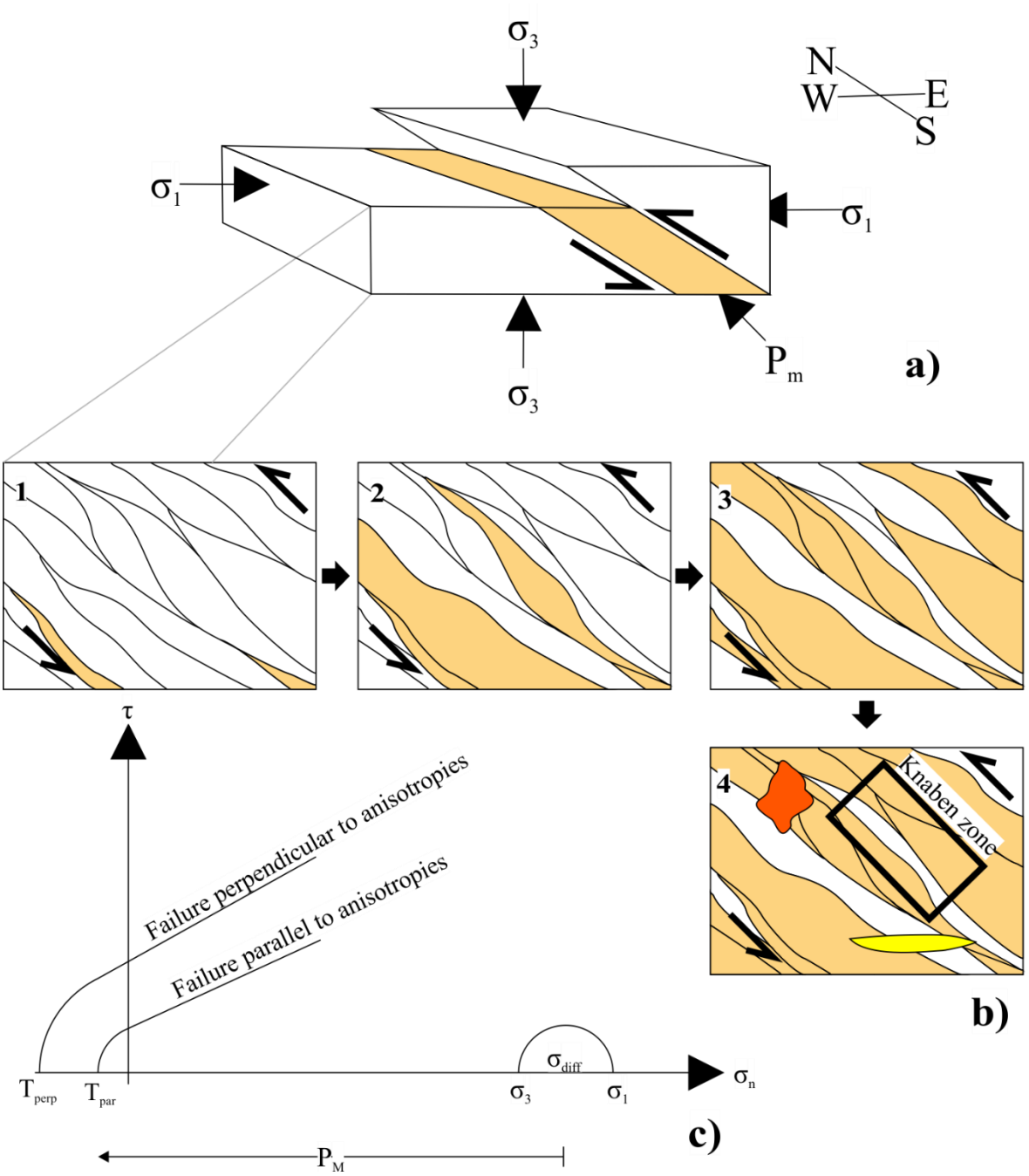

Figure 49: *Schematic emplacement model, illustrations modified after Brown and Solar (1998). The model can be viewed as scale-invariant, causing the small scale Knaben Zone sheets and the larger scale SMB intrusions.* ***a)*** *Model indicating the principle stress axis and the melt-pressure (Pm). Orange colour represents a granitoid sheet, intruded along an anisotropy in the country rock, represented by a thrust shear zone.* ***b)*** *Stepwise emplacement model of the SMB in a continuous kinematic setting. 1-3 represents sheet-intrusions parallel to the anisotropies. Internal sheeted intrusions are also important. 4 represents later stages with intrusion at an angle to the anisotropies and irregular intrusions. It is shown that the Knaben Zone represents a zone with remaining country rock, but similar intrusive processes occur on a local scale in the Knaben Zone.* ***c)*** *Mohr diagram illustrating that failure parallel to the anisotropies is favourable, relative to failure at an angle to the anisotropies, as is the case for b1-b3. Large differential stress (σ_{diff}) or extreme melt-pressure results in failure at an angle to the anisotropies (yellow in b4), and destabilizes the system, making it possible for irregular intrusions (red in b4) to form, which is the case for b4.*

intrusions, hence internal sheeted intrusions were common, resulting in poorly defined pluton-pluton contacts.

The Great Tonalite Sill is a highly elongate batholith in south Alaska, interpreted to intrude synkinematically in a convergent setting (Ingram and Hutton, 1994). Similar to the SMB, the batholith is elongated orthogonally to the compression, and consists largely of parallel granitoid sheets, at places separated by xenolith screens representing country rock. Importantly for further comparison, the Great Tonalite Sill intruded at pressures of 5-7 kbar (Ingram and Hutton, 1994), similar to the 4-5 kbar pressure in the SMB (Coint et al., in press). The sheets are interpreted to intrude as repeated dykes, into an active, compressive, crustal-scale shear zone. Ingram and Hutton (1994) argue that more voluminous domains have formed in dilating thrust flats in the Great Tonalite Sill, similarly to Fig 48c.

4.3.2 Emplacement of the Sirdal Magmatic Belt

The SMB-batholith is largely a N-S-elongated, orogen-parallel batholith consisting of length parallel sheet-like intrusions, inferred from magnetic anomalies and field observations (Coint et al., in press), with a relatively consistent east-dipping geometry. Anomalous domains occur in the north-western parts of the batholith, with poorly documented flat-lying structures (pers. comm. Slagstad) and metavolcanic xenoliths (Roberts et al., 2011; Roberts et al., 2013) and the well-constrained equidimensional garnet granite pluton in the NW domain (Fig 2a), with ages correlating with the SMB (1030Ma) (Coint et al., in press). Regionally, the SMB displays a dominant sheeted structure, and a number of N-S oriented zones with an increased amount of xenolith screens, deformation (pers. comm. Henderson), and molybdenite deposits. The Knaben Zone represents one of these zones. The zones are folded in a complex pattern (Fig 2a).

The lateral strike-length consistency of these xenolith-zones, in addition to the typical parallel sheets of the granitoid rocks in the SMB and the melt-present deformation, suggest that the xenolith-zones on a large scale represent structures with a bearing on the evolution of the SMB, rather than passive rafts of pre-existing bedrock. Coint et al. (in press) speculates that the xenolith zones could represent boundaries between separate intrusions, similar to those exemplified for other convergent plutons in the previous section (Ingram and Hutton, 1994; Mahan et al., 2003). As indicated in the results-chapter, there is a paleo-magnetic contrast between the porphyritic granite on the eastern and western side of the Knaben Zone (Appendix 4) which, together with an age difference of 10My (Slagstad et al., unpublished TIMS data, 2015), supports this hypothesis. Geochemical signatures, presented in the previous chapter, do not show any clear differences between the porphyritic granite on either side of the Knaben Zone (Fig 40, Fig 41). On the eastern margin of the Knaben Zone the xenolith screens are increasingly continuous (Map 1, Fig 5). This is suggested to represent the boundary between the western intrusion of porphyritic granite and the 10My younger eastern intrusion of porphyritic granite (Fig 5). The grey granite is likely to be related to the western intrusion, as there are no molybdenite deposits east of the xenoliths.

Assuming that the Knaben Zone is representative for the N-S-striking xenolith zones, a synkinematic model for the SMB (Fig 49) is within reason, but this should be confirmed by

future studies of these zones. Regionally, the SMB has a similar geometry to that observed on a smaller scale in the Knaben Zone (Henderson, pers. comm.). A regional scale E-W-compressive, top-to-the-W kinematic shear zone network with synkinematic magmatism is proposed for the SMB. This suggests that the structures, kinematics and geometry of the SMB, are scale-invariant, with a bearing for the SMB at whole. In addition, the model allows the SMB to be evaluated in the context of orogen-scale tectonics in the Sveconorwegian orogeny.

The SMB is proposed to intrude as multiple sheets over a period of 50 My (Coint et al., in press), exploiting anisotropies and shear zones within the pre-Sveconorwegian bedrock (Fig 49). For this to be mechanically possible, the magmatic pressure and/or differential stress needs to be significant (Fig 49c) (Hutton, 1992), which is highly likely in a converging Sveconorwegian orogen. Further migration of the sheets is aided by deformation, in the anastomosing duplex network. Extrusion affects the migration and melt-pressure, at least locally. With time, after multiple sheeted intrusions, internal sheeting and increasing assimilation of the country rock, the volume of intrusive granitoid sheets exceeds the volume of country rock screens. At this stage, more voluminous batches of melt are able to intrude, and the sheet-screen-geometry is only preserved locally and in between the larger melt batches, but at large, the emplacement mechanism remains unchanged. In this model, the Knaben Zone represents one of these zones (Fig 49b4), and it can be regarded as a boundary between two significant batches of melt.

Understanding the kinematics within the sheets and on their margins is important for determining the relationship between shearing and intrusion, as pointed out above (Mahan et al., 2003). The consistent top-to-the-W kinematics in the Knaben Zone with the continuation from magmatic flow to solid-state flow suggests that the kinematics reflect the regional tectonics. If the kinematics reflect strain caused by magma emplacement, opposing kinematics would initially be expected on either side of an intruding granitoid sheet. With continuing deformation and passive migration of the sheets evolving into solid-state deformation, such opposing sense of shear is likely to be overprinted, as the sheets possibly migrate with the top-to-the-W movement. Ingram and Hutton (1994) do not present evidence for an opposing sense of shear on either side of the sheets for the Great Tonalite Sill, and they assume that the strain along the hanging wall of a intruding sheet is unlikely to be well-recorded.

The late, irregular bodies of leucocratic granite do not follow the general sheeted model. As argued above, increasing differential stress or increased melt-pressure would destabilize the general intrusion mechanism and facilitate irregular intrusions. With cooling of the SMB, the internal anisotropies are likely to be less pronounced and could also result in late irregular intrusions. Alternatively, they could be explained by increments of extension. A similar discussion would apply to the larger equidimensional garnet granite further west in the SMB (Coint et al., in press).

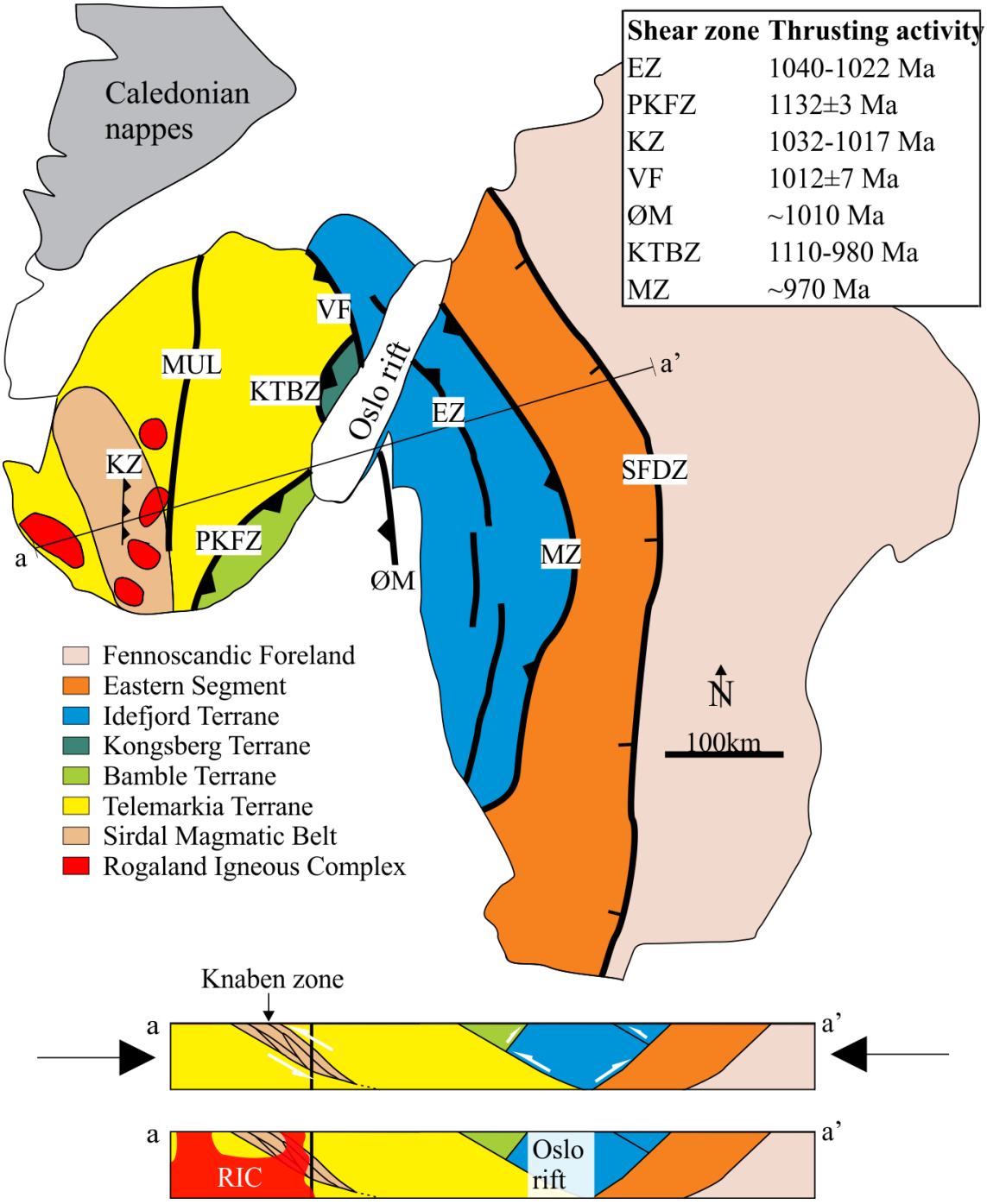

Figure 50: *Regional geology of the Sveconorwegian orogen, modified after (Bingen et al., 2008), showing the different terranes and segments, separated by major shear zones. The shear zones with thrusting activity are marked with triangles, and the approximate timing of the thrusting is shown in table. A simplified profile through the orogen is shown, and a late to post-Sveconorwegian profile including the Rogaland Igneous Complex and the Oslo Graben. The SMB and the Knaben Zone is included within Telemarkia Terrane. Orientation and kinematics from the emplacement of the Knaben Zone are interpreted to be representative for the sheeted intrusions constituting the SMB, and the SMB can hence be evaluated within the orogen-scale tectonic framework. See text for further discussion. Abbreviations for the shear zones. KZ (Knaben Zone), MU (Mandal-Ustaoset shear zone), PKFZ (Porsgrunn Kristiansand Fault Zone), KTBZ (Kongsberg Telemark Boundary Zone), VF (Vardefjell shear zone), ØM (Østfold Marsstrand shear zone), EZ (Elverum shear zone), MZ (Mylonite Zone), SFDZ (Sveconorwegian Frontal Deformation Zone).*

4.3.3 The Sirdal Magmatic Belt in the Sveconorwegian orogeny

The proposed emplacement model allows an interpretation of the SMB as a N-S-striking, eastward-dipping batholith, representing top-to the-W shearing at crustal scale with implications for the Sveconorwegian orogeny. Ages for the SMB between 1040Ma and 1020Ma are presented in this thesis, though SMB ages as old as 1066Ma are presented by (Coint et al., in press). The geometry, kinematics and timing of the SMB fit well with the majority of compressive shear zones elsewhere in the Sveconorwegian orogen (Fig 50).

The Porsgrunn Kristiansand Fault Zone (PKFZ) defines the boundary between the Telemarkia terrane and the Bamble terrane, and is interpreted as an E-dipping shear zone, with west-vergent thrusting subsequent to 1132±3Ma (Fig 50) (Henderson and Ihlen, 2004). Further north, a similar boundary towards the Kongsberg terrane records thrusting activity between 1110Ma and 980 Ma, evolving from an E-W-directed compression towards NW-SE directed compression (Scheiber et al., 2015). Additionally, a west-verging shear zone in the Elverum area, (Fig 50), is proposed to be active between 1040Ma and 1022Ma (Viola et al., unpublished data).

E-verging shear zones in the Sveconorwegian orogen are generally interpreted to occur at a later stage. The SW-dipping contact between the Telemarkia terrane and the Idefjord terrane (Fig 50), referred to as the Vardefjell shear zone (VF), records sinistral deformation at 1012±7Ma (Bingen et al., 2008a). Further west, the Mylonite Zone (MZ) marks the boundary between the Idefjorden terrane and the Eastern segment. Kinematics along the MZ are complex, much due to the arcuate shape of the shear zone and varying dip-direction, but the dominating deformation is interpreted as SE-directed back-thrusting occurring at approximately 970Ma (Viola et al., 2011). The boundary towards the Fennoscandian foreland (SFDZ) dips towards the east, but records minor deformation, and the Eastern segment is regarded as parautochthonous (Fig 50) (Wahlgren et al., 1994; Bingen et al., 2008).

Later extensional structures are well documented along the major shear zones, but with variable ages ranging from 985Ma at the VF to 890Ma in the PKFZ (Bingen et al., 2008). These structures are generally accepted to be a result of gravitational collapse of the Sveconorwegian orogen (Bingen et al., 2006). It is likely that the indications of a later extensional event in the Knaben Zone (Stage 2d) are related to this event.

Delimiting the different shear zones in time is difficult, and has led to the present temporal poorly constrained tectonic model with a converging phase lasting 130My followed by 100My of extension (Bingen et al., 2008; Scheiber et al., 2015). As pointed out by Coint et al. (in press) and shown in this thesis, the geochemistry of the SMB has a distinct subduction signature with significant crustal contamination, but this signature does not necessarily reflect the setting in which the rocks formed. These ambiguities have led to an ongoing discussion about the tectonic setting of the Sveconorwegian orogen (Slagstad et al., 2013; Möller et al., 2013) .

The long-lasting magmatism and elongated shape of the SMB points towards a setting in the vicinity of an active margin (Weaver et al., 1990), in addition to the large heat flow required to create such volumes of melt (Coint et al., in press). Domains within the Sveconorwegian orogen appear to have experienced extension simultaneously (due to the resolution of the

geochronological data) with the general convergence, represented by the equidimensional garnet granite spatially and temporally related to the SMB, at 1030Ma (Coint et al., in press), and lamprophyre dykes in the Bamble terrane (Dahlgren, 1991) at 1034Ma. Switching between compressional and extensional regimes within a few million years is largely accepted for accreting margins (Collins, 2002), and could explain such local differences. Alternatively, obliquities in the convergence can cause local extension, and this is a likely scenario for a large-scale orogen. Hence, the SMB itself reflects a complex tectonic model for the Sveconorwegian orogen, involving domains of extension and compression which are closely temporal and spatially linked.

Similarly to the research presented here, future research aiming to determine the evolution of the Sveconorwegian orogeny should evaluate the emplacement process and, if possible, kinematics of plutons, as they provide a method of acquiring kinematical and more precise temporal data. This will improve the resolution of possible extensional domains within an overall converging setting, and the evaluation of a precise tectonic framework will be less ambiguous.

Chapter 5 – Conclusions

5.1 Conclusions

Detailed fieldwork and microscopic analysis have redefined the understanding of the processes behind the formation of the Knaben Zone. The project has resulted in an updated and extended geological map (Digital Appendix) and a detailed description of the geological evolution (summarised in Fig 46) of the Knaben Zone. Zircon geochronology and whole rock geochemical analysis have provided corroborating evidence for important relations in the Knaben zone, and have allowed correlation on the regional scale.

The main findings considering the Knaben Zone are:

- Pre-Sveconorwegian bedrock (1252.8±8.7 Ma and older) is deformed, resulting in moderate E-dipping structures that are exploited by Sveconorwegian west-verging trusting and related emplacement of the SMB granitoid rocks (an age of 1043.3±5.6 Ma obtained in this project).
- Synkinematic magmatism of continuously evolving granitic rocks intrude as sheets guided by anisotropies and west-verging duplex shear zones, resulting in an anastomosing screen-sheet geometry. Strain is concentrated along the contacts between intrusive sheets and xenolith screens.
- Partial melting and assimilation of the pre-Sveconorwegian bedrock, represented by the xenolith screens, influences the evolved SMB melt, and provide chemical traps where molybdenite rich melts precipitate. The ore forming melts are directed by the top-to-the-W duplex structures, and emplace larger volumes where dilation is possible in such settings. Related late ore forming melts are emplaced in thrust-related pegmatites.
- Continued compression results in local and confined solid-state deformation of the granitoid rocks, and corresponding stretching lineations. The majority of the SMB granitoid rocks remain undeformed, to weakly deformed, with magmatic to submagmatic flow structures.
- Indications of ductile extension reactivating the structures and anisotropies are documented.
- The orientation and petrography of the E-W-striking dykes correspond to the 850 Ma Hunnedalen dykes described further west in the region (Mauer and Verschure, 1998).

Together with relevant research in the region, the findings from the Knaben Zone invite following conclusions and speculations considering Sirdal Magmatic Belt (SMB) and the Sveconorwegian orogeny:

- The synkinematic emplacement model described for the Knaben Zone is considered valid on a larger scale, resulting in the N-S-striking belts of xenolith screens and the N-S-striking magnetic anomalies constituting large parts of the SMB. Hence, the N-S striking xenolith screen zones can be regarded as boundaries between larger intrusions and/or domains where internal intrusions have dominated. This is supported by an age difference of 10My between porphyritic granite on the E and W side of the Knaben zone (Slagstad et al., unpublished TIMS data, 2015), and preliminary paleomagnetic studies indicating a significantly different magnetic inclination on either side.

- Similarly, major volumes of molybdenite bearing grey granite in a thrust setting ought to be confined to domains allowing extensive dilation, such as ramp-flats, and the Knaben Zone should be possible to distinguish geometrically from the less mineralized N-S-striking zones.
- The timing and kinematics of the Knaben Zone correlate well with thrusting activity along major shear zones in the Sveconorwegian orogen. Vast amounts of melt and long-lasting magmatism is well documented in the Knaben Zone and the SMB, together with a clear active margin geochemical signature. Together with indications of extension (presented in discussion) occurring synchronously with the main compressive event defined for the Sveconorwegian orogeny, the findings from the SMB point towards an overall converging tectonic setting allowing voluminous batholiths and domains of extension.

5.2 Further work

The distribution of magmatic, submagmatic and solid-state flow in the SMB is important to constrain the relationship between deformation and intrusion. Studying quartz lattice preferred orientations, similarly to Duguet and Faure (2004), would more precisely determine the relationship between different types of flow, and would be most precise through Electron Backscatter Diffraction (EBSD) analysis. Analysing the anisotropy of magnetic susceptibility (AMS) is a commonly used method for determining the direction of igneous flow (Cañón-Tapia, 2004), and would be especially interesting on a local scale, evaluating extrusion and dyke flow.

Extrusion of granitoid melt is proposed on the basis of lineations and pure-shear structures orthogonal to the compression. Preferably, a relationship between the dip of the foliation and the extrusion related structures (boudinage and magmatic to submagmatic lineations) should be documented, and the extrusion related structures would be expected to occur where the foliation is at its steepest. A detailed study of the relationship between domains that have experienced extrusion and larger screens that have acted as anisotropies would help to determine the amount of shortening.

Separating different plutons based on geochemistry has proved difficult. It is possible that isotopic signatures would improve the delineation of pluton boundaries. Regarding the molybdenite deposits, it is possible that neodymium, strontium, sulphur and possibly oxygen isotopes could determine if the grey granite is genetically related to the flaser gneiss, the porphyritic granite, and possible relations to the lithospheric mantle.

As indicated, it is possible that differences in the palaeomagnetic vector can distinguish different plutons. Ground-magnetic surveys are likely to have the resolution needed to map out different igneous bodies.

On a larger scale, studying and comparing the regional kinematics and geometry of the N-S-striking xenolith and molybdenite zones, similar to the Knaben Zone, would add to the understanding of the emplacement of the SMB. Such studies would possibly demonstrate differences from the Knaben Zone related to the grey granite and molybdenite, and/or geometry and kinematics, with a bearing on local ore-forming processes and large-scale emplacement.

References

Andersen, T., 2005, Terrane analysis, regional nomenclature and crustal evolution in the Southwest Scandinavian Domain of the Fennoscandian Shield: Gff, v. 127, no. 2, p. 159-168.

Bang, S., 2015, Geochemical analysis of molybdenite and other sulphides from Knaben, MSc thesis, Norwegian University of Science and Technology (NTNU).

Bard, J., 1986, Principal Textures of Metamorphic Rocks, Microtextures of Igneous and Metamorphic Rocks, Springer, p. 182-253.

Berthé, D., Choukroune, P., and Gapais, D., 1979, Orientations préférentielles du quartz et orthogneissification progressive en régime cisaillant: l'exemple du cisaillement sud-armoricain: Bull. Minéral., v. 102, no. 2–3, p. 265-272.

Bingen, B., Corfu, F., Stein, H. J., and Whitehouse, M. J., 2015, U–Pb geochronology of the syn-orogenic Knaben molybdenum deposits, Sveconorwegian Orogen, Norway: Geological Magazine, p. 1-20.

Bingen, B., Davis, W. J., Hamilton, M. A., Engvik, A. K., Stein, H. J., Skar, O., and Nordgulen, O., 2008a, Geochronology of high-grade metamorphism in the Sveconorwegian belt, S. Norway: U-Pb, Th-Pb and Re-Os data: Norsk Geologisk Tidsskrift, v. 88, no. 1, p. 13.

Bingen, B., Nordgulen, O., and Viola, G., 2008, A four-phase model for the Sveconorwegian orogeny, SW Scandinavia: Norsk Geologisk Tidsskrift, v. 88, no. 1, p. 43.

Bingen, B., Stein, H. J., Bogaerts, M., Bolle, O., and Mansfeld, J., 2006, Molybdenite Re–Os dating constrains gravitational collapse of the Sveconorwegian orogen, SW Scandinavia: Lithos, v. 87, no. 3, p. 328-346.

Bingen, B., and Van Breemen, O., 1998, Tectonic regimes and terrane boundaries in the high-grade Sveconorwegian belt of SW Norway, inferred from U–Pb zircon geochronology and geochemical signature of augen gneiss suites: Journal of the Geological Society, v. 155, no. 1, p. 143-154.

Boyer, S. E., and Elliott, D., 1982, Thrust systems: AAPG Bulletin, v. 66, no. 9, p. 1196-1230.

Brown, M., 2013, Granite: From genesis to emplacement: Geological Society of America Bulletin, v. 125, no. 7-8, p. 1079-1113.

Brown, M., and Solar, G. S., 1998, Granite ascent and emplacement during contractional deformation in convergent orogens: Journal of Structural Geology, v. 20, no. 9, p. 1365-1393.

Buettner, S. H., 1999, The geometric evolution of structures in granite during continous deformation from magmatic to solid-state conditions: An example from the central European Variscan Belt: American Mineralogist, v. 84, p. 1781-1792.

Bugge, A., 1963, Norges molybdenforekomster, Universitetsforlaget, v. 217.

Burnham, C., 1979, Magmas and Hydrothermal Fluids: in HL Barnes, ed.. Geochemistry of Hydrothermal Ore Deposits (2nd Edit.), New York, John Wiley and Sons.

Candela, P. A., and Holland, H. D., 1984, The partitioning of copper and molybdenum between silicate melts and aqueous fluids: Geochimica et Cosmochimica Acta, v. 48, no. 2, p. 373-380.

Cañón-Tapia, E., 2004, Anisotropy of magnetic susceptibility of lava flows and dykes: a historical account: Geological Society, London, Special Publications, v. 238, no. 1, p. 205-225.

Casini, G., Decandia, F. A., and Tavarnelli, E., 2007, Analysis of a mesoscopic duplex in SW Tuscany, Italy: implications for thrust system development during positive tectonic inversion: Geological Society, London, Special Publications, v. 272, no. 1, p. 437-446.

Coint, N., Slagstad, T., Roberts, N., Røhr, T., Marker, M., and Sørensen, B. E., in press, The late Mesoproterozoic Sirdal Magmatic Belt, SW Norway; relationships between magmatism and metamorphism and implications for Sveconorwegian orogenesis: Precambrian Research.

Collins, W., 2002, Hot orogens, tectonic switching, and creation of continental crust: Geology, v. 30, no. 6, p. 535-538.

Corfu, F., Hanchar, J. M., Hoskin, P. W., and Kinny, P., 2003, Atlas of zircon textures: Reviews in mineralogy and geochemistry, v. 53, no. 1, p. 469-500.

Dahlgren, 1991, Unpublished report; SNF workshop Bamble.

Drüppel, K., Elsäßer, L., Brandt, S., and Gerdes, A., 2012, Sveconorwegian mid-crustal ultrahigh-temperature metamorphism in Rogaland, Norway: U–Pb LA-ICP-MS geochronology and

pseudosections of Sapphirine granulites and associated paragneisses: Journal of Petrology, p. egs070.
Duguet, M., and Faure, M., 2004, Granitoid emplacement during a thrusting event: structural analysis, microstructure and quartz c-axis patterns. An example from Hercynian plutons in the French Massif Central: Journal of structural geology, v. 26, no. 5, p. 927-945.
Duuring, P., Hagemann, S. G., and Love, R. J., 2001, A thrust ramp model for gold mineralization at the Archean trondhjemite-hosted Tarmoola deposit: The importance of heterogeneous stress distributions around granitoid contacts: Economic Geology, v. 96, no. 6, p. 1379-1396.
Falkum, T., and Petersen, J., 1980, The Sveconorwegian orogenic belt, a case of Late-Proterozoic plate-collision: Geologische Rundschau, v. 69, no. 3, p. 622-647.
Fein, J. B., and Walther, J. V., 1987, Calcite solubility in supercritical CO 2 · H 2 O fluids: Geochimica et Cosmochimica Acta, v. 51, no. 6, p. 1665-1673.
Ferré, E. C., Galland, O., Montanari, D., and Kalakay, T. J., 2012, Granite magma migration and emplacement along thrusts: International Journal of Earth Sciences, v. 101, no. 7, p. 1673-1688.
Fowler, T., 1994, Sheeted and bulbous pluton intrusion mechanisms of a small granitoid from southeastern Australia: implications for dyke-to-pluton transformation during emplacement: Tectonophysics, v. 234, no. 3, p. 197-215.
Frost, B. R., Barnes, C. G., Collins, W. J., Arculus, R. J., Ellis, D. J., and Frost, C. D., 2001, A geochemical classification for granitic rocks: Journal of petrology, v. 42, no. 11, p. 2033-2048.
Gellein, J., 2007, Aeromagnetic anomaly map, Mandal. Scale 1:250,000. Geological Survey of Norway.
Gill, J. B., 1976, Composition and age of Lau Basin and Ridge volcanic rocks: implications for evolution of an interarc basin and remnant arc: Geological Society of America Bulletin, v. 87, no. 10, p. 1384-1395.
Gower, C., Ryan, A., and Rivers, T., 1990, Mid-Proterozoic Laurentia–Baltica: an overview of its geological evolution and a summary of the contributions made by this volume: Mid-Proterozoic Laurentia-Baltica, v. 38, p. 1-20.
Gvein, Ø., and Rui, I., 1980, The Knaben area. Report from the field-season 1979 and a compilation of results from previous drilling and exploration work. (For Sydvaranger A/S).
Henderson, I. H., and Ihlen, P. M., 2004, Emplacement of polygeneration pegmatites in relation to Sveco-Norwegian contractional tectonics: examples from southern Norway: Precambrian Research, v. 133, no. 3, p. 207-222.
Hirth, G., and Tullis, J., 1992, Dislocation creep regimes in quartz aggregates: Journal of Structural Geology, v. 14, no. 2, p. 145-159.
Hoskin, P., and Black, L., 2000, Metamorphic zircon formation by solid-state recrystallization of protolith igneous zircon: Journal of metamorphic Geology, v. 18, no. 4, p. 423-439.
Hutton, D. H., 1992, Granite sheeted complexes: evidence for the dyking ascent mechanism: Geological Society of America Special Papers, v. 272, p. 377-382.
Hutton, D. H., 1996, The'space problem'in the emplacement of granite: Episodes-Newsmagazine of the International Union of Geological Sciences, v. 19, no. 4, p. 114-119.
Ingram, G. M., and Hutton, D. H., 1994, The Great Tonalite Sill: Emplacement into a contractional shear zone and implications for Late Cretaceous to early Eocene tectonics in southeastern Alaska and British Columbia: Geological Society of America Bulletin, v. 106, no. 5, p. 715-728.
Jakubiak, Z., and Maund, N. H., 2012, AN EVALUATION OF MOLYBDENUM POTENTIAL, KNABEN AREA, KVINESDAL, VEST-AGDER, NORWAY (for Variscan Mines s.a.s.).
Jones, R. R., Holdsworth, R. E., and Bailey, W., 1997, Lateral extrusion in transpression zones: the importance of boundary conditions: Journal of Structural Geology, v. 19, no. 9, p. 1201-1217.
Jourdan, C., 2003, Molybdenum mining in the mountains around Knaben. Unpublished report.
Karlstrom, K., Miller, C., Kingsbury, J., and Wooden, J., 1993, Pluton emplacement along an active ductile thrust zone, Piute Mountains, southeastern California: interaction between deformational and solidification processes: Geological Society of America Bulletin, v. 105, no. 2, p. 213-230.

Küster, D., 2009, Granitoid-hosted Ta mineralization in the Arabian–Nubian Shield: ore deposit types, tectono-metallogenetic setting and petrogenetic framework: Ore Geology Reviews, v. 35, no. 1, p. 68-86.
Leake, R., 1972, The geology and petrology of the pre-camhrian basement" between Sirdal and Åseral, Vest Agder, Norway: Durham University.
Ludwig, K., 2012, Isoplot/Ex Version 4: A Geochronological Toolkit For Microsoft Excel: Geochronology Center, Berkeley.
Lysberg, K., 1976, Geologi og mineralisering ved Knaben molybdengruber. Thesis. Universitetet i Bergen. 84 p. (in Norwegian).
Mahan, K. H., Bartley, J. M., Coleman, D. S., Glazner, A. F., and Carl, B. S., 2003, Sheeted intrusion of the synkinematic McDoogle pluton, Sierra Nevada, California: Geological Society of America Bulletin, v. 115, no. 12, p. 1570-1582.
Mauer, C., and Verschure, R., 1998, Petrology and isotope geology of the Hunnedalen Monzonoritic Dyke Swarm, SW Norway: a possible late expression of Egersund Anorthosite magmatism: NORGES GEOLOGISKE UNDERSOKELSE, v. 434, p. 83-108.
Möller, C., Bingen, B., Andersson, J., Stephens, M. B., Viola, G., and Scherstén, A., 2013, A non-collisional, accretionary Sveconorwegian orogen–Comment: Terra Nova, v. 25, no. 2, p. 165-168.
Müller, A., 2014, Quartz chemistry of molybdenite mineralizations and host rocks of the Knaben mining district: NGU Field Work Report.
Müller, A., Wanvik, J. E., and Ihlen, P. M., 2012, Petrological and chemical characterisation of high-purity quartz deposits with examples from Norway, Quartz: deposits, mineralogy and analytics, Springer, p. 71-118.
Muñoz, M., Charrier, R., Fanning, C., Maksaev, V., and Deckart, K., 2012, Zircon trace element and O–Hf isotope analyses of mineralized intrusions from El Teniente ore deposit, Chilean Andes: Constraints on the source and magmatic evolution of porphyry Cu–Mo related magmas: Journal of Petrology, p. egs010.
Olerud, 1980, Molybdenforekomster mellom Flottorp og Ørsdalen, sammenstilling av enkeltundersøkelser, NGU rapport nr.: 1650/50A.
Parsons, I., Thompson, P., Lee, M. R., and Cayzer, N., 2005, Alkali feldspar microtextures as provenance indicators in siliciclastic rocks and their role in feldspar dissolution during transport and diagenesis: Journal of Sedimentary Research, v. 75, no. 5, p. 921-942.
Passchier, C. W., and Trouw, R. A., 1996, Microtectonics, Springer.
Paterson, S. R., Fowler, T. K., Schmidt, K. L., Yoshinobu, A. S., Yuan, E. S., and Miller, R. B., 1998, Interpreting magmatic fabric patterns in plutons: Lithos, v. 44, no. 1, p. 53-82.
Paterson, S. R., Vernon, R. H., and Tobisch, O. T., 1989, A review of criteria for the identification of magmatic and tectonic foliations in granitoids: Journal of structural geology, v. 11, no. 3, p. 349-363.
Pearce, J. A., and Stern, R. J., 2006, Origin of back-arc basin magmas: Trace element and isotope perspectives: Back-Arc Spreading Systems: Geological, Biological, Chemical, and Physical Interactions, p. 63-86.
Philpotts, A. R., 1989, Petrography of igneous and metamorphic rocks, Pearson College Div.
Platt, J., and Vissers, R., 1980, Extensional structures in anisotropic rocks: Journal of Structural Geology, v. 2, no. 4, p. 397-410.
Roberts, N. M., Parrish, R. R., Horstwood, M. S., and Brewer, T., 2011, The 1.23 Ga Fjellhovdane rhyolite, Grøssæ-Totak; a new age within the Telemark supracrustals, southern Norway: Norwegian Journal of Geology, v. 91, p. 239-246.
Roberts, N. M., Slagstad, T., Parrish, R. R., Norry, M. J., Marker, M., and Horstwood, M. S., 2013, Sedimentary recycling in arc magmas: geochemical and U–Pb–Hf–O constraints on the Mesoproterozoic Suldal Arc, SW Norway: Contributions to Mineralogy and Petrology, v. 165, no. 3, p. 507-523.
Sandstad, J., Bjerkgård, T., Boyd, R., Ihlen, P., Korneliussen, A., Nilsson, L., Often, M., Eilu, P., and Hallberg, A., 2012, Metallogenic areas in Norway, Metallogeny of Fennoscania. Geological Survey of Finland Special Paper 53, p. 35-138.

Scheiber, T., Viola, G., Bingen, B., Peters, M., and Solli, A., 2015, Multiple reactivation and strain localization along a Proterozoic orogen-scale deformation zone: The Kongsberg-Telemark boundary in southern Norway revisited: Precambrian Research.
Shand, S. J., 1943, Eruptive rocks: Their genesis, composition, and classification, with a chapter on meteorites, J. Wiley & sons, Incorporated.
Simakin, A., Salova, T., and Bondarenko, G., 2012, Experimental study of magmatic melt oxidation by CO2: Petrology, v. 20, no. 7, p. 593-606.
Slagstad, T., Roberts, N. M., Marker, M., Røhr, T. S., and Schiellerup, H., 2013, A non-collisional, accretionary Sveconorwegian orogen: Terra Nova, v. 25, no. 1, p. 30-37.
Stipp, M., Stuènitz, H., Heilbronner, R., and Schmid, S. M., 2002, The eastern Tonale fault zone: a 'natural laboratory'for crystal plastic deformation of quartz over a temperature range from 250 to 700 C: Journal of Structural Geology, v. 24, no. 12, p. 1861-1884.
Streckeisen, A., 1974, Classification and nomenclature of plutonic rocks recommendations of the IUGS subcommission on the systematics of igneous rocks: Geologische Rundschau, v. 63, no. 2, p. 773-786.
Sun, S.-S., and McDonough, W., 1989, Chemical and isotopic systematics of oceanic basalts: implications for mantle composition and processes: Geological Society, London, Special Publications, v. 42, no. 1, p. 313-345.
Vander Auwera, J., Bogaerts, M., Liégeois, J.-P., Demaiffe, D., Wilmart, E., Bolle, O., and Duchesne, J. C., 2003, Derivation of the 1.0–0.9 Ga ferro-potassic A-type granitoids of southern Norway by extreme differentiation from basic magmas: Precambrian Research, v. 124, no. 2, p. 107-148.
Vel, v. d., 1981, Åmlandsheia molybdenfelt, NGU rapport nr.:1750/71A.
Vernon, R. H., 2004, A practical guide to rock microstructure, Cambridge university press.
Vigneresse, J. L., 2004, A new paradigm for granite generation: Transactions of the Royal Society of Edinburgh: Earth Sciences, v. 95, no. 1-2, p. 11-22.
Viola, G., Henderson, I., Bingen, B., and Hendriks, B., 2011, The Grenvillian–Sveconorwegian orogeny in Fennoscandia: Back-thrusting and extensional shearing along the "Mylonite Zone": Precambrian Research, v. 189, no. 3, p. 368-388.
Wahlgren, C.-H., Cruden, A. R., and Stephens, M. B., 1994, Kinematics of a major fan-like structure in the eastern part of the Sveconorwegian orogen, Baltic Shield, south-central Sweden: Precambrian Research, v. 70, no. 1, p. 67-91.
Walderhaug, H. J., Torsvik, T. H., Eide, E. A., Sundvoll, B., and Bingen, B., 1999, Geochronology and palaeomagnetism of the Hunnedalen dykes, SW Norway: implications for the Sveconorwegian apparent polar wander loop: Earth and Planetary Science Letters, v. 169, no. 1, p. 71-83.
Weaver, S. G., Bruce, R., Nelson, E. P., Brueckner, H. K., and LeHuray, A. P., 1990, The Patagonian batholith at 48 S latitude, Chile; geochemical and isotopic variations: Geological Society of America Special Papers, v. 241, p. 33-50.
Whitney, D. L., and Evans, B. W., 2010, Abbreviations for names of rock-forming minerals: American mineralogist, v. 95, no. 1, p. 185.
Winter, J. D., 2010, Principles of igneous and metamorphic petrology, Prentice Hall New York.
Zellmer, G. F., and Annen, C., 2008, An introduction to magma dynamics: Geological Society, London, Special Publications, v. 304, no. 1, p. 1-13.
Zhang, L., Audétat, A., and Dolejš, D., 2012, Solubility of molybdenite (MoS 2) in aqueous fluids at 600–800 C, 200MPa: A synthetic fluid inclusion study: Geochimica et Cosmochimica Acta, v. 77, p. 175-185.

Appendix

Appendix 1 – Localities

Locality	lat	lon
L1	58.711842	7.06609299
L2	58.710743	7.066138
L3	58.710363	7.09236003
L4	58.707701	7.07074
L5	58.707129	7.06477099
L6	58.706521	7.09573802
L7	58.704649	7.10016199
L8	58.704196	7.07844699
L9	58.703145	7.10076104
L10	58.70313	7.08460702
Kvina	58.702918	7.0861
L11	58.702362	7.09707996
L12	58.702317	7.09639499
L13	58.701634	7.09574497
L14	58.701466	7.08994302
L15	58.701071	7.08802197
L16	58.700843	7.09178997
L17	58.700254	7.08734798
L18	58.698797	7.07708401
L19	58.698502	7.07461604
L20	58.698388	7.10455502
L21	58.698009	7.09159903
L22	58.697714	7.07289004
L23	58.697354	7.07391699
L24	58.69645	7.10033197
L25	58.696069	7.057367
L26	58.695238	7.083295

L27	58.695238	7.083295
L28	58.694957	7.05543498
L29	58.694589	7.09274702
L30	58.694144	7.08585399
L31	58.689785	7.07214396
L32	58.689746	7.075516
L33	58.689693	7.07744803
L34	58.689581	7.07391196
L35	58.687926	7.07222301
L36	58.68774	7.07517897
L37	58.68746	7.08123799
L38	58.687346	7.079455
L39	58.686913	7.08463401
L40	58.684355	7.08432497
L41	58.683793	7.06153398
L42	58.681523	7.07619896
L43	58.680696	7.09524902
L44	58.679062	7.05933298
Upper Roma	58.678078	7.08274196
L45	58.678077	7.08272402
Upper Ørnehommen	58.676948	7.06719504
Lower Ørnehommen	58.676652	7.06671903
L46	58.67519	7.09159803
L47	58.675084	7.08113599
L48	58.674912	7.08155097
L49	58.674207	7.05214298
L50	58.673476	7.05612003
L51	58.673188	7.05570504
L52	58.67315	7.04693204

L53	58.673146	7.08265998
L54	58.672981	7.06886396
L55	58.672896	7.07085399
Lower Roma	58.672367	7.08402397
L56	58.671074	7.08281304
L57	58.671032	7.07064704
L58	58.67068	7.07209401
L59	58.66944	7.06701399
L60	58.669428	7.07270899
L61	58.669378	7.07078802
L62	58.668856	7.07015896
L63	58.667415	7.08875103
L64	58.667395	7.088889
L65	58.665701	7.08919502
L66	58.66487	7.08198901
L67	58.664751	7.08390797
L68	58.664524	7.08460501
L69	58.664189	7.08332802
L70	58.663582	7.08344897
L71	58.663556	7.08326398
L72	58.663342	7.05132399
L73	58.661567	7.08943298
L74	58.661399	7.083166
L75	58.661266	7.08278697
L76	58.66094	7.08127999
L77	58.660604	7.07678896
L78	58.660584	7.07669098
L79	58.660553	7.07981399
L80	58.660463	7.08498102
L81	58.660381	7.08448104

L82	58.660035	7.08044699
L83	58.659885	7.07574097
L84	58.659826	7.07914696
L85	58.659813	7.07725399
L86	58.659636	7.08140597
L87	58.659244	7.07797903
L88	58.657798	7.08498697
L89	58.657716	7.08252403
L90	58.657345	7.08159397
L91	58.657191	7.07801096
L92	58.65707	7.08042302
L93	58.65695	7.07675301
L94	58.656055	7.06151303
L95	58.650858	7.05868104
L96	58.650626	7.07088701
L97	58.650399	7.05716902
L98	58.650261	7.05855397
L99	58.650259	7.06991396
L100	58.649756	7.06917501
L101	58.649677	7.08061396
L102	58.649295	7.08029503
L103	58.649007	7.07987996
L104	58.648648	7.07824498
L105	58.647446	7.04581297
L106	58.6469	7.05652203
L107	58.646791	7.04486498
L108	58.644425	7.05728201
L109	58.64441	7.05724698
L110	58.644257	7.07821498

Appendix 2 – Sample list

sample	lat	lon	rock type	thin section	geochemistry	geochronology
K1	58.694957	7.055434976	porphyritic granite		x	x
K2	58.696069	7.057367004	biotite gneiss	x	x	
K3	58.697714	7.072890038	porphyritic granite/biotite gneiss	x		
K4	58.697354	7.073916988	amphibolite			
K5	58.698797	7.077084007	amphibolite			
K6	58.700254	7.087347982	flaser gneiss		x	
K7	58.702362	7.097079959	biotite gneiss		x	
K8	58.698388	7.104555024	porphyritic granite		x	
K9	58.68746	7.081237994	melanocratic granite	x	x	
K10	58.68746	7.081237994	amphibolite			
K11	58.676652	7.066719029	leucocratic granite	x	x	
K12	58.676652	7.066719029	grey granite	x	x	
K13	58.676948	7.067195037	grey granite	x	x	
K14	58.671074	7.082813038	amphibolite		x	
K15	58.66487	7.081989013	porphyritic granite	x	x	
K16	58.664189	7.083328022	biotite gneiss	x	x	
K17	58.659885	7.075740974	grey granite	x	x	
K18	58.65695	7.076753005	porphyritic granite			
K19	58.657191	7.078010961	amphibolite	x	x	
K20	58.657345	7.081593974	magnetite rich layer	x		
K21	58.704196	7.078446988	porphyritic granite, altered			
K22	58.707701	7.070739996	aplite	x	x	
K23	58.704649	7.100161985	melanocratic granite		x	(x)
K24	58.702317	7.09639499	flaser gneiss	x	x	
K25	58.694589	7.092747018	mafic dyke			
K26	58.650399	7.057169024	porphyritic granite		x	(x)
K27	58.644425	7.057282012	leucocratic granite		x	
K28	58.649756	7.069175011	qz granite	x	x	
K29	58.650259	7.069913959	grey granite		x	(x)
K29A	58.648648	7.078244984	biotite gneiss	x	x	

K30	58.649677	7.080613961	porphyritic granite	x	x	
K31	58.689785	7.072143964	grey granite		x	(x)
K32	58.695238	7.083294997	migmatite	x	x	
K33	58.689693	7.077448033	amphibolite	x	x	
K34	58.68774	7.075178968	migmatite		x	
K35	58.689855	7.075210987	migmatite	x	x	
K36	58.686913	7.084634006	flaser gneiss	x	x	x
K100	58.659885	7.075740974	porphyritic granite/flaser gneiss	x		
K101	58.678077	7.082724022	melanocratic granite	x	x	
K102	58.678077	7.082724022	porphyritic granite/flaser gneiss	x		
K103	58.673188	7.055705041	hbl vein	x		
K104	58.673188	7.055705041	magnetite rich layer	x		
K105	58.674207	7.052142983	porphyritic granite		x	
K106	58.671032	7.07064704	porphyritic granite-deformed	x		
K107	58.67519	7.091598026	porphyritic granite		x	
K108	58.672896	7.07085399	aplite			
K109	58.668856	7.070158962	grey granite/porphyritic granite	x		
K110	58.650858	7.058681035	porphyritic granite with mol			
K111	58.647446	7.04581297	grey granite/biotite gneiss	x		
K112	58.646791	7.044864977	porphyritic granite		x	
K113	58.64441	7.057246976	leucocratic granite			
K114	58.707129	7.064770991	leucocratic granite		x	
K115	58.710743	7.066137996	aplite		x	
K116	58.710363	7.092360025	migmatite	x		
K117	58.679062	7.05933298	dyke	x	x	
K118	58.659826	7.079146961	porphyritic granite		x	
K119	58.660553	7.079813993	flaser gneiss		x	
K120	58.660035	7.080446994	aplite		x	
K121	58.661266	7.08278697	amphibolite	x		
K122	58.661567	7.089432981	porphyritic granite	x	x	

K123	58.667395	7.088888995	migmatite		
K124	58.667395	7.088888995	migmatite		
K125	58.665701	7.089195019	porphyritic granite		x
K126	58.659885	7.075740974	grey granite	x	x
K127	58.678078	7.082741959	flaser gneiss	x	
K128	58.678078	7.082741959	porphyritic granite-deformed	x	
K129	58.683793	7.061533984	porphyritic granite		x
K130	58.70313	7.084607016	biotite gneiss		x
K131	58.703145	7.100761039	porphyritic granite		x
K1000	58.659885	7.075740974	grey granite		
K1001	58.698009	7.091599032	pegmatite with chalcopyrite		
K1002	58.659813	7.077253992	btgneiss	x	x
K1003	58.650626	7.070887014	pegmatite with molybdenite		
K1004	58.6469	7.056522025	porphyritic granite-deformed with mol	x	x
K1005	58.650261	7.058553966	grey granite		x
P	58.501885	7.194833	flaser gneiss		x

Appendix 3 – Zircon geochronological data

	Isotope ratios										Age estimates (ma)								Concentrations			
	Concordia output					Terra-Wasserburg output																
Analysis_#	Pb207/U235	1s%	Pb206/U238	1s%	roh	238/206	1s%	207/206	1s%		Pb207/Pb206	1s	Pb207/U235	1s	Pb206/U238	1s	conc		Th/U	U	Th	Pbtot
K-1_01	1.8149	1.29	0.17726	1.17	0.56	5.6414	1.17	0.07431	1.16		1049.9	23.19	1050.9	8.46	1052	11.41	100.2		0.19	302	58	60
K-1_02	1.5714	1.21	0.15995	1.17	0.60	6.2520	1.17	0.07130	1.07		966.1	21.62	959	7.54	956.5	10.37	99.0		0.16	899	144	160
K-1_03	1.8196	1.19	0.17707	1.16	0.61	5.6475	1.16	0.07458	1.05		1056.9	21.1	1052.5	7.81	1050.9	11.29	99.4		0.16	1032	164	205
K-1_04	2.3838	1.45	0.20991	1.20	0.50	4.7639	1.20	0.08242	1.35		1255.5	25.93	1237.7	10.40	1228.3	13.38	97.8		0.32	95	31	23
K-1_05	1.7727	1.29	0.17365	1.17	0.56	5.7587	1.17	0.07409	1.16		1044	23.24	1035.5	8.39	1032.2	11.20	98.9		0.44	393	173	82
K-1_06	1.7494	1.20	0.17004	1.16	0.60	5.8810	1.16	0.07467	1.06		1059.6	21.12	1026.9	7.78	1012.3	10.91	95.5		0.16	837	134	159
K-1_07	1.8477	1.24	0.17903	1.12	0.53	5.5857	1.12	0.07486	1.15		1064.7	22.97	1062.6	8.18	1061.7	11.01	99.7		0.17	443	75	89
K-1_08	1.7736	1.19	0.17407	1.12	0.56	5.7448	1.12	0.07390	1.08		1038.8	21.79	1035.8	7.70	1034.5	10.69	99.6		0.36	577	206	119
K-1_09	1.8123	1.16	0.1742	1.12	0.57	5.7405	1.12	0.07546	1.06		1080.7	21.17	1049.9	7.62	1035.2	10.68	95.8		0.56	705	392	155
K-1_10	1.7639	1.21	0.17447	1.12	0.55	5.7316	1.12	0.07333	1.10		1023	22.3	1032.3	7.82	1036.7	10.73	101.3		0.35	349	121	72
K-26_01	1.5336	1.20	0.13487	1.16	0.60	7.4145	1.16	0.08253	1.05		1258.1	20.34	943.9	7.39	815.6	8.91	64.8		1.01	1591	1611	279
K-26_02	1.5150	1.20	0.13687	1.16	0.60	7.3062	1.16	0.08034	1.06		1205.4	20.6	936.5	7.33	826.9	9.02	68.6		0.74	1808	1342	309
K-26_03	1.0460	1.20	0.09338	1.17	0.60	10.7089	1.17	0.08131	1.06		1228.9	20.67	726.9	6.25	575.5	6.40	46.8		0.37	2531	928	282
K-26_04	2.0126	1.25	0.17797	1.17	0.57	5.6189	1.17	0.08208	1.12		1247.5	21.75	1119.8	8.50	1055.9	11.38	84.6		1.41	186	262	48
K-26_05	1.6764	1.21	0.16217	1.17	0.60	6.1664	1.17	0.07503	1.07		1069.4	21.29	999.6	7.69	968.8	10.46	90.6		0.65	1543	1006	312
K-26_06	1.6956	1.28	0.16667	1.17	0.56	5.9999	1.17	0.07384	1.15		1037.2	23.1	1006.9	8.18	993.8	10.77	95.8		0.16	661	107	123
K-26_07	1.7946	1.17	0.16647	1.12	0.56	6.0071	1.12	0.07819	1.07		1151.8	21.13	1043.5	7.65	992.6	10.29	86.2		0.51	855	439	177
K-26_08	1.1891	1.18	0.12289	1.11	0.56	8.1374	1.11	0.07018	1.08		933.6	21.97	795.6	6.51	747.2	7.89	80.0		0.14	1564	226	219
K-26_09	1.7948	1.44	0.16989	1.15	0.46	5.8862	1.15	0.07663	1.37		1111.5	27.15	1043.6	9.39	1011.5	10.75	91.0		0.33	122	40	25
K-26_10	1.0629	1.29	0.10113	1.13	0.51	9.8883	1.13	0.07623	1.21		1101.2	23.99	735.3	6.77	621	6.69	56.4		0.42	621	259	76
K-29_01	1.0867	1.22	0.11145	1.16	0.59	8.9726	1.16	0.07078	1.07		950.9	21.9	746.9	6.43	681.2	7.50	71.6		0.69	4370	2995	592
K-29_02	0.9421	1.25	0.10682	1.16	0.58	9.3615	1.16	0.06402	1.11		742.3	23.37	674	6.13	654.3	7.23	88.1		0.27	3425	935	415
K-29_03	1.4076	1.26	0.10458	1.17	0.57	9.5621	1.17	0.09770	1.13		1580.7	20.97	892.1	7.46	641.2	7.12	40.6		0.36	1944	702	263
K-29_04	1.4161	1.21	0.13912	1.16	0.59	7.1880	1.16	0.07389	1.07		1038.6	21.4	895.7	7.17	839.7	9.12	80.8		0.07	2344	175	357
K-29_05	1.3519	1.53	0.10844	1.20	0.46	9.2217	1.20	0.09050	1.45		1436	27.25	868.4	8.91	663.7	7.56	46.2		0.34	348	120	45
K-29_06	1.8450	1.21	0.16382	1.16	0.59	6.1043	1.16	0.08176	1.08		1239.7	20.98	1061.7	7.99	978	10.52	78.9		0.56	1199	667	246
K-36_01	2.4355	1.30	0.21287	1.17	0.55	4.6977	1.17	0.08306	1.18		1270.7	22.72	1253.2	9.33	1244.1	13.21	97.9		0.31	143	45	36
K-36_02	2.4114	1.30	0.21105	1.17	0.54	4.7382	1.17	0.08295	1.18		1268	22.77	1246	9.32	1234.4	13.12	97.4		0.28	229	63	57
K-36_03	2.4120	1.33	0.21315	1.17	0.53	4.6915	1.17	0.08215	1.22		1249.1	23.72	1246.2	9.57	1245.6	13.27	99.7		0.37	135	50	35
K-36_04	2.3460	1.29	0.20593	1.17	0.55	4.8560	1.17	0.08270	1.17		1262.2	22.59	1226.3	9.19	1207.1	12.84	95.6		0.26	329	85	79
K-36_05	2.4459	1.27	0.21427	1.16	0.56	4.6670	1.16	0.08287	1.15		1266.2	22.2	1256.2	9.17	1251.5	13.24	98.8		0.28	269	76	68
K-36_06	2.1541	1.23	0.19318	1.16	0.58	5.1765	1.16	0.08095	1.10		1220.3	21.5	1166.4	8.52	1138.6	12.09	93.3		0.18	1165	212	258
K-36_07	2.4724	1.24	0.21608	1.12	0.53	4.6279	1.12	0.08299	1.16		1269	22.22	1264	8.98	1261.1	12.88	99.4		0.28	220	62	58
K-36_08	2.4956	1.24	0.2136	1.12	0.53	4.6816	1.12	0.08474	1.16		1309.6	22.21	1270.8	9.00	1247.9	12.76	95.3		0.26	204	54	51
K-36_09	2.5356	1.21	0.21957	1.12	0.54	4.5544	1.12	0.08376	1.12		1286.8	21.66	1282.3	8.83	1279.6	13.02	99.4		0.36	241	88	64
K-36_10	2.4275	1.18	0.21306	1.12	0.56	4.6935	1.12	0.08264	1.08		1260.7	20.75	1250.8	8.47	1245.1	12.65	98.8		0.28	437	123	109
K-36_11	1.8835	1.17	0.18127	1.11	0.56	5.5166	1.11	0.07537	1.07		1078.3	21.33	1075.3	7.76	1073.9	11.04	99.6		0.17	738	126	150
K-36_12	2.4017	1.89	0.21294	1.22	0.35	4.6962	1.22	0.08180	1.86		1240.8	35.83	1243.1	13.56	1244.5	13.80	100.3		0.47	65	31	17

Porphyritic granite sample K1 – outliers included

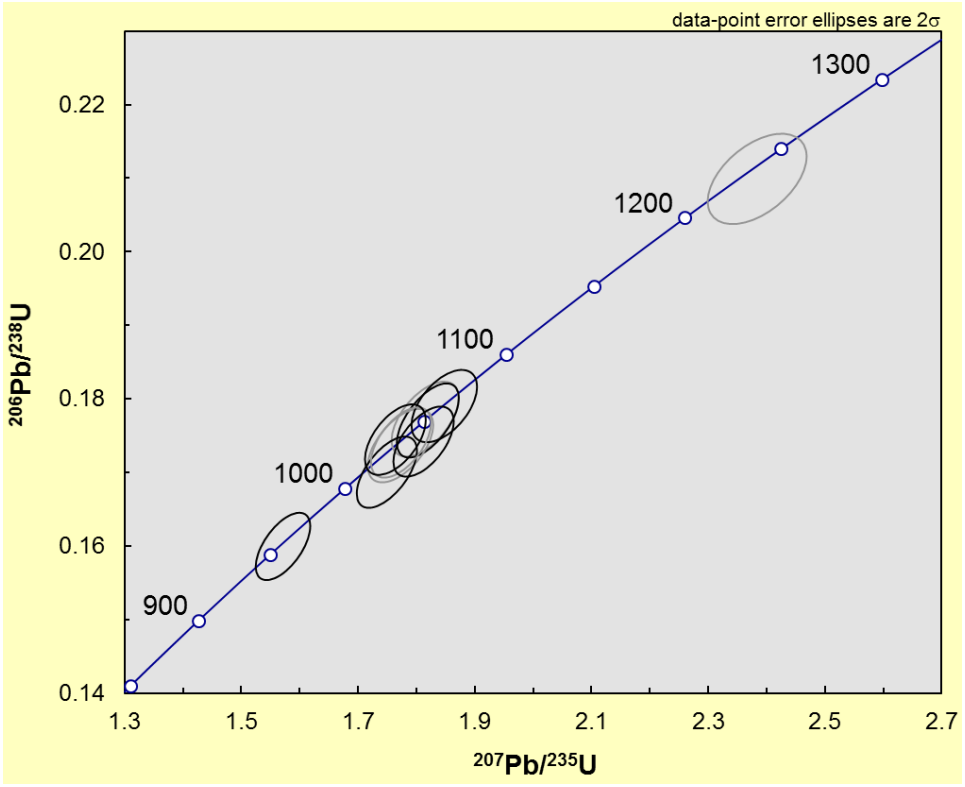

Flaser gneiss sample K36 – outliers included

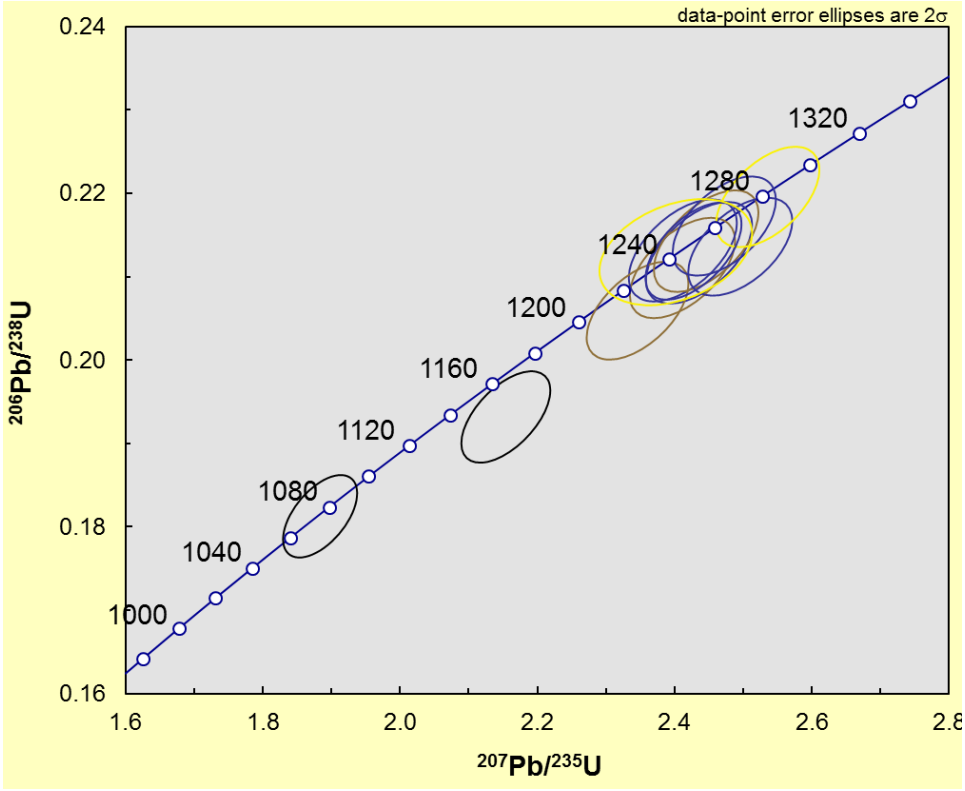

Porphyritic granite sample K26 – discordant data

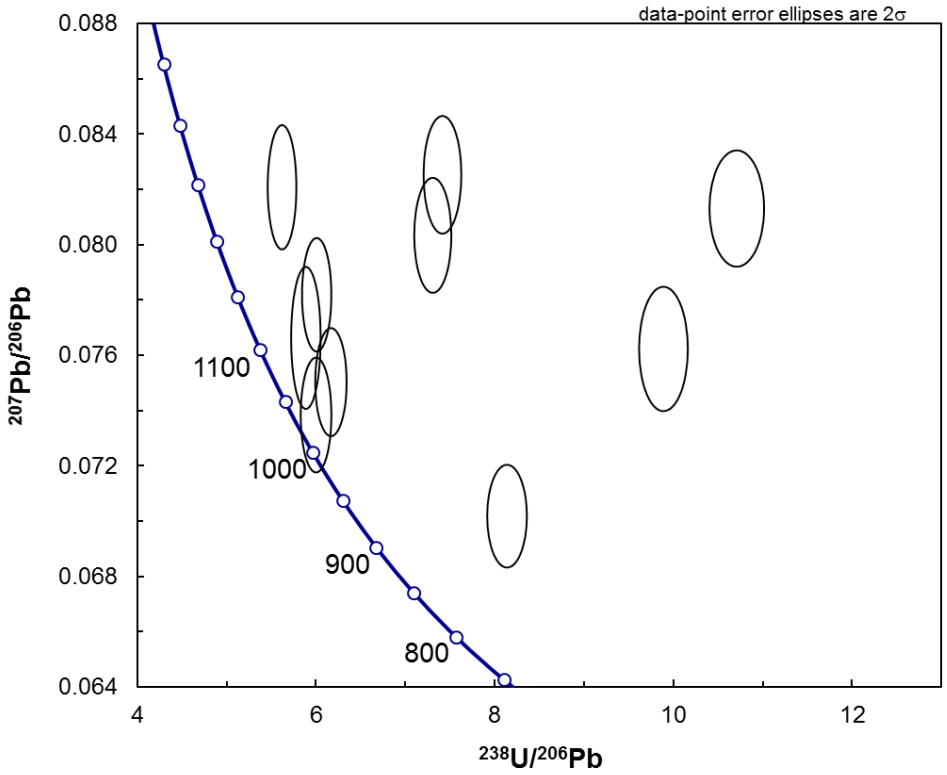

Grey granite sample K29 – discordant data

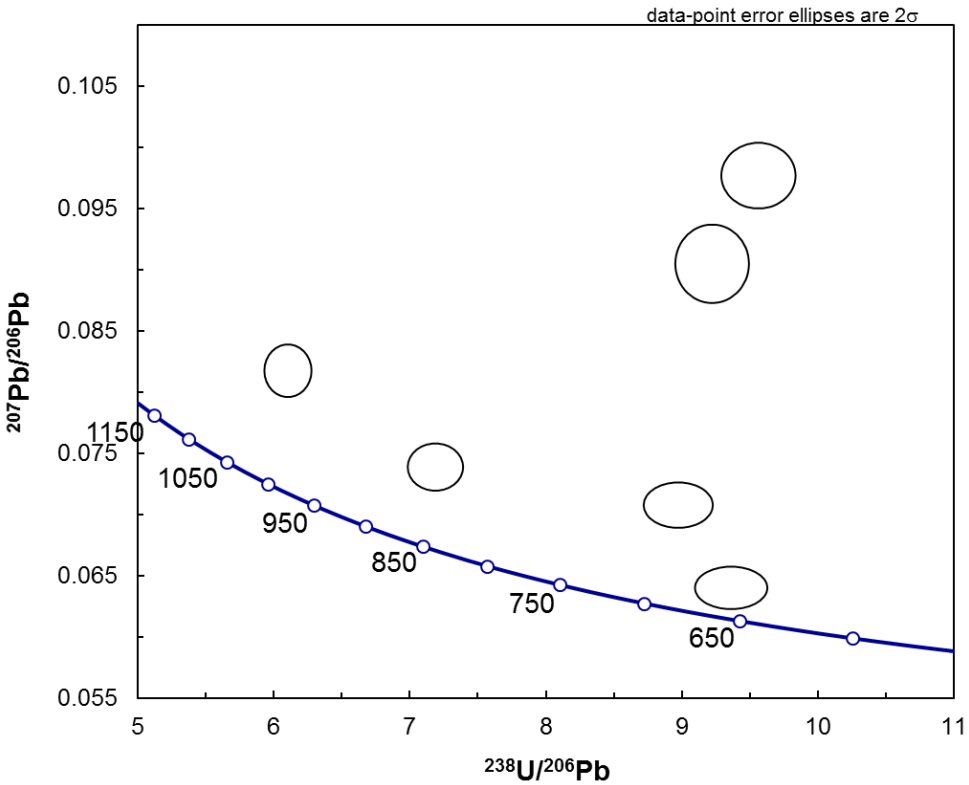

Appendix 4 – Results from magnetic analysis

	GeoDec	GeoInc	Susc. (SI)	Jr (A/m)	Ji (A/m)	Q	% Mt
K2	314,2	3,5	0,0538	0,2723	2,1628	0,1259	1,549
	313,4	-25,1	0,0358	0,4614	1,4405	0,3203	1,032
	101,5	79,5	0,0505	0,0564	2,0317	0,0278	1,455
K26	157,8	-27,1	0,0035	0,0439	0,1389	0,3158	0,100
	149,9	-52,3	0,0056	0,1105	0,2267	0,4876	0,162
	91,5	-56,7	0,0087	0,0704	0,3490	0,2017	0,250
	142,5	-34	0,0086	0,0251	0,3451	0,0727	0,247
	268,3	-52,4	0,0058	0,0322	0,2318	0,1388	0,166
	158,7	-65,2	0,0083	0,1018	0,3356	0,3034	0,240
K29A	260,1	84,7	0,0607	0,4771	2,4438	0,1952	1,751
	208,4	58,5	0,0301	0,1488	1,2109	0,1229	0,867
	57,6	22,4	0,0485	0,2343	1,9507	0,1201	1,397
	144,7	53,6	0,0498	0,2808	2,0047	0,1401	1,436
K30	115,8	26,9	0,0098	0,2273	0,3934	0,5777	0,282
	134,1	41,2	0,0055	0,1469	0,2210	0,6645	0,158
	134,7	28	0,0074	0,2009	0,2967	0,6772	0,213
	88,2	40,7	0,0084	0,1990	0,3398	0,5855	0,243
	93,5	34,7	0,0083	0,2531	0,3349	0,7559	0,240
K31	210,6	53,5	0,0017	0,0061	0,0671	0,0908	0,048
	62,5	17,3	0,0007	0,0026	0,0274	0,0950	0,020
	233,4	-44,2	0,0012	0,0114	0,0468	0,2443	0,034
	166,1	40,5	0,0012	0,0056	0,0486	0,1161	0,035
K32	167,7	51,2	0,0401	0,6635	1,6144	0,4110	1,156
	289,3	62,1	0,0466	0,3235	1,8755	0,1725	1,344
	262,2	31,7	0,0440	0,1846	1,7707	0,1043	1,268
	259,4	82,9	0,0359	0,2270	1,4425	0,1573	1,033
K33	71,8	55,6	0,0008	0,0169	0,0315	0,5349	0,023
	101,5	79,5	0,0008	0,0564	0,0341	1,6558	0,024
	186,3	54,1	0,0008	0,0095	0,0314	0,3024	0,022
	134,8	18,9	0,0007	0,0047	0,0274	0,1705	0,020
K36	306,5	-57,4	0,0003	0,0025	0,0128	0,1957	0,009
	235,7	-59,2	0,0002	0,0107	0,0063	1,6894	0,005
	240,4	-58,8	0,0001	0,0089	0,0055	1,6016	0,004

Background field: 40,23A/m, 056/71 (http://www.ngdc.noaa.gov)

Note the difference in inclination (GeoInc), Q-value (Jr/Ji) and Jr for the porphyritic granite from the west side of the Knaben Zone, K26, and from the east side K30. This suggests that different plutons could be possible to distinguish by their palaeomagnetic vector.

Amphibolite	Banded granite	Grey MoS granite	Porphyry Granite	Strained granite
0,64	5,78	0,156	1,91	0,05
0,66	9,78	0,16	2,86	0,08
14,64	18,22	0,51	3,51	0,09
47,44	29,06		3,63	0,4
	46,6		4,86	0,46
			4,98	0,64
			5,04	0,73
			5,18	1,4
			5,29	4,61
			5,66	4,8
			6	6,02
			6,09	6,76
			6,44	7,19
			6,62	8,17
			6,63	10,19
			6,74	11,78
			6,86	15,52
			7,11	22,9
			7,28	31,42
			7,47	73,34
			7,53	
			7,63	
			7,69	
			7,85	
			8,34	
			8,65	
			9,29	
			9,5	
			9,54	
			9,76	
			11,9	
			12,07	
			14,06	
			15,74	
			26,35	
			28,32	

Average field measurements of magnetic susceptibility from different localities. Note that the grey granite displays much lower values than the porphyritic granite, which is usefull for distinguishing between the two in field.

Digital appendix

Map 1 – Geological map with structure measurements and samples

Map 2 – Geological map with structure interpretations, profiles and localities

Map 3 – Geological map with data from key localities

Whole-rock geochemical data

Zircon geochronological data

Abstracts from conferences

(Unggeo 2014, EGU General Assembly 2014, NGF's annual winter conference 2015)